Universitat Internacional de Catalunya
Departament de Ciències Bàsiques

Tesis doctoral

G1-Cdk modulation by time and stress

Alexis E. Pérez Paredes

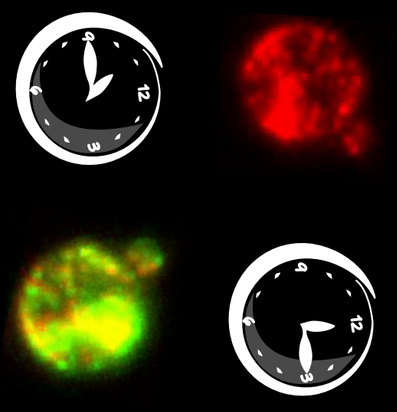

G1-Cdk modulation by time and stress

Alexis Pérez

DOCTORAL THESIS

Universitat Internacional de Catalunya, 2022

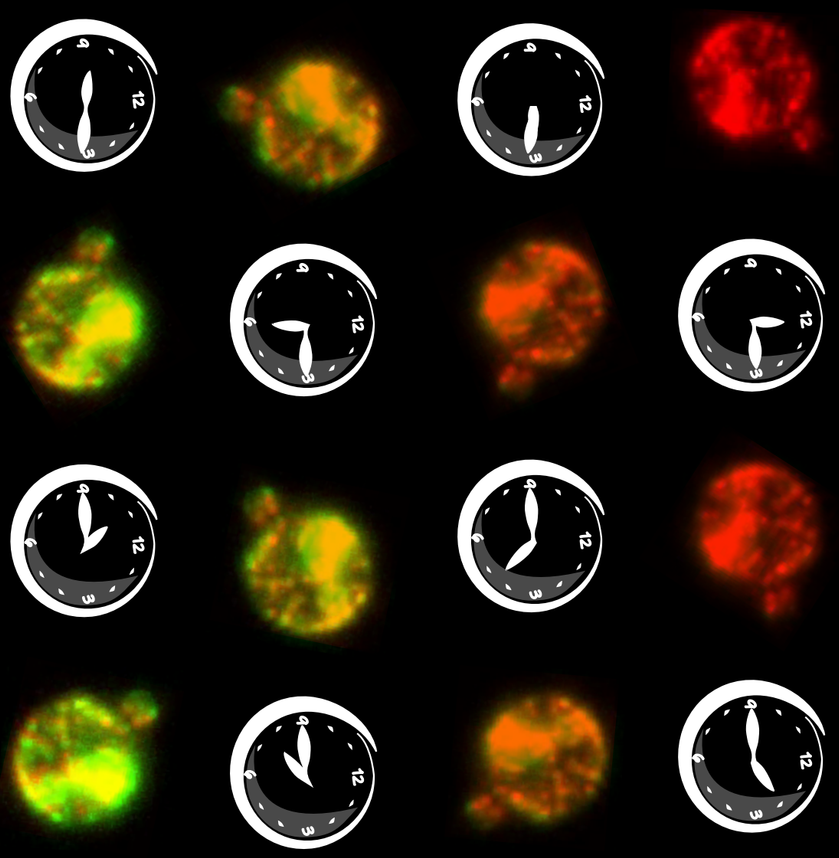

G1-Cdk modulation by time and stress

Alexis E. Pérez Paredes

Doctoral thesis

International University of Catalonia

Health sciences doctoral program

Barcelona, 2022

Work and research co-supervised by Dr. Martí Aldea Malo, and Dr. Josep Clotet Erra, in the cell cycle and molecular biology research line at the International University of Catalonia (UIC) and the Molecular Biology Institute of Barcelona (IBMB-CSIC) laboratories.

A todos a quien quiero,

Abstract

The cell cycle is regulated at different layers of control in either homeostatic or non-homeostatic conditions. Hence, in this work we analyse how time and stress modulate the cell cycle through the activity of the G1 Cdk.

Cell growth and division are coordinated processes that ensure life perpetuation with optimal cell fitness. One fundamental trait that emerges from this interplay is cell size. Despite being a seemingly basic attribute, little is known about the molecular machinery that ensures a homeostatic cell size control. In budding yeast, cell size control is mostly established in G1 and relies on the machinery that regulates the Start checkpoint transition. It is at this point where the G1 Cdk, formed by the Cdc28 Cdk and cyclin Cln3, promotes the inhibitory phosphorylation of the Whi5 repressor at the same time that activates the function of RNA polymerase II at specific SBF/MBF loci. Three models have been proposed to orchestrate these factors in size control: sizers, timers, and adders. So far, cell size control has been reported to be exerted through the dilution of Whi5 repressor acting as sizer. Even so, cell size still depicts high single-cell variability and thus warms the debate about a stochastic or deterministic size control. Favouring the latter, our work adds a time-dependent control layer executed by the interplay of APC^{Cdh1}, the mitotic-exit protein-degradation machine, Mad3, a centromeric-signalling protein, and Cln3, the G1 cyclin. APC^{Cdh1} is activated during exit from the previous mitosis and degrades Mad3 decreasing its protein levels as cells progress through G1. At the same time, since Mad3 actively participates in the degradation of Cln3 by SCF, levels of active G1 Cdk increase in the nucleus throughout G1 until Start, where cells become committed to enter the next cell cycle. Our model bestows a timer control in G1 emerging from the intertwined coordination of APC and SCF degradation machineries.

Aside of its role in the cell cycle, here we show that the G1 Cdk is also an active regulator of cell fitness under stress conditions. Many strategies conform the so-called stress response and its adaptation to a wide range of stresses and intensities. Among them, the rapid formation of stress granules (SGs) upholds cell survival and growth recovery to optimal levels upon stress relief. Stress granules are membraneless condensates rich in translationally-inhibited mRNAs and RNA-binding proteins. Their internal multivalent interactions settle a proper thermodynamic environment that generates the formation of protein-RNA assemblies by liquid-liquid phase separation. Among the diverse transcriptome and proteome composition of SGs, we have found Whi8 as a key element that connects the stress response to the cell cycle control machinery. Whi8 modulates the budding volume and interacts with both the *CLN3* mRNA and the Cdc28 kinase. Interestingly, Whi8 is also a *bona fide* component of SGs that recruits Cdc28 and the *CLN3* mRNA into these condensates. The consequence of this recruitment directly influences on both the kinetics of SG dissolution and the inactivation of the yeast Cdk. Our results designate Caprin1 as the mammalian functional homolog of Whi8 that interacts with Cdk4 and the mRNA of cyclin D1. In summary, the G1 Cdk favours disassembly of stress granules which, in turn, inhibit the activity of the Cdk. This mutual inhibition relationship generates a bistable system that ensures a rapid and abrupt SG formation only when stress exceeds a level that would otherwise endanger cell viability.

Resum

El cicle cel·lular regula diferents nivells de control tant en condicions homeostàtiques com no homeostàtiques. En aquest treball analitzem com el temps i l'estrès modulen el cicle cel·lular a través de l'activitat de la Cdk de G1.

El creixement cel·lular i la divisió són processos coordinats que asseguren la perpetuació de la vida amb una adaptació òptima. Un tret fonamental que sorgeix d'aquesta interacció és la mida de la cèl·lula. Tot i ser un atribut aparentment bàsic, es coneix poc sobre la maquinària molecular que assegura un control de la mida de la cèl·lula homeostàtica. En el llevat de gemmació, el control del tamany cel·lular s'estableix principalment en G1 i es basa en la maquinària que regula la transició del punt de control d'Start. És en aquest punt on el complex format per la Cdk Cdc28 i la ciclina Cln3 promou la fosforilació inhibidora del repressor Whi5 al mateix temps que activa la funció de l'ARN polimerasa II en el loci SBF/MBF. S'han proposat tres models que poden executar aquests factors per controlar el tamany cel·lullar: "sizers", "timers" i "adders". Fins ara, el repressor transcripcional Whi5 ha estat reportat com modulador del control del volum de la cèl·lula a través de la seva dilució. Tot i així, la mida cel·lular encara mostra una gran variabilitat a nivell de cèl·lula única i ,per tant, això escalfa el debat sobre si el control de la mida és estocàstic o determinista. Afavorint aquesta darrera opció, el nostre treball afegeix un nivell de control dependent del temps i executat per la interacció de l'APC^{Cdh1} (la màquina de degradació de proteïnes de sortida mitòtica), Mad3 (una proteïna de senyalització centromèrica) i Cln3, la ciclina de G1. L'APC^{Cdh1} s'activa durant la sortida de la mitosi anterior i degrada Mad3 reduint els seus nivells a mesura que les cèl·lules progressen en G1. Al mateix temps, donat que Mad3 participa activament en la degradació de Cln3 per SCF, els nivells de Cdk actiu augmenten en el nucli durant G1 fins a Start, on les cèl·lules estableixen l'entrada en el següent cicle cel·lular. El nostre model proporciona un control de temps en G1 que sorgeix de la coordinació entrellaçada de les màquines de degradació APC i SCF.

A més del seu paper en el cicle cel·lular, hem demostrat que la Cdk de G1 també és un regulador actiu de la supervivència cel·lular en condicions hostils. Moltes estratègies conformen l'anomenada resposta a estrès i la seva adaptació a diferents tipus d'estrès i intensitat. Entre ells, la ràpida formació de grànuls d'estrès manté la supervivència cel·lular i la recuperació del creixement a nivells òptims post-estrès. Els grànuls de l'estrès són condensats sense membrana rics en ARN missatgers (ARNm) no traduïts i proteïnes d'unió a l'ARN. Les seves interaccions internes multivalents s'estableixen en un entorn termodinàmic adequat que facilita associacions de proteïna-ARN que genera separació de fase líquida. Entre la diversa composició transcriptòmica i proteòmica dels grànuls d'estrès, hem trobat Whi8 com un element clau que connecta la resposta d'estrès amb la maquinària de control del cicle cel·lular. Whi8 modula el volum de gemmació i interacciona tant amb l'ARN missatger de CLN3 com amb la Cdk Cdc28. Curiosament, Whi8 és també un component canònic de grànuls d'estrès que recluta Cdc28 i el mRNA de CLN3 en aquests condensats. La conseqüència d'aquest reclutament influeix directament en la cinètica de la dissolució dels grànuls d'estrès i la inactivació de la Cdk de llevat. Paral·lelament, els nostres resultats designen Caprin1 com l'homòleg funcional de Whi8 en mamífer ja que interacciona amb Cdk4 i l'ARNm de la ciclina D1. En resum, la Cdk de G1 afavoreix la dissolució dels grànuls d'estrès que, al seu torn, inhibeixen l'activitat de la Cdk. Aquesta relació d'inhibició mútua genera un sistema biestable que assegura una formació ràpida i abrupta dels grànuls d'estrès només quan aquest supera un nivell que podria posar en perill la viabilitat cel·lular.

Acknowledgements

Sin ser muy consciente de lo rápido que pasa el tiempo, de repente me veo escribiendo estas líneas de agradecimiento. La verdad, este no ha sido un camino en línea recta. Como casi todo, hacer el doctorado ha sido una montaña rusa de emociones, y aunque ha habido veces que podía desbordarme siempre he sentido el apoyo de mucha gente. Ojo, tampoco quiero parecer catastrofista, volvería a hacer el doctorado y lo haría con gusto por que el placer de aprender y los buenos momentos con tanta gente me bastan para saber que no me he equivocado. Así pues, vengo con una maleta cargada de gracias.

Si tiro hacia atrás me doy cuenta de que primero me gustaría agradecer el trabajo de todos los profesores y profesoras brillantes que he tenido durante toda mi etapa académica. En especial a Guillermina y a Antonio mis profesores de biología y filosofía. Vosotros despertasteis mi interés en saber algo más de lo que pone en los libros y querer entender un poco mejor cómo funciona esto de la vida.

Esta vez no quiero dejar pasar de agradecer el apoyo de Marga, Eva y Arnau durante mi etapa en el máster de inmunología. Gracias por darme la oportunidad de aprender en uno de los primeros laboratorios en los que trabajé. Guardo muy buenos recuerdos con vosotros. Mención especial a Eva, que tuvo la paciencia de enseñarme y ayudarme con la portada de esta tesis. Gracias por tu alegría y tu forma resolver problemas en un pispás.

Es curioso por que en su momento ni siquiera me plantee que podría hacer una tesis sobre ciclo celular. Fue genial descubrir los proyectos que se estaban haciendo sobre el tema y eso me empujó a probar suerte con el grupo de Pep. Gràcies Pep per acollir-me al grup de noves ciclines. Gràcies per transmetre'm les teves ganes i saber fer de ciència. Sens dubte has estat el catalitzador d'aquesta aventura doctoral i realment t'agraeixo la confiança durant tota aquesta etapa. Siguiendo con lo que comentaba antes, tampoco me imaginé que me centraría en ciclo celular usando el modelo de levadura. Un buen día Pep me comentó que qué me parecería hacer la tesis en Barcelona junto con Martí Aldea. Me pareció buena idea y poco podía imaginar lo que eso iba a significar. Gràcies Martí per aquests anys de pura ciència. Gràcies per sempre estar disposat a discutir de qualsevol tema, donar-me un cop de ma i fer de guia quan tot estava embolicat. He pogut veure la teva forma d'entendre aquesta feina i crec que això m'ha fet ser millor científic. Gràcies també Carme per sempre estar present per qualsevol dubte i per col·laborar sempre amb tots els teus comentaris i observacions.

Hay mucha gente de la Universidad Internacional de Cataluña a la que estoy agradecido. Gracias a Javi Jiménez por los consejos y por estar siempre dispuesto a ayudarme a nivel docente y científico. Igualmente, a Natalia y Samu por el apoyo y las charlas sobre las clases. A Mariana porque siempre está ahí para ayudarte con una sonrisa y también a Joan Marc por tu buen humor, estar siempre dispuesto ayudarme con las clases o la tesis y ¡por pasarme el testigo de Mad3! No me olvido de toda la gente del laboratorio de la UIC, Anna Fosch per les xarredes sobre drets laborals dels predocs i per ajudar-me en l'aplicació de l'EPIF. A l'Helena Muley pels seus completíssims apunts de pràctiques, a la Cristina Miralpeix (ara ja d'aventura postdoc) y gracias a Eva y Abril por ayudarme en mis primeros pasos en el laboratorio de la UIC. No quiero dejarme a Blanca y Tadeo por ser tan buenos compañeros de clases de prácticas y un gracias enorme a Marta y Andrea como pilares del laboratorio de ciencias básicas, es genial poder contar siempre con vosotras y vuestro buen hacer.

Finalment, no em puc deixar a la ja Dra. Núria. No vam treballar gaire temps junts però no va caler més per saber que seríem bons amics. Gràcies per totes les xerrades de la vida, els dinars compartint

preocupacions i bones notícies i per fer-me tant suport desde la UIC. A tu Martí també t'agraeixo el poder compartir tants dinars a casa vostra i el teu bon humor sempre. Us desitjo el millor de tot cor.

Continuemos, pues. Aún me quedan gracias que repartir, por suerte. Mi llegada al IBMB al principio me resultó un poco confusa. Cambiaba de modelo y algunas cosas funcionaban de forma distinta. Mi primer gracias va ir a Eva Parisi, literalmente la conocí el día que ya se iba del laboratorio pero me dio un par de consejos e incluso me invitó a comer. Las primeras técnicas con levadura las aprendí con Pedro y David. Mis profundos agradecimientos por ayudarme a entender mejor el modelo y por toda la asistencia en los experimentos. Pedro gracias por aquellos platos típicos de Murcia y David per encara a día d'avui compartir experiments i solucions. Gracias también a Raúl por la ayuda en el laboratorio y sus charlas divertidas. Un placer poder trabajar con vosotros.

A veces, uno cuando empieza no sabe bien qué ambiente se va a encontrar en el laboratorio. Sobre todo sabiendo lo incompatible que puede ser eso con una buena salud mental. La verdad, no puedo quejarme. Por delante van mis gracias de todo corazón a todos mis compañeros de laboratorio que de alguna manera u otra forma siempre han estado ahí, ya realmente como amigos con los que he compartido muchos buenos momentos, anécdotas y a la vez tantas confidencias e inquietudes. Es algo que me llevo como un gran recuerdo de todo este recorrido. Una de las primeras personas que conocí fue Mònica. No estoy seguro de conocer a alguien que le guste más la playa y que tenga esa energía para hacer tantas cosas. Gracias por todo el apoyo en el laboratorio, los consejos científicos y las risas en tantos ya míticos "afterwork". Eso sí, que nadie ose retarnos a jugar a esconder la moneda. Me hace gracia recordar que los primeros 2 minutos que conocí Marcos no imaginé que fuera predoc por que iba trajeadísimo. Tío gracias por tantas discusiones de resultados, por compartir tu pasión por la cocina (¡y tus platos!) y estar siempre dispuesto a echar una mano. No imaginaréis lo que hay detrás del Ponceau y el Bitter Kas. Desde luego estos años no habrían sido lo mismo sin las carcajadas que me he pegado por todos los chistes o chorradas que hemos compartido. Aunque un tiempo fuimos un poco los tres mosqueteros con Mònica y Marcos, luego Raquel y Emese pasaron un tiempo en el laboratorio. La verdad que lo pasamos muy bien. Gracias a las dos por el soporte con los experimentos y por todos los buenos momentos… y el Unicum.

Pronto llegarían Blanca y Marta al laboratorio. Amigas con las que agradezco poder compartir lugar de trabajo. Blanca, gràcies per tots els consells i perquè crec que d'alguna manera ens assemblem i pots comprendre quan t'explico moltes situacions. Gràcies per les llargues xerrades, el suport al laboratori i portar tanta cultura mallorquina al lab. Marta, gràcies per ser tan bona companya de feina i per tirar endavant els projectes sempre amb ganes de treballar i dedicació. Fent duo ens va passar de tot al lab però al final sempre hem aconseguit en sortir-nos. Gràcies per les xarrades valencianes i la teva passió fallera. Digueu no als pèsols a la paella, per favor. Us desitjo de veritat un doctorat ple de bons records. Gràcies a la Laia també, espero igualment que vagi genial aquesta etapa doctoral i que el peu et deixi en pau una mica. No quiero dejarme a Alba y Ester, gracias por los comentarios y por las charlas a la hora de comer. Ester admiro tu forma de ver la vida y espero que te vaya genial en esta nueva etapa. Gracias a Bea que aunque hizo una estancia corta en nuestro laboratorio, me llevo muy buenos recuerdos de las charlas y las risas en las comidas y los afterwork.

No quiero dejarme a Laura. Gracias por los consejos en ciencia, el apoyo y las charlas que se me hacen siempre interesantes de alguna u otra forma. Gracias por tu forma de reírte de muchas cosas de la vida. Ya míticas esas vueltas corriendo a pillar el último tren por que claro… el Vallès…es el Vallès.

Con el tiempo en el IBMB se ha ido formando un buen rollito que de verdad agradezco y disfruto a partes iguales. Gracias primero a nuestras vecinas del laboratorio de topología del ADN: Joana, Sílvia, Belén y Alba. Probablemente sin vuestra ayuda habría palmado al segundo experimento. En especial

gracias a Joana por entender perfectamente lo que es vivir en Mollet y a Sílvia por los consejos sobre la tesis y algunos protocolos de levadura. Gracias a Pilar por su alegría y lo divertida que es siempre, a Mar porque siempre está ahí para dar ánimos y preguntar que qué tal va todo. Gracias también a Jose (memorable Blancanieves) y Paula por formar parte de esta etapa. Un gran gracias a Mónica Salinas por las charlas sobre el protocolo de ChIP y las qPCR y gracias también a Núria y a Carles. Esto sin dejarme por supuesto a Marta Vicioso, Samuel, María Logroño, Omar, Elena, Ramiro (gracias por las Pichia), Alex, Mariajo, Arkadiusz, Isabel e Inés (maravilloso el híbrido Sebastian + mi cabeza para, ojo, el pesebre navideño). Todos habéis formado parte de alguna u otra forma de este viaje.

Gracias a Elena Rebollo por toda la ayuda y los consejos sobre microscopía. No quiero dejarme a todo el personal del PCB: Leonor por todo tu trabajo desde administración, Patricia por encargarte de traernos los pedidos y a Antonia por que eres un cielo y encargarte de todo nuestro material.

Si algo ha sido también fundamental ha sido todo el apoyo que he recibido fuera del laboratorio. Gracias a los amigos de la "secta". Nos conocemos ya desde hace muchos años y espero que, aunque cada uno siga su vida, podamos seguir reuniéndonos de tanto en tanto. Gracias en especial a Alex y Esther por ser mis mejores amigos y ser como una segunda familia. Espero que pronto vuelvan esos viajes y excursiones. También a las personas con las que descubrí esto del rol junto a Axel, Bea, Sara, Mariana y Ramón. Gracias por seguir siempre ahí de alguna u otra forma. Esto sin olvidarme de Vílchez, Sergi y Eric, colegas entre colegas de la carrera a los que les debo muchas horas de charlas y buenos recuerdos.

Ya va quedando menos. La música ha sido y será siempre una parte muy importante en mi vida. Y así ha sido durante el doctorado, más si uno puede compartir esta pasión con personas a las que admiro como Isma y Enric. Gracias Isma por todas las horas (gustosamente) dedicadas a la música y por todos los consejos sobre networking y sobre cómo hacer currículums. Son muchos ya los años que nos conocemos y me alegra seguir compartiendo esta pasión juntos. Enric, muchas gracias, siempre estás dispuesto a echar una mano y sé que si surge un problema lo más probable es que sepas o aprendas a resolverlo. Es un placer poder ser compañeros de grupo y amigos. No imagino mejores personas con las que tirar adelante este proyecto. Ah, por supuesto no quiero dejarme a Anna (hermana Garriga), por aguantar nuestros ensayos y recibirnos siempre con una sonrisa.

Finalmente, nada de esto que escribo estaría completo si no mencionara a mi familia. Gracias de verdad, a la que está lejos, en especial a mis abuelos porque siempre me envían su cariño y apoyo. Y por supuesto a la familia que siempre he tenido cerca. A mi madre, por enseñarme siempre a ser buena persona y a esforzarme un poco más. Gracias por trabajar siempre tan duro, por los tuppers y por anticiparte y de alguna forma saber siempre la mejor forma de estar ahí. A mi padre, por todas las veces que has tenido que doblar en el trabajo, por todos los consejos de la vida, por saber comprenderme y acompañarme siempre que te he necesitado. A mi hermano, no sé qué habría hecho solo. Eres una de las personas que más admiro en este mundo, gracias por estar siempre a mi lado, por todos los momentos, las charlas, las confidencias…gracias…no puedo más que agradecer tu apoyo. En resumen, que os quiero.

Hola noia, sabías que no me iba a olvidar de ti. Mi maleta de gracias ya casi está vacía, pero me queda uno enorme y es para ti. Gracias por ser un apoyo constante durante estos años, por tus consejos y por comprenderme cuando llegaba ofuscado del trabajo. Hay muchas cosas aún por descubrir ahí fuera y espero poder hacerlo a tu lado, allá donde nos lleve esta locura de la vida. T'estimo.

Index

INTRODUCTION

Life is perpetuated based on self-replicating organisms

In the late 1940s, John von Neumann, an outstanding mathematician, taught his first lectures about self-replicating systems and cellular automata. His thoughts about the relation between the "constructor", the "description" and "the thing that is constructed" (von Neumann, 1951) reached the theories of some molecular biologists for whom the structure of the DNA was still a mystery. Nevertheless, on that time it seemed clear that DNA contained the descriptive information for generating a self-replicating living system, including the instructions for the constructor itself. Nowadays, we know that, as a general rule, DNA contains the instructions and enzymes have the role of "constructors".

The importance of DNA in this self-replicating context has commanded the basis of life perpetuation across evolution. This relies on organisms capable of accurately duplicate their DNA and then evenly distribute it to a descendant organism. The resulting organism is born with exactly the same capacities of the "mother" organism and so it can repeat again all the process. Given its loopy essence, at a cellular level this is called the cell cycle and is composed of sequential phases based on the duplication/segregation state of DNA. The cell cycle reproduces the "necessity" of each cell to accurately transfer its genetic information from the mother cell to the daughter cell (Fig. 1).

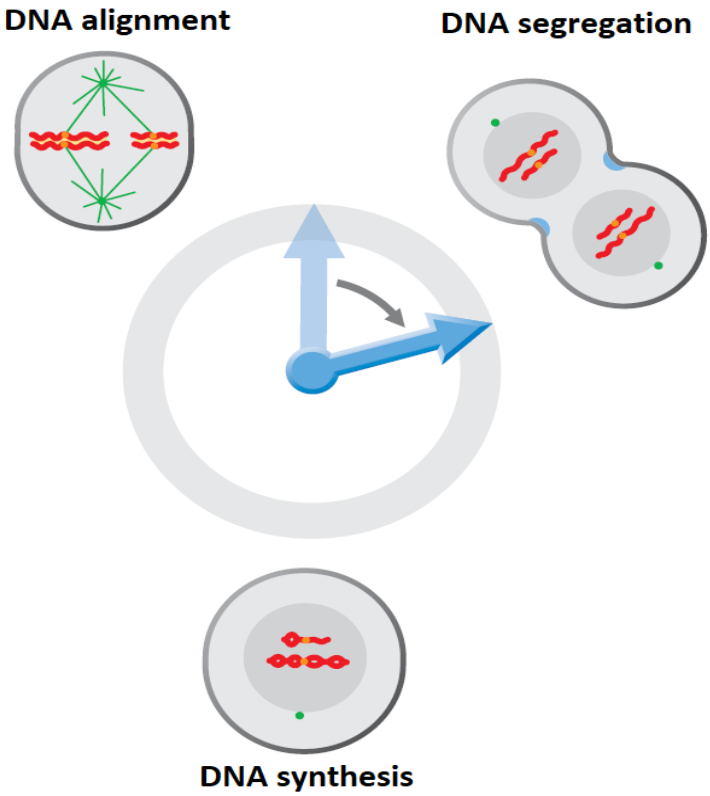

Fig. 1. The cell cycle emerges from the different DNA replication-segregation states (Morgan, 2007)

Budding yeast as a cell cycle model

Many reasons make budding yeast (*Saccharomyces cerevisiae*) a suitable model organism for studying the molecular ins and outs of cell cycle. Over a century after the introduction of budding yeast as an experimental organism, we deeply know the genetic details and the molecular biology of this microorganism (Liti, 2015). We know how to culture yeast cells in the laboratory in a feasible and controlled way. We also know how yeast genetics work and how can we neatly manipulate them by using homologous recombination. The early availability of the whole genome sequence facilitated the genomic manipulation in budding yeast. Although vertebrates are evolutionarily far positioned from budding yeast, the pillars on which the foundations of life are well preserved in most of the fundamental aspects of life.

Budding yeast cells are cell-wall delimited unicellular organisms of about 10 µm of diameter (Fig. 2). They cycle in about 90 min with a closed-asymmetric mitosis (Boettcher and Barral, 2013). This means that daughter cells are born smaller than mothers, and also, that mitosis is performed without the disassembly of the nuclear membrane. Another advantageous trait is that it is possible to visually follow the budding yeast cell cycle by just observing cells under the microscope: the presence and the subsequent growth of the bud occurs just after G1 phase.

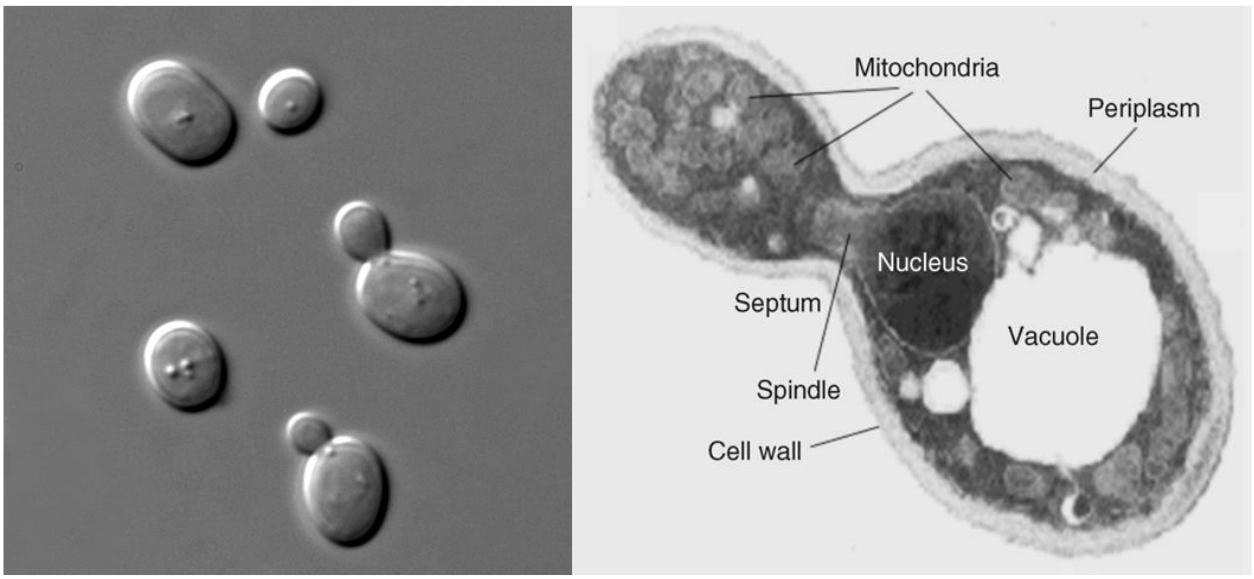

Fig. 2. The *Saccharomyces cerevisiae* yeast is also known as "budding yeast" due to the emergence of the characteristic bud. **(Left)** Changes in cell morphology are related to different cell cycle phases (Masur, 2009). **(Right)** Budding yeast micrograph with some highlighted parts. The nucleus is moving to the mother-daughter intersection where it will be fragmented once closed mitosis finishes (Horst Feldmann, 2012).

It is important to consider that in nature, budding yeast has evolved to adapt the many hostile conditions of the environment. Most of its adaptations are focused on nutrient availability. In this context, budding yeast can use many carbon sources for obtaining energy, such as glucose, raffinose, galactose and even amino acids (Dann and Thomas, 2006). They can also respond to changes in pH, temperature or osmotic pressure.

Cell cycle elements are well conserved in budding yeast, and also the underlying regulatory networks. Historically, cell cycle research has leveraged the use of budding yeast for uncovering the presence of the so-called CDC (cell division cycle) genes. As a result, in 2001, Leland H. Hartwell (*S. cerevisiae*), Paul M. Nurse (*Schizosaccharomyces pombe*) and R. Timothy Hunt (*Spisula solidissima*) were awarded with the Nobel prize for shedding light on the molecular mechanisms that drive the cell cycle.

General aspects of the cell cycle

Evolution has shaped the cell cycle to similar scenarios across living organisms (Cross et al., 2011). Most functions of the cell cycle are preserved in all organisms even with unrelated aminoacidic sequences. In general, complex multicellular organisms increase the layers of regulation at different stages, while simpler organisms do not depict that level of control. This raises doubts about how the cell cycle has evolved to the current high-regulated complexity. On one hand, maybe diverged protein sequences conserved its original function. On the other hand, many organisms may have converged to identical cell cycle networks.

In cell cycle control, the spatiotemporal order is crucial. DNA must not be segregated before it is totally replicated. In the same way, it must be well positioned for its segregation. Cells strive to accurately control that duplication and segregation happen both in the correct order and with the optimal fidelity. This relies on the role of the cell-cycle control system, that ensures the proper alternation of DNA replication phase (S) with the segregation mitotic phase (M). If any problem affects the cell cycle network, the control system delays the progress of the cell cycle by arresting the cell in a specific phase. In this line, cell cycle shows some level of environmental plasticity. This attribute gives the cell the opportunity to adapt to the environment status such as nutrient availability or other hostile conditions.

If S and M where the unique phases in the cell cycle, cells at each generation would get smaller and smaller. In addition, many other important organelles must be present in sufficient quantities so that they can be half-split between two cells. Additional time is needed for cell growth. G1 and G2 (gap) phases fulfil this mission and also serve as surveillance phases. In general, G1 phase precedes S phase while G2 phase precedes M phase. The maintaining of cell growth and division homeostasis in cell

populations depends on the connection of these phases. Nevertheless, in specific contexts, such as human oocytes, cell division occurs in the absence of cell growth, producing even more and more smaller daughter cells.

In general, G1 sets the initial phase of the cell cycle. At this point, cells grow to a specific cell size and predisposes the molecular machinery for DNA replication. In parallel, it monitors internal and external signals that influence in the commitment to triggering the cell cycle. The following S phase (S stands for synthesis) begins at DNA replication origins, where DNA is untangled for allowing the access of the enzymes that will synthesize the new DNA strands. At this level, protein production is also increased, partly due to the histone requirements that should package the extra copy of DNA (Günesdogan et al., 2014). Although last studies have showed that histone production starts in late G1 (Armstrong and Spencer, 2021). G2 phase allows for the preparation of the following mitosis by, depending on the organism, promoting protein synthesis and cell growth. Mitosis comprises the last phase of the cell cycle. In this context, DNA replication generates two sister chromatids that condense forming chromosomes. Sister chromatids are positioned in the middle of the cell by a protein polymer called the mitotic spindle and composed of microtubules. Microtubules are generated from structures that are strategically placed at both poles of the cell, the centrosomes. Once all microtubules are correctly attached to DNA, anaphase is triggered, and sister chromatids separate in an equal proportion. Last studies have reported that DNA replication overlaps with anaphase in late M phase (Ivanova et al., 2020). This occurs mainly at subtelomeric regions when M-cyclin-Cdk activity decreases by the action of protein degradation. Finally, cytokinesis promotes the division of the initial cell in two cells capable to initiate a new cell cycle from the initial G1 phase. Although evolutionary conserved, the presence of all these phases is not ubiquitous to all cellular contexts.

The cell cycle control system

The oscillatory nature of the cell cycle is based at the molecular level on the cell cycle control system. The dominant family of proteins that drives the cell cycle are cyclin-dependent kinases (Cdks) and their activity depend on cyclins, a different family of proteins. The Cdk-cyclin complex phosphorylates many partners within pathways that control the advance of the cell cycle. As it is referred by its name, cyclin levels oscillate in time and so the activity of Cdks. Given that Cdk concentration is constant along the cell cycle (Keaton, 2007), the oscillation of the kinase activity is mainly promoted by cyclins.

The underlying regulatory pathways stablish a “switch-like” mode of action for cyclin-Cdk complexes. This is mainly acquired by a crew of enhancers or inhibitors that modulate the kinase response and set an all-or-none response to cell cycle progression. Also, different Cdk-cyclin complexes govern

different cell cycle phases, providing a dominant cyclin-Cdk combinational pattern in S, M, and G1/G2 phases.

Certain points exist during the cell cycle where cells monitor the viability of maintaining its progression (Fig. 3). They are called checkpoints and three are the principal ones. The first one is named Start, where the cell commits or not to entering the cell cycle. It depends on many parameters both coming from internal signals (is cell size correct?) and external signals (are nutrients available?). Later in the cell cycle we find the G2/M checkpoint. It assures that different mitotic proteins are present at sufficient levels for mitosis. Also, here the cell examines DNA status searching for damage in any of the copies. Studies with phleomycin, which generates DNA double-strand brakes, have shown that Tel1 and Mec1 kinases are firstly activated when DNA damage is detected. Their activity is cell-cycle phase dependent and promotes the delay of S/G2 phase by inhibiting the settlement of late origins of replication (Santocanale and Diffley, 1998). They also promote the production of dNTPs needed for DNA repair (Nakada et al., 2003; Weinert et al., 1994).

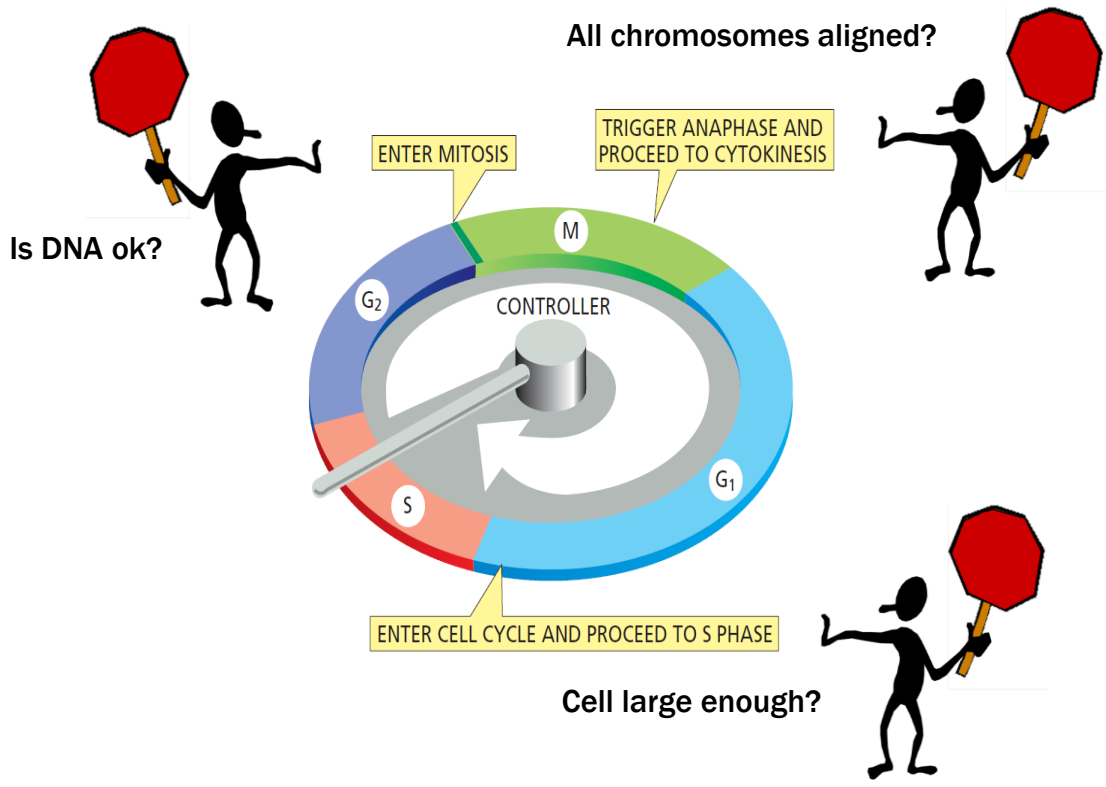

Fig. 3. G1 and G2 gap phases are intercalated between S and M cell cycle phases. Cell cycle starts in the G1 growth phase followed by both DNA synthesis phase (S) and G2 growth phase. DNA segregation and cell division occurs in the last mitotic (M) phase. The main checkpoints are placed at G1, S and M phases, where cells validate the advance of the cell cycle through "molecular questions". Modified from (Bruce Alberts (University of California, San Francisco et al., 2018).

The third one is called the spindle assembly checkpoint (SAC) and operates at M phase (Fig. 4). At this point cells check if kinetochore-microtubule complexes are correctly bound to DNA and orientated for properly distributing sister chromatids between mother and daughter cells. Treating cells with microtubule depolymerizing agents causes M-phase arrest and the activation of the SAC. When kinetochores are well attached to the centromeric sequences of chromosomes, high physical tension is maintained. However, attachment problems generate low-tension states that promote structural changes in the kinetochore. This is detected by Mps1, a kinase that phosphorylates the Spc105 kinetochore subunit and recruits members of the SAC through Bub1 protein (Foley and Kapoor, 2013). The molecular effector of the SAC is the mitotic checkpoint complex (MCC) that is composed of Mad2, Mad3, Bub3 and Cdc20. In this way, M cyclin-Cdk complexes remain intact, and sister-chromatids are kept together. Inhibition of the Cdc20 adaptor is mostly mediated by a closed conformational state of Mad2 that prevents the activation of the anaphase-promoting complex (APC) and promotes a delay in metaphase (Luo et al., 2004; Skinner et al., 2008). These guard systems directly target cyclin-Cdk complexes, thus affecting the main drivers of cycle. The proper functioning of the checkpoints determines that cells are produced when they are really needed and also when DNA integrity is assured. However, the checkpoint inhibitory strength depends on each specific context and thus it is possible that in certain circumstances, checkpoints could be surpassed even under unfavourable conditions.

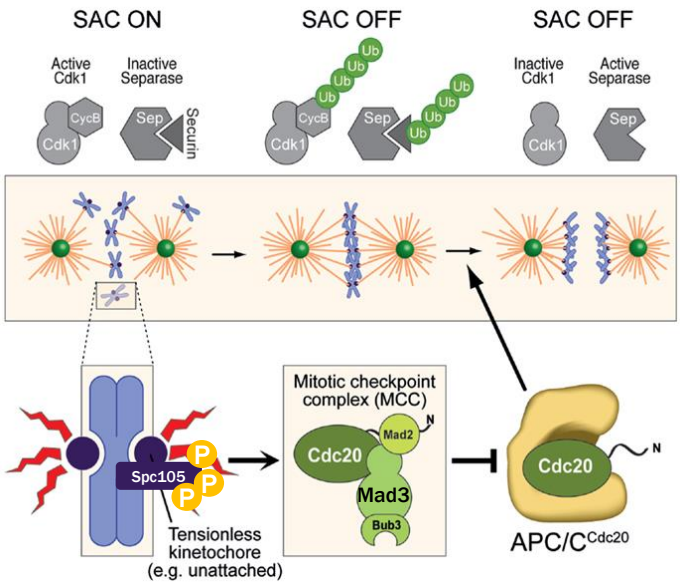

Fig. 4. The spindle assembly checkpoint. The phosphorylation of tensionless kinetochores (Spc105) promotes the assembly and recruitment of the mitotic checkpoint complex (MCC) composed of Mad2, Mad3, Bub3 and Cdc20. This complex sequesters Cdc20 and hinders the APC ubiquitination activity over securin. Once chromosome – kinetochore attachment is solved, Cdc20 is released and the APC^{Cdc20} complex degrades securin (and M cyclins) and unleashes the anaphase promoting activity of the separase. Modified from (Krenn and Musacchio, 2015).

Cdks

At different organism levels, Cdks have a conserved serine-threonine kinase activity. The target sequence is generally composed of a serine or threonine (S/T), followed by a proline (P) and a basic amino acid (K/R) two positions away of the target residue. The phosphorylation consensus sequence is thus referred as [S/T]PX[K/R], where X corresponds to any amino acid.

The whole Cdk family portrait varies depending on the organism. For instance, animals possess at least nine different Cdks, although not all of them with cell-cycle related roles. Conversely, some fungi like *S. cerevisiae* in normal conditions trusts most of the Cdk activity to just one multifaceted Cdk (Cdc28). Interestingly, under nutrient scarcity, other Cdks like Pho85 take over cell survival and are fundamental for cell cycle re-entry and Cln3 stability (Menoyo et al., 2013).

Full Cdk activation is mediated by cyclin binding and phosphorylation by Cdk-activating kinases (CAK), specialized enzymes that fully stimulate the Cdk activity. Under normal conditions, CAK expression and activity are maintained at high levels. This promotes a state in which Cdk is permanently phosphorylated and thus cyclin binding becomes the limiting step in full Cdk activation. However, phosphorylation has a dual role in Cdk functionality. In mitosis, Wee1 (Swe1 in budding yeast) kinase intercedes the inhibitory phosphorylation of Cdk. On the other hand, the Cdc25 phosphatase removes this Cdk inhibitory phosphorylation modulating its activity in terms of kinase-phosphatase opposing forces. Both Wee1 and Cdc25 are also phosphorylated by mitotic cyclin-Cdk complexes. In the case of Wee1, this phosphorylation has an inhibitory behaviour while it acts as an activation signal for Cdc25. As a whole, this system works as a positive feedback loop where the cyclin-Cdk is able to activate system components that promote their own activation. This settles the basis of the “switch-like” functioning of the cell cycle.

Cdk activation is well reflected in its protein structure (Fig. 5). The catalytic site is assembled in a cleft between two lobes: a small N-terminal lobe and a large C-terminal lobe. ATP is placed inside the cleft and the substrate binds to the C-terminal lobe for receiving the phosphate group. One structural regulatory unit is the T-loop. This structure blocks the entrance of the cleft from the C-terminal loop and so prevents ATP binding in the absence of cyclin. In this line, the residues that properly face ATP to the substrate are misoriented and thus phosphate transference is blocked. Finally, one last important regulatory structure is the conserved PSTAIRE helix that includes two alpha helices that interact with the cyclin and predisposes the catalytic residues to ATP phosphate binding.

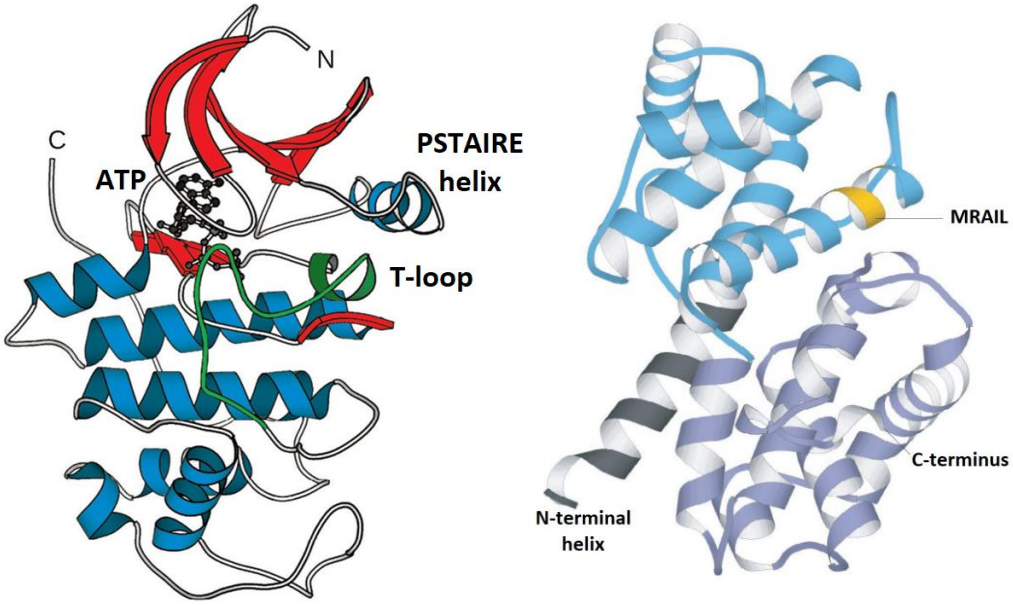

Fig. 5. **(Left)** The general structure of a Cdk consists of two lobes: one minor N-terminal lobe (red) plus one major C-terminal lobe (blue). The ATP is placed in the depths of the groove formed by the two lobes. The PSTAIRE helix modulates the interaction with cyclin while the T-loop regulates the entry of ATP. **(Right)** Structure of the central core of a cyclin. The MRAIL is also called the hydrophobic patch and contributes to substrate recognition. Modified from (Morgan, 2007).

Cyclins

Cyclins are mainly defined by two features: their capacity of binding and activating Cdks and their oscillating protein levels along cell cycle. This is managed by both increased expression levels and proteolysis as opposite collaborators. Cyclins peak throughout the cell cycle and define what happens in the different cell-cycle phases (Fig. 6). In consequence, they can be classified as G1, S, G2 and M cyclins (Table 1).

Canonical Cyclins and Cdks of Vertebrates and Budding yeast				
	Vertebrates		Budding yeast	
Cdk-cyclin complex	Cyclin	Cdk	Cyclin	Cdk
Cdk-G1	Cyclin D1,2,3	Cdk4,6	Cln3	Cdk1 (Cdc28)
Cdk-G1/S	Cyclin E	Cdk2	Cln1,2	Cdk1 (Cdc28)
Cdk-S	Cyclin A	Cdk2, Cdk1	Clb5,6	Cdk1 (Cdc28)
Cdk-M	Cyclin B	Cdk1	Clb1,2,3,4	Cdk1 (Cdc28)

Table 1. Cyclins and Cdk complexes in vertebrates and budding yeast.

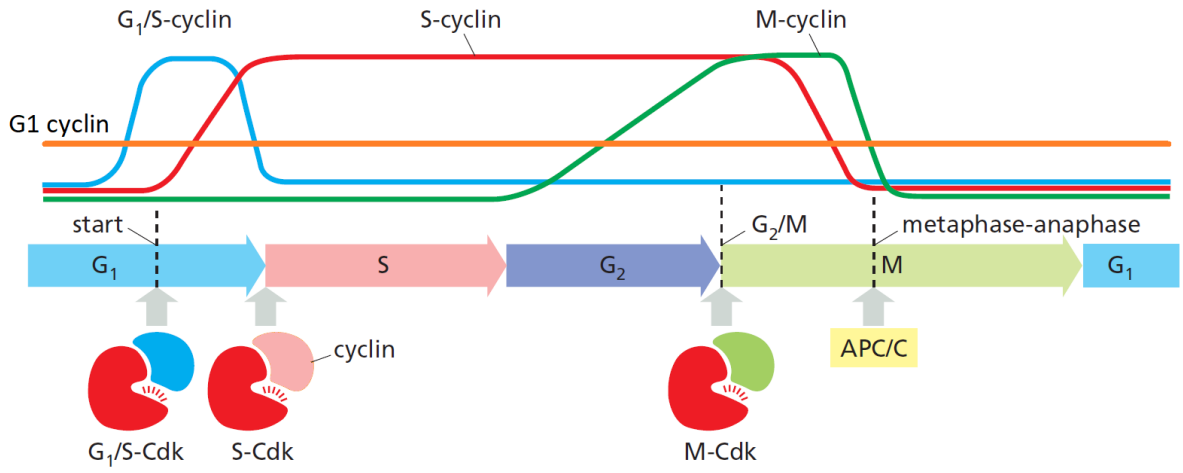

Fig. 6. Different Cdk-cyclin complexes drive the advance of the cell cycle according to different phases. Cyclins depict oscillatory expression, and, in the case of budding yeast, they all bind to the same Cdk (Cdc28). Also, the G1 cyclin of budding yeast, Cln3 has not an oscillatory behaviour. Modified from (Bruce Alberts (University of California, San Francisco et al., 2018).

The amino acid sequences strongly diverge across species. Nevertheless, a 100 amino acid region called the cyclin box depicts the greatest similarity among other cyclin regions and it is mainly devoted to bind and activate the Cdk. Additionally, cyclin consensus sequences can also be restricted to specific cell cycle phases. That is the case of the G1-type PEST conserved sequence that is present in proteins with fast turnover rates such as G1 cyclins.

G1 cyclins (Cln3 in budding yeast and cyclin D in vertebrates) monitor internal and external signals for the onset of the cell cycle. This allows the coordination of cell growth with the commitment to entering the cell cycle. G1/S cyclins (Cln1 and Cln2 in budding yeast, cyclin E in vertebrates) are stably expressed in late G1 and they promote Start and DNA replication by relieving all the mechanisms that prevent S-cyclin action. S cyclins (Clb5 and Clb6 in budding yeast, cyclin A in vertebrates) are mainly devoted to trigger DNA replication. M cyclins (Clb1 to Clb4 in budding yeast and cyclin B in vertebrates) coordinate the complexity of the mitotic spindle and the later chromosome segregation between cells. The action of the proteolytic complexes degrades M cyclins and paves the way for the execution of cytokinesis.

The great variability in sequence does not hinder the fact that the 3D structure of cyclins is similar between species (Fig. 5). The cyclin fold is made up of two domains of five alpha helices, one of them contains the referred cyclin box and also contributes to target recognition, and the other one participates in regulatory roles and contains, for example, the destruction motifs that modulate cyclin levels.

Cyclin-Cdk complexes specificity

Cdk-cyclin complexes target a wide range of partners. Since the number of Cdk-cyclin complexes are very limited in comparison with the number of targets, the specificity of the system could be compromised. Some possibilities tackle this problem. On one hand, it has been described that cyclins interact with Cdk-associated substrates (Örd et al., 2020). This property is not manifested in all cyclin-Cdk contexts and relies on different interaction domains. S cyclins have been reported to interact with Cdk substrates through a hydrophobic patch. This cyclin patch targets proteins that contain a RXL motif. Intrinsically disordered regions have also demonstrated a role in cyclin-mediated target recognition (Holt et al., 2009a). On the other hand, cyclins can also lead Cdks to specific cellular compartments. That is the case for the Cln3-Cdc28 cyclin-Cdk complex (Wang et al., 2004). Cln3 contains a nuclear localization signal that promotes the entry of Cdc28 to the nucleus and thus the activation of late G1 transcription factors.

Controlled protein degradation drives cell cycle

So far, we have seen that the cell cycle is sustained by oscillating elements that define different phases. These elements are the cyclin-Cdk complexes. The dramatic drop of cell-cycle related proteins is caused by the ubiquitin-dependent proteolysis machinery. This mode of regulation guarantees the irreversibility and orderly sequence of cell cycle events.

Ubiquitin is a short polypeptide that acts as a “destroy me” post-translational signal covalently attached to the target protein (Guo and Tadi, 2020). Many enzymes perform the transference of ubiquitin to the target protein in a procedure called ubiquitination. The ultimate goal of this process is directing proteins to the proteasome, a large complex where proteins are chemically fragmented to peptide and amino acids. Given the wide scope of ubiquitin action, the mechanism is preserved across species. Three main steps define ubiquitination (Fig. 7). First, ATP is consumed for activating ubiquitin by creating a thioester bond with the E1 ubiquitin activating enzyme. Second, the E2 ubiquitin-conjugating enzyme binds to the E1-ubiquitin complex and catalyses the transference of ubiquitin from E1 to E2 complex. Finally, the E3 ubiquitin ligase relocates ubiquitin from the E2 complex to the target protein by creating an isopeptide bond between a lysine in the target protein and the C-terminal glycine of ubiquitin. Often, this process is repeated on the same target but at different lysines. The result is a poly-ubiquitinated protein with destination to the proteasome.

Considering that E1 and E2 enzymes perform functions that do not directly involve the target protein, the specificity of ubiquitination is determined by the E3 ubiquitin ligase. These complexes recognize amino acid-conserved sequences called destruction motifs that allow the proper assembly of E3

ligases to selected proteins. Nevertheless, the presence of the destruction motif is not required in all protein-destruction contexts. Two main E3 ligases regulate the levels of many cell cycle components: The SCF and APC RING-type E3 ligases. SCF takes its name from Skp1, Cullin (Cdc53 in budding yeast) and F-box, the three main components of this complex (Ang and Harper, 2005). The U shape of the SCF complex faces on one hand the target protein -bound to the F-box adaptor- and on the other hand the E2-ubiquitin complex bound to Rbx1, that contains a conserved domain called the RING finger. The F-box acts as an adaptor protein that defines SCF specificity. A wide range of F-box proteins modulates E3 activity on different cell cycle proteins. For instance, Cdc4 F-box protein targets both G1 cyclin Cln3 and the Clb-inhibitor Sic1 to SCF-mediated ubiquitination. The role of F-box proteins is especially important in G1 cyclins. Cdc4 and Grr1 redundantly target Cln3 and Cln2 for degradation, but *in vivo* evidence shows that in fact, F-box specificity is dominated by subcellular localization. Grr1 is found in the cytoplasm while Cdc4 is predominantly localized in the nucleus and thus they just interact with G1 cyclins that move to their respective cellular localizations (Landry et al., 2012). Aside of subcellular location, the activity of SCF is mainly regulated at the F-box protein level and the rate of ubiquitination relies on the affinity of the target-F-box partners.

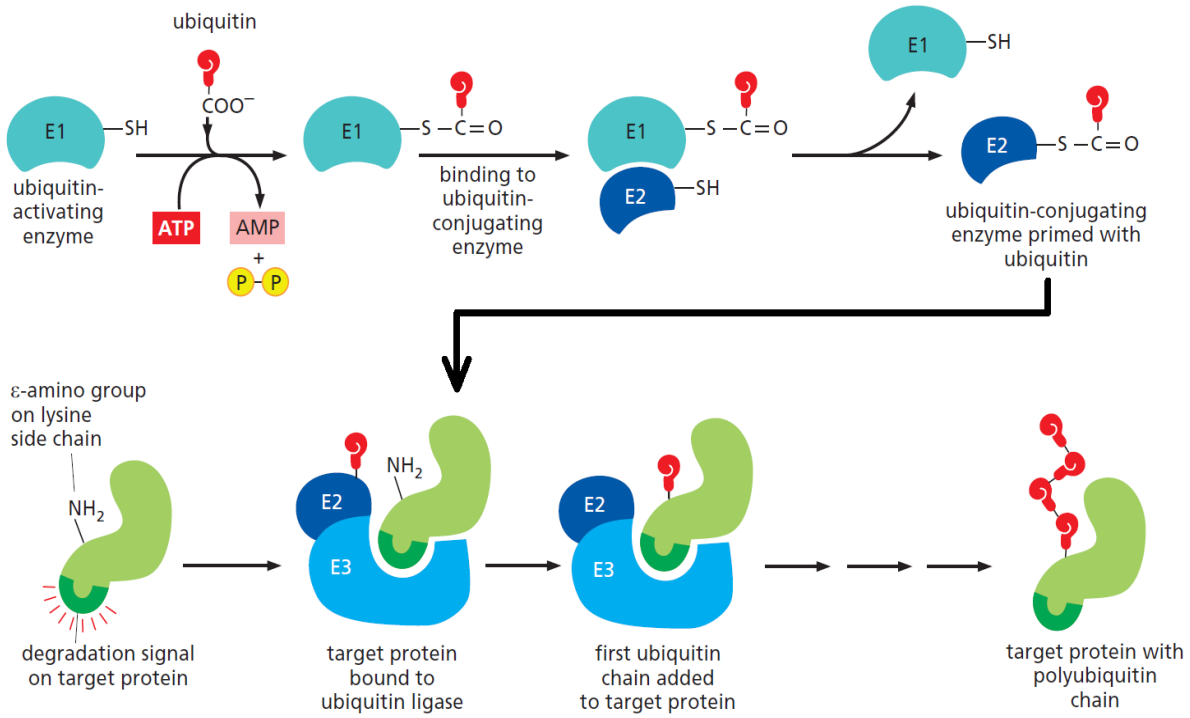

Fig. 7. The three main steps of ubiquitination. First the ubiquitin activating enzyme (E1) activates ubiquitin consuming ATP. Next, the ubiquitin is transferred to the ubiquitin conjugating enzyme (E2) that binds to the ubiquitin ligase enzyme (E3) that catalyses the ubiquitination of the target protein (in a lysine side chain) from the E2 enzyme. The process is repeated and generates polyubiquitinated proteins. Modified from (Bruce Alberts (University of California, San Francisco et al., 2018).

The phosphorylation state of the target protein, generally mediated by the Cdk, increases the affinity to the F-box proteins and thus cyclin-Cdk complexes also command the elimination of different cell cycle components in a phase-dependent manner. APC stands for anaphase-promoting complex. It constitutes a vast and conserved multisubunit system with multiple targets. It has a central role in M phase, where it is in charge of triggering anaphase by the degradation of securin. This unblocks the protease activity of separase, an enzyme that targets and cleaves cohesins, the complexes that maintain chromatid sister cohesion. The human APC is composed of 20 subunits that adopt a triangular shape (Chang et al., 2014). Tetratricopeptide repeat -containing proteins are placed in a TPR lobe that bends over a structural platform to form an assembly similar to the SCF. In this space Cdh1 and related activator subunits are able to promote an allosteric change that activates the complex. Ubiquitination activity of APC is mainly modulated by two WD40-repeat activators: Cdc20 and Cdh1 in a cell-cycle dependent manner.

In metaphase, the phosphorylation of many APC subunits by mitotic cyclin-Cdk complexes facilitates the interaction with Cdc20. The APC^{Cdc20} directs both securin and M cyclins to destruction. This constitutes a negative loop since M cyclin-Cdk complexes lead the activation of their own destruction. In consequence, APC phosphorylation decreases and Cdc20 is disassembled eventually inactivating APC in this phase. However, APC activity is also maintained in the next G1 phase. This is mediated by the Cdh1 activator subunit. The APC^{Cdh1} complex maintains some effectors at low level for resetting and avoiding premature entry in the cell cycle. In parallel, the previous APC^{Cdc20} activity virtually removes Cdk activity at the end of M phase and thus cells begin G1 in a low-Cdk activity state (Fig. 8). In consequence, APC^{Cdh1} is mostly active when Cdk activity is low following the activation of the mitotic APC^{Cdc20}. The rise of Cdk activity inhibits the APC^{Cdh1} leaving the APC no longer active until the next M phase with Cdc20. All in all, the creation of positive feedbacks mediated by cyclin-Cdk drives the abrupt advance of the cell cycle while negative feedbacks (where SCF/APC complexes have a crucial role) promote oscillatory behaviour.

The pro-destruction role of either SFC or APC complexes is counteracted by the action of the less studied deubiquitinating enzymes (DUBs), that remove the ubiquitin chains from targeted proteins. Last studies show an important contribution of DUBs to cell cycle progression. Namely, Ubp10 overexpression stabilizes a wealth of cycle-related proteins and delays mitosis. On the other side, Ubp10 deletion decreased the stability of the S phase Dbf4 kinase promoting a delay in G1/S transition. In budding yeast, Ubp15 directly deubiquitinates and stabilizes the S phase cyclin Clb5. Regarding G1, Ubp7 strongly stabilizes Cln1/Cln2 cyclins (Mapa et al., 2018), and Bre5 and Otu1 prevent excessive degradation of Cln3 (Parisi et al., 2018a).

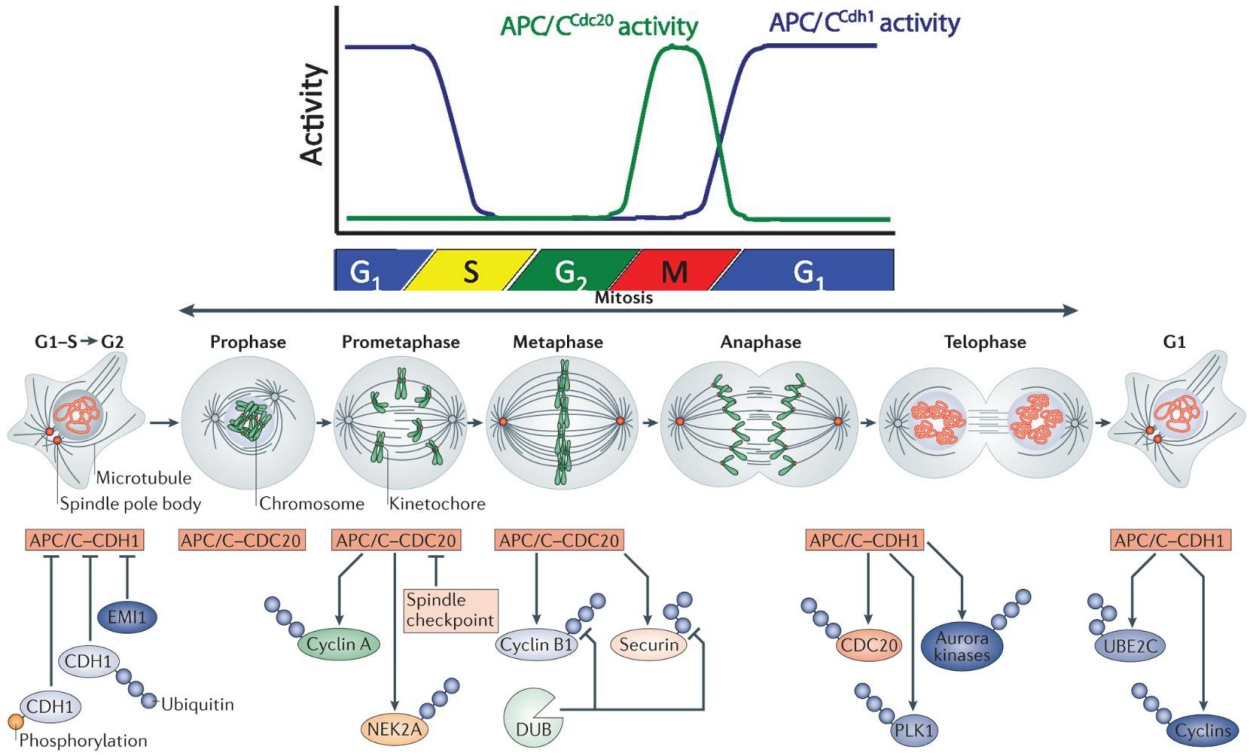

Fig. 8. The activity of the anaphase-promoting complex (APC) is cell cycle regulated. **(Above)** The APC is active at G2-M and G1 phases by means of different adaptors. Cdc20 modulates the specificity of the APC in G2/M and Cdh1 in post-anaphase and G1 phases. **(Below)** The activation of the APC depicts different targets (cyclins among them) according to different phases. In the same way many regulators influence or block the activation of the APC, like the spindle assembly checkpoint. Modified from: (Sivakumar and Gorbsky, 2015; Tsunematsu et al., 2015).

Cell cycle biochemical switches and positive feedbacks

The characteristic directionality and all-or-none triggering of some cell cycle events have long been studied. Cell cycle control ensures that phase transitions are irreversible and behave like molecular switches. These switches are based on the relation between a stimulus and a response, considering cyclins as the stimulators of the Cdk driving response. In the simplest context, increasing amounts of stimulus provoke a linear increase in the Cdk response. Given that there is a limiting number of binding sites in the Cdk, the final response becomes saturated once all Cdk are active. This relation is similar to a Michaelis-Menten plot and is called a hyperbolic response (Fig. 9). However, the relation between the stimulus and the response is far more complex in real biochemical switches. The final outcome in cell cycle must provide a quick an irreversible transition between two states: one of basal Cdk activity and the other one of high and maintained Cdk activity. Given that this system depicts well stability at both states, it is called a bistable system. Bistability can explain the behaviour of some molecular switches. In vivo, kinases can be activated not only by ligand binding but also by phosphorylation. In consequence, one kinase activated by ligand can stimulate the activity of other kinases by

phosphorylating them and generating positive feedback. At this point, this system would be too sensitive to small variations in the amount of ligand and thus bistability could be set off without control. Phosphatases negatively modulate the activation of kinases by phosphorylation and thus stablish a threshold for bistability. At the beginning, the activation of kinases is well compensated by the opposing action of phosphatases. As stimulus increases, it reaches a point in which kinases phosphorylate an overwhelming number of additional kinases that abruptly overcome the phosphatase activity (Fig. 9). This mechanism involves an important trait: the burst of kinase activity is maintained even when the ligand or the stimulus is removed from the system. This stimulus-independent activation is mediated by phosphorylation and mediates the directionality of cell cycle progression.

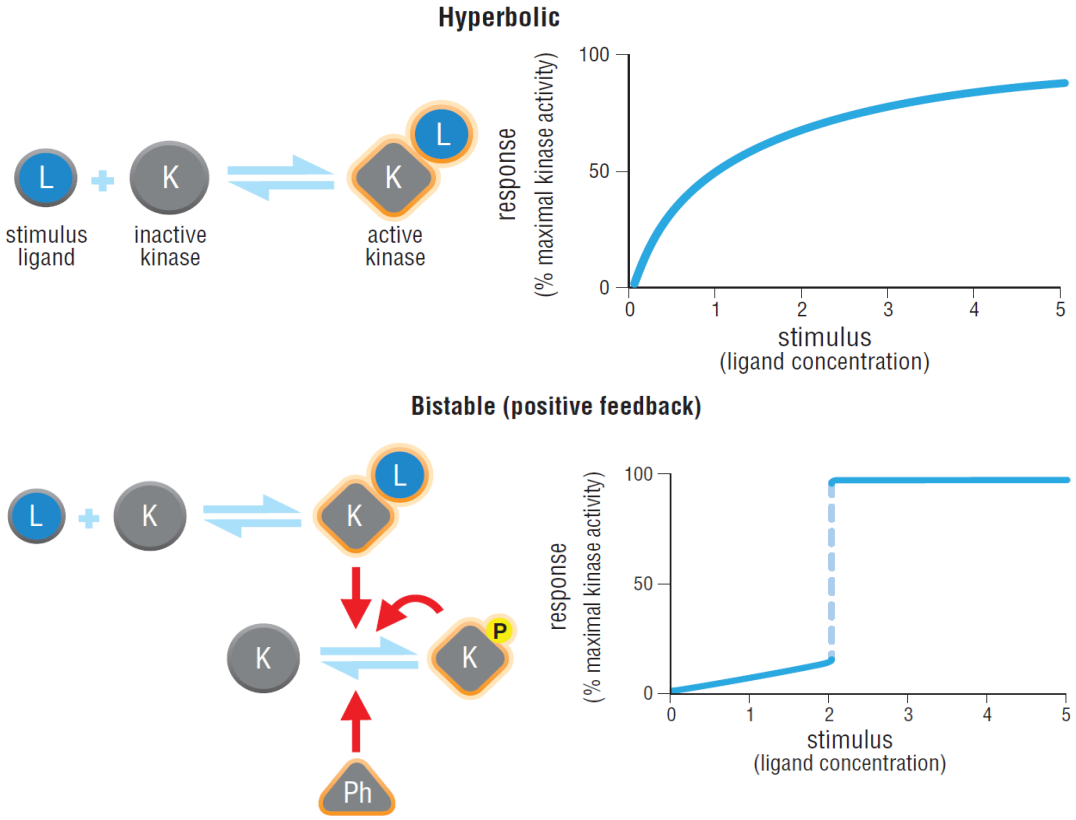

Fig. 9 **(Above)** In a simple situation, the relation of stimulus (cyclin) and response (Cdk activity) is limited by the availability of Cdks. This results in a prominent Michaelis-Menten-like behaviour. **(Below)** Bistable systems can emerge from modulated positive feedbacks. Noteworthy, at the beginning the kinase is active when is bound to the ligand. This kinase can in turn phosphorylate and activate other kinases. This generates a positive feedback modulated by the action of phosphatases. The combination of both processes generates bistable molecular switches. L = ligand K = kinase Ph = phosphatase. Modified from (Morgan, 2007).

Positive feedbacks modulated by the opposing effects of negative regulators settles the basis of bistable switches. One *in vivo* example is shown by the activation of the Cdk1-B cyclin complex. Given

that Cdk – cyclin affinity is very high, the generation of a molecular switch relies on the opposing actions of Wee1 and Cdc25. As explained before, Wee1 phosphorylation inhibits the Cdk1-B cyclin complex while the Cdc25 phosphatase removes the phosphate groups and favours the advance of the cell cycle. Here, the positive feedback is established by the Cdk-cyclin activation of additional Cdk-cyclin complexes that can inactivate Wee1 and stimulate Cdc25. The raised Cdk activity is sustained until B cyclin is degraded by the APC complex. Still, little is known about how Cdk1-B cyclin complexes begin to raise their activity for unleashing this positive feedback. Regarding budding yeast, considering that Cdc28 is the main Cdk, molecular switches could depend on the equilibrium between cyclin degradation and expression in each phase.

Cdk oscillatory activity and negative feedbacks

The cycling essence of replicating organisms is molecularly translated to oscillations in the activity of the main commanders of the cell cycle: the Cdk-cyclin complexes. In the last section, positive feedbacks explained the drastic increase in Cdk activity as a mechanism for ensuring the directionality of the cell cycle. Nonetheless, different cell cycle stages involve different Cdk-cyclin complexes and so one Cdk-cyclin complex must cease its activity to make way for the next Cdk-cyclin complex. This results in sharp ups and downs of Cdk activity that produce an oscillatory pattern. In parallel to positive feedbacks, self-promoted negative feedbacks cause the radical decrease of Cdk activity. This scenario occurs when Cdks phosphorylate and activate the Cdk inhibitors that block their own function. As with positive feedbacks, phosphatases modulate the triggering of the negative feedback. In addition to phosphatases acting on activated kinases, phosphatases also react to Cdk inhibitors, suppressing their function. The increasing activation of Cdks (mediated by cyclins) can bypass the action of phosphatases, in one case for triggering a feedback loop, and in the other one for inducing their own inhibition mediated by Cdk phosphorylated inhibitors. Eventually, when Cdk activity decreases, phosphatases return the system to the initial unphosphorylated state where the addition of stimulus can promote again a state of high Cdk activity (Fig. 10). Not only molecular inhibitors lead negative feedbacks. Ubiquitination and proteasomal degradation can work in a similar fashion if Cdks stimulate the degradation of their own stimulus.

An oscillator would only be competent if there is a balanced delay between the drastic activation of Cdks and their final self-inhibition mediated by the inhibitor. Otherwise, the kinase activity would be early repressed without reaching a high-activity state. A temporary delay can be achieved by means of phosphatase activity or affinity to the inhibitor or by using kinase intermediates that phosphorylate it and promote a lag in the inhibition of the Cdk. In addition to this time delay, molecular oscillators also demand a bistable system with stable low-high activation states. As before, one well described

oscillator arises from the Cdk1-B cyclin complex. The negative feedback involves the activation of the APC^{Cdc20} ubiquitinase due to phosphorylation by Cdk1. The APC^{Cdc20} complex essentially drives the degradation of B cyclins while triggers anaphase. Once Cdk phosphorylation decreases, APC^{Cdc20} activity concurrently drops to pre-mitotic levels. Eventually, this molecular oscillator emerges from the positive feedback mediated by Wee1-Cdc25 and the delayed (and not well understood) negative feedback from the APC^{Cdc20} complex.

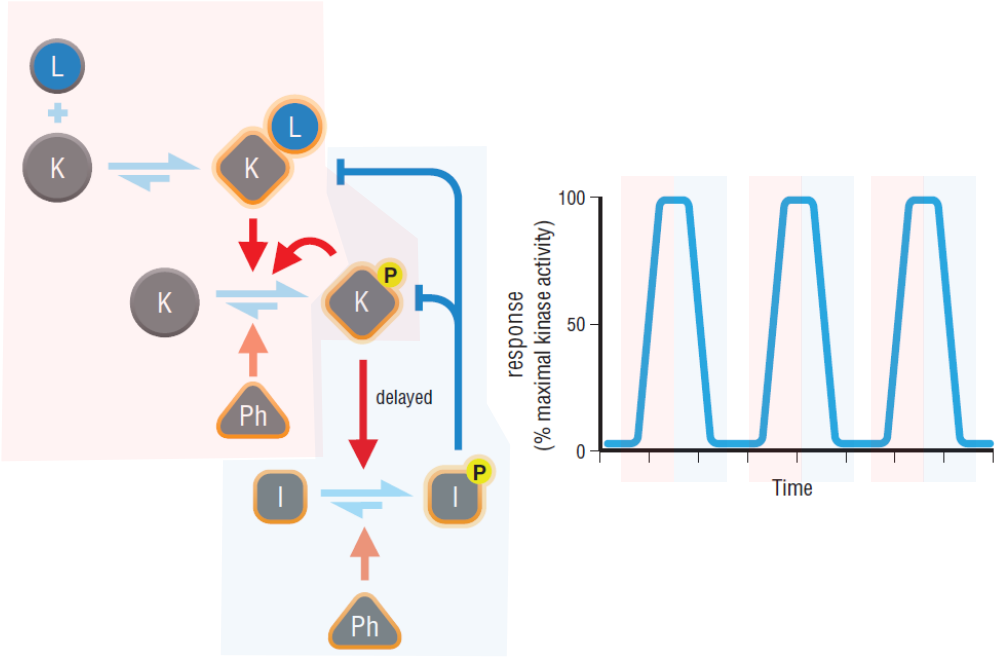

Fig. 10. Biochemical oscillators emerge from the combination of self-regulated positive feedbacks (red background) and negative feedbacks (blue background). The Cdk activity modulates its activation in the same way that activates its own inhibitor. L = ligand K = kinase Ph = phosphatase I = kinase inhibitor. Modified from (Morgan, 2007).

The G1 phase and Start machinery

As been said, cell cycle phases are sequentially ordered events in which cells strive for DNA replication and segregation. Cell population fitness depends on the quality of this process, that in parallel coordinates growth to cell division. The commitment to cell cycle entry is decided in late G1, at the Start checkpoint. This mechanism allows cells to trigger Start when external and internal conditions are favourable. Otherwise, G1 can be delayed or blocked by altering the functionality of the Start partners.

As mentioned before, budding yeast possess just one essential Cdk (Cdc28) that modulates its activity by switching cyclin partners in different phases. In G1, Cdc28 is predominantly bound to the most

upstream cyclin: Cln3. Total amounts of both Cdc28 and Cln3 remain nearly constant through the cycle (Tyers et al., 1993). By mechanisms not yet well understood (Aldea et al., 2017), cell growth modulates the Cln3-Cdc28 complex to phosphorylate elements that restrict the pass through Start and promote the positive feedback that unleashes entry into the cell cycle. The transition through Start involves a burst of expression of G1/S and S regulatory genes, like Cln1,2 G1/S cyclins and Clb5,6 S cyclins. Most of these genes are regulated by the SBF (SCB-binding factor) and MBF (MCB-binding factor) transcription factors (Iyer et al., 2001). Each one of them is composed of one protein that recognizes DNA (Swi4 in SCF and Mbp1 in MBF) and a second common regulatory protein that does not directly interact with DNA (Swi6). (Fig. 11).

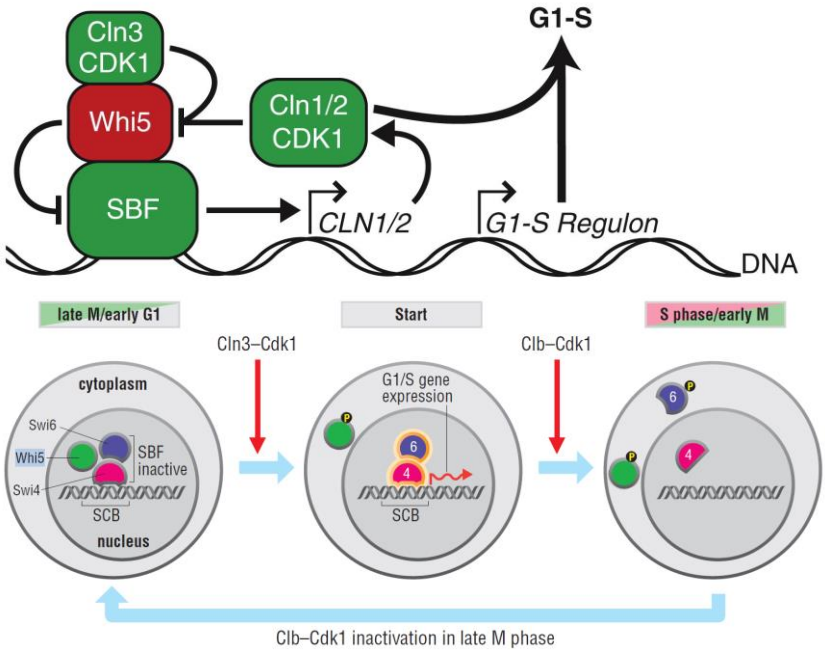

Fig. 11. **(Above)** The canonical molecular machinery that control Start transition. At early G1, Whi5 represses the SBF/MBF loci. The Cdc28-Cln3 complex phosphorylates Whi5 and releases the SBF/MBF sites for unleashing the expression of G1/S genes and trigger Start. **(Below)** Regulation of SBF activity along the cell cycle. The phosphorylation of Whi5 stimulates its nuclear to cytoplasm localization that unleash the expression of G1-S genes through SBF transcription factors. Modified from (Morgan, 2007; Turner et al., 2012).

The SBF complex is activated in late G1 when basal levels of cyclin-Cdk activity rise. However, the Swi4/Swi6 complex is blocked by the presence of the inhibitor protein Whi5 (Costanzo et al., 2004). In early G1, Whi5 binds and inhibits SBF complexes along with MBF/SBF-related TFs (transcription factors). As other Start regulators, Whi5 senses the environmental conditions that may limit the advance of the cycle (Liu et al., 2015). Whi5 acts a structurally disordered transcriptional repressor (Hasan et al., 2014). It is regulated by inhibitory phosphorylations that release Whi5 from G1/S TFs and trigger export from the nucleus to the cytoplasm (Fig. 11). During G1 Whi5 is generally hypophosphorylated, probably mediated by basal G1 cyclin-Cdk activities (Kõivomägi et al., 2021).

Since Whi5 has shown to be a poor Cln3-Cdc28 substrate, it is thought that in this context the activity of Cln3-Cdc28 is more focused on generating a positive feedback loop (with Cln1/Cln2) that shifts Whi5 to a hyperphosphorylated state. As Whi5 is inhibited, SBF/MBF complexes promote the abrupt expression of a large number of S genes and *CLN1,2* genes that reinforce the positive feedback and ensure the irreversibility of the Start transition. In addition to this mechanism, it has been reported that Cln3-Cdc28 phosphorylates the C-terminus of RNApol II localized at the SBF/MBF promoters (Kõivomägi et al., 2021) (Fig. 12). This stimulates the transcription of G1/S genes that triggers Start.

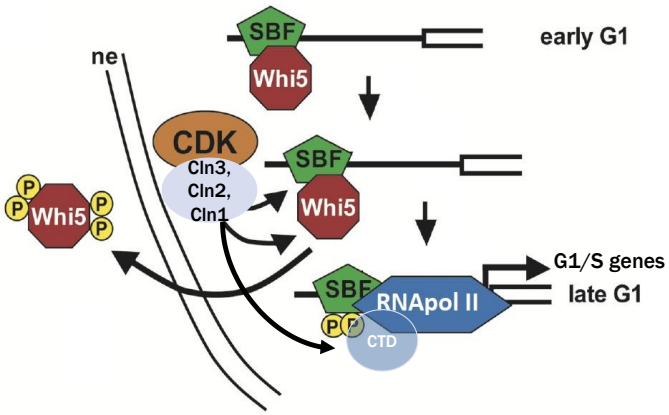

Fig. 12. Last reports indicate that Cdc28-Cln3 complexes phosphorylate basal amounts of Whi5 with low efficiency. Instead, the phosphorylation of the C-terminal domain (CTD) of RNApol II at SBF/MBF sites is suggested to be more relevant in the Start context. Modified from (Costanzo et al., 2004).

It seems that the functional role of Whi5 is mimicked by the Stb1 protein. The mutation of Cdk phosphorylation targets in either Whi5 or Stb1 does not have any relevant effect at Start. However, if both proteins are mutated, the Cln3-Cdk complex is unable to induce G1/S gene expression (Honey and Futcher, 2021). In summary, although Stb1 shares activation-repressor roles, Whi5 and Stb1 display redundant functions in Start control.

At the transcriptional level, Start is not only regulated by the Whi5 repressor. Bck2 protein works stimulating the expression of genes at diverse cell cycle phases, including late G1 and G1/S genes (Ferrezuelo et al., 2009). In fact, when Cln3 is not present, it becomes essential. Importantly, Bck2 overexpression can bypass the deletion of all G1 – G1/S cyclins (Cln1, Cln2, Cln3) (Epstein and Cross, 1994). In spite of this genetic interactions, the detailed mode of action of Bck2 is still unknown. So far, we know that Bck2 acts as an activating cofactor for transcription through a mechanism that is independent of Swi6 and thus independent of Cln3 activity. Mcm1 has also been reported as a Bck2 interactor. In this context, Bck2 participates in the expression of early cell cycle box genes that are mainly manifested in G1/S phase.

Given the surveillance nature of the G1 phase, the activity of the Cln3-Cdc28 complex is tightly regulated at different levels. For instance, Cln3 mRNA levels, Cln3 mRNA translation and Cln3 protein stability all depend on nutrient availability (Gallego et al., 1997a; Menoyo et al., 2013; Parviz and Heideman, 1998). On the other hand, the nuclear concentration of the Cln3-Cdc28 complex is regulated by Whi3/Whi7 proteins (Wang et al., 2004; Yahya et al., 2014) (Fig. 13). Whi3 has a dual role in Cln3-Cdc28 regulation. It specifically binds and retains Cln3 mRNA in the cytoplasm. On the other hand, it interacts with Cdc28 in the cytoplasm and modulates the nucleocytoplasmic localization of the Cdk. Whi7, a Whi5 paralog, associates and repress G1/S promoters (Gomar-Alba et al., 2017). Previously, it was also shown that Whi7 regulates the nuclear localization of Cln3-Cdc28 by positive feedback. Whi7 phosphorylation disassembles Cln3-Cdc28 from the reticulum-located Whi7 which in turn phosphorylate additional Whi7 repressors that release more Cln3-Cdc28 complexes (Yahya et al., 2014). In parallel, chaperones act as pivotal regulators of cytoplasmatic G1 cyclins. Ssa1-Ydj1 chaperones are important for nuclear accumulation of Cln3 by releasing it from the endoplasmic reticulum (ER) (Vergés et al., 2007a). Curiously, Ydj1 also promotes the phosphorylation of Cln3 that drives it to degradation (Yaglom et al., 1996). This duality present in some chaperons remains to be fully understood.

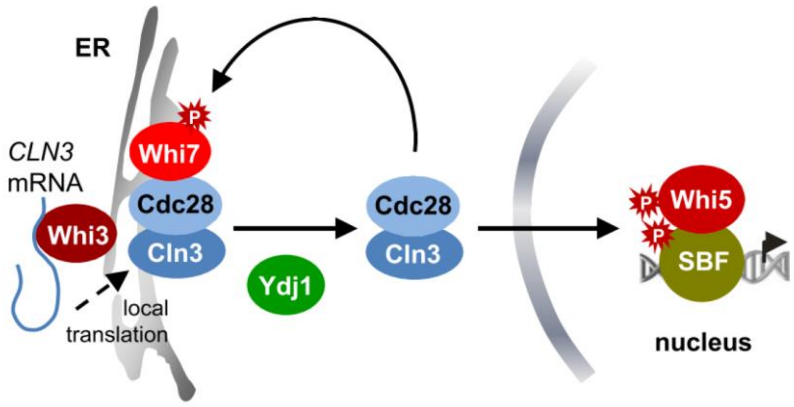

Fig. 13. Although Cln3 and Cdc28 levels remain constant along the cycle, different cytoplasm retaining mechanisms regulate Cln3 – Cdc28 nuclear entry. Whi3 arrest the mRNA of Cln3 in the ER (endoplasmic reticulum). Whi7 also retains the Cdc28-Cln3 complexes bound to the ER. The release of Cdc28-Cln3 stimulate their own release by phosphorylating Whi7. This process is assisted by chaperones like Ydj1 (Yahya et al., 2014).

Segregase chaperones add another level of control over Cln3. Involved in a wide range of cellular protein-folding processes, segregases bind ubiquitinated proteins and “segregate” them from their partners (Jentsch and Rumpf, 2007). Some segregases have influence on cell cycle progression. As it is specified in its name, cell division cycle 48 segregase (Cdc48) inhibits Cln3 proteasomal degradation by the associated action of deubiquitination enzymes and spurs Start transitioning by releasing Cln3 from the ER (Parisi et al., 2018a). This results in an accumulation of Cln3 in the nucleus.

Following the activation of the Start machinery through G1/S cyclin activity, S cyclins (Clb5,6) bind Cdc28 and form the first S-Cdk complexes. However, S-Cdk activity is still low at this point due to the inhibitory effect of Sic1. Sic1 specifically inhibits Clb-Cdc28 but not Cln-Cdc28 complexes. As a result, many inhibited Sic1-Clb-Cdc28 complexes accumulate in late G1/S phase. Phosphorylation by Cln-Cdc28 at multiple Sic1 sites stimulates the interaction of Sic1 with Cdc4, a SCF F-box protein (Verma et al., 1997). The specific characteristics of these phosphorylations set a threshold for the degradation of Sic1 in a switch-like degradation mechanism (Nash et al., 2001) (Fig. 14). As a result of the Cln1,2-Cdc28 feedback loop, Sic1 is sent to proteolytic degradation and Clb-Cdc28 complexes are released for triggering DNA replication. During S phase, G1/S cyclin expression is negatively regulated at DNA and protein level. S and M cyclin-Cdk complexes promote the dissociation of SBF/MBF transcriptional factors. In consequence, the dominant role of the new Clb-Cdc28 phosphorylation complexes leads the export of Swi6 from the nucleus to the cytoplasm.

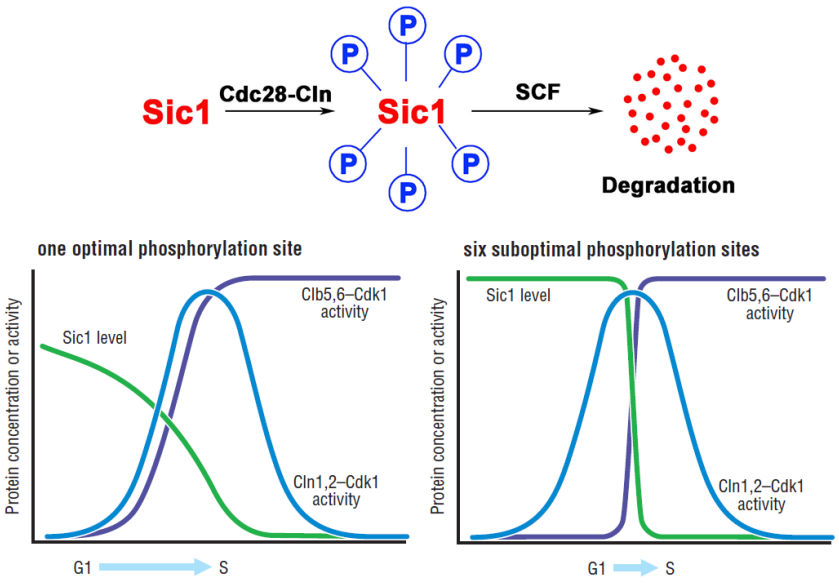

Fig. 14. Multisite phosphorylation of Sic1 shows a switch-like drop of the Sic1 inhibitor. Low Cdc28-Cln3 activity promote low phosphorylation states of Sic1 that poorly bind to Cdc4. Once Cdc28-Cln3 activity surpasses certain levels, Sic1 is multiphosphorylated and rapidly degraded by Cdc4-SCF. The activation of Cdc28-Clb complexes also contribute to Sic1 multisite phosphorylation. One single phosphorylation site in Sic1 would extend the G1-S transition and cause premature Sic1 one degradation. G1-S transition is quick and coordinated with Start if Sic1 degradation occurs abruptly. Modified from (Morgan, 2007).

Whi5 and Cln3-Cdc28 constitute the main opposing forces that control Start, but they are not the only ones. Cdk inhibitor proteins (CKIs) play a major role in G1 progression. Sic1 and Cip1 belong to this group. As stated before, Sic1 inhibitor modulates the unleash of the S phase response. Cip1, a functional analogue of human p21, also constitutes an important G1 inhibitor with a dual role (Li et al., 2020). It is able to repress Start either blocking the action of Cln3-Cdc28 or hindering the activity

of Ccr4, a protein involved in mRNA processing that destabilizes the Whi5 mRNA. As a whole, Cip1 is a negative regulator of Whi5 inhibitors and thus it delays the transition through Start by stabilizing the functions of Whi5.

Another regulatory network is present in the particular case of budding yeast. G1 delay takes place during mating. Briefly, when members of opposed mating type meet, the production of mating factors synchronize the yeast populations in G1. To do so, a Cln-Cdc28 inhibitor (Far1) is activated when the correct mating factor is perceived in the environment. Mating factors activate a G-protein signalling pathway that in the end mobilizes the Fus3 activated kinase that phosphorylates Far1 to arrest cells in late G1 (Gartner et al., 1998).

G1 controls cell size homeostasis in budding yeast

When examining cell populations under the microscope one of the most evident traits that we can observe is the homogeneity in cell shape and size. Most cell components and processes, such as organelles and protein synthesis, scale with cell size and so it is a critical physical feature that cells strive to control. Otherwise, unbalanced cell growth to cell division coordination produces serious imbalances that compromise cell survival. However, not all cell types and organisms fulfil this condition. Neuron and muscle cells grow without experiencing division. Conversely, embryos from certain species keep division without intermediate growth phases. But in general, cell cycle events are coordinated with the synthesis rates that drive the increase in cell mass. This allows the maintenance of a critical size that varies across different cell populations. In fact, the presence of multiple sizes in the same cell population is referred as a diagnostic hallmark in cancer (Shashni et al., 2018; Zatulovskiy and Skotheim, 2020) (Fig. 15).

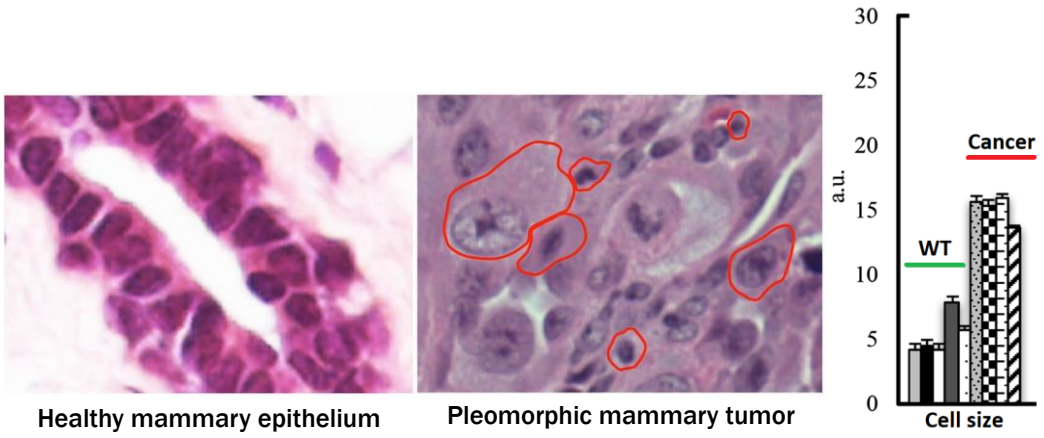

Fig. 15. Cell size as hallmark for cancer diagnosis. **(Left)** Cancer unbalances cell size homeostasis and depicts diverse cell sizes. Hematoxylin-eosin staining of mammary tissue comparing healthy with tumoral histological samples. Different cells with diverse sizes have been outlined red. **(Right)** Cancer cell lines show larger sizes than their non-cancer counterparts. Modified from (Ginzberg et al., 2015; Shashni et al., 2018).

Many strategies seem to link the machineries responsible for biomass synthesis (this includes proteins, membranes, and organelles) to the networks that drive the cell cycle. In pluricellular organisms, the production of new cells acts on demand and thus cell size is mostly modulated by signalling pathways that rely on growth factors. However, this is different in a context in which environmental conditions like nutrient availability or pH affects the coordination of growth and division. This is the case for unicellular organisms such as budding yeast or fission yeast. Yeast cells subjugate some cell cycle phases to a deterministic/stochastic critical size. While fission yeast shows a pre-mitotic size control, budding yeast control cell size in G1 (Fig. 16). In consequence, smaller G1 cells extend G1 phase until they get a critical cell size. Conversely, bigger cells spend less time in G1 and trigger Start quickly. Due to the asymmetric characteristics of budding yeast division, daughter cells are born smaller than mothers, which in normal conditions (almost) already have the critical size. The first mechanistic description of this phenomenon is based on the asymmetrical activation of Ace2 and Ash1 daughter-specific transcription factors (Di Talia et al., 2009). Both of them promote a Start delay by repressing the expression of Cln3 on daughter cells.

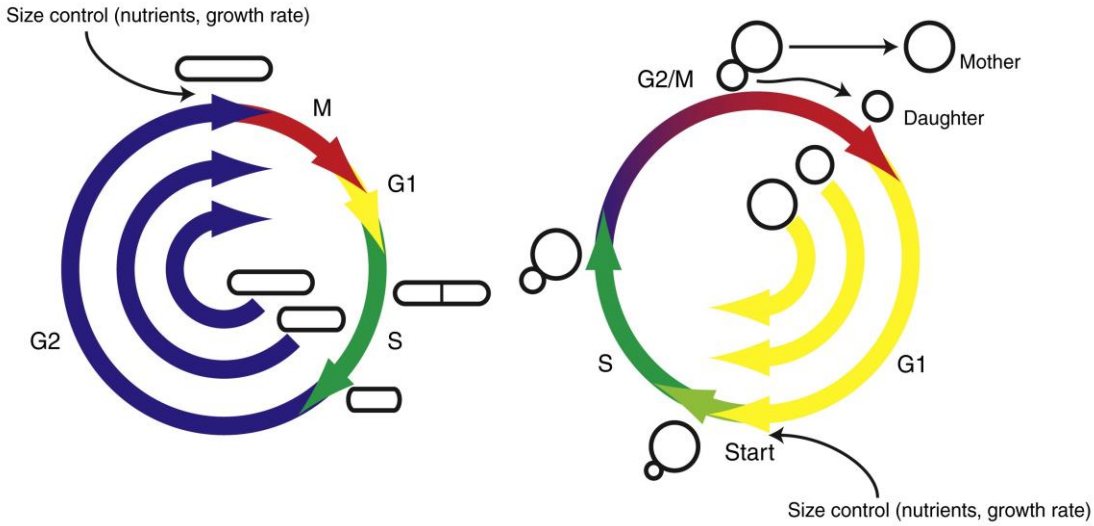

Fig, 16. Size control is organism-dependent and modulates distinct phases of the cell cycle. Fission yeast controls size mainly in G2 **(Left-blue)** while Budding yeast controls it in G1 phase **(Right-yellow)**. As a general rule, small cells delay either G2 (Fission yeast) or G1 (Budding yeast) for attaining bigger and suitable volumes for continuing the cell cycle. Bigger cells do just the opposite. Modified from (Turner et al., 2012).

Modes of cell size control

When measuring budding yeast cell volume at different points of the cell cycle, cell size variability is limited mainly at late G1 and G2/M transition (Garmendia-torres et al., 2017; Hartwell et al., 1974;

Johnston et al., 1977). Although, some G2/M size control exists, the main size-control mechanisms mainly influence Start transition in G1 (Lord and Wheals, 1981) (Fig. 17).

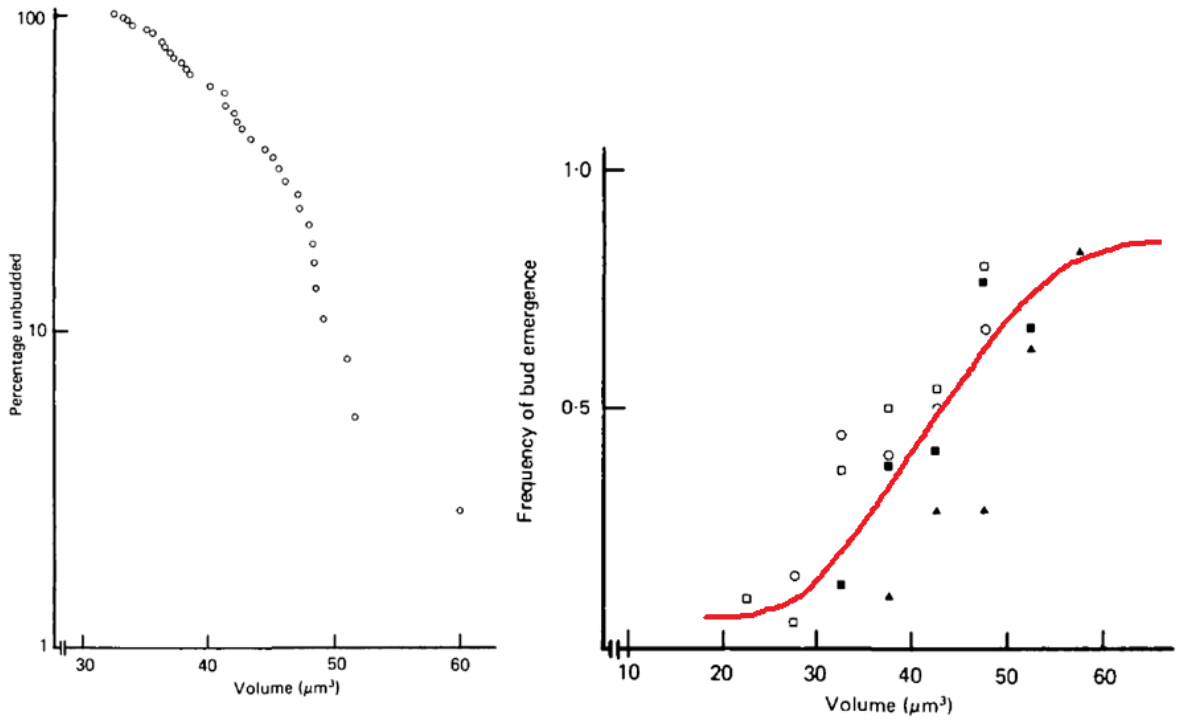

Fig. 17. Budding yeast depict G1 size control. Bud emergence occurs after Start transition. **(Left)** Percentage of unbudded cells according to volume. **(Right)** Frequency of bud emergence as a function of size. The bigger are G1 cells, the higher is the number of budded cells. Different shaped points indicate difference carbon sources (glucose, raffinose, sorbitol, galactose). Modified from (Lord and Wheals, 1981).

Three main model concepts explain cell size control behaviour: sizers, timers, and adders. When size control is mostly regulated by a sizer, cells monitor that size meets a critical range as a requirement for cell cycle normal transition. Timers modulate cell size as a function of a fixed amount of growth time and adders are based on a constant addition of a fixed size (Facchetti et al., 2017) (Fig. 18). So, the main difference between all of them is what is monitoring the cell. Is it checking the increment in size? the time spent? Or is it monitoring the size itself?

The presence of one or other mode of size control is not restricted. Some mammalian cells show a dominant G1 sizer control (Xie and Skotheim, 2020) while microbes are reported to control size by always growing the same amount of it (adder) irrespective of size at birth (Campos et al., 2014). Studies in *Chlamydomonas* found that cells divided when they reached a critical size, however, this was concomitant with a timer mode of control. If *Chlamydomonas* cells were unable to get a suitable size, they experienced a delay time that triggered cell division regardless of size control (Matsumura et al., 2003). Growth control modes can be different depending on the cell cycle phase, or they can

even combine for generating intermediate size control states (Chandler-Brown et al., 2017). In budding yeast, there is extensive data aiming at prominent sizer control in G1 (Chandler-Brown et al., 2017; Johnston et al., 1977; Lord and Wheals, 1981; Turner et al., 2012). However, daughter cells also add a constant amount of size along cell cycle that is independent of birth size. This adder control does not confront the sizer regulator in G1. Actually, it has been shown that the adder phenomenon emerges from different pre-Start and post-Start size control modes (Chandler-Brown et al., 2017).

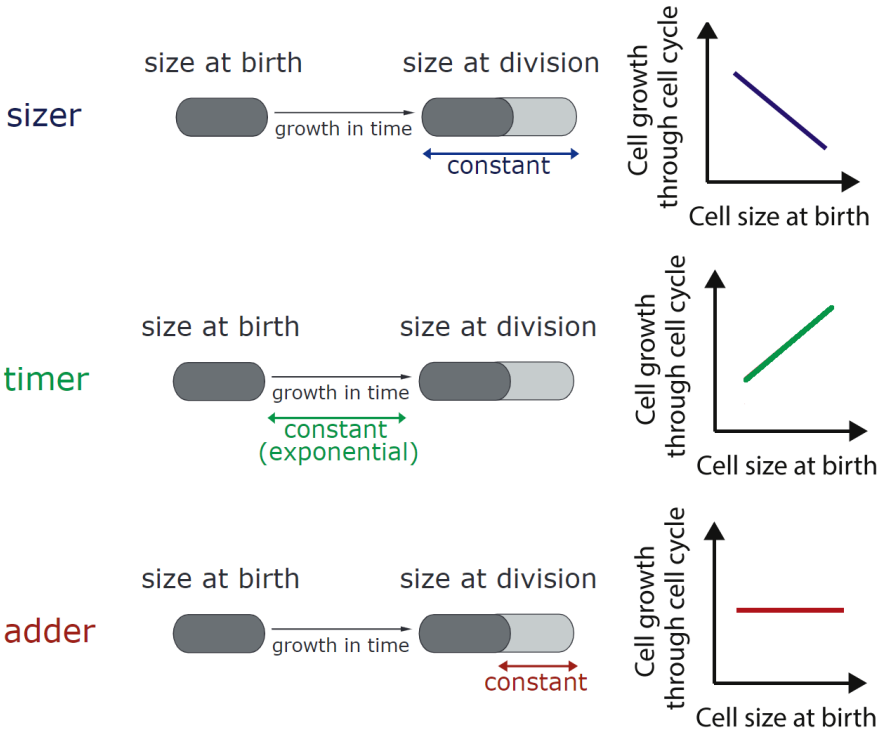

Fig. 18. Modes of size control. Sizers stablish a critical size that cells monitor in each cycle. Timers stablish that each cell grow the same amount of time each cycle. In case of adders, cells monitor the amount of growth in each cycle. Assuming exponential growth, different relations emerge from birth size vs cell growth according to different modes of size control. In case of sizers, the smaller is the cell the bigger is the amount of growth and vice versa. When there are only timers, cells grow the same amount of time, but since growth rate depends on volume, we have a positive correlation. Regarding adders, each cell adds the same amount of growth regardless birth size. Modified from (Morcinek-Orlowska et al., 2019; Zatulovskiy and Skotheim, 2020).

With this framework, the adder does not emerge directly from a specific molecular mechanism. This does not discard the presence of other size-control modes, mostly because sizers do not completely explain cell size variability at Start and also because basal molecular noise contributes to such variability (Talia et al., 2007). Moreover, part of this variability can also be explained by single-cell differences in growth rate (Ferrezuelo et al., 2012). Thus, according to different nutritional or hostile environment characteristics, growth rate (as a reporter of biomass synthesis) is affected, and thus a

poor culture medium generates slow growth rates that produce cells with smaller critical sizes and vice versa (Fig. 19).

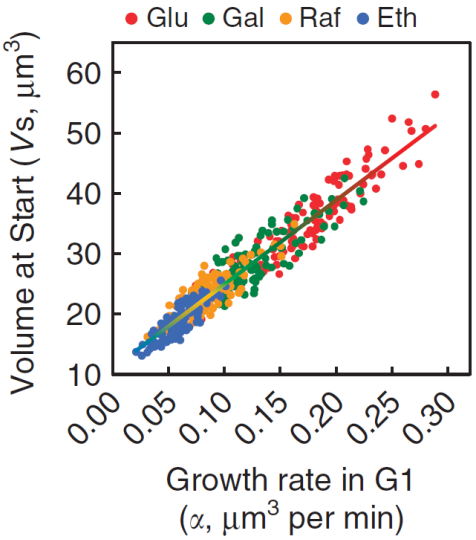

Fig. 19. Positive correlation between growth rate and budding volume. Faster growth rates promote bigger cells in rich culture mediums like glucose. Restricting the carbon source (ethanol, blue), shows a drop in the growth rate with the consequent decrease in budding volume (Ferrezuelo et al., 2012).

At a molecular level, the sizer model is supported by evidence from Whi5 in budding yeast. The Whi5 repressor is mainly synthesized in the previous G2/M phase in a way that is independent of cell size. Since Whi5 is not produced in G1, as volume increases its concentration decreases (Fig. 20). The smaller is a cell, the higher is the Whi5 concentration and G1 is extended until Whi5 dilution reaches a low-concentration level. In this context, Whi5 would work as a size-sensing protein with a sizer behaviour that emanates from its dilution in G1. Conversely, the Cln3 positive regulator of Start is produced in scale with cell volume and thus its concentration is predominantly constant along G1 (Schmoller et al., 2015). The mechanistic sub-scaling production of Whi5 has been recently described (Swaffer et al., 2021). Like histones, Whi5 production is uncoupled from cell size. However, mother to daughter biomass inheritance usually maintains an asymmetric distribution corresponding to asymmetric cell sizes. Whi5 overcomes this mode of distribution by binding to chromatin (SBF promoters) to evenly segregate from mothers to daughters in a way that is independent of cell size (Swaffer et al., 2021). The role of Whi5 as sizer has been a matter of debate. One fundamental trait of the Whi5 sizer is the fact that it is linearly accumulated in the previous G2/M phase regardless of cell size. This assigns a crucial role to the Whi5 promoter or the transcriptional system. Recently, it has been shown that switching the endogenous Whi5 promoter to a constitutive and size-scaling promoter has no effect on the next G1 cell size (Barber et al., 2020). In this new scenario, Whi5 concentration remains constant during G1 without any loss of size control. The fact that chromatin-

based partitioning is still intact even with a constitutive promoter and also the redundant control of cell cycle may reconcile the role of Whi5 in G1.

SBF/MBF promoters also have some level of control of cell size through Start. The artificial addition of SBF binding sites delays Start (Wang et al., 2009). This mechanism would suggest a role for the titration of Cln3-Cdc28 complexes at a number of available SBF/MBF promoters (Fig. 20). In consequence, as G1 phase advances, a fixed amount of SBF promoters must be titrated by the increasing activity of Cln3-Cd28, that inhibits the function of the Whi5 transcriptional repressor and the Rpd3 deacetylase complex.

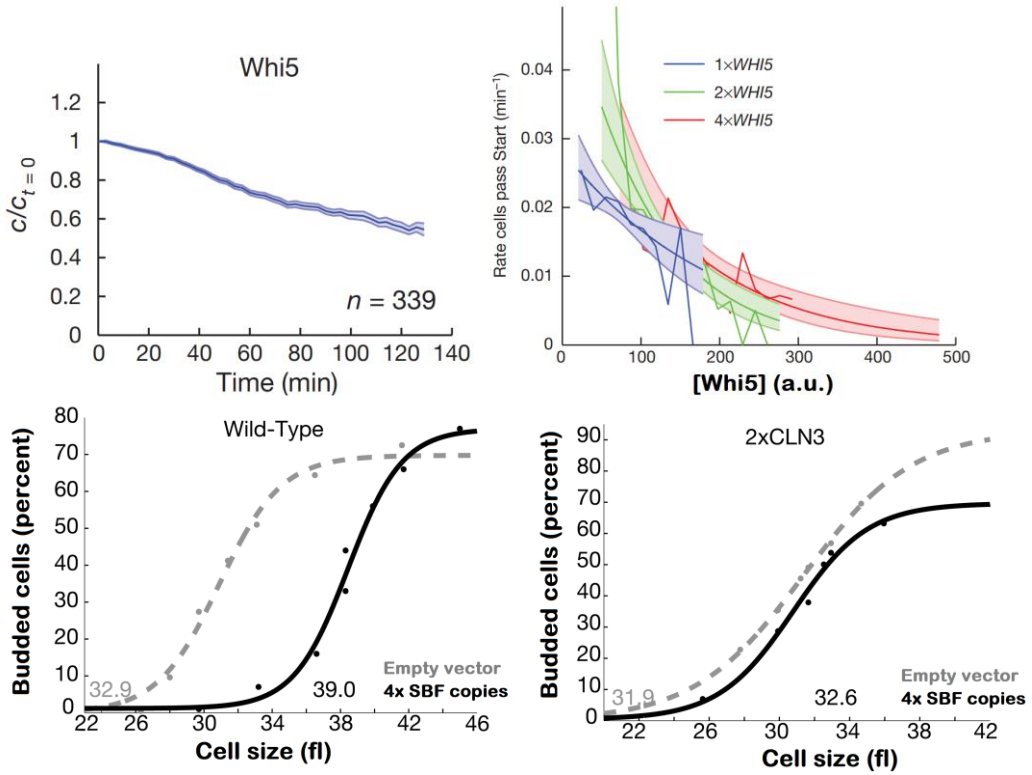

Fig. 20. Molecular regulators underlying size control in budding yeast. **(Above)** Whi5 is diluted in G1 in the same way that its concentration acts as a dose-dependent modulator of Start triggering. **(Below)** The addition of four tandem copies of SBF loci increases the volume at which cells start to bud. This phenotype is reversed by the addition of extra copies of Cln3 supporting the SBF-Cln3 titration model. Modified from (Schmoller et al., 2015; Wang et al., 2009).

Cln3 also has a deep influence on size in budding yeast (Futcher, 1996; Wijnen et al., 2002). Cln3 overexpression accelerates Start in a dose dependent manner (Cross et al., 2002; Schmoller et al., 2015). The same happens with Cln1 and Cln2, whose overexpression bypass G1 phase by triggering Start after cytokinesis (B. Futcher unpublished results). In these experiments, the resulting phenotype directly affects cell size producing extremely small cells. In this line, Cln3 deletion produces cells with a bigger cell size at Start. However, the involvement of Cln3 in setting a critical size remains obscure.

As stated before, the levels of Cln3 remain nearly constant during the cycle, suggesting that protein localization could be a key regulatory step. However, although nuclear import depends on chaperones (Verges et al 2007), there is no evidence giving support to this possibility.

As a general rule, the alteration of any of the main Start factors promote a size effect in budding yeast. And even do so some indirect regulators. This means that any mechanism that monitors and modulates important changes in size should affect molecular regulators that drive Start.

Environmental influence on cell size

As described many years ago (Schaechter et al., 1958), the influence of the environment can also be translated into effects on cell size, Nutrient scarcity is commonly one of the environmental challenges that budding yeast faces. In consequence it possesses a wealth of molecular mechanisms that sense and act as a result of any alteration in the availability of the source of carbon (Smets et al., 2010). As a central orchestrator of nutrient sensing, the TOR pathway impacts on size by monitoring nutrient availability through the TORC1 and TORC2 complexes. On one hand, TORC1 coordinates growth with Start by stimulating the expression of G1 cyclins and modulating the phosphorylation status of the Sic1 inhibitor through the opposed activities of Mpk1 kinase and Cdc55 phosphatase (Moreno-Torres et al., 2015). On the other hand, nutrient availability influences TORC2 which in turn modulates ceramide lipids synthesis (Lucena et al., 2018). Ceramides possess crucial structural and signalling roles in the plasma membrane. In this context, Cdc55 phosphatase partnered with the Rts1 regulator coordinate the response of TORC2 to nutrient availability through Ypk1/2. These kinases limit the synthesis of ceramides which are important for growth rate and cell size control (Nickels and Broach, 1996).

Organisms of higher complexity depict comparable nutrient-cell size dependence. Fruit flies (*Drosophila melanogaster*) that lack S6 kinase, a prominent target of TORC1 involved in ribosome regulation, show to be half-sized in comparison to their wild-type counterparts (Montagne et al., 1999). The subsequent analysis noted that cell size and not the cell number was the responsible of this phenotype. A similar phenotype was found in mouse cells (Shima, 1998). In this line, inhibitors (mimicking the effects of nutrient scarcity) of the mTOR pathway promote reduced cell size in human U2OS osteosarcoma cells (Fingar et al., 2002). Low glucose availability or blocking glucose uptake also promote small HEK293 cells (Inoki et al., 2003) (Fig. 21). It is in the TOR pathway where nutrient signalling and the consequent molecular reactions confluence. However, the upstream nutrient sensor is the AMPK protein, that monitors the amount of AMP and acts by inhibiting the TOR pathway through the GAP (GTPase-activating protein) TSC2 regulator when AMP levels rise. In consequence, in

mammalian cells, one mechanism that connects cell size to nutrient scarcity involves AMPK-dependent inhibition of TOR, thus restricting protein translation and cell size (Inoki et al., 2003).

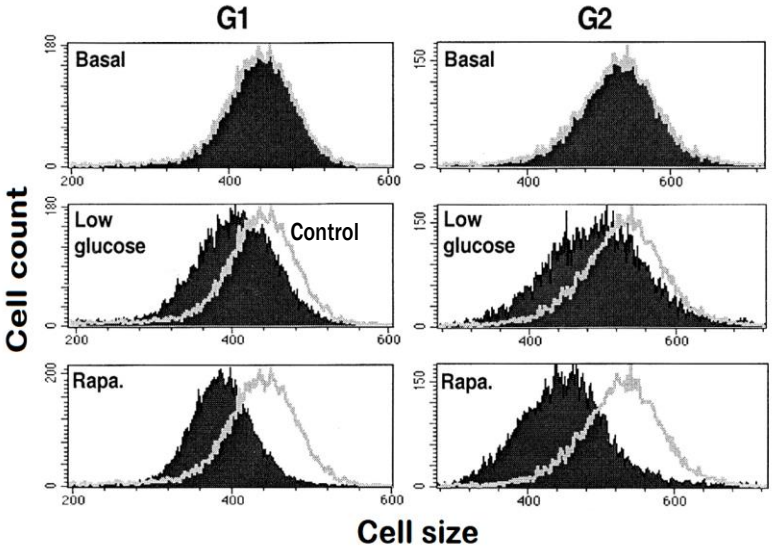

Fig. 21. Nutrient availability affects cell size in mammalian cells. HEK293 cells were subjected to either low glucose conditions or rapamycin treatment (mTOR inhibitor). Both conditions reduced cell size at G1 and G2 cell cycle phases. Size measured by fluorescence assisted cell sorting (FACS). Modified from (Inoki et al., 2003).

At a different environmental control level, the budding yeast 5' UTR region of Cln3 includes a short open reading frame (ORF) that misleads ribosomes when they are not abundant under poor medium conditions. In contrast, higher amounts of available ribosomes can bypass this hurdle and increase Cln3 translation in a well-fed state (Polymenis and Schmidt, 1997a). This nutrient mediated effect is directly aimed at one of the main drivers of G1 un budding yeast and thus, aside of TOR regulation, alternative mechanisms may influence on cell size according to nutrient availability.

In case of S. pombe, cell size and growth rate are mainly controlled in G2 phase, so environmental effects on cell cycle are prone to influence on this interval. The activity of the Cdc13-Cdk1 complex, the major G2 impeller, is modulated by the action of Wee1 inhibitory kinase and the Cdc25 phosphatase. On one hand, protein synthesis has a dominant role in Cdc25 and Cdc13 levels (Daga and Jimenez, 1999)and, on the other one, Wee1 activity is decreased when nutrients are abundant (Moseley, 2017).

As a whole, one important and visible fact about nutrient influence on cell growth is that cell critical size has evolved to be adaptable to the environment (Fig. 22). This means that rich culture mediums promote bigger cells than the ones that grow in poor conditions. In nutrient abundant conditions, cells quickly get an optimal growth rate at the same time that PKA hinders transcription of *CLN1* and *CLN2*. This slightly delay for passing Start allows the cell to maintain an optimal growth rate and promote

cells with an adjusted big size in rich mediums. The opposite effect occurs in a nutrient-deprived state where growth rate is decreased, and cells trigger Start at a reduced size.

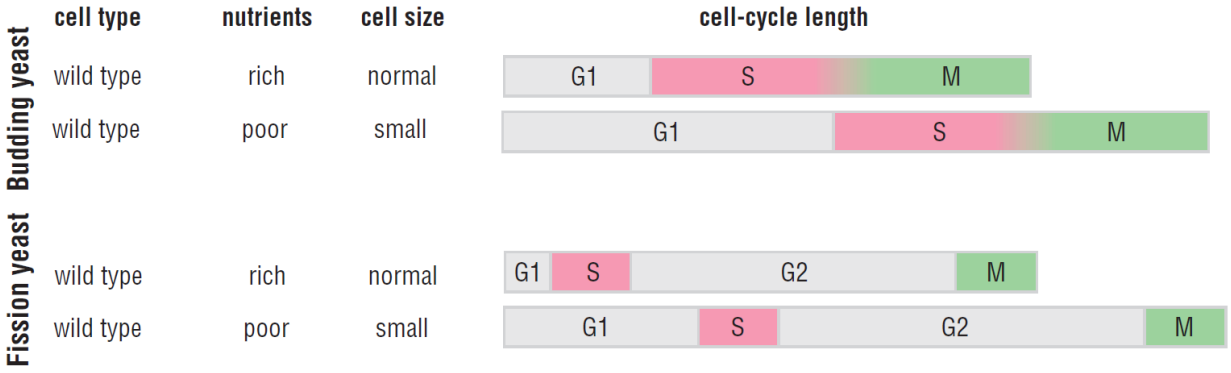

Fig. 22. Nutrient scarcity reduces cells size and extends the time of size-control phases in yeast. Budding yeast extends G1 phase while Fission yeast extends G2. In the end, cells adapt to nutrient availability and trigger the cell cycle even with non-optimal and small volumes. Modified from (Morgan, 2007).

Ploidy effects on cell size

From the 20th century it was evident to researchers that the number of chromosomes were directly proportional to the cell volume. Being settled as a universal correlation across living organisms (Gregory, 2001) (Fig. 23), Artom Cesare claimed the first correlations between ploidy and size in *Artemia salina*, a species of shrimp (Artom, 1926). He found that *A. salina* could be classified in two groups depending on the ploidy-size relationship. Tetraploid organisms were much bigger than their diploid counterparts in proportion to their respective DNA dose.

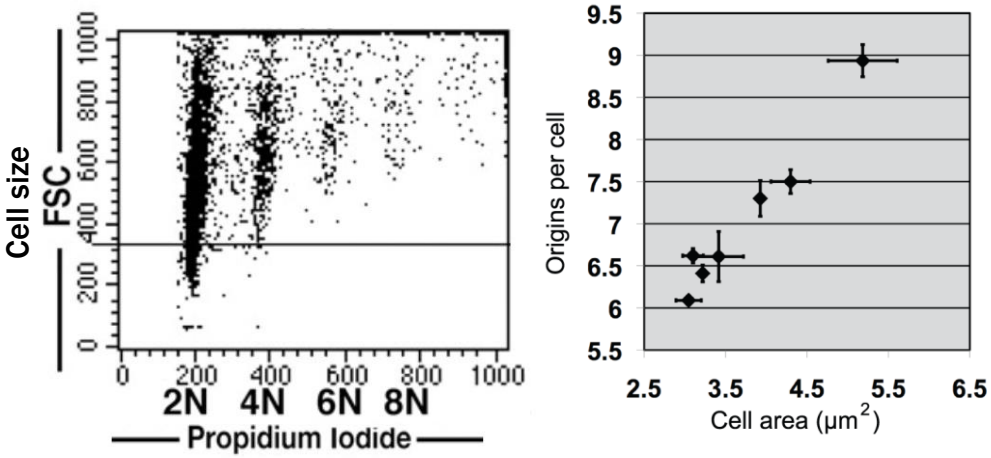

Fig. 23. Size scales with ploidy as a conserved and universal correlation. **(Left)** Hepatocyte populations increase cell size in relation to ploidy content. **(Right)** A similar scenario is present in bacteria (*B. subtilis*) where the number of DNA replication origins correlates with the cell area. Modified from (Baena et al., 2005; Hill et al., 2012).

The simpler hypothesis explains this occurrence by directly linking additional gene copy number and protein synthesis to an increased cell size. However, simply doubling all cellular components would compromise cell fitness by producing excessive amounts of two-dimensional components such as membranes. This means that active genetic regulation balances cell size with ploidy. Depending on their gene target, different mutations affect or not cell size and polyploidy correlations without modifying the amount of DNA. This points to a genetic machinery that underlies this universal phenotype (Tsukaya, 2008).

In this line, cells integrate ploidy to the cell size regulating machinery by a mechanism that goes further than the solely increase in gene expression due to additional amounts of DNA. However, the underlying mechanism that scales cell volume with DNA dose are still poorly understood. In a theoretical study, it has been proposed that ploidy molecular sensing could depend on either the production of a specific factor according to ploidy or the titration of a factor against the number of chromosomes (Marshall et al., 2012). In the first case, the pulsed expression of a factor according to DNA content and not cell size may underlie ploidy sensing. This is better complemented if this factor acts as an inhibitor in the phase in which cells stablish the critical size. By this way, the amount of inhibitor would depend on ploidy and thus higher DNA doses would inhibit the cell cycle for a larger period of time with the consequent increase in cell size. At the molecular level, Whi5 could enact this role. As stated before, Whi5 levels increase during G2/M phase. What there was also found was that this increment was proportional to the gene dose (Schmoller et al., 2015). As Whi5 acts as a G1 inhibitor, it is reasonable to think that greater amounts of DNA would extend G1 and thus cause an additional size. Nonetheless, the model predicts that the deletion of one copy of the genes in diploid cells should result in a smaller haploid-like size in diploid cells and this does not occur with Whi5. It looks clear that ploidy sensing does not depend on only one factor with a hierarchical command that links size to ploidy. As many other biological processes, redundant and compensatory mechanisms adapt cell survival to different scenarios.

The titration of a molecular activator to the DNA content could also accomplish ploidy cellular perception. If we imagine that the activator binds to specific DNA sequences for executing Start, additional copies of DNA should concomitantly extend G1 and cell size given a fixed amount of DNA. In fact, some studies point that Cln3 could be the activator that is titrated against the number of SBF/MBF positions. This hypothesis alleges that in early G1, SBF/MBF copy number exceeds the number of Cln3 molecules. As G1 goes by, Cln3 number increases (holding a constant concentration, though) titrating the SBF/MBF positions and triggering Start. The experimental addition of SBF/MBF binding sites promotes an increase in size during G1 (Wang et al., 2009). Regarding cyclin – Cdk activity,

diploid cells would display lower levels than haploid cells, pointing to a DNA inhibitory function in this framework (Patterson et al., 2021).

Alternatively, one recently found mechanism shed light to the molecular regulation of ploidy and size (Martínez-láinez et al., 2018). Using different approaches to manipulate the number of active centromeres in a haploid cell, these authors observed that cell size scaled with the number of centromeres. Being G1 the phase in which the critical size is established, they reasoned that this observation could be mediated by any of the Start effectors. Among them, the deletion of Cln3 neutralized this correlation. The same happened when some participants of the spindle assembly checkpoint (SAC) such as Mad3 were removed. Given that Mad3 is the only reported interactor of Cln3 and the Cdc4 ubiquitinating protein, it was proposed that cells may sense ploidy by counting the number of centromeres through the kinetochore – SAC machineries and the subsequent Cln3 degradation by a Mad3-mediated Cdc4 interaction (Fig. 24). A similar idea has been proposed for sex-determination in Drosophila (Sánchez et al., 1994)

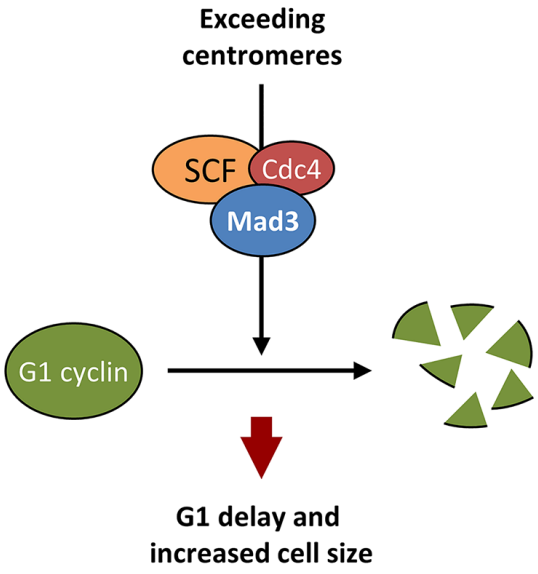

Fig. 24. One mechanism that may link ploidy with the molecular regulators of cell size. Exceeding number of centromeres promote the degradation of the G1 cyclin Cln3 through the interaction of Mad3 (a protein from the spindle assembly checkpoint) and Cdc4 (a F-box protein from the SCF ubiquitin ligase complex). The prominent phenotype depicts an increase in cell size according to the number of centromeres. Modified from (Martínez-láinez et al., 2018).

Plants have been widely used for understanding this phenotype. In fact, many human cultivated plants have evolved artificially to polyploidy genomes that depict bigger and appealing traits for consumption (Kondorosi et al., 2000). In *Arabidopsis thaliana* studies show that polyploidy alters cell size in a tissue-dependent manner. Bigger cells produce bigger roots, seeds, or flowers while bigger cells in leaves do

not significantly alter the final organ size. This shows that the relation between cell division and cell elongation is differentially coordinated according to each different plant organ (Del Pozo and Ramirez-Parra, 2015). In *Arabidopsis sepal*, cell and nuclear size also increase with ploidy albeit cell size increases in relation to ploidy rather than nuclear size (Robinson et al., 2018). As other living organisms, plants sense DNA content by a regulated molecular mechanism. The ratio between these parameters is not constant and depicts a cell-specific behaviour, assigning adjusted molecular responses in different contexts.

Cell cycle adaptation to stress: Stress granules

The environment set the framework in which living systems have evolved across millions of years. Life has shown a tremendous capacity to adapt to different environments. However, hostile conditions are unpredictable, and the lack of any general response could have seriously hindered life evolution. At the cellular level, checkpoints modulate cell cycle progression at certain time periods. However, these mechanisms coexist with other stress responses that can be triggered at any point of the cell cycle. This is molecularly reflected in the so-called stress granules, which are generated after oxidative or osmotic stress, heat shock or nutrient deprivation. The first seminal works were related to heat-shock experiments in *Drosophila melanogaster* and the observation of mRNA-containing cytoplasmatic structures (Storti et al., 1980).

Stress granules (SGs) are membrane-less organelles composed of mRNAs and protein assemblies that produce independent entities by liquid-liquid phase separations (LLPS) (Fig. 25). The rapid formation of SGs minimizes damage by stress and promotes cell survival by stalling mRNA translation (Mahboubi and Stochaj, 2017). They are assembled in few minutes but endure many hours. Conversely, the disassembly usually takes from several minutes to many hours. This stress-dealing mechanism is well preserved across all eukaryotic kingdoms ranging from plants and yeasts to mammals.

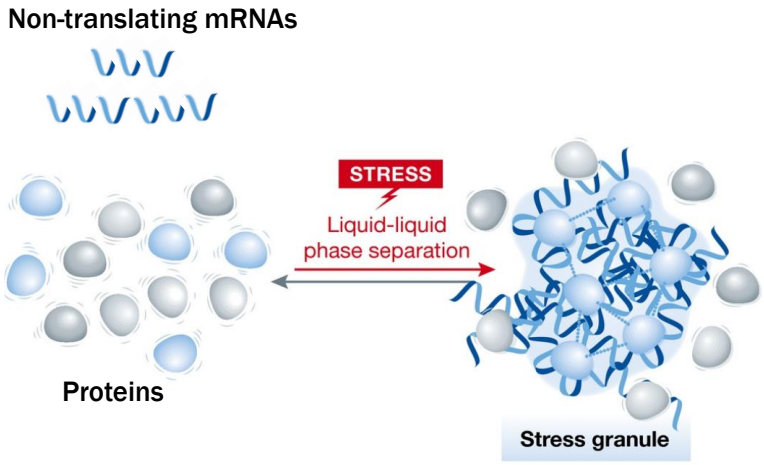

Fig. 25. Cellular stress (osmotic, temperature, nutrient scarcity) induces the formation of mRNA-protein cytoplasmatic structures called stress granules (SGs). SGs are membraneless entities thermo-dynamically stabilized by internal interactions from which emerge liquid-liquid phase separation. Modified from (Siwach and Kaganovich, 2017).

Stress granules impose a biosynthesis standby by recruiting mRNAs, RNA-binding proteins (RBPs), and other proteins mainly from the initial translational machinery. The final result is an RNA-structured entity stabilized by RNA-RNA, RNA-protein, and protein – protein interactions. In fact, the addition of cycloheximide, a drug that blocks translation by immobilizing ribosome-mRNA complexes, inhibits the formation of SGs (Kedersha et al., 2000). Drugs that block the initial steps of protein translation and raise the levels of untranslated mRNAs have just the opposite effect to cycloheximide (Anderson and Kedersha, 2009). Cells take profit of SGs formation for rearranging mRNAs and modulating many signalling pathways, some of them involved in antiviral responses (Valiente-Echeverría et al., 2012). As a result, storing these crucial components of protein translation ensures a fast biosynthetic recovery when stress is alleviated.

Aside of the fundamental role of mRNAs in SGs structure and function, a heterologous group of either RNA binding proteins or proteins that do not directly interact with RNA are directed to stress granules. Approximately 50% of SGs proteins belong to the RBPs group, while the other half includes metabolic enzymes, RNA remodelling components, post-translation modification enzymes, ATP-dependent helicases and many signalling elements like kinases (Jain et al., 2016). The analysis of the stress granule transcriptome in mammalian cells showed that virtually all mRNAs can be found in SGs with high variabilities depending on the efficiency of mRNA targeting to SGs (Khong et al., 2017). Curiously, the quantification of SG-associated mRNA in relation to the total amount revealed that just 10% of the total mRNA was accumulated in stress granules, with good correlations with large and poorly translated mRNAs found in SGs (Khong et al., 2017). As a whole, RNA and protein composition modulate stress granule dynamics. On one hand, some RNA binding proteins such as Pub1, TIA-1, Ataxin-2 or G3BP1/2 locate in the innermost part of SGs and thus it is thought that they participate in SGs nucleation. On the other hand, many translation machinery components such as eIF4E or eIF4G and other signalling-associated proteins are concurrently recruited to stress granules (Tian et al., 2020). Defining the protein composition of SGs could be a daunting task mainly because it is stress-dependent and because although structurally conserved, stress granule composition may vary depending on the organism. In some cases, SGs composition is related to the nucleation mechanism. For instance, in mammals, some kinases like PKR (double stranded RNA-dependent protein kinase), PERK (PKR-like endoplasmic reticulum kinase) or HRI (heme-regulated inhibitor) act as stress sensors that cause the inhibitory phosphorylation of eIF2α. This converts eIF2α into an inhibitor of eIF2B, causing the arrest of protein translation. In consequence, the phosphorylation of eIF2α serves as a nucleation stimulus for stress granules loaded with translation initiation factors (Mahboubi and Stochaj, 2017).

Many RNA-containing granules arise in normal non-stress conditions in the same way that they coexist with SGs under stress conditions. This highlights the fact that other structures depicting high RNA densities are also present in cells regardless of stress. In this line, some RNA liquid-liquid phase structures similar to SGs emerge in cells in a tissue-specific manner. This is the case of neuronal or germ cell granules with respective roles in synaptic remodelling or maternal mRNA storage (Barbarese et al., 2013; Brangwynne et al., 2009). Actually, the abnormal formation and disassembly of both stress granules and other related structures connects with neurodegenerative diseases (Ramaswami et al., 2013). Shared by mammals and budding yeast, P bodies also arise from pools of non-translated mRNA under normal environmental conditions. Within this framework, P bodies gather mRNAs related to translational repressors and members of the mRNA decay machinery, assigning RNA stabilizing functions to P bodies (Aizer et al., 2014). Stress granules and P bodies interact dynamically by exchanging mRNAs and some proteins, which discards specific mRNA commitment to one or the other structure (Kedersha et al., 2005) (Fig. 26). In a more general scenario, the nucleolus also concentrates ribosomal RNAs forming membrane-less intra-nuclear organelles.

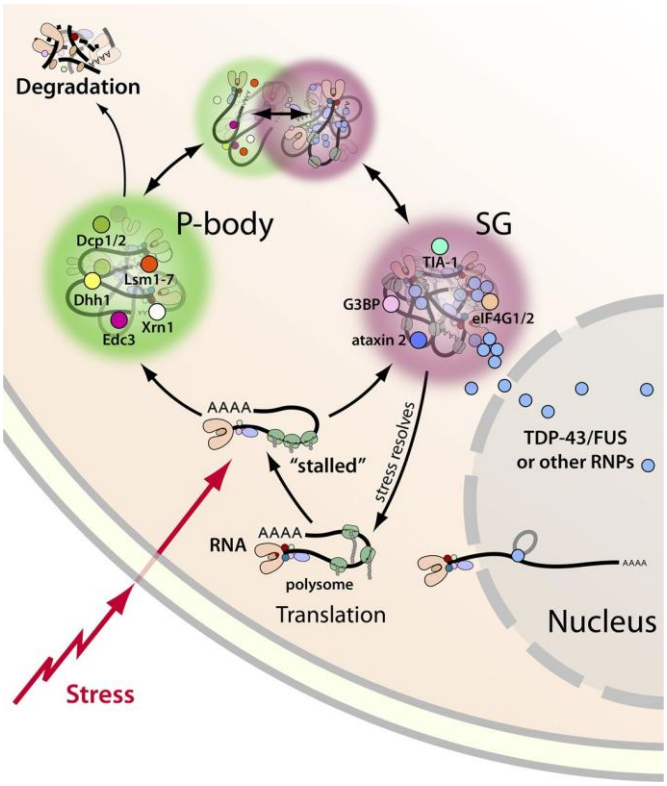

Fig, 26. Stress granules and P-bodies are independent RNA-protein condensates with different functions. Cellular stress promotes the accumulation of non-translated mRNAs that are directed to stress granules and remain stored. A fraction of mRNAs is distributed to P-bodies where they can be sent to degradation. P-bodies and stress granules depict different specific markers albeit they interact and exchange material. Modified from (Li et al., 2013).

Structure of stress granules

Many experimental clues point to different substructure stratums with different associated dynamics in stress granules (Niewidok et al., 2018). As dynamic entities, SGs are subjected to fusion, fission, and flow in the cytosol (Kedersha et al., 2005). Electron micrographs show SGs regions with different electron density (Fig. 27). This is supported by fluorescence microscopy experiments that identified regions with elevated concentrations of proteins and mRNAs (Souquere et al., 2009). In this line, FRAP (fluorescence recovery after photobleaching) experiments also distinguished both high and low mobile components (Buchan and Parker, 2009). The SGs internal part depicts general low protein dynamics and corresponds to regions with high electron density, these areas are referred as the stress granule "cores" of about 190 nm.

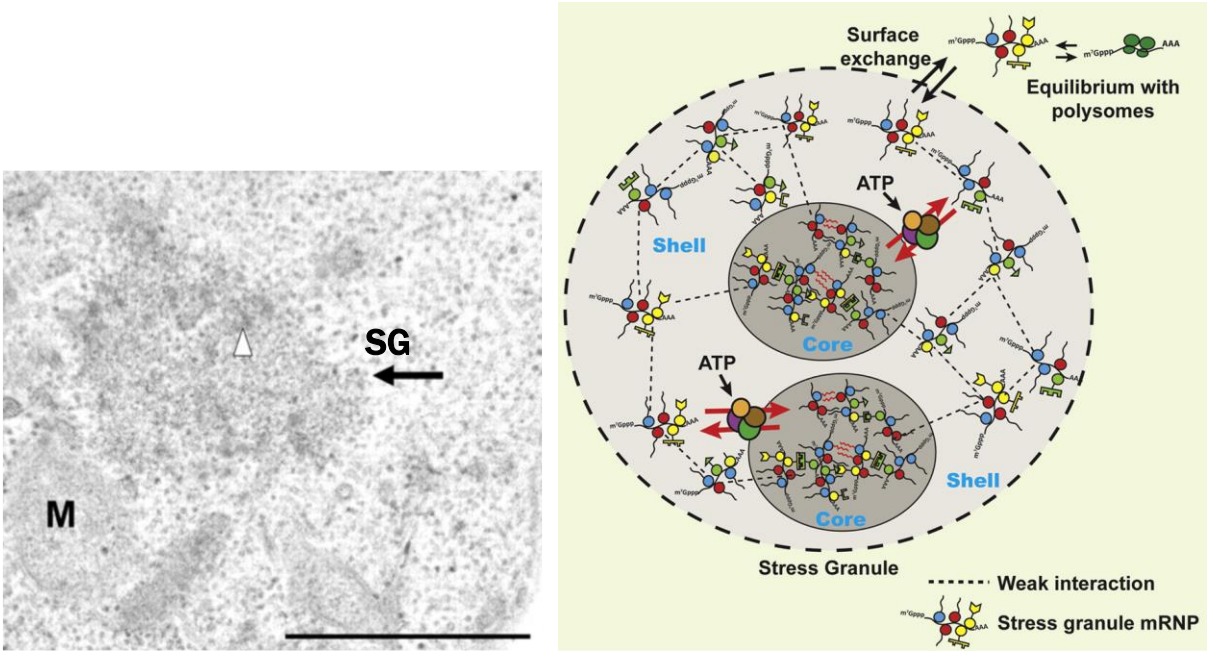

Fig. 27. Stress granules structure. **(Left)** Stress granules depict internal electrodense sub-structures (white arrow) under electron microscopy. M = mitochondria. Scale bar: 1µM. **(Right)** Stress granules are formed by multiple core structures with stable interactions along with more diffuse shells stabilized by multivalent and weak interactions. Shells stablish a dynamic equilibrium with external entities. Modified from (Jain et al., 2016; Souquere et al., 2009).

Mammalian cells possess multiple cores embedded in each stress granule, which contributes to scaffold and stabilize them (Wheeler et al., 2016). The most commonly found proteins in SGs cores are G3BP1,2 in mammalian cells and Pab1p/Pub1 in budding yeast. The situation is different in the shallower layers, where RNPs interchange is high and mRNA-protein composition is potentially more variable (Protter and Parker, 2016). The labile nature of the superficial sections makes difficult to natively purify intact stress granules. In consequence, proteomic studies conceivably shed light mainly

to SGs cores with some protein variations among studies probably due to the nature of SGs and the composition of the superficial layers. The stiffness of the core may emerge from stable protein-RNA interactions that nucleate the assembly of stress granules by recruiting additional mRNAs that reinforce this "solid" state. Last data suggest that the structural contribution of these mRNAs to SGs is mediated by RNA secondary structures, RNA-RNA interactions and by RNA-induced conformational changes in some RBPs such as G3BP1 (Campos-Melo et al., 2021).

Liquid-Liquid phase separation structurally distinguishes stress granules from other biological entities. Multivalent and sometimes unspecific interactions propel phase separation, but this mode of interaction is also present in other structures that do not generate phase separation. Instead, liquid phase states are generated according to the interaction turnover among different SGs components. Proteins or mRNAs that interact with slow turnover rates induce more solid entities while fast turnovers lead to liquid-liquid phase separations (Protter and Parker, 2016a).

Macromolecular interactions within stress granules

Stress granule formation relies on the redundant and mainly unspecific interactions that arise from mRNAs, RBPs and non-RNA binding proteins. Although many proteins such as TIA1 or Pub1 have been commonly found in stress granules, the unspecific requirements to SG formation suppresses the necessity of specific participants for stress granule assembly (Buchan et al., 2008; Gilks et al., 2004). Consequently, the deletion of any of these proteins does not completely inhibit SG formation. The fact that stress granule components vary according to the nature of the stress and the cell framework makes even more difficult to assign specific roles to particular proteins in SG formation. Therefore, this suggests that the assembly of stress granules is context dependent and is stabilized by the balanced interactions among the internal constituents. For instance, G3BP1,2 proteins depict relevant roles in SG formation under oxidative stress but not after osmotic stress (Kedersha et al., 2016; Tourrière et al., 2003). In parallel, post translational modifications (PTMs) deeply modulate SG stability by altering the internal interaction pattern. This includes phosphorylations, methylations, acetylations or glycosylations. Phosphorylations typically hinder protein multimerization in stress granules or stimulate proteins like Grb7 or DYRK3 kinase that promote SG disassembly (Tsai et al., 2008; Wippich et al., 2013). Glycosylations, namely O-GlcNAc, stimulate the formation of stress granules (Ohn et al., 2008), Methylations in arginine RGG motifs recruit proteins containing Tudor domains such as TDRD3, that has roles as a transcriptional activator (Goulet et al., 2008). The last studied PTM in the context of stress is sumoylation. Firstly, RANBP2 and UBE21 SUMO ligases localize in SGs (Marmor-Kollet et al., 2020). Secondly, the knockdown of SUMO-targeted ubiquitin ligases disrupts SG disassembly (Keiten-Schmitz et al., 2020) (Fig. 28).

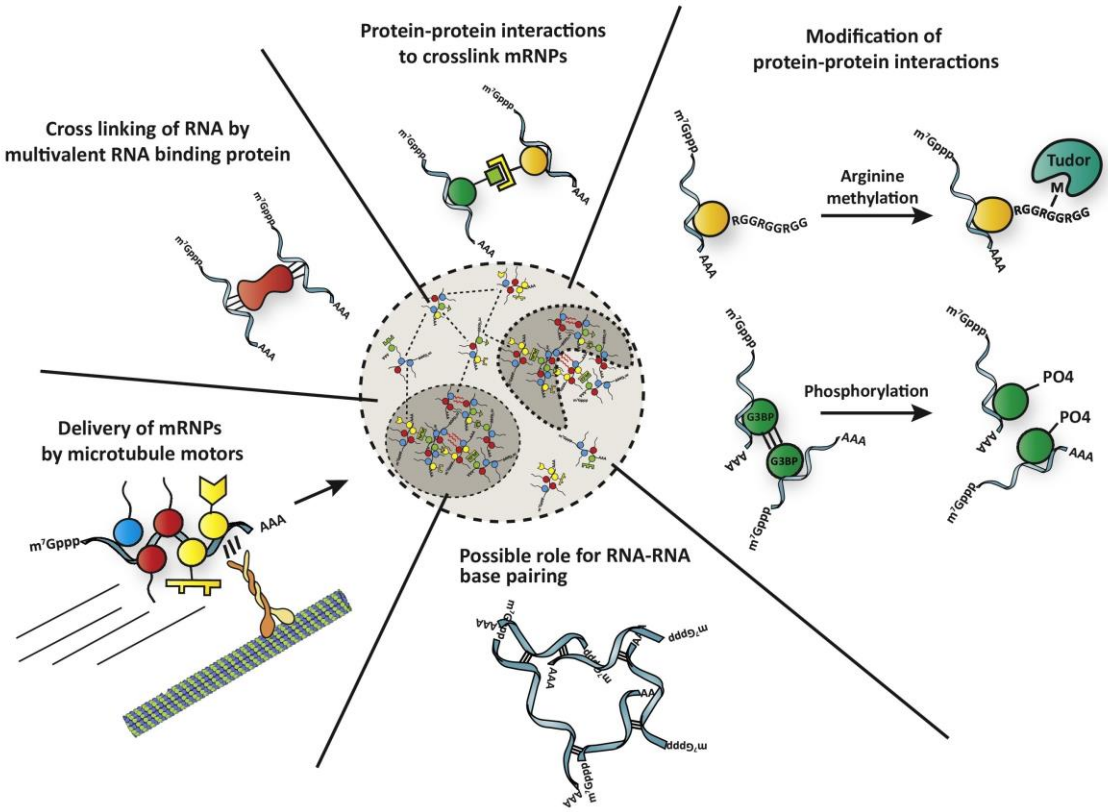

Fig. 28. Highly diverse interactions modulate the dynamics of stress granules. mRNAs, proteins, and ribonucleoproteins (RNPs) promote multivalent interactions through different combinations and intensities. Protein modifications such as phosphorylations and methylations are of special importance in the stability of SGs. Modified from (Protter and Parker, 2016).

In addition to PTMs, crucial protein domains favour or even could drive the assembly of stress granules. The most prominent ones correspond to intrinsic disordered domains (IDRs), to prion like domains (PrLDs) and the related RNA-recognition motifs (RRMs). Stress granules and other RNPs are referred as liquid-liquid phase separations that emerge from a network of multivalent weak interactions. At the molecular level, the promiscuous nature of IDRs generates LLPS and thus engages in stress granule formation (Elbaum-Garfinkle et al., 2015; Lin et al., 2015; Molliex et al., 2015; Nott et al., 2015). For example, the IDR and PrLD found in human TIA-1 favour the production of stress granules. This phenotype is maintained even with the substitution of the human PrLD with a yeast PrLD domain (Gilks et al., 2004).

IDRs contribution to SG assembly involves different mechanisms according to different models. Firstly, IDRs contain versatile Short Linear Motifs (SLiMs) that can easily fetter the binding site of a wide range proteins. This is the case for SLiMs in P body assembly (Jonas and Izaurralde, 2013). SLiMs are enriched in polar, aromatic, or charged side chains and thus they promote a variety of interactions spanning from electrostatic and hydrogen to hydrophobic bonds (Boeynaems et al., 2018). IDRs can also interact

with mRNAs and modulate the stability of stress granules (Lin et al., 2015). In this line, IDRs can form amyloid-like fibres and stabilize SGs trough cross-strand beta zippers (Kato et al., 2012; Lin et al., 2015; Protter and Parker, 2016a). Finally, as stated before, IDRs produce weak, multivalent, and dynamic interactions that can promote liquid-liquid phase separations typical in stress granules (Elbaum-Garfinkle et al., 2015; Zhang et al., 2015).

Aside of proteins, mRNA forms secondary structures that may modulate the stability of stress granules. RNA-RNA interactions involve Watson-Crick base-pairing or helical stacking and sometimes require ionic cofactors such as Mg^{+2} and K^{+} in certain concentration ranges (Langdon et al., 2018; Van Treeck and Parker, 2018). Hence, RNA structure and concentration provide the specificity for inducing liquid-liquid phase separation (Langdon et al., 2018). Additionally, RNA containing CAG, GGGCC and CUG repeats boost phase separation in cells and *in vitro* through G-quadruplex (rich in guanine) secondary structure, among other three-dimensional space arrangements (Fay et al., 2017; Jain and Vale, 2017). mRNA is also altered through N6-methyladenosine (m6A) modifications. Interestingly, m6a is only depicted in mRNAs associated to stress granules and thus it distinguishes them from the ones that move freely in the cytoplasm (Anders et al., 2018). YTH protein domains recognize m6a modifications and promote the formation of LLPS through multivalent binding patterns (Fu and Zhuang, 2020; Ries et al., 2019).

Assembly of stress granules

In general, little is known about the details of stress granule construction. The initial signals for stress granule formation firstly come from translation inhibition, often mediated by the phosphorylation of eIF2α and the dismantling of ribosomal polysomes (Hofmann et al., 2021). The biphasic properties of stress granules point to different stages during the assembly. Two models propose an explanation to this process based on the order in which cores or the superficial layers are assembled (Protter and Parker, 2016a; Wheeler et al., 2016) (Fig. 29). One model alleges that the formation of liquid-liquid phase separation precedes the formation of cores. In this context, the dynamic and multivalent nature of mRNA and RNPs stalled at translation commands the generation of liquid phase entities. As time goes by, an increasing number of IDR-containing proteins would increase the structural complexity and thus slow the turnover of interactions defining the core section of stress granules. Is in this part where protein concentration would be high with a different interaction pattern, in part possibly due to amyloid-like substructures (Molliex et al., 2015; Patel et al., 2015). In the second model, cores prime the assembly of larger liquid phase stress granules. The first step would depend on the oligomerization of RNPs in substructures that can grow over time. The subsequent fusion of different cores would function as a platform able to recruit partners with fast turnover interactions (like IDRs-containing

proteins). In consequence, the superficial shell would behave as a liquid phase entity emanating from the initial cores (Protter and Parker, 2016a; Wheeler et al., 2016).

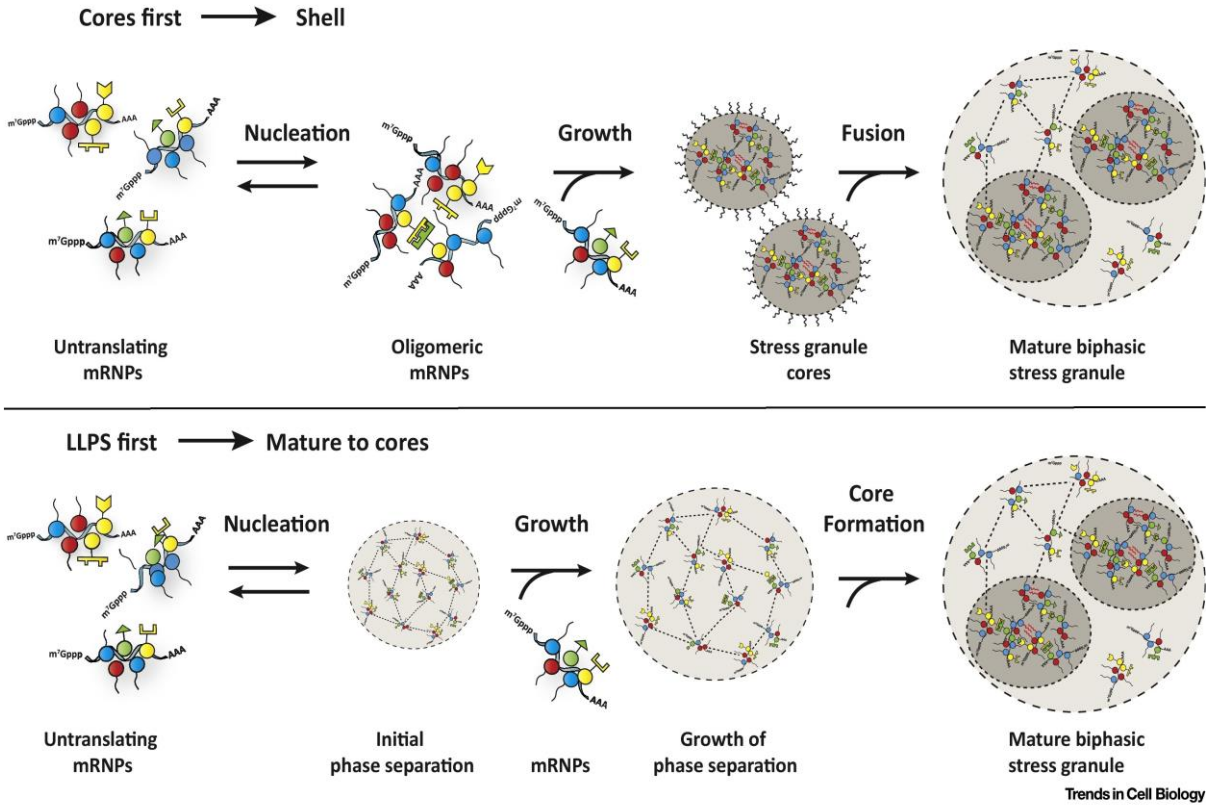

Fig. 29. Two models explain stress granules assembly. **(Above)** One model stablishes the primary formation of stable cores that can fusion and generate phase separation. **(Below)** In the phase separation model, the interactions of mRNAs and proteins drive phase separation preceding the assembly of stable cores. Modified from (Protter and Parker, 2016a).

The first experimental data that tested these possibilities point to the "initial core" as the potential model that explains stress granule assembly (Wheeler et al., 2016). In early stages of SG formation, solid structures resistant to isolation from cell lysates were found at the very first moment in which SGs were detectable under the microscope. The microscopy analysis of stress granules with SIM (Structured Illumination Microscopy) confirms the early presence of substructures in stress granules. In addition, knowing that low temperatures enhance liquid-liquid phase separation, the formation of stress granules should be improved under low temperatures if LLPSs are able to prime SG assemblies (Kato et al., 2012; Molliex et al., 2015; Nott et al., 2015). However, under low temperatures the formation of stress granules is greatly delayed even with effective translational repression and similar mRNA levels as the right-temperature control. These lines of evidence suggest that cores precede the formation of LLPS.

The initial formation of cores in stress granules is potentially nucleated by a bunch of proteins where TIA-1 and G3BP play a prominent role in mammalian models. On one hand, TIA-1 contains Q/N-rich (glutamine/asparagine rich) domains that mediate its aggregation and stimulate the formation of stress granules (Gilks et al., 2004). In turn, the presence of RRM motifs is needed for TIA-1 recruitment to SGs (Kedersha et al., 1999). In the case of G3BP1,2 proteins, removing both proteins strongly hinders the assembly of stress granules under specific stress conditions (Kedersha et al., 2016). This phenotype relies in both NTF2 (a dimerization domain) and RRM sections of G3BP1,2, but not in IDRs, that were dispensable for SGs assembly (Guillén-Boixet et al., 2020; Sanders et al., 2020; Yang et al., 2020). In this context, suppressing G3BP1,2 could interfere with the function of some G3BP-associated proteins such as Caprin1 and USP10, whose binding sites are close enough for promoting a competition between these two proteins. Caprin1 impels stress granule formation while USP10 hinders this process. This places G3BP proteins at the centre of Caprin1 and USP10 activity, with Caprin1 triggering a conformation change in G3BP that promote the unleash of its IDRs domains. On the other side, it is thought that USP10 stabilizes more soluble forms of G3BP (Hofmann et al., 2021; Kedersha et al., 2016). In parallel, active remodelling complexes also assist SG construction through RNA helicases. Members of the Dead-box helicase family are commonly found in stress granules promoting their assembly (Hilliker et al., 2011). As a whole, the intra- and intermolecular interaction networks drive the assembly of stress granules for generating their biphasic facet.

Disassembly of stress granules

Once the stress is lessened, cells trigger again all the translational machinery for advancing the cell cycle. This means that stress granule disassembly is also crucial for recovering the cell cycle after a period of stress-induced translational arrest. Although of general importance, the molecular mechanisms underlying stress granule disassembly are still not well understood. In this regard, many ATP-dependent remodelling complexes modulate the dynamics of stress in a way that under ATP scarcity, SGs mobility, fusion and disassembly is highly compromised (Jain et al., 2016; Protter and Parker, 2016). The loss of function of MCM (minichromosome maintenance) helicase alters the pace of SGs disassembly in a role independent of DNA (Bell and Botchan, 2013; Jain et al., 2016a). Other group of ATPases are the ubiquitin segregases. In this context, removing Cdc48 causes the accumulation of stress granules in the cytosol possibly due to the lack of extraction of ubiquitinated proteins from the SGs. The same happens for some members of the family of Hsp70 and Hsp40 chaperones that localize in SGs (Cherkasov et al., 2013; Mateju et al., 2017). Namely, Ydj1 motivates the disassembly of stress granules while Sis1 drives their autophagy (Walters et al., 2015). When the ubiquitin-proteasome system is inhibited, some kinases phosphorylate the eIF2α factor for stalling

translation initiation. This induces the formation of stress granules that, in this context, are disassembled mainly through the Hsp72 chaperone (Mazroui et al., 2007).

Phosphorylation is one of the most important modifiers that is dependent on ATP availability. As a general rule, increased phosphorylation contexts transiently disrupt the internal network interaction of stress granules by modifying the interplay turnover of many participants. Concurrently, the action of kinases prompts the SGs inhibitory function of chaperones, RNA helicases and microtubule-dependent motors (Chernov et al., 2009; Nadezhdina et al., 2010). As a result, kinase activity stimulates SGs disassembly. For instance, DYRK3 dual specificity kinase is recruited to SGs via a N-terminal low complexity domain. In this situation it modulates both SGs disassembly and the release of mTORC1 (Wippich et al., 2013). Once mTORC1 is released, DYRK1 also repressed the PRAS40 mTORC1 inhibitor. Importantly, in a screening for chemical inhibitors of SGs disassembly, many kinase-directed drugs deeply impaired SGs dissolution. Among them, Cdk2 and Cdk4 specific inhibitors almost abolished the disassembly of SGs with little effects on their formation. This points to a link between the sporadic and quick stress response and the cell cycle control machinery (Wippich et al., 2013). Besides phosphorylation, the inner PTM pattern also changes during this process. It has been reported that G3BP1 undergoes acetylation that prevents it from binding mRNAs once stress is relieved (Gal et al., 2019). Arginine-rich motifs, close related to the RNA binding domains, are also subjected to methylations that loosen the strength of cores and promote the re-mixing of cytosolic and stress granule components (Hofmann et al., 2021).

One proposed mechanism for stress granule dissolution claims that it is driven by a multistep process in which firstly the external layers are dismantled followed by the dissolution of the cores and the final destruction through autophagy (Wheeler et al., 2016) (Fig. 30). The re-establishment of mRNA translation alters the equilibrium between cytosolic and SG-associated mRNA. In consequence, the rapid ins and outs from SGs to cytosolic sections (and vice versa) appear to be the trigger that initiate the dissolution of stress granules. This is consistent with the multivalence nature that stabilizes LLPS in stress granules. When multivalency drops, the stability of SGs is compromised because many RNPs are either degraded or return to their original task. Hence, they cannot longer sustain the multivalent interactions required for LLPS formation (Protter and Parker, 2016; Wheeler et al., 2016). The last experimental data reinforces the regulated multistep model and discards the disassembly of SGs as a matter of passive dissolution. By means of proximity labeling, a subset of proteins found specifically at the dissociation phase of stress granules was identified (Marmor-Kollet et al., 2020). They were termed as DEPs (disassembly engaged proteins). For example, several SUMO ligases were identified as DEPs during the disassembly process. This suggests that SUMOylation has a prominent role in protein multivalence modulation, not just by SUMO binding to SG targets but also by SUMO-targeted

ubiquitin ligation (StUbL). In this line, removing key components of the StUbL pathway delays the disassembly of stress granules (Keiten-Schmitz et al., 2020).

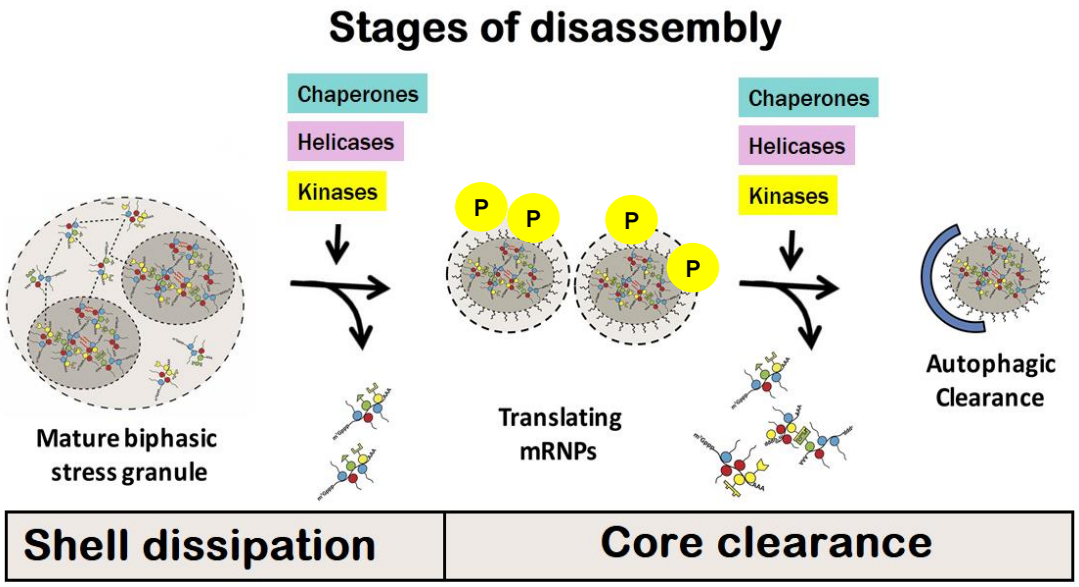

Fig. 30. A model for stress granule disassembly. Little is known about stress granule dissolution but some data point to a coordinated and multi-step process. Resuming mRNA translation may alter the inner SG multivalency and destabilize firstly SGs shells and then the inner cores. The role of chaperones, helicases and kinases is fundamental for attaining proper SG dissolution. Modified from (Wheeler et al., 2016).

Stress granules as crucibles of pathogenesis

Cells engage complex stress responses to different hostile conditions. This is objectified through the formation of stress granules; LLPSs entities composed of mRNAs and RBPs that promote cell survival upon stress relieve. The detection of any kind of stress condition demands a homeostatic control of stress granule dynamics: granulostasis. This means that any imbalance in both stress granule formation and dissolution could be responsible of many pathogenic conditions. Mutations that alter the kinetics and dynamics of stress granules are related to degenerative diseases like amyotrophic lateral sclerosis (ALS) and frontotemporal lobar degeneration (FTLD) (Li et al., 2013; Ramaswami et al., 2013). So, the neuronal system is highly susceptible to stress granule homeostasis. Disease-associated proteins like FUS, Tau and TDP-43 linked to neurodegenerative diseases are commonly present in stress granules (Bentmann et al., 2013; Shukla and Parker, 2016; Vanderweyde et al., 2016). In ALS patients, TDP-43 mutations increase protein aggregation and hyper-assembly of stress granules via early TDP-43 association to larger SGs. Hyper formation of SGs is also promoted by the interplay between Tau and TIA-1, where TIA-1 primes Tau misfolding (Vanderweyde et al., 2016). On the other

hand, the disease-causing isoform of C9ORF72 (with hexanucleotide repeat expansions) hinders the assembly of stress granules in ALS and FTD patients, generating a SG hypo-assembly state (Shukla and Parker, 2016). When SGs clearance is diminished, they can seed the formation of protein aggregates that promote Parkinson's and Alzheimer's disease (Repici et al., 2019; Vanderweyde et al., 2012). In this line, mutations in hnRNPA1,2 proteins promote the formation of amyloid fibres that, once associated with SGs, interfere with the dissolution process. The final step for some SGs disassembly is autophagy, a process controlled by granulostasis. Mutations in either the valosin-containing protein (VCP) or the HspB8-Bag3-Hsp70 chaperon complex impairs correct granulostasis and causes the accumulation of persistent stress granules linked to pathogenesis (Buchan et al., 2013; Ganassi et al., 2016).

In the case of cancer, high levels of reactive oxygen species and low nutrient availability trigger SGs assembly in different tissues (Adjibade et al., 2015; Vilas-Boas et al., 2016). Anti-cancer chemotherapy treatments along with radiotherapies also stimulate the formation of stress granules with consequences that negatively affect the effectiveness of such treatments (Anderson et al., 2015; Moeller et al., 2004; Szaflarski et al., 2016). This is the case of doxorubicin, a DNA intercalant, that induces the formation of SG (Morita et al., 2012). Given the positive function of SGs in cancer maintenance, some drugs inhibit SGs formation in the same way that they hinder tumour growth and stimulate cancer cell death (Fournier et al., 2013). Cancer metastasis is also influenced by the arise of stress granules. Sarcoma cells loaded with SGs are resistant to chemotherapy and also easily metastasize to lungs (Somasekharan et al., 2015). These events were prevented with the knockdown of G3BP1, which increased survival in animal models (Somasekharan et al., 2015).

Viral infections trigger wide stress responses in cells. However, last data assign protective roles to the emergence of stress granules in these circumstances. Firstly, the presence of viral RNA activates the PKR kinase that phosphorylates eIF2α and stimulates SGs formation (Poblete-Durán et al., 2016; Yoneyama et al., 2015). In this way, stress granules confine mRNA and translation proteins and prevent them from viral replication. The formation of SGs also induces the expression of the specific immune response to viral infection, mainly through the interferons (Yoneyama et al., 2015). Actually, viral adaptation has produced mechanisms that hinder SG assembly and stimulate their dissolution. For example, some viruses block or drive the degradation of G3BP1 while others, like the dengue virus, capture SGs-related proteins such as TIA-1 (Dougherty et al., 2015; Panas et al., 2015; Valiente-Echeverría et al., 2014).

HYPOTHESIS & OBJECTIVES

We had previously observed that supernumerary centromeres cause a G1 delay by increasing degradation of Cln3, the yeast G1 cyclin, by Mad3, a centromeric-signalling protein that interacts with Cln3 and Cdc4, an F-box component of the protein ubiquitination SCF complex. As Mad3 stability is in turn regulated at the protein level by the APC^{Cdh1} ubiquitin ligase complex, **we hypothesized that Mad3 would set a molecular timer based on the oscillatory pattern of two ubiquitination devices as a novel mechanism of G1 regulation.**

The main objectives are:

1.1. Quantify G1 Cdk nuclear localization during G1 in wild-type cells
1.2. Analyse nuclear levels of Cln3 during G1 in *mad3* mutant cells
1.3. Study Mad3 levels and the dynamics of the Mad3–Cdc4 complex along the cell cycle
1.4. Characterize the activity of the APC^{Cdh1} complex on Mad3 levels
1.5. Accurately measure the relation of the budding volume to the volume extension in G1
1.6. Test the properties of the model as a timer control device

Conversely, under non-homeostatic environmental conditions, cells unleash the stress response. Among different mechanisms, the emergence of stress granules (SGs) has showed to be crucial for cell survival. In fact, problems in SGs formation or clearance are responsible for many degenerative diseases. In a search for Cdc28 interactors that could affect cell size control in G1 we had found Whi8, a protein that localizes in stress granules and contains RNA-binding motifs. **We hypothesized that Whi8 could recruit Cdc28 and the *CLN3* mRNA to stress granules and thus connect the stress response to the key drivers of cell cycle entry.**

The main objectives are:

2.1. Characterize the sequestration of the *CLN3* mRNA to SGs and its dependency on Whi8
2.2. Study the role of Whi8 in recruiting Cdc28 to SGs
2.3. Assess the functional role of Cdc28 in stress granules.
2.4. Identify and characterize homologous mechanisms in mammalian cells

RESULTS

ScienceAdvances AAAS

Mad3 modulates the G1 Cdk and acts as a timer in the Start network

Alexis P. Pérez[1,2], Marta H. Artés[1], David F. Moreno[1], Josep Clotet[2,*], Martí Aldea[1,2,*]

[1] Molecular Biology Institute of Barcelona (IBMB), CSIC, 08028 Barcelona, Catalonia, Spain

[2] Department of Basic Sciences, Universitat Internacional de Catalunya, 08195 Sant Cugat del Vallès, Spain

[*] Corresponding authors: jclotet@uic.es and marti.aldea@ibmb.csic.es

Science Advances 10.1126/sciadv.abm4086 (2022)

Alexis Pérez contribution: Investigation and data analysis.

Abstract

Cells maintain their size within limits over successive generations to maximize fitness and survival. Sizer, timer and adder behaviors have been proposed as possible alternatives to coordinate growth and cell cycle progression. Regarding budding yeast cells, a sizer mechanism is thought to rule cell cycle entry at Start. However, while many proteins controlling the size of these cells have been identified, the mechanistic framework in which they participate to achieve cell size homeostasis is not understood. We show here that intertwined APC and SCF degradation machineries with specific adaptor proteins drive cyclic accumulation of the G1 Cdk in the nucleus, reaching maximal levels at Start. The mechanism incorporates Mad3, a centromeric-signaling protein that subordinates G1 progression to the previous mitosis as a memory factor. This alternating-degradation device displays the properties of a timer and, together with the sizer device, would constitute a key determinant of cell cycle entry.

Short title: G1 is modulated by a time-dependent mechanism

Teaser: Interlaced protein degradation machineries impose a timer mechanism that tempers cell size control at Start

Introduction

The scale and efficiency of most molecular processes that take place within a cell depend on its size. Hence, as an important factor of fitness and survival, cell size is maintained within constant limits under unperturbed conditions of growth (Chen and Futcher, 2021; D'Ario and Sablowski, 2019; Wood and Nurse, 2015; Zatulovskiy and Skotheim, 2020). In budding yeast, although cells show a size checkpoint at the G2/M transition (Garmendia-torres et al., 2017; Spiesser et al., 2015; Zapata et al., 2014), they primarily control their size prior to S-phase entry at a point termed Start (Hartwell and Unger, 1977; Johnston et al., 1977), where cell size displays the lowest variability compared to other cell cycle transitions. In principle, size homeostasis can be attained by means of three different model mechanisms: sizers, timers and adders (Facchetti et al., 2017). A sizer allows cells to test their size and can be based on accumulation of inducers or dilution of inhibitors of cell cycle entry as cells grow. Timers are able to trigger a molecular event as a function of time, and they may be originated by enzymatic reactions functioning at saturation. Finally, the adder allows cells to measure a fixed size increment and may emanate from the combination of molecular mechanisms acting as timers and sizers (Chandler-Brown et al., 2017; Heldt et al., 2018). However, available evidence addressing whether G1 is controlled by sizer, timer or adder mechanisms is inconclusive in yeast (Facchetti et al., 2019; Ferrezuelo et al., 2012; Talia et al., 2007) and mammalian cells (Cadart et al., 2018a).

Cyclin Cln3 is the most upstream activator of Start (Tyers et al., 1993). This G1 cyclin forms a complex with Cdc28, the cell cycle Cdk in budding yeast, to activate transcription of the G1/S regulon (Bertoli et al., 2013) by phosphorylation of RNAPolII C-terminus (Kõivomägi et al., 2021), where *CLN1* and *CLN2,* two additional G1 cyclins under the control of Whi5, create a positive feedback loop that makes Start a robust and irreversible transition (Johnson and Skotheim, 2013). Alteration of key molecules of the Start network has prominent effects on the critical size (Jorgensen and Tyers, 2004). In particular, Cln3 and Whi5 modulate cell size in a precise dose-dependent manner. Whi5 is synthesized during the previous cycle independently of cell mass and is diluted by growth in G1 (Schmoller et al., 2015b), thus offering the key properties to function as a sizer molecule at Start (Heldt et al., 2018; Schmoller and Skotheim, 2015). The Cln3 cyclin is present at low but nearly constant levels throughout G1 (Garí et al., 2001a; Tyers et al., 1993) and its nuclear accumulation depends on Hsp70/Hsp40 chaperone systems and the Cdc48 segregase (Parisi et al., 2018a; Vergés et al., 2007b; Yaglom et al., 1996), which would be important for subjugating cell cycle entry to growth rate and aging (Ferrezuelo et al., 2012b; Moreno et al., 2019a, 2019b). Cln3 is recruited to G1/S promoters and its titration as a function of the mass/DNA ratio has been proposed as a sizer mechanism (Wang et al., 2009). Nonetheless, no evidence exists showing that changes in Cln3 levels or subcellular distribution during G1 play a role in a sizer or timer mechanism.

Here we analyze the mechanisms regulating nuclear accumulation of Cln3 during G1 progression and entry into the cell cycle, and we find that Mad3, a nuclear centromeric-signaling factor (Hardwick et al., 2000), plays an active role in SCF-driven degradation of Cln3 in the nucleus. In turn, Mad3 levels decrease during G1 by APC-dependent degradation, thus raising the nucleo-cytoplasmic ratio of Cln3 as cells progress in G1 to reach a maximal level at cell cycle entry. Our results reveal a new regulatory layer in G1 control and provide a mechanism with a timer behavior in the Start network.

Results

Cyclin Cln3 accumulates in the nucleus in G1 and peaks during entry into the cell cycle

We previously observed by indirect immunofluorescence methods a prominent nuclear signal of Cln3 when cells enter the cell cycle (Vergés et al., 2007b; Wang et al., 2004). To characterize the temporal dynamics of this phenomenon, we decided to monitor G1 cyclin localization in live cells during G1 progression by time-lapse microscopy. Cln3 is too short-lived to be detected as a fluorescent-protein fusion in single cells unless partially-stabilizing mutations are used (Liu et al., 2015; Schmoller et al., 2015b). To avoid premature entry into the cell cycle caused by elevated G1 cyclin levels, a hypoactive mutation in the cyclin box was also introduced that maintains size within a physiological range. As previously described (Schmoller et al., 2015b), mCit-Cln3^{11A} displayed a distinct nuclear signal in most asynchronously growing cells. However, after careful measurement of images obtained by wide-field fluorescence microscopy (fig. S1A), we observed that nucleo-cytoplasmic ratios of mCit-Cln3^{11A} increased during G1 progression and reached maximum values at budding (Fig. 1A-C), thus confirming previous observations obtained with 3HA-tagged wild-type Cln3 by immunofluorescence (Wang et al., 2004). To support the nucleo-cytoplasmic ratio data, we also directly measured the nuclear concentration of mCit-Cln3^{11A} by confocal time-lapse microscopy and obtained comparable results (fig. S1C-E) to those obtained by wide-field microscopy (fig. S1B). Interestingly, the nuclear concentration of mCit-Cln3^{11A} did not change significantly with cell size at birth (Fig. 1D), suggesting Cln3 is passively segregated during cell division, likely due to free diffusion between mother and daughter compartments. Finally, intercellular variability of the nuclear concentration of mCit-Cln3^{11A} decreased during G1 and reached a minimum about 10 minutes prior to budding (Fig. 1E), which points to nuclear levels of Cln3 as a likely key parameter ruling entry into the cell cycle.

Cln3 contains a bipartite nuclear localization signal (NLS) at its C terminus that is essential for proper entry into the cell cycle (Edgington and Futcher, 2001a; Miller and Cross, 2001a). Since Cdc28 depends on the cyclin Cln3 NLS to accumulate in the nucleus in G1 cells (Wang et al., 2004), we decided to study a Cdc28-GFP fusion in a wild-type *CLN3* background to test the results observed with the mCit-Cln3^{11A} protein.

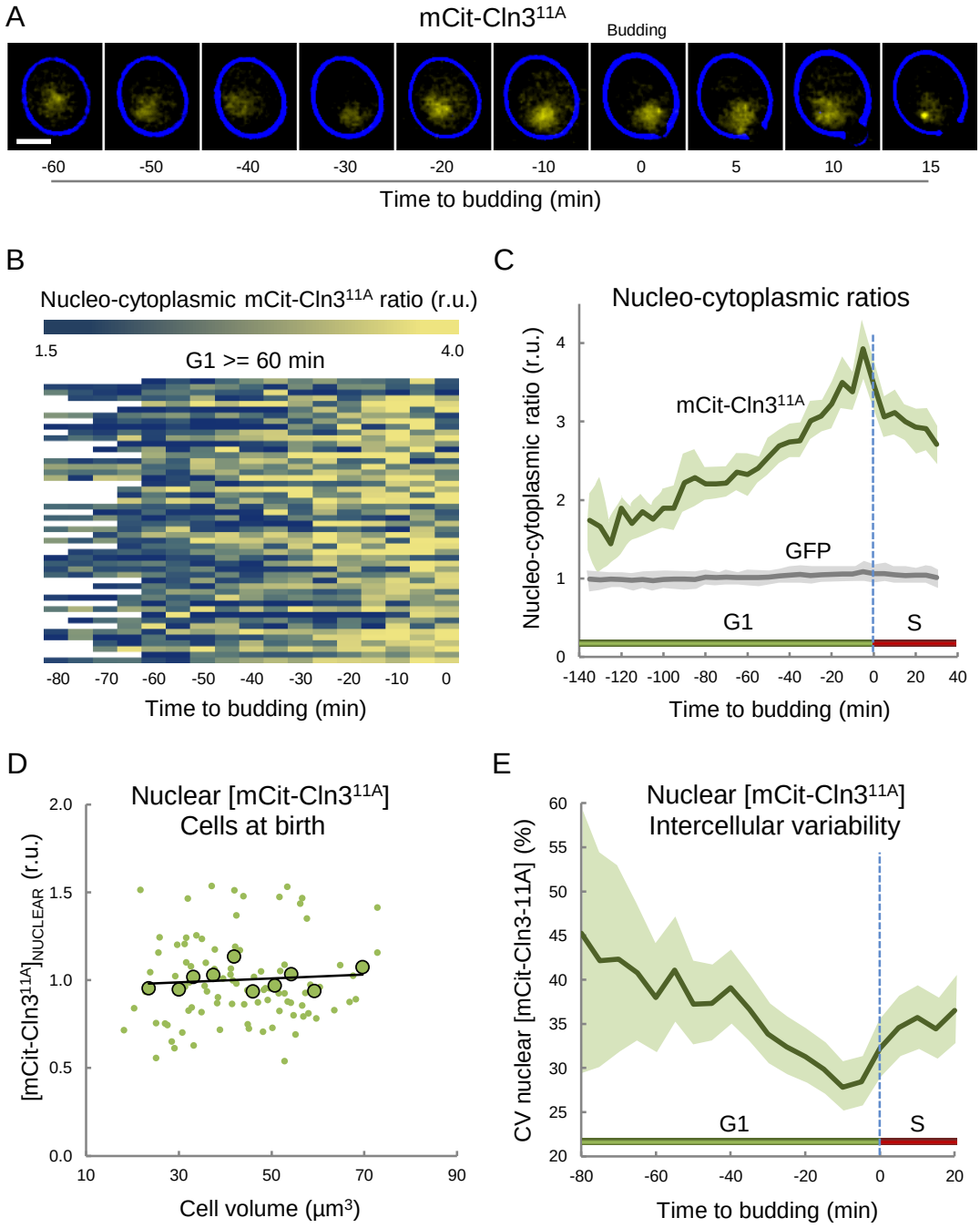

Fig. 1. Cln3^{11A} accumulates specifically in the nucleus during G1 and reaches a maximum around Start
(A) Cells expressing mCit-Cln3^{11A} were analyzed by wide-field time-lapse microscopy during G1 progression and entry into the cell cycle. The fluorescence signal of mCit-Cln3^{11A} (yellow) and the bright-field contour (blue) from a representative cell at different times relative to budding are shown. Bar is 2 µm. **(B)** Heatmap displaying nucleo-cytoplasmic ratios of mCit-Cln3^{11A} during G1 and entry into the cell cycle. Relative data were obtained from single cells (N=50) every 5 min and aligned to budding time. **(C)** Nucleo-cytoplasmic ratio of mCit-Cln3^{11A} in G1 cells as in panel A aligned to budding. Relative mean ± se values (N=100) are plotted. Data obtained from GFP-expressing cells are shown as control. **(D)** Nuclear concentration of mCit-Cln3^{11A} in cells at birth as a function of cell volume. Relative single-cell (N=100, small circles) and binned data (N=10, large circles) with the corresponding regression line are plotted. **(E)** Intercellular variability of nuclear mCit-Cln3^{11A} concentration during G1 and entry into the cell cycle. Coefficient of variation ± se values of nuclear mCit-Cln3^{11A} concentration are plotted as a function of time to budding.

While total Whi5-mCherry concentration showed a steady decrease during G1 as described (Schmoller et al., 2015b), overall Cdc28-GFP concentration was kept constant (fig. S2A). However, Cdc28-GFP displayed a progressive accumulation in the nucleus until late G1, with a maximal value at Start as determined by completion of Whi5-mCherry export, approximately 12 minutes before budding (Fig. 2A,B). Notably, the nuclear concentration of Cdc28-GFP correlated ($p<10^{-11}$) with the total concentration of Whi5-mCherry in single cells at Start (Fig. 2C), in which the fitted slope attained maximal values (fig. S2B). As expected, we observed no correlation between the nuclear concentration of Cdc28-GFP and the total concentration of mCherry expressed from a constitutive promoter (fig. S2C). These data support the idea that critical nuclear Cdc28 and Whi5 levels are main determinants of Start, where cells would integrate signals on both the G1 Cdk and the G1/S inhibitor when entering the cell cycle (Liu et al., 2015; Schmoller et al., 2015b). Regarding the role of Cln3, we found that nuclear accumulation of Cdc28-GFP was delayed in Cln3-deficient cells aligned at budding time, and nucleo-cytoplasmic ratios of Cdc28-GFP were always lower throughout entry into the cell cycle (Fig. 2D). Likely due to the fact that Cdc28 is present at much higher levels than Cln3 (Cross et al., 2002; Tyers et al., 1993) differences in the steady-state nucleo-cytoplasmic ratio of Cdc28-GFP in late G1 cells were only modest. Thus, we decided to analyze directly the import kinetics of Cdc28-GFP by nuclear fluorescence-loss in photobleaching (FLIP) (Moreno et al., 2019a). We found that the nuclear import rate of Cdc28-GFP required Cln3 and was minimal in early G1 compared to all other stages during G1 progression (Fig. 2E and fig. S2D,E). Although the Cln3 nuclear localization signal is essential for its role at Start, Cln1 and Cln2 would likely contribute to Cdc28 import (Quilis and Igual, 2012a) once the positive feedback loop is triggered, thus explaining the residual import rate of Cdc28 observed in the *cln3* mutant. Overall, these data are consistent with a post-translational mechanism that progressively increases the nuclear levels of Cln3 during G1 for the timely execution of Start.

Cln3 cyclin stability in the nucleus is modulated by Mad3 and increases with cell size in G1 cells

The Cln3 NLS is constitutively active through all stages of the cell cycle (Edgington and Futcher, 2001a; Miller and Cross, 2001a) and, contrary to Cln1 and Cln2 (Quilis and Igual, 2012a), Cln3 does not seem to have a nuclear export signal (NES). Thus, we speculated that the post-translational control of the nuclear levels of Cln3 that we observed could be due to protein stability. Cln3 is ubiquitinated by SCF with the aid of two alternative F-box proteins, Grr1 in the cytoplasm and Cdc4 in the nucleus (Landry et al., 2012), thus pointing to Cdc4 as a putative factor modulating Cln3 stability in the nucleus during G1. The dependence of Cln3 degradation on Cdc4 is almost absolute in the absence of Grr1 (Landry et al., 2012), suggesting that fine-tuning Cdc4 activity by regulatory factors could produce moderate but relevant changes in Cln3 levels in the nucleus.

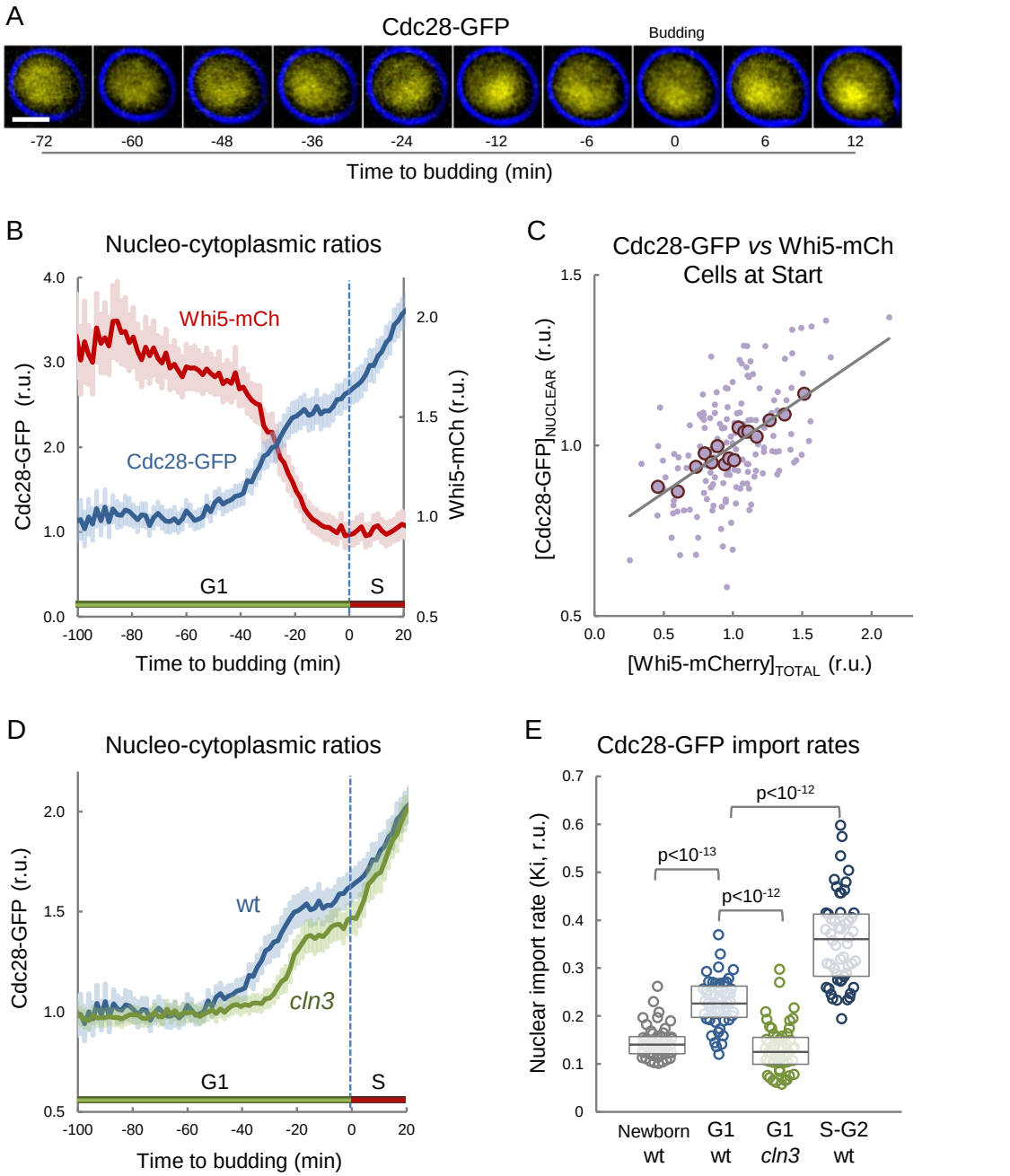

Fig. 2. Cln3 boosts nuclear import of Cdc28-GFP during cell cycle entry
(A) Cells expressing Cdc28-GFP and Whi5-mCh were analyzed by time-lapse microscopy during G1 progression and entry into the cell cycle. The fluorescence signal of Cdc28-GFP (yellow) and the bright-field contour (blue) from a representative cell at different times relative to budding are shown. Bar is 2 µm. **(B)** Nucleo-cytoplasmic Cdc28-GFP and Whi5-mCh ratios in cells as in panel A aligned to budding. Relative mean ± se values (N=100) are plotted. **(C)** Nuclear Cdc28-GFP concentration as a function of cellular Whi5-mCherry concentration at Start. Relative single-cell data (N=100, small circles) are plotted. Mean values of binned data (N=10, large circles) are also shown. **(D)** Nucleo-cytoplasmic Cdc28-GFP ratios in wild-type (wt) and Cln3-deficient (*cln3*) cells aligned to budding. Mean ± se values (N=100) are plotted. **(E)** Nuclear import rates of Cdc28-GFP in individual wild-type (wt) and Cln3-deficient (*cln3*) G1 cells. Data from wt cells in early G1 (newborn) or S-G2-M phases are shown for comparison. Median (N=50) and quartile values are plotted. Pairwise comparisons were performed with a Mann-Whitney U test, and the resulting p-values are indicated.

In this respect, we recently identified Mad3 as a nuclear centromeric-signaling protein that increases the critical size when cells contain an exceeding number of centromeres (Martínez-láinez et al., 2018). During the course of these experiments we found that Mad3 interacts with Cln3 and Cdc4 and increases nuclear degradation of the G1 cyclin. Thus, we wanted to test whether Mad3 plays a role in the degradation of nuclear Cln3 in G1 phase under normal conditions. As shown in Fig. 3A, while mCit-Cln3^{11A} half-life in wild-type G1 cells was *ca*. 20 min, degradation kinetics in Mad3-deficient cells were slower, producing a two-fold extension in the half-life of mCit-Cln3^{11A}. Next, we analyzed degradation rates in G1 at the single-cell level and found a strong negative correlation with cell size in the wild-type strain, but not in Mad3-deficient cells, in which the degradation rate was constant independently of cell size (Fig. 3B). Remarkably, we found that the nucleo-cytoplasmic ratio and the concentration of mCit-Cln3^{11A} in the nucleus remained high from early G1 to budding in Mad3-deficient cells (Fig. 3C and fig. S3A). Mad3-deficient cells are smaller at budding (Martínez-láinez et al., 2018), which is consistent with the idea that, by contributing to degradation of Cln3 during G1, Mad3 acts as an inhibitor of Start. Accordingly, Cln3 was required for the reduction in budding volume caused by a *mad3* deletion (fig. S3B). Execution of Start not only depends on G1 cyclin levels but also on Whi5 (Litsios et al., 2019; Schmoller et al., 2015b; Xie et al., 2015). Unexpectedly, deletion of *MAD3* in Whi5-deficient cells did not cause a further reduction in cell size (fig. S3B). On the other hand, we found no significant changes in Whi5 export kinetics and overall levels at Start when comparing wild-type and Mad3-deficient cells (fig. S3C,D). Thus, although Mad3 would act specifically to restrain cyclin Cln3, the resulting effects on cell cycle entry would require an intact Start network.

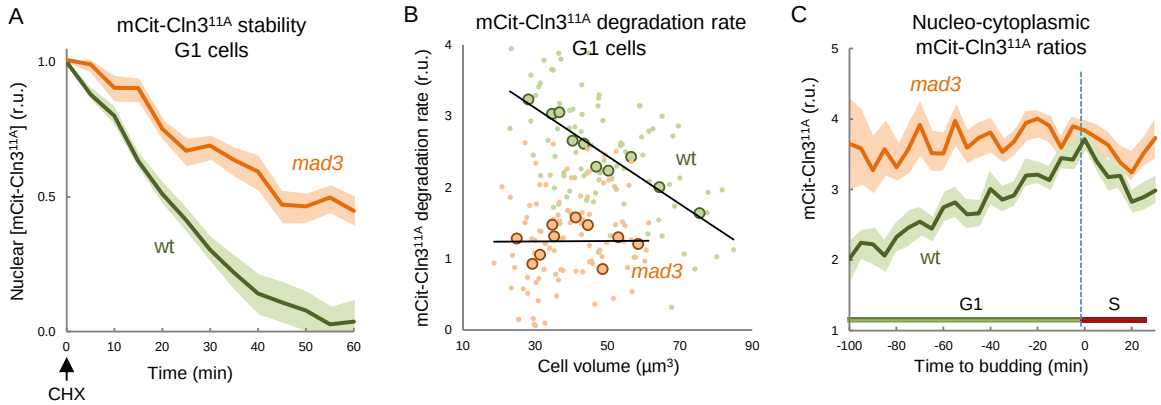

Fig. 3. Cln3^{11A} stability in the nucleus is modulated by Mad3 and increases with cell size in G1 cells
(A) Analysis of mCit-Cln3^{11A} stability in the nucleus of wild-type (wt) and Mad3-deficient (*mad3*) G1 cells. Nuclear concentrations of mCit-Cln3^{11A} were determined at the indicated times after cycloheximide (CHX) addition. Mean ± se values (N=100) are plotted. **(B)** Degradation rate of mCit-Cln3^{11A} in wild-type (wt) and Mad3-deficient (*mad3*) G1 cells. Relative single-cell data (N=100, small circles) are plotted. Mean values of binned data (N=10, large circles) and the corresponding regression lines are also shown. **(C)** Nucleo-cytoplasmic mCit-Cln3^{11A} ratios in wild-type (wt) and Mad3-deficient (*mad3*) cells aligned to budding. Mean ± se values (N=100) are plotted.

Mad3 protein levels oscillate during the cell cycle as a function of APC activity

Transcription of *MAD3* and *CDC4* is not cell cycle regulated (Spellman et al., 1998), which prompted us to analyze levels of these two proteins when expressed from constitutive promoters during the cell cycle. While a GFP-Cdc4 fusion protein was maintained at constant levels (fig. S4A), mCh-Mad3 levels decreased during G1 progression (Fig. 4A,B,D) by post-transcriptional mechanisms (fig. S4B). By contrast, the concentration of mCh-Mad3 progressively recovered during the S-G2-M period in the mother cell compartment, and decreased during the last 10-15 min due to nuclear division (Fig. 4C,E). Amounts of the mCh-Mad3 protein were segregated during mitosis following a 1:1 ratio in mother and daughter cells but, due to their smaller size, daughter cells were born with a higher concentration of Mad3 (Fig. 4F), similar to data from early-G1 cells in Fig. 4D. Finally, by using FRET, we found that levels of the Mad3-Cdc4 complex were proportional to mCh-Mad3 from birth to budding (Fig. 4G and fig. S4C), indicating that Mad3 levels are limiting at setting steady-state levels of the Mad3-Cdc4 complex during G1 progression.

Mad3 is an unstable protein that has been shown to be degraded in G1 with the key contribution of the anaphase-promoting complex (APC) and Cdh1 (King et al., 2007). Taking into account that APC^{Cdh1} is activated late in mitosis and remains active throughout G1 until entry into S phase, Mad3 stability should be sharply reduced during mitotic exit, thus providing an explanation to the observed progressive decline in Mad3 protein levels during the ensuing G1 phase until the new steady state set by APC^{Cdh1} activation is reached. To test this prediction, we analyzed a Mad3 mutant lacking the KEN30 box that mediates degradation by Cdh1 (King et al., 2007), and found that protein concentration at budding was higher compared to wt (fig. S4D) and, notably, did not decrease during G1 phase (fig. S4E).

Next, we wanted to test whether Cdh1 is not just necessary but also limiting for Mad3 degradation in G1 cells. As the *CDH1* gene is normally expressed at low levels, we analyzed *GAL1p-CDH1* cells in medium with raffinose to limit *GAL1p* activity to basal levels and attain a low level of expression. These conditions, which caused a moderate 3.2-fold increase in *CDH1* expression over wild-type cells, decreased levels of Mad3 by 2.7-fold in G1 cells and produced a clear reduction in cell size (Fig. 4H,I), similar to that observed in Mad3-deficient cells (Martínez-láinez et al., 2018). Confirming the dependence of Mad3 stability on anaphase completion, the concentration of Mad3 readily increased in cells arrested in metaphase by turning off *GAL1p-CDC20* expression (fig. S4F). In summary, these results indicate that Mad3 protein levels oscillate during the cell cycle, reaching a minimum value in daughter cells at the G1/S transition, and point to the cyclic activation APC^{Cdh1} as a new layer of control in the Start network.

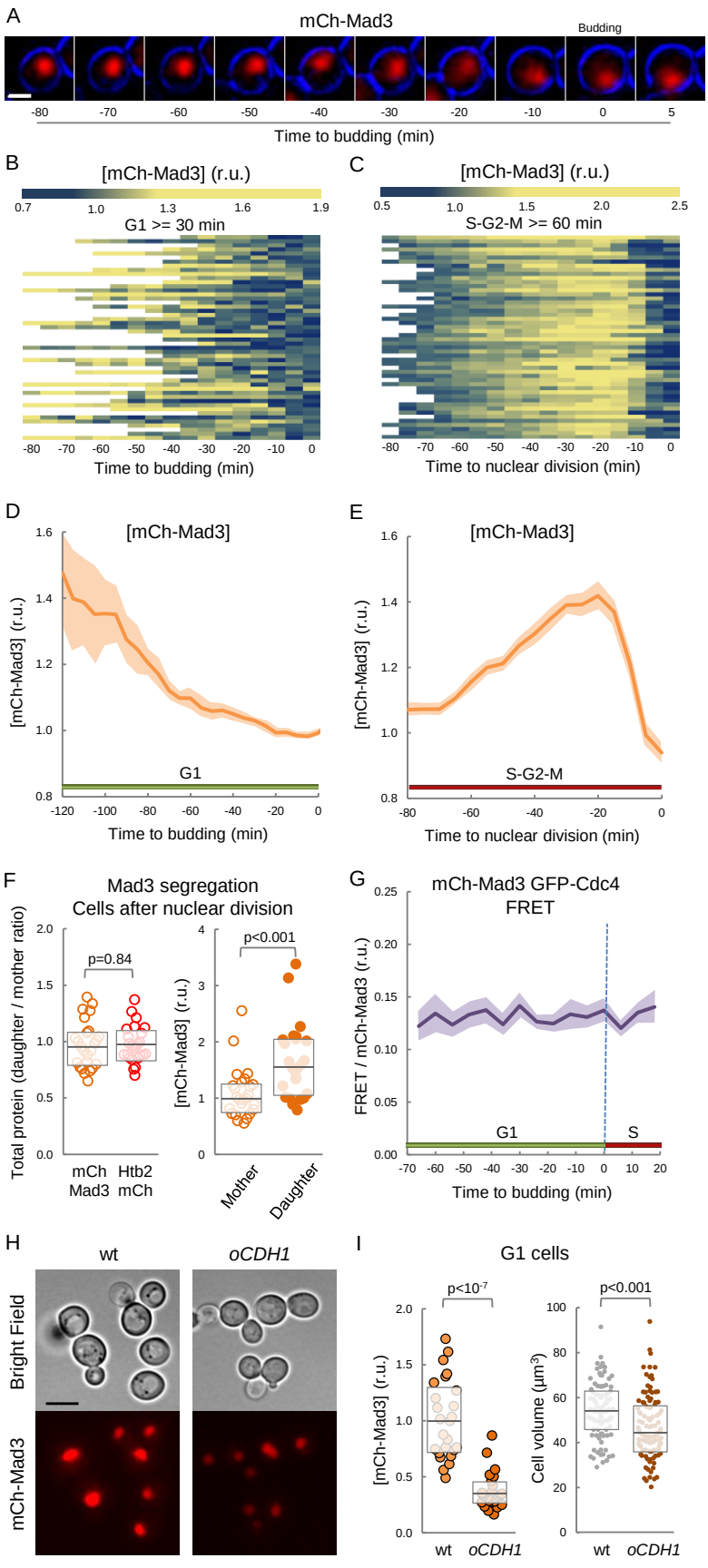

Fig. 4. Mad3 protein levels oscillate during the cell cycle as a function of APC activity

(A) Cells expressing mCh-Mad3 from a constitutive promoter during G1 progression and entry into the cell cycle. A representative cell at different times relative to budding is shown. Bar is 2 µm. **(B, C)** Heatmaps displaying mCh-Mad3 concentration during the cell cycle. Relative data from single cells (N=50) were obtained every 5 min and aligned to budding (B) or nuclear division (C). **(D, E)** Cellular concen-tration of mCh-Mad3 in cycling cells as in panel A aligned to budding (D) or nuclear division (E). Relative mean ± se values (N=100) are plotted. **(F)** Nuclear segregation of mCh-Mad3. Total amounts (left) and concentrations (right) of mCh-mad3 were determined in daughter and mother cell compartments after nuclear division and the corresponding relative data with median (N=25) and quartile values are plotted. Pairwise comparisons were performed with a Mann-Whitney U test, and the resulting p-values are indicated. Histone Htb2 fused to mCherry (Htb2-mCh) was used as control. **(G)** Mad3-Cdc4 interaction efficiency in G1 cells. Cells expressing mCh-Mad3 and GFP-Cdc4 were analyzed by FRET during G1 progression and cell-cycle entry. Relative mean ± se values (N=50) of the inferred Mad3-Cdc4 complex relative to mCh-Mad3 levels in cells aligned to budding are plotted. **(H)** Representative images of cells with empty vector (wt) or expressing a *GAL1p-CDH1* construct (*oCDH1*) in raffinose medium to limit *GAL1p* expression to basal levels. **(I)** Concentration of mCh-Mad3 (left, N=25) and cell volume (right, N=100) in G1 cells as in panel H. Single-cell data with the corresponding median and quartile values are plotted. Pairwise comparisons were performed with a Mann-Whitney U test, and the resulting p-values are indicated.

We previously observed a SAC-dependent delay in mitosis in cells containing an exceeding number of centromeric sequences (Martínez-láinez et al., 2018), which prompted us to test the effects on Mad3. We found that Mad3 levels increased in newborn cells with centromere-containing plasmids (fig. S4G). Interestingly, Mad3 levels displayed a positive correlation with cell size at birth in cells transformed with three centromeric vectors (fig. S4H), suggesting that longer delays in the previous mitosis upregulate Mad3 to higher levels. In all, these data point to Mad3 as a sensor of the metaphase-anaphase transition that modulates the duration of the ensuing G1 phase.

Mad3 adds a timer component to the mechanisms of G1 cyclin activation at Start

Protein degradation normally follows apparent first-order kinetics determined by a half-life parameter in time units (McShane et al., 2016; Varshavsky, 2011) and provides oscillators with robust temporal dynamics (Freire et al., 2012). Thus, we asked whether Mad3 degradation would introduce a time-dependent mechanism in G1 control. Early work in fission yeast established a theoretical framework based on simple cell-size measurements to test the existence of timer and sizer mechanisms controlling a cell cycle phase (Fantes, 1977). Briefly, concerning control of G1 in budding yeast, the increase in size from birth to budding should be independent of the birth size if G1 length is only determined by a timer (Fig. 5A), which would produce a null or positive slope depending whether linear or exponential growth is considered. By contrast, if the end of G1 is determined by a critical size (Fig. 5B), cells born with a smaller size than average must increase their size to a larger extent than those born larger, i.e. cell volume extension during G1 would negatively correlate with birth volume and display a slope of -1. However, available experimental data do not univocally discriminate between these two possible scenarios. Wild-type cells of budding yeast display a negative slope, from -0.4 to -0.3 depending on strain background

(Ferrezuelo et al., 2012b; Talia et al., 2007), but far from the theoretical -1 value predicted by the sizer mechanism. In agreement with previous data, wild-type cells used in this study displayed a slope of -0.283 in asynchronous cultures (Fig. 5C) and -0.296 in newly born cells (fig. S5A). Notably, Mad3-deficient cells exhibited a slope of -0.835 in asynchronous cultures (Fig. 5D) and -0.773 in newly born cells (fig. S5B), significantly different ($p=2.10^{-4}$) to those obtained from wild-type cells (fig. S5C), which indicates that Mad3 weakens the sizer behavior of G1 control, perhaps by adding a timer mechanism. To analyze this possibility, we used experimental data on cycle time, G1 length and cell volumes at birth and budding, and simulated the dependence of cell volume extension in G1 on birth volume with the aid of a pure sizer model or alternative models wherein the sizer device coexists with either timer or adder mechanisms. In order to reproduce the observed variability in cell volume and G1 length, experimental coefficients of variation were introduced in the models (Fig. 5E,F, Supplementary Data).

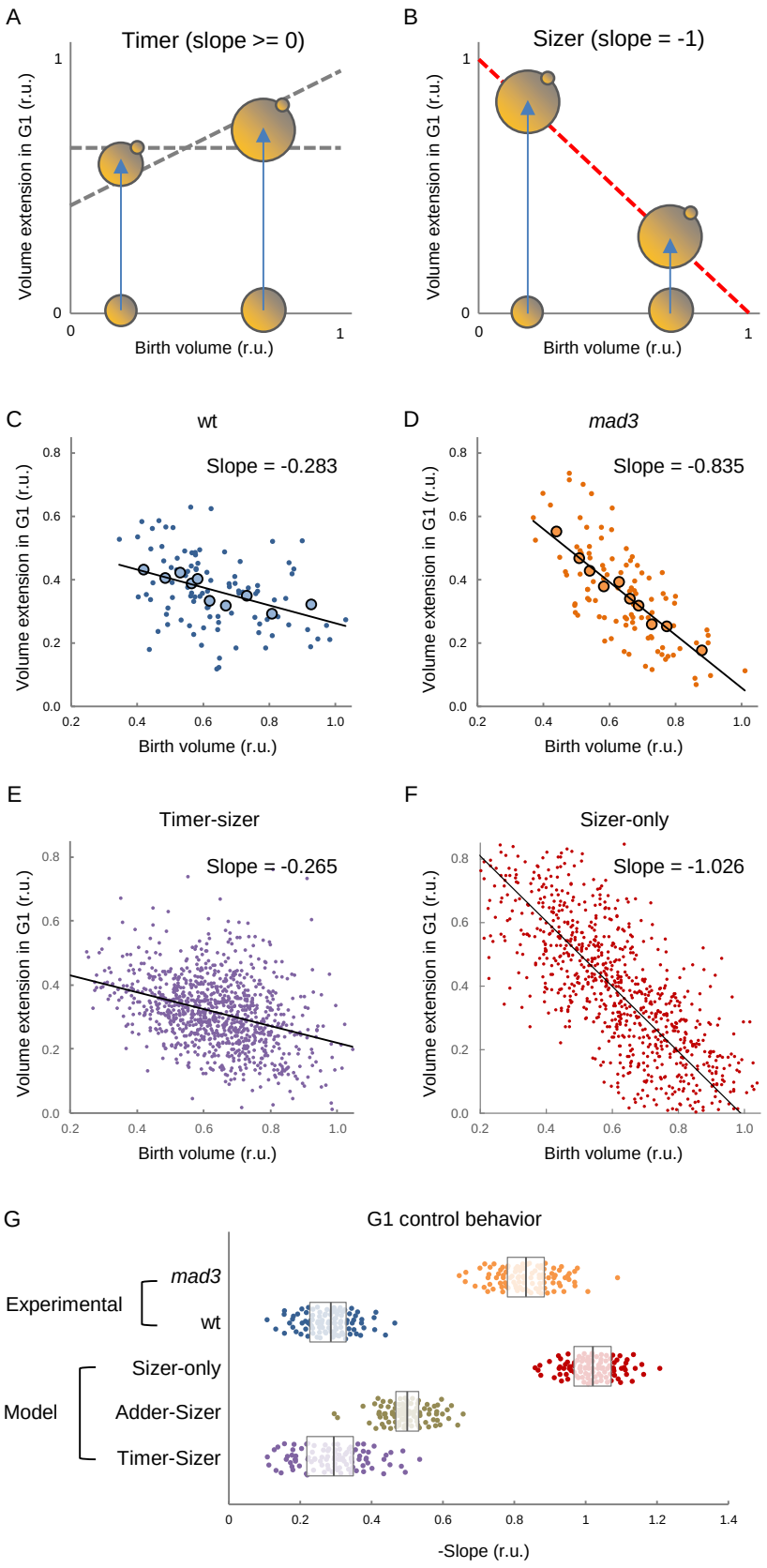

Fig. 5. Mad3 tilts the sizer behavior of G1 control

(A, B) Schemes of timer and sizer mechanisms in G1 control. If G1 length is only determined by time (A), the increase in size from birth to budding should be greatly independent of the birth size and produce a null or positive slope depending on whether linear or exponential growth in G1 is considered. By contrast, if G1 length only depends on the time required to reach a critical size (B), cells born with a smaller size than average would have to increase their size to a larger extent than others, i.e. cell volume extension during G1 should negatively correlate with birth volume (slope -1). **(C, D)** Cell volume extension in G1 as a function of birth volume in wild-type (wt, C) and Mad3-deficient (mad3, D) cells. Relative single-cell data (N=100, small circles) are plotted. Mean values of binned data (N=10, large circles) and the corresponding regression lines are also shown. **(E, F)** Simulations of the cell volume extension in G1 as a function of birth volume in the mixed timer-sizer (E) or sizer-only (F) models. Relative single-cell data (N=1000, small circles) are plotted. Mean values of binned data (large circles) and regression lines are also shown. **(G)** G1 control behavior of wild-type (wt) and Mad3-deficient (mad3) cells as measured by the absolute value of the slope from volume extension vs birth volume data. Bootstrapped values (N=100) with the corresponding median and quartile values are plotted. Simulations produced from sizer, timer-sizer and adder-sizer models are also shown.

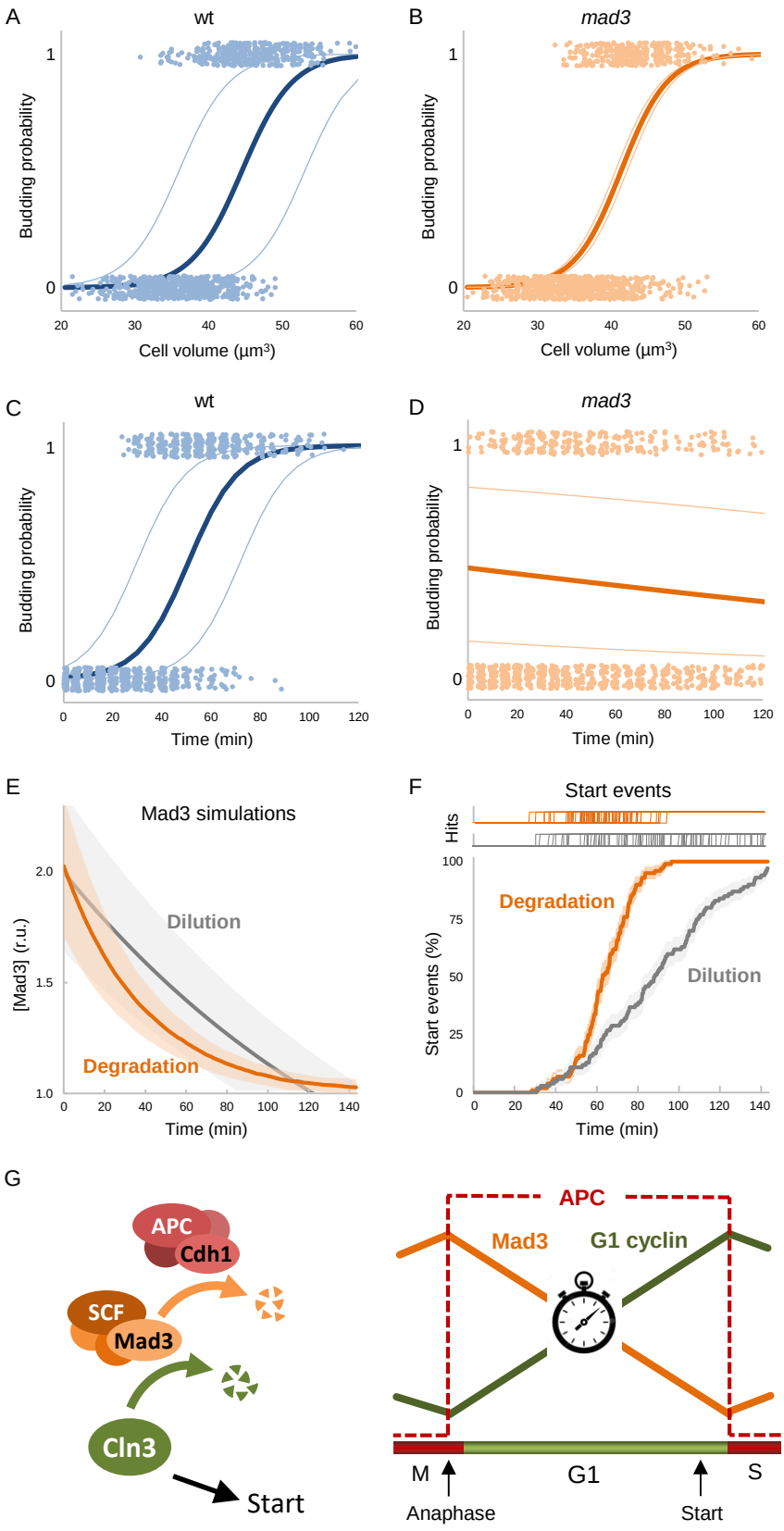

Fig. 6. Mad3 as a timer mechanism in G1 cyclin activation at Start

(A-D) Logistic regression analysis of cell volume (A,B) and time from birth (C,D) as predictors of cell budding in wild-type (A,B) and Mad3-deficient (C,D) cells. Data from sampled time frames (N=1000, small dots) of cells growing in G1 are plotted with the corresponding logistic regression curves (mean ± sd). **(E)** Simulation of the decrease in Mad3 levels by degradation or dilution as deduced from experimental data on protein half-life and mass doubling time, respectively. The experimental coefficient of variation of mCh-Mad3 in cells at birth was used to obtain single trajectories (N=100) and the resulting mean ± sd values are plotted. **(F)** Simulation of the time needed to reach a Mad3 threshold equivalent to 60% of the mean value at cell birth. Experimental parameters were as in panel A and the resulting mean frequencies ± se values are plotted. Individual events (hits) are also shown at the top. **(G)** Intertwined degradation machineries are coupled to modulate G1-cyclin activity for timely execution of cell-cycle entry. Degradation of cyclin Cln3 depends on Mad3, which in turn is degraded by APC. Hence, due to the activation of APC in anaphase, Mad3 levels decrease with time during the subsequent G1 phase, thus allowing the progressive accumulation of Cln3 in the nucleus to trigger Start. Once entered the cell cycle, high Cdk activity turns off APC and Mad3 levels are allowed to recover until anaphase, which boosts again G1-cyclin degradation to high levels before a new cycle is initiated.

While sampled simulations of the sizer and adder-sizer models produced median slopes of -1 and -0.49, respectively, the timer-sizer model exhibited a median slope of -0.3, very similar to that obtained from bootstrapped samples of wild-type cells (Fig. 5G). By contrast, the dependence of cell volume extension on birth volume displayed by Mad3-deficient cells was stronger, with a negative slope much closer to that predicted by the pure sizer model. Taken together, these data point to the notion that Mad3 contributes with a timer behavior to the mechanisms that trigger entry into the cell cycle. Supporting this idea, Mad3 concentration displayed similar average values and variability in cells born with different sizes (fig. S5D), which would rule out a function as a sizer molecule (Schmoller and Skotheim, 2015).

To assess the relative contribution of the sizer and timer mechanisms in cell-cycle entry we analyzed the probability of budding as a function of cell size and time by multivariable logistic regression. We found that both cell volume ($p<10^{-3}$) and time from birth ($p<10^{-3}$) were significant predictors of budding in wild-type cells (Fig. 6A,C). However, whereas cell volume accurately ($p<10^{-4}$) predicted budding in *mad3* cells, time from birth had no effect (p=0.26) (Fig. 6B,D).

Finally, to test further whether Mad3 degradation could act as a timer, we asked if degradation and dilution mechanisms would be equally effective. To this end we simulated the decrease in Mad3 levels by degradation or dilution as deduced from experimental data on protein half-life (King et al., 2007; Liu et al., 2011a) and mass doubling times, respectively. Applying the experimental coefficient of variation of mCh-Mad3 in cells at birth, we observed that Mad3 levels rapidly converged by degradation but not by dilution when G1 progression was simulated (Fig. 6E). As a consequence, only degradation upshift predicted reaching a threshold in a range of times compatible with experimental G1 lengths (Fig. 6F).

Discussion

G1 cyclins are highly unstable (Diehl et al., 1997; Yaglom et al., 1995), and this property allows cells to rapidly downregulate their levels after transcriptional shut-off and, hence, quickly prevent entry into the cell cycle as a response to unfavorable conditions. In budding yeast, whereas G1 cyclins are unstable throughout the cell cycle (Schneider et al., 1998), the overall levels of Cln3 display a slight but significant increase during G1 under non-perturbed conditions (Sommer et al., 2021).

Despite the relevance of degradation in cyclin regulation, its modulation during G1 progression and cell cycle entry has not been analyzed. By using a partially-stabilized hypoactive cyclin that allows live single-cell analysis (Liu et al., 2015; Schmoller et al., 2015b), we found that the nuclear concentration of Cln3 increases as cells progress in G1 and reaches a maximal level at cell cycle entry. As a

consequence, Cln3 increased nuclear import and triggered accumulation of Cdc28 in the nucleus during mid-G1 to reach a plateau later at Start that displayed a strong correlation with Whi5, the key inhibitor of the G1/S regulon. We also found that Cln3 degradation by SCF is reduced as cells progress in G1 in a Mad3-dependent manner. Mad3 levels, in turn, decreased during G1 by APC-mediated degradation, thus defining a new layer for G1 control (Fig. 6G).

While synthesis of Cln3 is assumed to be the key mechanism sensing the nutritional (Gallego et al., 1997b; Menoyo et al., 2013; Newcomb et al., 2002; Polymenis and Schmidt, 1997b; Talarek et al., 2017) and metabolic (Litsios et al., 2019) status of the cell, modulation of Cln3 activity by growth rate, stress and aging would be exerted at chaperone-dependent steps of protein folding and ER release (Moreno et al., 2019a, 2019b; Parisi et al., 2018a; Vergés et al., 2007b). Regarding the specific physiological roles of the Mad3-based mechanism described here, we propose that Mad3 acts as a timer component in the Start network, thus explaining a longstanding question in cell size control. Wild-type cells of budding yeast display a negative correlation between cell volume extension and birth volume (Ferrezuelo et al., 2012b; Talia et al., 2007), but the observed slopes are at odds with the theoretical -1 value produced by the sizer mechanism. This important discrepancy has been attributed to different factors such as noise in the Start network (Chandler-Brown et al., 2017; Talia et al., 2007) and single-cell variability in growth rate (Ferrezuelo et al., 2012b). Here we show that, compared to wild-type, Mad3-deficient cells display a slope very close to that predicted by the pure sizer model, indicating that Mad3-dependent degradation of Cln3 counteracts the sizer properties of other mechanisms of G1 control such as dilution of Whi5 (Heldt et al., 2018; Schmoller et al., 2015b). Nevertheless, the negative correlation of cell volume extension with birth volume in cells lacking Mad3 displayed a median slope (-0.827) significantly different from -1, which suggests that other factors and/or a noisy molecular design of the Start network also contribute to reduce the sizer behavior in G1 control.

The dynamic properties of Mad3 downregulation by APC are perfectly compatible with a timer mechanism. The half-life of Mad3 is *ca*. 30 minutes in G1, which makes it possible to decrease its steady-state levels about two-fold in 60-70 minutes, and cause relevant changes in Cln3 stability during the time period spent by cells in G1 phase. Mad3 may increase the binding affinity of Cdc4 for Cln3, or the intrinsic rate of ubiquitination once the G1 cyclin is bound to SCF. The latter possibility would set Cln3 degradation in a cell-size independent manner, reinforcing Mad3 as a timer modulator of Start. In this regard, Mad3 could also modulate the role of Cdc4 on the stability of Cln1 and Cln2 in the nucleus (Landry et al., 2012), thus impinging on the positive feedback loop driven by these two G1 cyclins to inactivate Whi5 (Skotheim et al., 2008).

We found that the total amount of Mad3 segregated 1:1 during cell division but, due to their smaller size, daughter cells initiate their cycle with a higher Mad3 concentration. This feature provides an additional daughter-specific mechanism to modulate Start (Di Talia et al., 2009). Although Mad3 has been shown to interact with kinetochore components of the spindle-assembly checkpoint, its presence is not restricted to centromeres and displays a diffuse pattern in the nucleus that is maintained throughout mitosis. Thus, the question remains as to how Mad3 attains equal segregation. As a possibility, very dynamic non-saturating interactions with kinetochore (Bub1, Scm3) or DNA-binding (Ccr4, Sin4) proteins could uncouple Mad3 scaling from cell size at division as shown for stably chromatin-bound proteins (Swaffer et al., 2021).

The reason why Start is not only controlled by a timer may reside on the fact that making G1 length a constant parameter would preclude size homeostasis if exponential growth is assumed. In this case, cells born larger would grow faster and differences in cell size would increase with time. On the other hand, if only a sizer mechanism operated, cells displaying very low growth rates would spend much longer periods of time in G1 and, hence, would be strongly counterselected in populations with intrinsic growth-rate variability. Thus, a timer component in G1 control would particularly assist slow growing cells to execute Start in spite of being smaller than the critical size, and would provide an explanation to our previous finding that cell size at Start is modulated by growth rate at the single-cell level (Ferrezuelo et al., 2012b).

In Whi5-deficient cells, the abovementioned slope drops to -0.2, indicating that the sizer mechanism is considerably compromised (Talia et al., 2007). However, cells lacking or expressing constant levels of Whi5 display similar cell-size population variabilities compared to wild-type cells (Barber et al., 2020; Jorgensen et al., 2004), suggesting that other mechanisms contribute to maintain cell size within limits. In this regard, differential scaling of transcription with cell size affecting inducers and inhibitors of cell cycle entry has been proposed as a complex sizer mechanism (Chen et al., 2020).

Mad3 mutant cells are only slightly smaller compared to wild-type cells. We have shown here that lack of Mad3 produces constant levels of nuclear Cln3 throughout G1 similar to those attained at Start by wild-type cells. If this were the only mechanism upholding entry into the cell cycle, Mad3-deficient cells should be very small. However, considering that Start is triggered when a threshold ratio between Cdc28 and Whi5 is attained in the nucleus, Whi5 would still delay Start unless sufficiently diluted by growth to the normal critical size (Schmoller et al., 2015b). The recent finding that the Cdc28-Cln3 complex phosphorylates the RNAPolII C-terminus to activate transcription of a subset of the G1/S regulon genes (Kõivomägi et al., 2021), including *CLN1* and *CLN2,* suggests that Cln3 and Whi5 would work in successive but different substeps of Start. This order of function could explain the observed

epistatic interaction between *MAD3* and *WHI5*. Moreover, the Mad3-Cln3 timer and Whi5 sizer mechanisms could act in a largely independent but synergistic manner providing the Start network with a more robust design and stable output.

Although the underlying molecular basis remains unclear, the combined participation of sizer with timer or adder factors may also control proliferation in bacterial and mammalian cells. In bacteria, while DNA replication is initiated at a constant size, a growth-rate dependent time sets cell division (Wallden et al., 2016). On the other hand, in an exhaustive analysis of mammalian cell lines, cell-cycle time was proposed as an important modulator of cell size (Cadart et al., 2018a). Our results on the negative correlation of cell volume extension with birth volume in wild-type cells are better explained by the addition of a timer component compared to the mixed adder-sizer device. In addition, the mechanistic and kinetic properties of Mad3-based degradation of Cln3 strongly support the role of Mad3 in a timer mechanism. The contribution of the timer component could largely depend on the specific growing conditions, particularly on growth rate. Thus, cells slowly progressing through G1 in the mouse epidermis offer a strong sizer behavior (Xie and Skotheim, 2020). By contrast, as a result of the timer component, rapidly growing cells would adapt their size to growth rate.

Finally, we also show that an exceeding number of centromeres causes increased levels of Mad3 in newborn cells, which would explain the observed faster degradation of Cln3 in G1 phase and the larger budding size compared to control cells (Martínez-láinez et al., 2018). We attribute the increase in Mad3 levels to the delay in the metaphase/anaphase transition -and APC activation- caused by tensionless kinetochores in centromeric vectors (Futcher and Carbon, 1986). When cells encounter difficulties in mitosis and become larger at birth, increased levels of Mad3 would prevent their premature entry into the subsequent cycle and ensure pre-replicative complex assembly. Thus, Mad3 would constitute a mother-to-daughter memory factor for cell size determination, perhaps also transmitting information on ploidy. The role of a chromosome-bound Cdk-inhibitor in plants (D'Ario et al., 2021) suggests that size-independent mechanisms operate throughout evolution in cell cycle entry. As it would be likely stabilized by downregulation of Fbl17 in response to DNA damage (Pan et al., 2021), this Cdk inhibitor could also act as a memory factor transmitting information of DNA synthesis and/or mitotic defects to the next G1 phase in plant cells.

We envisage that Mad3 degradation kinetics would have been evolutionarily optimized to set the most appropriate G1 length and, perhaps more important, to diversify cell dimensions in unpredictable environments.

Materials and Methods

Strain constructions. Yeast strains used in this study are listed in Table S1. Methods for chromosomal gene transplacement and PCR-based directed mutagenesis have been described (Ferrezuelo et al., 2012b; Gallego et al., 1997b; Wang et al., 2004). Unless stated otherwise, all gene fusions were expressed at endogenous levels at their respective loci. C-terminal fusions of fluorescent proteins to Cdc28 (Maekawa et al., 2003), Whi5 (Schmoller et al., 2015b) or Htb2 (Skotheim et al., 2008) have been previously characterized. The N-terminal mCitrine $Cln3^{11A}$ fusion protein contains a hypoactive and hyperstable cyclin with 11 amino acid substitutions (R108A, T420A, S449A, T455A, S462A, S464A, S468A, T478A, S514A, T517A, T520A) that allows its detection by fluorescence microscopy with no gross effects on cell cycle progression (Schmoller et al., 2015b).

Fusion of mCherry to the N-terminus or C-terminus of Mad3 under the endogenous promoter decreased protein expression levels, likely due to the uncoupling of uncommon downstream transcriptional elements. Moreover, the C-terminal fusion did not accumulate in the nucleus as shown for wt Mad3 by immunofluorescence (31), suggesting that Mad3 mislocalization would affect protein stability. Thus, since we wanted to analyze post-transcriptional changes on Mad3 levels during the cell cycle, we opted for using an N-terminal fusion under the constitutive *GPD1* promoter at the *MAD3* locus. Similarly, the N-terminal GFP-Cdc4 fusions was expressed from the constitutive *TEF1* promoter at the corresponding locus. Gene fusions and specific constructs requiring multiple fragments were obtained by one-step recombination in yeast cells as described (Gibson et al., 2008).

Growth conditions. Cells were grown under exponential conditions for 7-8 generations in SC medium with 2% glucose at 30ºC before microscopy unless stated otherwise. Other carbon sources used were 2% galactose and 2% raffinose.

Where indicated, cycloheximide was added at 20 µg/ml. Small newly-born cells were isolated from Ficoll gradients (Mitchison, 1988).

Time-lapse microscopy. Cells were analyzed by time-lapse microscopy in 35-mm glass-bottom culture dishes (GWST-3522, WillCo) in SC-based media at 30ºC essentially as described (Ferrezuelo et al., 2012b) using fully-motorized Leica AF7000 or Thunder Imager microscopes. Time-lapse images were analyzed with the aid of BudJ (Ferrezuelo et al., 2012b), an ImageJ (Wayne Rasband, NIH) plugin (https://www.ibmb.csic.es/en/department-of-cell-biology-dcb/spatial-control-of-cell-cycle-entry/#lab-corner) to obtain cell dimensions and fluorescence data. Volume growth rate in G1 was obtained as described (Ferrezuelo et al., 2012b). Background autofluorescence from untagged cells was subtracted.

Determination of cellular and nuclear concentrations of fluorescent fusion proteins. Wide-field microscopy is able to collect the total fluorescence emitted by yeast cells and, consequently, cellular concentration of fluorescent fusion proteins was obtained by dividing the integrated fluorescence signal within the projected area of the cell by its volume. Regarding the quantification of nuclear levels, since the signal in the nuclear projected area is influenced by both nuclear and cytoplasmic fluorescence, determination of the nuclear concentration required specific calculations (fig. S1A) as described (Moreno et al., 2019a). In confocal microscopy the fluorescence signal is directly proportional to the concentration of the fluorescent fusion protein, and required no further calculations.

The nuclear compartment was estimated as described (Ferrezuelo et al., 2012b). Briefly, the center of the nucleus was set as the gravity center of pixels with a fluorescence 30% higher than the mean value and the radius was obtained as 0.4-times the cell radius (Jorgensen et al., 2007). This approach produced results that correlated well with those obtained by colocalization with Htb2-mCherry as a nuclear marker (Ferrezuelo et al., 2012b). Moreover, these procedures made unnecessary the co-expression of a tagged nuclear protein and helped minimize light-induced damage during growth. In some experiments (fig. S1C-D), the nuclear compartment was delimited by means of histone Htb2-mCh.

Nuclear import rate determinations by FLIP. To analyze nuclear import kinetics of Cdc28-GFP, a circle inscribed within the Htb2-mCherry nuclear region was repetitively photobleached at 488-nm while the cell was imaged every 0.5 sec to record fluorescence loss under a Zeiss LSM780 confocal microscope. After background subtraction, fluorescence data were corrected with those from a non-bleached cell, and fluorescence signals within nuclear and cytoplasmic areas were used to analyze import kinetics as described (Moreno et al., 2019a). Briefly, fluorescence signals within nuclear (F_n) and cytoplasmic (F_c) areas were used to obtain a nuclear to cytoplasmic ratio (F_n/F_c). At steady-state ratio the import (dF_n/dt) and export (dF_c/dt) rates are in equilibrium (i.e. $dF_n/dt = dF_c/dt$), and $dF_n/dt = K_i.F_c – (K_e+K_b)F_n$, and $dF_c/dt = K_e.F_n – K_i.F_c$, where K_i, K_e and K_b are the import, export and bleaching rate constants, respectively. Thus, $K_i.F_c – (K_e+K_b)F_n = K_e.F_n – K_i.F_c$, and $K_i = (F_n/F_c)\ (K_e+K_b/2)$. The bleaching rate constant was obtained from Htb2-mCherry fluorescence loss in the same cell, and the export rate constant from the recovery kinetics after nuclear FLIP as described (Moreno et al., 2019a).

Mad3-Cdc4 interaction by FRET. Cells expressing mCh-Mad3 and GFP-Cdc4 were analyzed by FRET under a Zeiss LSM780 confocal microscope. Briefly, GFP-Cdc4 was excited at 488 nm, and its emission was measured at 490-532 nm. Excitation of mCh-Mad3 was at 561 nm, and emission was measured at 563-695 nm. The FRET signal was measured at 563-695 when excited at 488 nm. The relative FRET

efficiency was calculated as $(I_F - k_D*I_D - k_A*I_A) / I_A$, where I_A, I_D and I_F are the fluorescence intensities recorded from the acceptor, donor and FRET channels, are k_A and k_D correcting acceptor cross-excitation and donor bleed-through constants, respectively. Background autofluorescence in all channels from untagged cells was subtracted. FRET efficiencies obtained from cells expressing Cdc4-GFP and Mad3-mCh, or GFP and mCh as control, are shown in fig. S4C. First, the FRET efficiency between GFP and mCh was not significantly different from zero and, second, FRET produced by the Cdc4-GFP Mad3-mCh pair did not change much over a 10-fold range of acceptor fluorescence values.

Cell size simulations in G1. We modeled volume growth during G1 progression in daughter cells following exponential kinetics with the following variables: initial volume (V_i), budding volume (V_b), G1 length (G_1) and duplication time (τ). When used as independent variables, they were parameterized with experimental average data and coefficients of variation shown in Supplementary Data. We assumed that independent variables followed normal distributions, which were used to generate random stochastic values and to calculate the dependent variables depending on different scenarios of G1 control: sizer, timer, adder, timer-sizer or timer-adder behaviors, as follows:

Sizer**:** New born cells were given V_i, V_b and τ as independent variables, and the length of the G1 period was calculated as $G_1 = \tau * ln_2 (V_b / V_i)$.

Timer**:** New born cells were given V_i, G_1 and τ as independent variables, and the budding volume was obtained as $V_b = V_i * 2^{(G1/\tau)}$.

Adder**:** New born cells were given V_i and ΔV as independent variables, and the budding volume was obtained as $V_b = \Delta V + V_i$.

Timer-sizer: Budding volumes were calculated following timer and sizer behaviors as above and, assuming an equal contribution to the final budding volume, the mean value was taken.

Adder-sizer: Budding volumes were calculated following adder and sizer behaviors as above and, assuming an equal contribution to the final budding volume, the mean value was taken.

Mad3 degradation simulations. We first parametrized Mad3 synthesis and degradation reactions to obtain a half-life of 60 min (King et al., 2007). To simulate Cdh1 activation in G1, we increased the degradation constant by two-fold (King et al., 2007; Liu et al., 2011a), and followed Mad3 with time as a function of initial levels stochastically generated from normal distributions with a coefficient of variation experimentally determined from wild-type cells (Fig. 6E). For comparison, dilution of Mad3 was also modelled using experimentally determined mass-doubling times from wild-type cells. As an approximation to G1 length, we used the time at which Mad3 levels decreased to 60% relative to cell birth by degradation or dilution (Fig. 6F).

Statistical analysis. Sample size is always indicated in the figure legend. For single-cell data, median and quartile values are shown. Pairwise comparisons were performed with a Mann-Whitney U test; and the resulting p-values are shown in the corresponding figure panels. Time-lapse data from single cells are represented as the mean value of the population along time, while the shaded area represents the standard error of the mean. Multivariable logistic regression using cell size and time from birth as predictors of budding was done using randomly-sampled individual time frames from time-lapse experiments with small newborn cells growing in G1. For each cell and time frame, cell volume and time from birth were determined and tested as predictors of budding in the next 30 min by fitting a logistic model. To obtain logistic regression curves of either cell volume or time from birth as single predictors, the other variable was fixed as the mean ± sd from all sampled time frames.

References

Barber, F., Amir, A., Murray, A.W., and Murray, A.W. (2020). Cell-size regulation in budding yeast does not depend on linear accumulation of Whi5. Proc. Natl. Acad. Sci. U. S. A. 117, 14243–14250.

Bertoli, C., Skotheim, J.M., and de Bruin, R.A.M. (2013). Control of cell cycle transcription during G1 and S phases. Nat. Rev. Mol. Cell Biol. 14, 518–528.

Cadart, C., Monnier, S., Grilli, J., Sáez, P.J., Srivastava, N., Attia, R., Terriac, E., Baum, B., Cosentino-Lagomarsino, M., and Piel, M. (2018). Size control in mammalian cells involves modulation of both growth rate and cell cycle duration. Nat. Commun. 9, 3275.

Chandler-Brown, D., Schmoller, K.M., Winetraub, Y., and Skotheim, J.M. (2017). The adder phenomenon emerges from independent control of pre- and post-Start phases of the budding yeast cell cycle. Curr. Biol. 27, 2774–2783.

Chen, Y., and Futcher, B. (2021). Scaling gene expression for cell size control and senescence in Saccharomyces cerevisiae. Curr. Genet. 67, 41–47.

Chen, Y., Zhao, G., Zahumensky, J., Honey, S., and Futcher, B. (2020). Differential scaling of gene expression with cell size may explain size control in budding yeast. Mol. Cell 78, 359–370.

Cross, F.R., Archambault, V., Miller, M., and Klovstad, M. (2002). Testing a mathematical model of the yeast cell cycle. Mol. Biol. Cell 13, 52–70.

D'Ario, M., and Sablowski, R. (2019). Cell Size Control in Plants. Annu. Rev. Genet. 53, 45–65.

D'Ario, M., Tavares, R., Schiessl, K., Desvoyes, B., Gutierrez, C., Howard, M., and Sablowski, R. (2021). Cell size controlled in plants using DNA content as an internal scale. Science 372, 1176–1181.

Diehl, J., Zindy, F., and Sherr, C. (1997). Inhibition of cyclin D1 phosphorylation on threonine-286 prevents its rapid degradation via the ubiquitin-proteasome pathway. Genes Dev. 11, 957–972.

Edgington, N.P., and Futcher, B. (2001). Relationship between the function and the location of G1 cyclins in S. cerevisiae. J. Cell Sci. 114, 4599–4611.

Facchetti, G., Chang, F., and Howard, M. (2017). Controlling cell size through sizers mechanisms. Curr. Opin. Syst. Biol. 5, 86–92.

Facchetti, G., Knapp, B., Chang, F., and Howard, M. (2019). Reassessment of the Basis of Cell Size Control Based on Analysis of Cell-to-Cell Variability. Biophys. J. 117, 1728–1738.

Fantes, P.A. (1977). Control of cell size and cycle time in Schizosaccharomyces pombe. J. Cell Sci. 24, 51–67.

Ferrezuelo, F., Colomina, N., Palmisano, A., Garí, E., Gallego, C., Csikász-Nagy, A., and Aldea, M. (2012). The critical size is set at a single-cell level by growth rate to attain homeostasis and adaptation. Nat. Commun. 3, 1012.

Freire, P., Vinod, P., and Novak, B. (2012). Interplay of transcriptional and proteolytic regulation in driving robust cell cycle progression. Mol. Biosyst. 8, 863–870.

Futcher, B., and Carbon, J. (1986). Toxic effects of excess cloned centromeres. Mol. Cell. Biol. 6, 2213–2222.

Gallego, C., Garí, E., Colomina, N., Herrero, E., and Aldea, M. (1997). The Cln3 cyclin is down-regulated by translational repression and degradation during the G1 arrest caused by nitrogen deprivation in budding yeast. EMBO J. 16, 7196–7206.

Garí, E., Volpe, T., Wang, H.Y., Gallego, C., Futcher, B., and Aldea, M. (2001). Whi3 binds the mRNA of the G1 cyclin CLN3 to modulate cell fate in budding yeast. Genes Dev. 15, 2803–2808.

Garmendia-Torres, C., Tassy, O., Matifas, A., Molina, N., and Charvin, G. (2018). Multiple inputs ensure yeast cell size homeostasis during cell cycle progression. Elife 7, e34025.

Gibson, D.G., Benders, G.A., Axelrod, K.C., Zaveri, J., Algire, M.A., Moodie, M., Montague, M.G., Venter, J.C., Smith, H.O., and Hutchison, C.A. (2008). One-step assembly in yeast of 25 overlapping DNA fragments to form a complete synthetic Mycoplasma genitalium genome. Proc. Natl. Acad. Sci. U. S. A. 105, 20404–20409.

Hardwick, K.G., Johnston, R.C., Smith, D.L., and Murray, A.W. (2000). MAD3 encodes a novel component of the spindle checkpoint which interacts with Bub3p , Cdc20p , and Mad2p. J. Cell Biol. 148, 871–882.

Hartwell, L.H., and Unger, M.W. (1977). Unequal division in Saccharomyces cerevisiae and its implications for the control of cell division. J. Cell Biol. 75, 422–435.

Heldt, F.S., Lunstone, R., Tyson, J.J., and Novak, B. (2018). Dilution and titration of cell-cycle regulators may control cell size in budding yeast. PLoS Comput. Biol. 14, e1006548.

Johnson, A., and Skotheim, J.M. (2013). Start and the restriction point. Curr. Opin. Cell Biol. 25, 717–723.

Johnston, G.C., Pringle, J.R., and Hartwell, L.H. (1977). Coordination of growth with cell division in the yeast Saccharomyces cerevisiae. Exp. Cell Res. 105, 79–98.

Jorgensen, P., and Tyers, M. (2004). How cells coordinate growth and division. Curr. Biol. 14, R1014–R1027.

Jorgensen, P., Rupes, I., Sharom, J.R., Schneper, L., Broach, J.R., and Tyers, M. (2004). A dynamic transcriptional network communicates growth potential to ribosome synthesis and critical cell size. Genes Dev. 18, 2491–2505.

Jorgensen, P., Edgington, N.P., Schneider, B.L., Rupes, I., Tyers, M., and Futcher, B. (2007). The size of the nucleus increases as yeast cells grow. Mol. Biol. Cell 18, 3523–3532.

King, E.M.J., van der Sar, S.J.A., and Hardwick, K.G. (2007). Mad3 KEN boxes mediate both Cdc20 and Mad3 turnover, and are critical for the spindle checkpoint. PLoS One 2, e342.

Kõivomägi, M., Swaffer, M.P., Turner, J.J., Marinov, G., and Skotheim, J.M. (2021). G1 cyclin-Cdk promotes cell cycle entry through localized phosphorylation of RNA polymerase II. Science (80-.). 374, 347–351.

Landry, B.D., Doyle, J.P., Toczyski, D.P., and Benanti, J.A. (2012). F-box protein specificity for G1 cyclins is dictated by subcellular localization. PLoS Genet. 8.

Litsios, A., Huberts, D.H.E.W., Terpstra, H.M., Guerra, P., Schmidt, A., Buczak, K., Papagiannakis, A., Rovetta, M., Hekelaar, J., Hubmann, G., et al. (2019). Differential scaling between G1 protein production and cell size dynamics promotes commitment to the cell division cycle in budding yeast. Nat. Cell Biol. 21, 1382–1392.

Liu, C., Van Dyk, D., Choe, V., Yan, J., Majumder, S., Costanzo, M., Bao, X., Boone, C., Huo, K., Winey, M., et al. (2011). Ubiquitin ligase Ufd2 is required for efficient degradation of Mps1 kinase. J. Biol. Chem. 286, 43660–43667.

Liu, X., Wang, X., Yang, X., Liu, S., Jiang, L., Qu, Y., Hu, L., Ouyang, Q., and Tang, C. (2015). Reliable cell cycle commitment in budding yeast is ensured by signal integration. Elife 4, e03977.

Maekawa, H., Usui, T., Knop, M., and Schiebel, E. (2003). Yeast Cdk1 translocates to the plus end of cytoplasmic microtubules to regulate bud cortex interactions. EMBO J. 22, 438–449.

Martínez-Láinez, J.M., Moreno, D.F., Parisi, E., Clotet, J., and Aldea, M. (2018). Centromeric signaling proteins boost G1 cyclin degradation and modulate cell size in budding yeast. PLoS Biol. 16, e2005388.

McShane, E., Sin, C., Zauber, H., Wells, J.N., Donnelly, N., Wang, X., Hou, J., Chen, W., Storchova, Z., Marsh, J.A., et al. (2016). Kinetic analysis of protein stability reveals age-dependent degradation. Cell 167, 803–815.

Menoyo, S., Ricco, N., Bru, S., Hernández-Ortega, S., Escoté, X., Aldea, M., and Clotet, J. (2013). Phosphate-activated cyclin-dependent kinase stabilizes G1 cyclin to trigger cell cycle entry. Mol. Cell. Biol. 33, 1273–1284.

Miller, M.E., and Cross, F.R. (2001). Mechanisms controlling subcellular localization of the G1 cyclins Cln2p and Cln3p in budding yeast. Mol. Cell. Biol. 21, 6292–6311.

Mitchison, J.M. (1988). Synchronous cultures and age fractionation. In Yeast, a Practical Approach, I. Campbell, and J. Duffus, eds. (Oxford, UK: IRL Press), pp. 51–64.

Moreno, D.F., Parisi, E., Yahya, G., Vaggi, F., Csikász-Nagy, A., and Aldea, M. (2019a). Competition in the chaperone-client network subordinates cell-cycle entry to growth and stress. Life Sci. Alliance 2, e201800277.

Moreno, D.F., Jenkins, K., Morlot, S., Charvin, G., Csikász-Nagy, A., and Aldea, M. (2019b). Proteostasis collapse, a hallmark of aging, hinders the chaperone-Start network and arrests cells in G1. Elife 8, e48240.

Newcomb, L.L., Hall, D.D., and Heideman, W. (2002). AZF1 is a glucose-dependent positive regulator of CLN3 transcription in Saccharomyces cerevisiae. Mol. Cell. Biol. 22, 1607–1614.

Pan, T., Qin, Q., Nong, C., Gao, S., Wang, L., Cai, B., Zhang, M., Wu, C., Chen, H., Li, T., et al. (2021). A novel WEE1 pathway for replication stress responses. Nat. Plants 7, 209–218.

Parisi, E., Yahya, G., Flores, A., and Aldea, M. (2018). Cdc48/p97 segregase is modulated by cyclin-dependent kinase to determine cyclin fate during G1 progression. EMBO J. 37, e98724.

Polymenis, M., and Schmidt, E. V (1997). Coupling of cell division to cell growth by translational control of the G1 cyclin CLN3 in yeast. Genes Dev. 11, 2522–2531.

Quilis, I., and Igual, J.C. (2012). Molecular basis of the functional distinction between Cln1 and Cln2 cyclins. Cell Cycle 11, 3117–3131.

Schmoller, K.M., and Skotheim, J.M. (2015). The biosynthetic basis of cell size control. Trends Cell Biol. 25, 793–802.

Schmoller, K.M., Turner, J.J., Kõivomägi, M., and Skotheim, J.M. (2015). Dilution of the cell cycle inhibitor Whi5 controls budding yeast cell size. Nature 526, 268–272.

Schneider, B., Patton, E., Lanker, S., Mendenhall, M., Wittenberg, C., Futcher, B., and Tyers, M. (1998). Yeast G1 cyclins are unstable in G1 phase. Nature 395, 86–89.

Skotheim, J.M., Di Talia, S., Siggia, E.D., and Cross, F.R. (2008). Positive feedback of G1 cyclins ensures coherent cell cycle entry. Nature 454, 291–296.

Sommer, R.A., DeWitt, J.T., Tan, R., and Kellogg, D.R. (2021). Growth-dependent signals drive an increase in early G1 cyclin concentration to link cell cycle entry with cell growth. Elife 10, e64364.

Spellman, P.T., Sherlock, G., Zhang, M.Q., Iyer, V.R., Anders, K., Eisen, M.B., Brown, P.O., Botstein, D., and Futcher, B. (1998). Comprehensive identification of cell cycle-regulated genes of the yeast Saccharomyces cerevisiae by microarray hybridization. Mol. Biol. Cell 9, 3273–3297.

Spiesser, T.W., Kühn, C., Krantz, M., and Klipp, E. (2015). Bud-localization of CLB2 mRNA can constitute a growth rate dependent daughter sizer. PLOS Comput. Biol. 11, e1004223.

Swaffer, M.P., Kim, J., Chandler-Brown, D., Langhinrichs, M., Marinov, G.K., Greenleaf, W.J., Kundaje, A., Schmoller, K.M., and Skotheim, J.M. (2021). Transcriptional and chromatin-based partitioning mechanisms uncouple protein scaling from cell size. Mol. Cell 81, 4861-4875.e7.

Talarek, N., Gueydon, E., and Schwob, E. (2017). Homeostatic control of START through negative feedback between Cln3-Cdk1 and Rim15/Greatwall kinase in budding yeast. Elife 6, e26233.

Di Talia, S., Skotheim, J.M., Bean, J.M., Siggia, E.D., and Cross, F.R. (2007). The effects of molecular noise and size control on variability in the budding yeast cell cycle. Nature 448, 947–951.

Di Talia, S., Wang, H., Skotheim, J.M., Rosebrock, A.P., Futcher, B., and Cross, F.R. (2009). Daughter-specific transcription factors regulate cell size control in budding yeast. PLoS Biol. 7, e1000221.

Tyers, M., Tokiwa, G., and Futcher, B. (1993). Comparison of the Saccharomyces cerevisiae G1 cyclins: Cln3 may be an upstream activator of Cln1, Cln2 and other cyclins. EMBO J. 12, 1955–1968.

Varshavsky, A. (2011). The N-end rule pathway and regulation by proteolysis. Protein Sci. 20, 1298.

Vergés, E., Colomina, N., Garí, E., Gallego, C., and Aldea, M. (2007). Cyclin Cln3 is retained at the ER and released by the J chaperone Ydj1 in late G1 to trigger cell cycle entry. Mol. Cell 26, 649–662.

Wallden, M., Fange, D., Lundius, E.G., Baltekin, Ö., and Elf, J. (2016). The synchronization of replication and division cycles in individual E. coli cells. Cell 166, 729–739.

Wang, H., Garí, E., Vergés, E., Gallego, C., and Aldea, M. (2004). Recruitment of Cdc28 by Whi3 restricts nuclear accumulation of the G1 cyclin-Cdk complex to late G1. EMBO J. 23, 180–190.

Wang, H., Carey, L.B., Cai, Y., Wijnen, H., and Futcher, B. (2009). Recruitment of Cln3 cyclin to promoters controls cell cycle entry via histone deacetylase and other targets. PLoS Biol. 7, e1000189.

Wood, E., and Nurse, P. (2015). Sizing up to divide: mitotic cell-size control in fission yeast. Annu Rev Cell Dev Biol 31, 11–29.

Xie, S., and Skotheim, J.M. (2020). A G1 Sizer Coordinates Growth and Division in the Mouse Epidermis. Curr. Biol. 30, 916-924.e2.

Xie, Z., Jay, K.A., Smith, D.L., Zhang, Y., Liu, Z., Zheng, J., Tian, R., Li, H., and Blackburn, E.H. (2015). Early telomerase inactivation accelerates aging independently of telomere length. Cell 160, 928–939.

Yaglom, J., Linskens, M.H.K., Sadis, S., Rubin, D.M., Futcher, B., and Finley, D. (1995). p34 Cdc28 -mediated control of Cln3 cyclin degradation. Mol. Cell. Biol. 15, 731–741.

Yaglom, J.A., Goldberg, A.L., Finley, D., and Sherman, M.Y. (1996). The molecular chaperone Ydj1 is required for the p34CDC28-dependent phosphorylation of the cyclin Cln3 that signals its degradation. Mol. Cell. Biol. 16, 3679–3684.

Zapata, J., Dephoure, N., Macdonough, T., Yu, Y., Parnell, E.J., Mooring, M., Gygi, S.P., Stillman, D.J., and Kellogg, D.R. (2014). PP2ARts1 is a master regulator of pathways that control cell size. J. Cell Biol. 204, 359–376.

Zatulovskiy, E., and Skotheim, J.M. (2020). On the molecular mechanisms regulating animal cell size homeostasis. Trends Genet. 36, 360–372.

Acknowledgments. We thank E. Rebollo for technical assistance, and J. Skotheim and F. Ferrezuelo for providing strains. We also thank C. Rose for editing the manuscript, and C. Gallego for helpful comments. *Funding***:** *Agencia Estatal de Investigación* Spain PID2019-109638GB-I00 (MA); *Agencia Estatal de Investigación* Spain PGC2018-096597-B-I00 (JC); *Agència de Gestió d'Ajuts Universitaris i de Recerca* Catalonia 2019FI_B 00452 (APP); *Agència de Gestió d'Ajuts Universitaris i de Recerca* Catalonia 2014FI_B 00074 (DFM). *Author contributions:* Conceptualization: JC, MA; Investigation: APP, MHA, DFM; Data analysis: APP, DFM; Supervision: JC, MA; Writing-original draft: JC, MA; Writing-review and editing: JC, MA. *Data and materials availability:* All data needed to evaluate the conclusions in the paper are present in the paper and the Supplementary Materials. BudJ can be obtained from https://www.ibmb.csic.es/en/department-of-cell-biology-dcb/spatial-control-of-cell-cycle-entry/#lab-corner. *Supplementary Materials.* Supplementary figures S1 to S6; Supplementary table S1 with yeast strains used in this study, and a dataset with **c**ell size predictions by sizer, timer, adder, timer-sizer and timer-adder models.

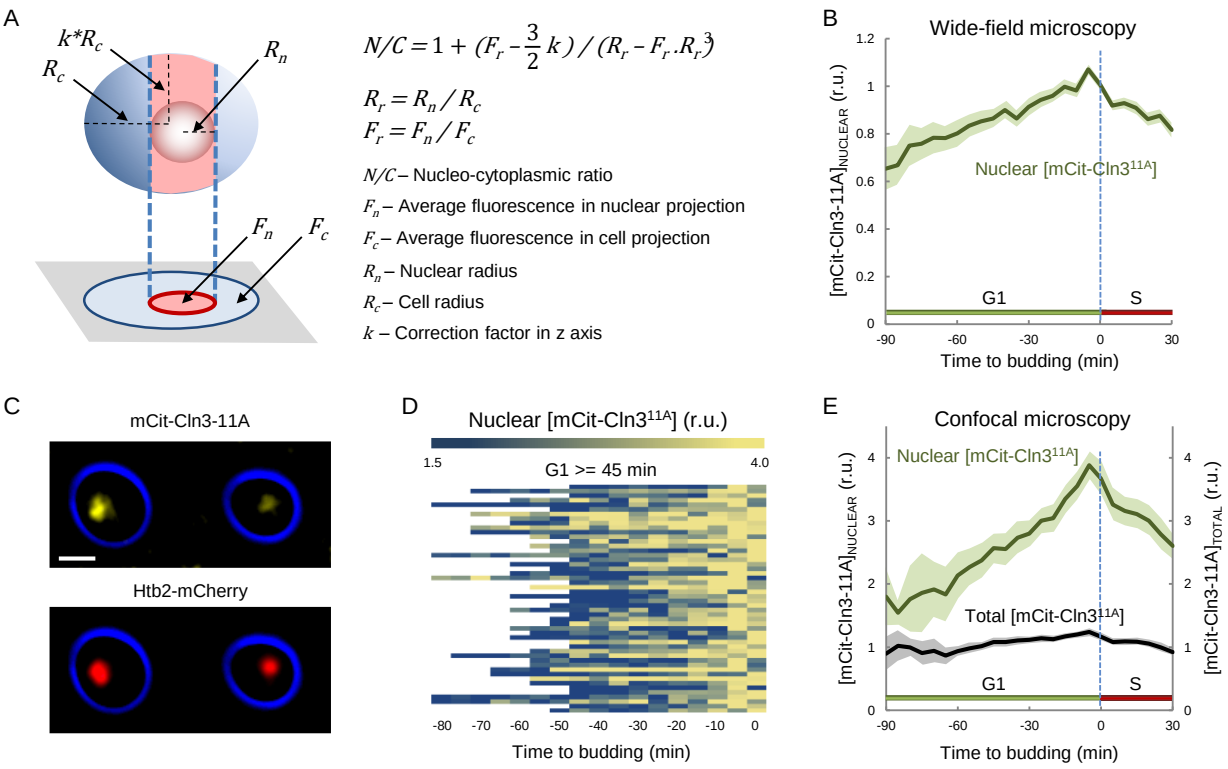

Fig. S1. Cln3^{11A} accumulates in the nucleus during G1 and reaches a maximum around Start

(A) Fluorescence within the nuclear projected area is influenced by fluorescence levels in both nuclear and cytoplasmic compartments. Briefly, the nuclear projection collects fluorescence originated from a column defined by the nuclear diameter and the cell height. Total fluorescence in the column is the weighted sum of nuclear and cytoplasmic concentrations of fluorophore assuming that the column is a cylinder and the nucleus a sphere with known dimensions relative to the cell. Cytoplasmic fluorescence (and concentration) is obtained from cell regions outside the nuclear projection, and the ratio of the nuclear to cytoplasmic concentration of the fluorescent protein is calculated as $N/C = 1 + \left(F_r - \frac{3}{2} * k\right) / \left(R_r - F_r * R_r^3\right)$, where F_r is the ratio of average fluorescence signal in nuclear (F_n) and cell (F_c) projected areas, R_r is the ratio of nuclear (R_n) and cell (R_c) radius, and k corrects for cell radius variation in the z axis, which was experimentally obtained from GFP-expressing wild-type cells. **(B)** Nucleo-cytoplasmic ratio of mCit-Cln3^{11A} measured by wide-field microscopy in G1 cells as in Fig. 1A aligned to budding. Relative mean ± se values (N=100) are plotted. (C) Cells expressing mCit-Cln3^{11A} and mCh-Htb2 were analyzed by confocal time-lapse microscopy during G1 progression and entry into the cell cycle. A representative cell at different times to budding is shown. Bar is 2 µm. **(D)** Heatmap displaying nuclear concentrations of mCit-Cln3^{11A} during G1 and entry into the cell cycle. Relative data were obtained from single cells (N=50) every 5 min and aligned to budding. **(E)** Cellular (total) and nuclear concentrations of mCit-Cln3^{11A} in G1 cells as in panel C aligned to budding. Relative mean ± se values (N=100) are plotted.

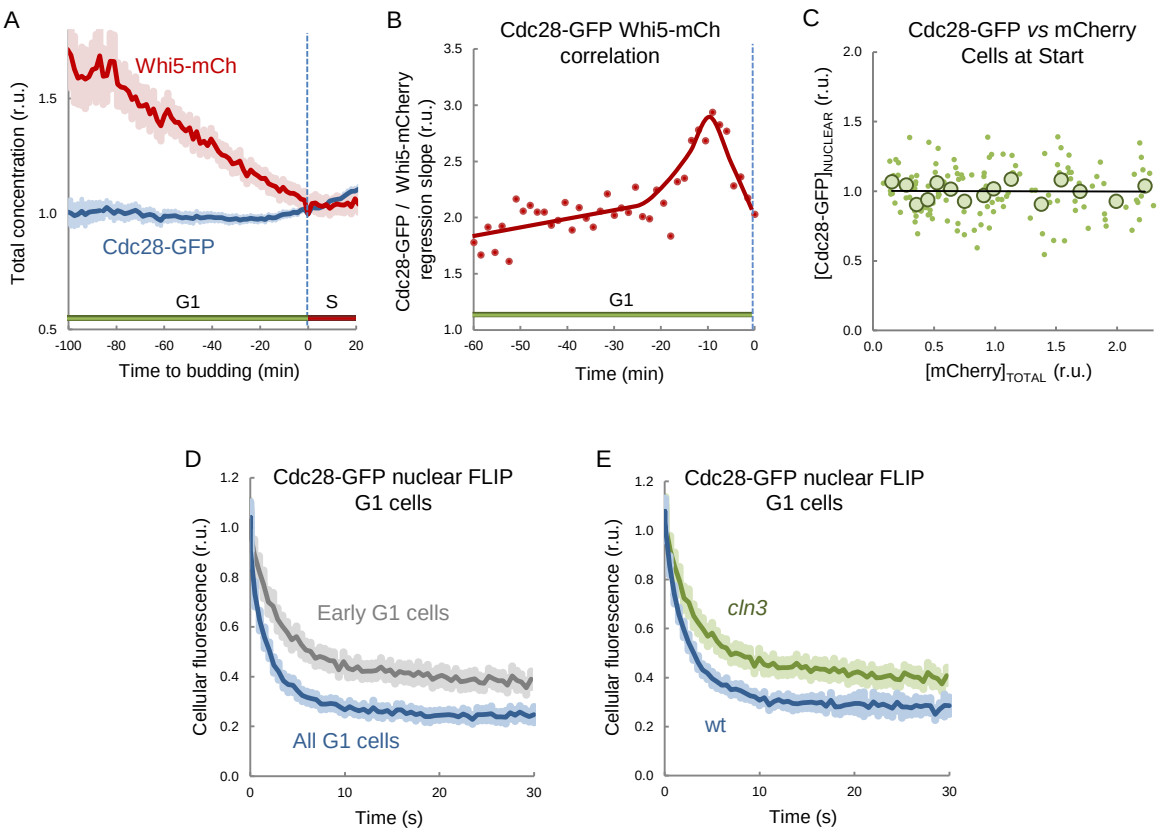

Fig. S2. Cln3 boosts nuclear import of Cdc28-GFP during cell cycle entry

(A) Cellular concentration of Cdc28-GFP and Whi5-mCh during G1 and entry into the cell cycle. Relative mean ± se values (N=100) from cells aligned to budding are plotted. **(B)** Cells as in panel A were analyzed to obtain cellular Whi5-mCherry and nuclear Cdc28-GFP relative concentrations, which were used to perform linear regressions at different times during G1. Slope values and a freehand line are plotted. **(C)** Nuclear Cdc28-GFP concentration as a function of cellular mCherry concentration at Start. Relative single-cell data (N=150, small circles) are plotted. Mean values of binned data (N=10, large circles) and a regression line are also shown. **(D)** Total fluorescence decay of Cdc28-GFP in newborn (early G1) and cycling cells in G1 (all). Relative mean ± se values (N=100) from cells aligned to budding are plotted. **(E)** Total fluorescence decay of Cdc28-GFP in wild-type (wt) and Cln3-deficient (*cln3*) cells in G1. Relative mean ± se values (N=100) from cells aligned to budding are plotted.

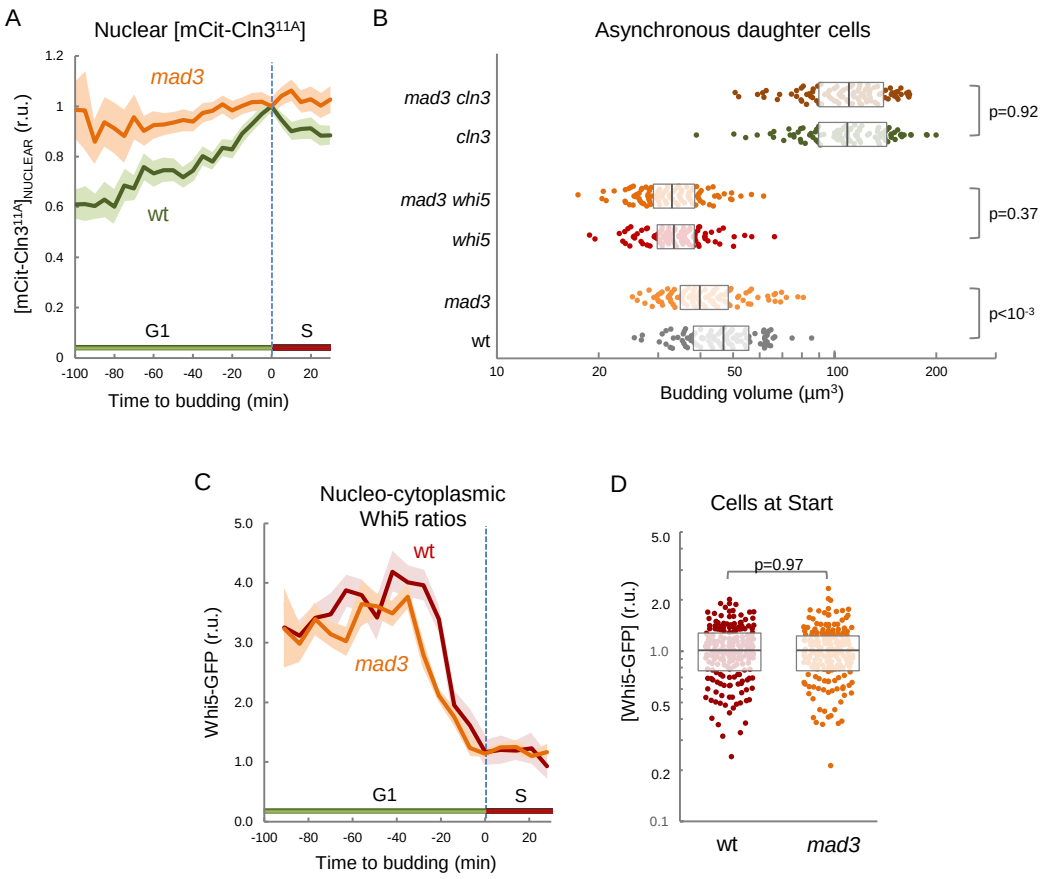

Fig. S3. Mad3 regulates Cln3 levels in G1 but does not modulate Whi5 levels at Start
(A) Nuclear concentration of mCit-Cln3^{11A} in wild-type (wt) and Mad3-deficient (*mad3*) cells aligned to budding. Mean ± se values (N=100) are plotted. **(B)** Budding volume of asynchronous daughter cells with the indicated genotypes. Single-cell data with the corresponding median and quartile values are plotted. Pairwise comparisons were performed with a Mann-Whitney U test, and the resulting p-values are indicated. **(C)** Nucleo-cytoplasmic Whi5-GFP ratios in wild-type (wt) and Mad3-deficient (*mad3*) cells aligned to budding. Mean ± se values (N=100) are plotted. **(D)** Concentration of Whi5-GFP in wild-type (wt) and Mad3-deficient (*mad3*) G1 cells (N=100) at Start. Single-cell data with the corresponding median and quartile values are plotted. Pairwise comparisons were performed with a Mann-Whitney U test, and the resulting p-values are indicated.

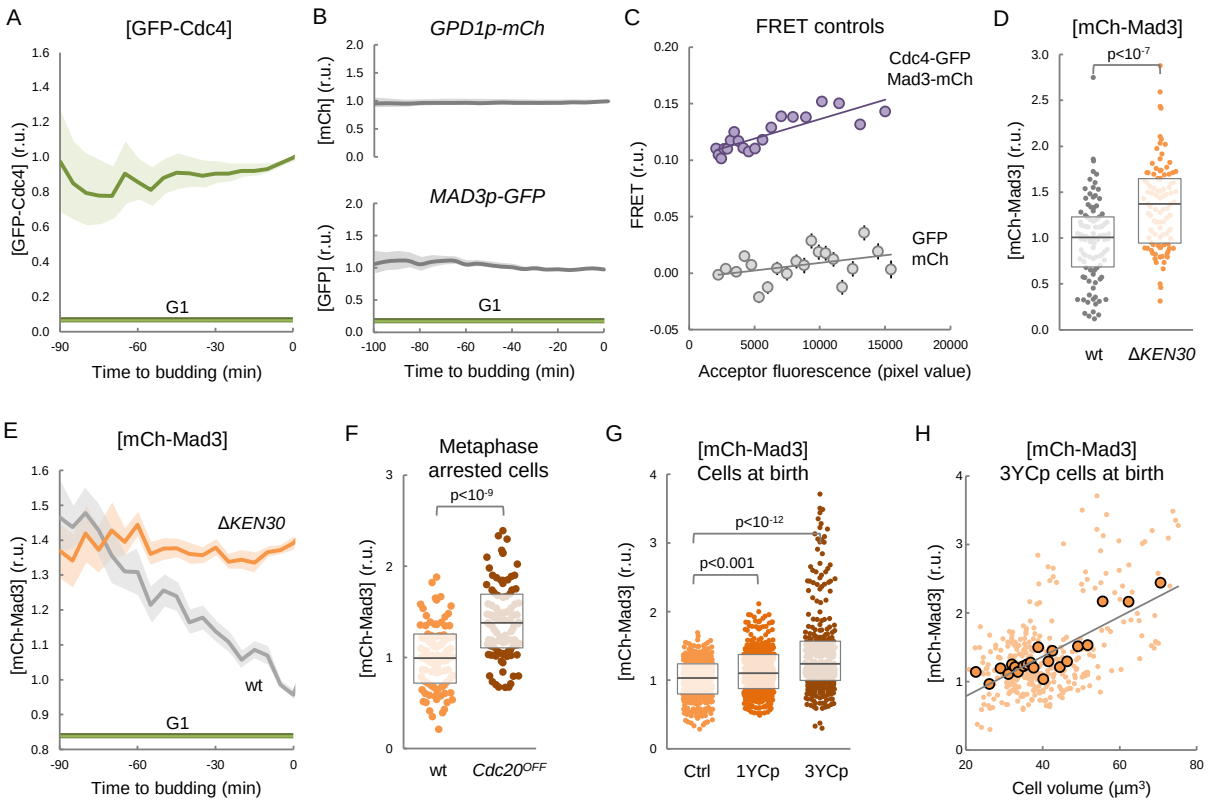

Fig. S4. Mad3 protein levels oscillate during the cell cycle as a function of APC activity

(A) Cellular concentration of GFP-Cdc4 expressed from a constitutive promoter in cycling cells aligned to budding. Relative mean ± se values (N=100) are plotted. **(B)** Cellular concentration of mCherry and GFP expressed from the *GPD1p* and *MAD3p* promoters, respectively, in cycling cells aligned to budding. Relative mean ± se values (N=100) are plotted. **(C)** FRET efficiencies of the GFP-Cdc4 / mCh-Mad3 and GFP / mCh pairs as a function of the acceptor (mCh) fluorescence level. Cells expressing the indicated pair of fluorescent proteins were imaged and the FRET efficiency in random pixels was calculated as described in Materials and Methods and binned by the acceptor fluorescence. Relative mean ± se values (N=1000) with the corresponding linear regression lines are plotted.

(D) Cellular concentration of mCh fused to wild-type or ΔKEN30 Mad3 proteins at budding. Single-cell data with the corresponding median and quartile values are plotted. Pairwise comparisons were performed with a Mann-Whitney U test, and the resulting p-values are indicated. **(E)** Cellular concentration of mCh fused to wild-type or ΔKEN30 Mad3 proteins in cycling cells aligned to budding. Relative mean ± se values (N=100) to that of wild-type cells at budding are plotted. **(F)** Concentration of mCh-Mad3 in Cdc20-arrested cells. Single-cell data with the corresponding median and quartile values are plotted. Pairwise comparisons were performed with a Mann-Whitney U test, and the resulting p-values are indicated. **(G)** Concentration of mCh-Mad3 in cells at birth containing none (Ctrl), one (YCp) or three (3YCp) centromeric vectors. Single-cell data with the corresponding median and quartile values are plotted. Pairwise comparisons were performed with a Mann-Whitney U test, and the resulting p-values are indicated. **(H)** Cellular concentration of mCh-Mad3 in wild-type cells at birth containing three centromeric vectors as a function of cell volume. Relative single-cell (N=300, small circles) and binned data (N=20, large circles) with the corresponding regression lines are plotted.

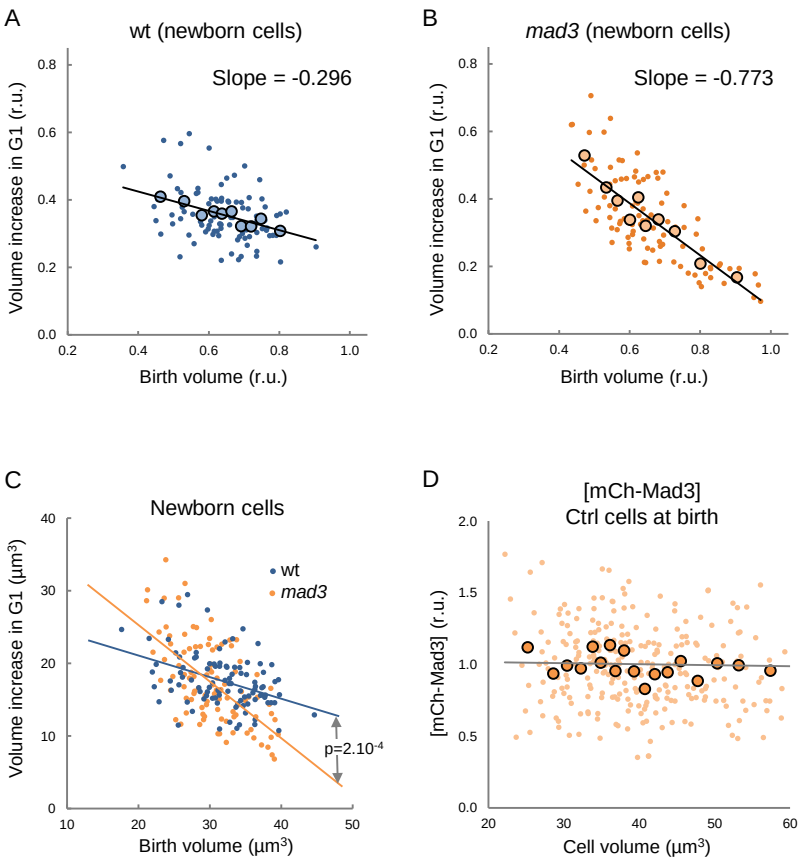

Fig. S5. Mad3 tilts the sizer behavior of G1 control

(A, B) Cell volume increase during G1 as a function of birth volume in newborn wild-type (wt, A) and Mad3-deficient (mad3, B) cells. Relative single-cell data (N=100, small circles) are plotted. Mean values of binned data (N=10, large circles) and regression lines are also shown. **(C)** Single-cell data of wild-type (wt) and Mad3-deficient (mad3) cells in panels A and B are plotted in non-normalized volume units (μm^3) with the corresponding regression lines. Slopes were compared with a t test, and the resulting p value is shown. **(D)** Cellular concentration of mCh-Mad3 in wild-type cells at birth as a function of cell volume. Relative single-cell (N=300, small circles) and binned data (N=20, large circles) with the corresponding regression lines are plotted.

Table S1. Yeast strains

Strain	Source
CML128 (Mat**a** *leu2-3,112 trp1-1 ura3-52 his4-1 can1-100*)	Our lab stocks
W303-1A (Mat**a** *leu2-3,112 trp1-1 ura3-1 ade2-1 his3-11,15 can1-100*)	Our lab stocks
KSY083-5 (*mCitrine-CLN3^{11A}::NAT*)	Jan Skotheim
CYC216 (*CDC28-GFP::KAN)*	This study
CYC228 (*CDC28-GFP::KAN cln3::LEU2*)	This study
CYC457 (*CDC28-GFP::KAN HTB2-mCherry::HYG*)	This study
CYC459 (*CDC28-GFP::KAN HTB2-mCherry::HYG cln3::LEU2*)	This study
MAG714 (*whi5::KAN*)	This study
MAG1092 (*CDC28-GFP::KAN WHI5-mCherry::HYG*)	This study
MAG1334 (*mCitrine-CLN3^{11A}::NAT HTB2-mCherry::HYG*)	This study
MAG1463 (*whi5::LEU2 mad3::KAN*)	This study
MAG2013 (*mCitrine-CLN3^{11A}::NAT mad3::KAN*)	This study
MAG2458 (*TEF1p-GFP-CDC4::NAT*)	This study
MAG2501 (*GPD1p-mCherry-MAD3::KAN*)	This study
MAG2509 (*GPD1p-mCherry-MAD3::KAN TEF1p-GFP-CDC4::NAT*)	This study
MAG2510 (*mad3::KAN*)	This study
MAG2621 (*GPD1p-mCherry-MAD3::HIS3 GAL1p- CDC20::KAN*)	This study
MAG2771 (*WHI5-GFP::KAN*)	This study
MAG2773 (*WHI5-GFP::KAN mad3::HIS3*)	This study
MAG2823 (*MAD3p-GFP::HIS3)*	This study
MAG2825 (*GPD1p-mCherry::KAN*)	This study
MAG2827 (*cln3::TRP1*)	This study
MAG2829 (*cln3::TRP1 mad3::KAN*)	This study

JCB Journal of Cell Biology

Rockefeller University Press

Stress granules display bistable dynamics modulated by Cdk

Galal Yahya[1,2,*], Alexis P. Pérez[1,3,*], Mònica B. Mendoza[1], Eva Parisi[1], David F. Moreno[1], Marta H. Artés[1], Carme Gallego[1,ŧ], Martí Aldea[1,3,ŧ]

[1]Molecular Biology Institute of Barcelona (IBMB), CSIC, Catalonia, 08028, Spain

[2]Department of Microbiology and Immunology, Zagazig University, 44519, Egypt

[3]Department of Basic Sciences, Universitat Internacional de Catalunya, 08195, Spain

[*]These authors contributed equally to this work

[ŧ] Corresponding authors: carme.gallego@ibmb.csic.es and marti.aldea@ibmb.csic.es

Alexis Pérez contribution: Investigation and data analysis.

Journal of Cell Biology 220: e202005102 (2021)

Abstract

Stress granules are conserved biomolecular condensates that originate in response to many stress conditions. These membraneless organelles contain nontranslating mRNAs and a diverse subproteome, but our knowledge on their regulation and functional relevance is still incipient. Here we describe a mutual-inhibition interplay between stress granules and Cdc28, the budding yeast Cdk. Amongst Cdc28 interactors acting as negative modulators of Start we have identified Whi8, an RNA-binding protein that localizes to SGs and recruits the mRNA of *CLN3*, the most upstream G1 cyclin, for efficient translation inhibition and Cdk inactivation under stress. However, Whi8 also contributes to recruiting Cdc28 to SGs, where it acts to promote their dissolution. As predicted by a mutual-inhibition framework, the SG constitutes a bistable system that is modulated by Cdk. Since mammalian cells display a homologous mechanism, we propose that the opposing functions of specific mRNA-binding proteins and Cdks subjugate SG dynamics to a conserved hysteretic switch.

eTOC summary: Stress granules are biomolecular condensates of nontranslating mRNAs and diverse proteins. Yahya et al. uncover a mutual-inhibition system between stress granules and the cyclin-dependent kinase, the key cell cycle regulator, whereby Cdks regulate SG dynamics and SGs contribute to inhibiting cyclin transcript translation.

Introduction

Phase separation of proteins and nucleic acids into condensates is emerging as a general mechanism for cellular compartmentalization without the requirement of surrounding membranes (Alberti and Dormann, 2019; Banani et al., 2017; Shin and Brangwynne, 2017). These biomolecular condensates are based on weak multivalent interactions among component molecules that are mobile and exchange with the adjoining medium, and play essential roles in cell physiology as reaction crucibles, sequestration centers or organizational hubs. In a dynamic environment, cells need to control phase separation to form or dissolve condensates as a function of spatial and temporal cues. Thus, the molecular mechanisms that modulate phase separation will be critical to understanding how cells use biomolecular condensates to execute and control a growing list of cellular processes (Alberti et al., 2019; Bratek-Skicki et al., 2020; Snead and Gladfelter, 2019).

Stress granules (SGs) are conserved cytoplasmic condensates that contain (1) pools of nontranslating mRNAs and (2) a variety of proteins, including translation initiation factors and RNA-binding proteins that form core stable substructures in SGs (Protter and Parker, 2016b). Non RNA-binding proteins such as post-translational modification factors, and protein or RNA remodeling complexes, are recruited to SGs by protein–protein interactions often mediated by intrinsically-disordered regions (IDRs), and modulate SG assembly and disassembly. However, a predominant role has been recently attributed to intermolecular RNA-RNA interactions as upstream determinants of stress granule composition (Van Treeck et al., 2018). Although SGs are thought to downregulate translation and protect recruited mRNAs in many different stress conditions, we still do not have sufficient experimental evidence to comprehend the relevance of SGs in cell physiology.

Stress restricts cell-cycle progression and budding yeast cells display a diverse set of mechanisms as a function of the stress signal. The HOG pathway constitutes a prominent paradigm, and operates on specific molecular targets to modulate different cell-cycle phases and transitions in response to osmotic stress (De Nadal et al., 2011; Solé et al., 2015). Regarding entry into the cell cycle, osmotic shock causes a temporary repression of the G1/S regulon (Bellí et al., 2001), in which Hog1-mediated phosphorylation of Whi5 and Msa1 contributes to inhibiting transcription (González-Novo et al., 2015). Downregulation of G1/S genes was also observed during heat and ER stress (Rowley et al., 1993; Vai et al., 1987) and, since chaperones play important but limiting roles at Start (Parisi et al., 2018b; Vergés et al., 2007b; Yahya et al., 2014), we proposed that, by compromising chaperone availability, all stressful conditions would target the chaperome as a common means to hinder entry into the cell cycle (Moreno et al., 2019a). However, the precise molecular environment in which diverse stress conditions would converge to modulate Start is still unknown.

Here we describe the interplay between a common actor in stress, SGs, and the budding yeast Cdk, Cdc28. In a screen for Cdc28 interactors acting as negative modulators of Start we identified Whi8, a putative RNA-binding protein previously localized to SGs. Whi8 is important for recruiting the mRNA of *CLN3*, the most upstream G1 cyclin, to SGs and contributes to inhibiting its translation under stress conditions. On the other hand, Whi8-dependent recruitment of Cdc28 is important for timely dissolution of SGs when stress conditions are relieved. We also identified the key elements of a homologue mechanism in mammalian cells, and we propose that Cdks create a conserved bistable system that regulates SG dynamics.

Results

Whi8 is a Cdc28 interactor that hinders cell cycle entry

We previously identified and characterized a $Cdc28^{wee}$ mutant that produces premature entry into the cell cycle causing a small cell-size phenotype and, to uncover new negative modulators of Start, we used quantitative proteomics to compare the interactomes of wild-type and wee Cdc28 proteins (Yahya et al., 2014) (Fig. 1A). The $Cdc28^{wee}$ mutant was expressed at similar levels to the wt Cdc28 protein but showed impaired retention at the ER and caused premature accumulation of the Cln3 cyclin in the nucleus (Yahya et al., 2014). The five amino-acid substitutions in the $Cdc28^{wee}$ mutant are found clustered in the C-terminal lobe of Cdc28, far from the cyclin-binding region and the kinase cleft, and mostly affect basic amino acids with likely exposed side chains, suggesting that the $Cdc28^{wee}$ mutant has altered interaction properties with negative regulators of the yeast Cdk. Among the group of proteins displaying a lower binding to $Cdc28^{wee}$ we found YGR250c, a putative RNA-binding protein that has been localized to stress granules (Buchan et al., 2008) and recently isolated as a multicopy suppressor of ER-mitochondria tethering complex defects (Kojima et al., 2016). To ascertain its role as a negative regulator of the yeast Cdk at Start we measured the budding volume of cells lacking YGR250c, and found a clear reduction that strictly required the presence of Cln3, the most upstream G1 cyclin (Fig. 1B). Since overexpression of YGR250c produced the opposite effect and increased the budding volume by nearly 50%, we named YGR250c as Whi8, following the nomenclature of genes modulating cell size at Start.

As expected, Whi8 levels were lower in $Cdc28^{wee}$ immunoprecipitates compared to wild-type Cdc28 (Fig. 1C), suggesting that the negative role of Whi8 at Start is mediated by physical interaction with the Cdc28 kinase. Notably, a bioinformatics analysis of 480 Cdc28 interacting proteins pinpointed Whi8 as the only gene product that (1) displays RNA-binding motifs, (2) is induced by heat shock and (3) is present in SGs (Fig. 1D). In all, Whi8 emerged as a putative mediator of SG-born signals restraining entry into the cell cycle.

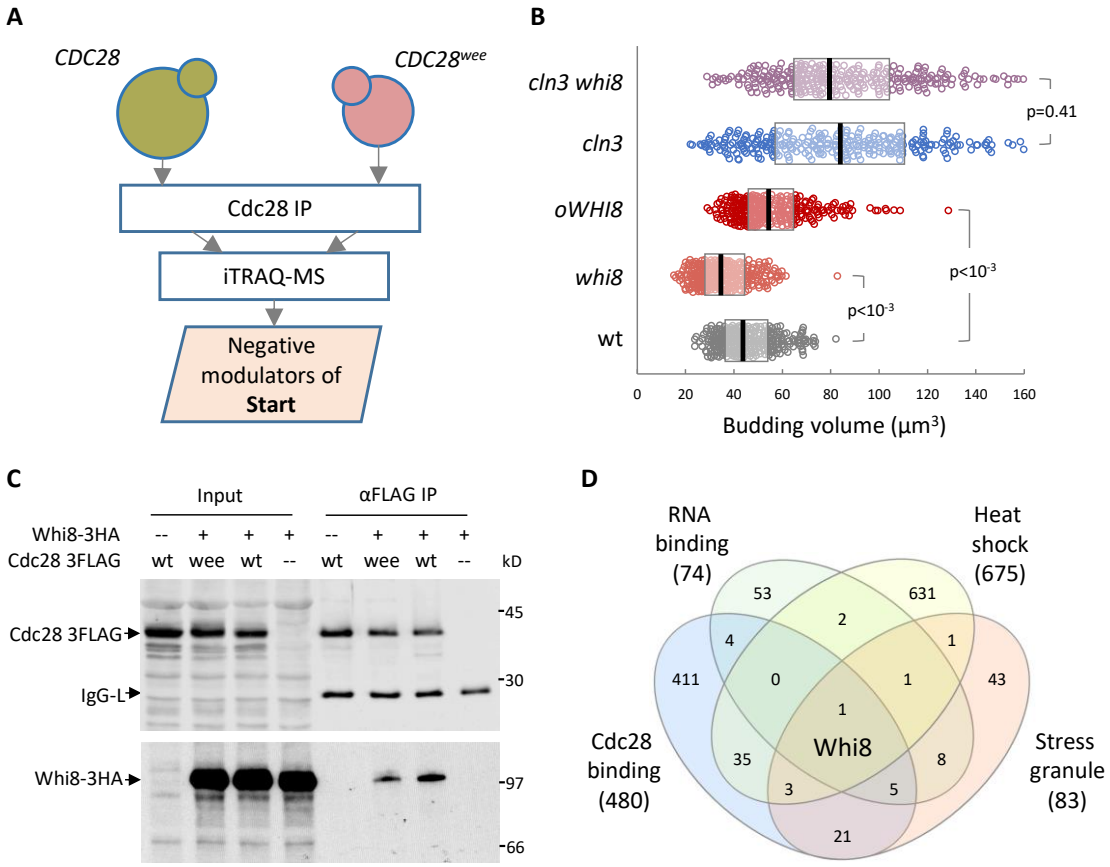

Fig. 1. Whi8 is a Cdc28 interactor that hinders cell cycle entry

(A) Schematic of the screen for Cdc28 interactors as negative regulators of Start (Yahya *et al*, 2014). Briefly, pulldowns of wild-type and *wee* Cdc28 were analyzed by iTRAQ-based proteomics to identify proteins with a reduced affinity for Cdc28^{wee}. **(B)** Cells with the indicated genotypes were analyzed to determine cell size at budding. Individual data (n>300) and median ± Q values are plotted. Shown p-values were obtained using a Mann-Whitney U test. **(C)** Immunoblot of input and αFLAG immunoprecipitation samples from *WHI8-3HA* cells with plasmids expressing wild-type or mutant (*wee*) Cdc28-3FLAG proteins. **(D)** Venn diagram showing the overlapping of proteins that are (1) physical interactors of Cdc28, (2) contain demonstrated or putative RNA-binding domains, (3) are upregulated by heat shock and (4) were identified as SG components.

Whi8 binds and recruits the CLN3 mRNA to SGs

Since *cln3* was totally epistatic to the loss of Whi8 with regards to the cell size phenotype, we wanted to test whether the role of Whi8 at Start would be exerted on *CLN3*, perhaps due to its RNA-binding properties. We found that the *CLN3* mRNA was enriched 10-fold in Whi8 immunoprecipitates (Fig. 2A), thus displaying a similar behavior to Whi3, a protein previously shown to bind the *CLN3* mRNA and regulate cell cycle entry (Colomina et al., 2008; Garí et al., 2001a). Supporting shared roles in modulating *CLN3* expression by their RNA-binding motifs, Whi8 and Whi3 were found to co-immunoprecipitate in an RNA-dependent manner (Fig. 2B). By contrast, the interaction between Whi8 and Pub1, a component of SGs, did not depend on RNA (Fig. 2C).

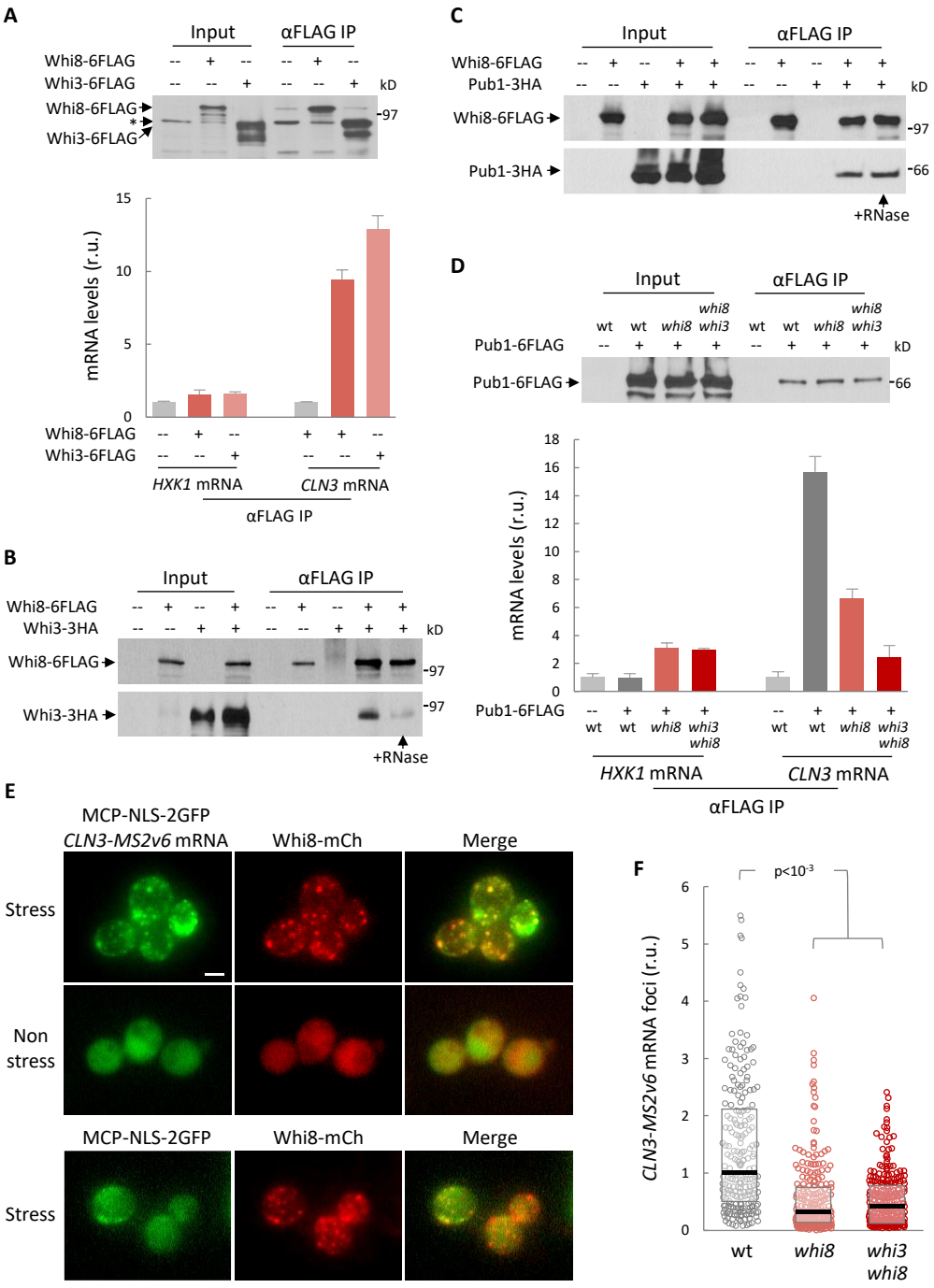

Fig. 2. Whi8 binds and recruits the *CLN3* mRNA to SGs

(A) Immunoblot of input and αFLAG immunoprecipitates (IP) from *WHI8-6FLAG*, *WHI3-6FLAG* or untagged cells (top). Levels of *CLN3* and *HXK1* (as control) mRNAs in IPs were determined and mean + SEM values (n=3) are plotted (bottom). **(B, C)** Immunoblots of input and αFLAG IPs from cells expressing the indicated proteins. RNase was added during immunoprecipitation when indicated. **(D)** Wild-type, *whi8* or double *whi8 whi3* mutant cells expressing Pub1-6FLAG were stressed at 42ºC for 30 min in the absence of glucose. An immunoblot of input and αFLAG IPs is shown at the top. Levels of *CLN3* and *HXK1* (as control) mRNAs were determined and mean + SEM values (n=3) are plotted (bottom). **(E)** *WHI8-mCh* cells with plasmids expressing *CLN3-MS2v6 and MCP-NLS-2GFP* after 30 min at 42ºC in the absence of glucose (top). Non-stressed (center) and stressed *CLN3* control (bottom) cells are also shown. Bar, 2 µm. **(F)** *PUB1-mCh* cells with the indicated genotypes with plasmids expressing *CLN3-MS2v6* and *MCP-NLS-2GFP* were stressed as above. MCP-NLS-2GFP foci (n>250) and median ± Q values are plotted. Shown p-values were obtained using a Mann-Whitney U test.

The *CLN3* mRNA was clearly enriched in Pub1 pulldowns in stressed cells (Fig. 2D) which, considering the abovementioned interactions, suggested that Pub1 could recruit the *CLN3* mRNA to SGs through Whi8. In agreement with this idea, enrichment of the *CLN3* mRNA in Pub1 pulldowns was strongly diminished in *whi8* cells and totally abrogated in double *whi8 whi3* cells under stress conditions (Fig. 2D). We next tested whether the *CLN3* mRNA colocalized with Whi8 in SGs using the MS2v6 system (Tutucci et al., 2018). We observed some autofluorescent foci in control cells under stress, but they were in much lower numbers per cell compared to those produced by MCP-NLS-2GFP in the presence of the *CLN3-MS2v6* mRNA (Fig S1A), which did not form foci in the absence of stress (Fig. 2E). As already described (Buchan et al., 2008), Whi8-GFP readily formed bright granules in the cytoplasm under stress conditions, where the *CLN3* mRNA readily colocalized (Fig. 2E). Although the *CLN3* mRNA was previously found in SGs with Whi3 (Cai and Futcher, 2013; Holmes et al., 2013), the presence of Whi3 was totally dispensable. We found that colocalization of the *CLN3* mRNA with Pub1-mCherry granules required Whi8 and, to a much lesser extent, Whi3 (Fig. 2F and S1B), which gives further support to the notion that the *CLN3* transcript is recruited to SGs with the essential role of Whi8.

Whi8 is recruited to SGs via an IDR and is required to inhibit CLN3 mRNA translation under stress

Whi8 contains a C-terminal region of 120 residues largely dominated by disorder-prone amino acids (Fig. 3A), suggesting that Whi8 could be recruited to SGs by an IDR. Deletion of these amino acids did not have any noticeable effect on cell size under normal growing conditions, but Whi8-ΔIDR was completely absent in the ER fractions as compared to the wild-type protein (Fig. 3B). Moreover, although Whi8-ΔIDR was still recruited to SGs under stress conditions, the number of foci per cell and the fraction of Whi8-ΔIDR in SGs were sharply reduced (Fig. 3C-F).

One of the hallmarks of SG-recruited mRNAs is translation inhibition which, particularly for short-lived proteins such as Cln3, may have important effects in the corresponding downstream processes. We found that Cln3 levels rapidly decreased under stress conditions (Fig. S2A), reaching a five-fold reduction in less than 30 min, while the *CLN3* mRNA was only reduced by 40% compared to unstressed cells (Fig. S2C). Notably, levels of Cln3 decreased very slowly in cells lacking Whi8 (Fig. S2A), thus reinforcing the notion that Whi8 would recruit the *CLN3* mRNA to SGs to inhibit its translation under stress conditions. Overexpression of SG components promotes SG formation and recapitulates inhibition of SG-reporter gene expression in non-stressed cells (Kedersha and Anderson, 2007). Accordingly, when we overexpressed Whi8 in the absence of stress we observed a significant decrease in Cln3 protein levels (Fig. S2B), while mRNA levels remained unchanged (Fig. S2C). Whi8 overexpression did not induce SG formation, suggesting that Whi8 would have a direct effect on *CLN3* mRNA translation. Similarly to Whi3 (Wang et al., 2004) and Whi7 (Yahya et al., 2014), loss or overexpression of Whi8 increased or decreased, respectively, the nuclear levels of Cln3 (Fig. S2D).

These data would explain the observed large cell-size phenotype of Whi8-overexpressing cells, and emphasize the idea that Whi8 acts as a negative regulator of Start by modulating expression of the *CLN3* mRNA.

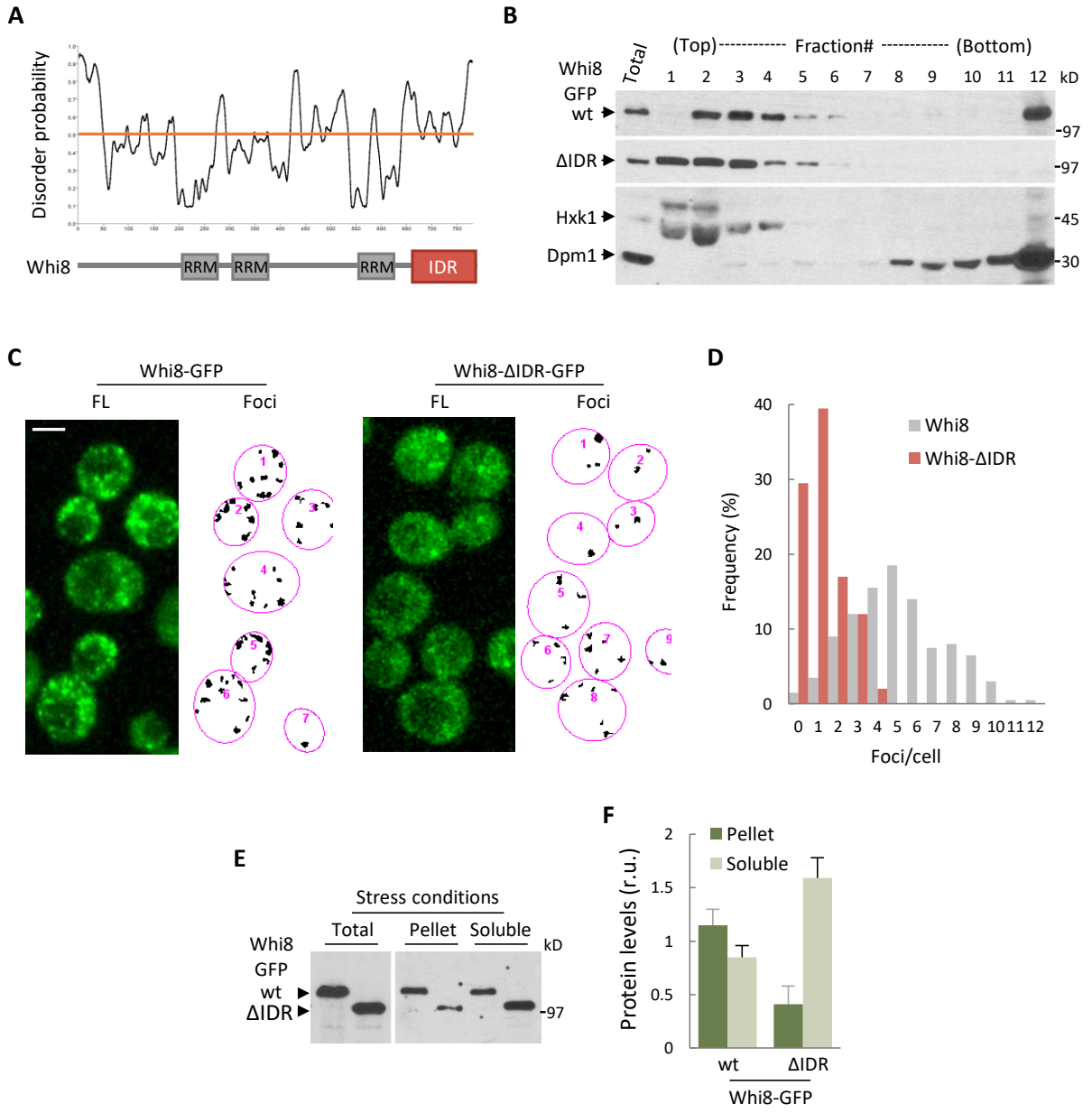

Fig. 3. Whi8 contains an IDR important for SG recruitment

(A) Disorder probability of Whi8 amino acids and predicted RRMs and IDR. **(B)** Immunoblot analysis of the distribution of wild-type and ΔIDR Whi8-GFP in sucrose gradients. Hxk1 and Dpm1 are shown as soluble and ER markers, respectively. **(C)** Maximum projections (FL) of confocal images from cells expressing wild-type and ΔIDR Whi8-GFP after 30 min at 42ºC in the absence of glucose. Bar, 2 µm. Foci detected above a fixed local threshold with the aid of BudJ are also shown. **(D)** Cells expressing wild-type and ΔIDR Whi8-GFP were treated at 42ºC in the absence of glucose, and analyzed as in Fig. 4A. Foci frequencies per cell are plotted (n=200). **(E)** Immunoblot of wild-type and ΔIDR Whi8-GFP in the indicated fractions from cells as in D. **(F)** Whi8-GFP levels as in **e** were quantified and mean + SEM values (n=3) are plotted.

Cdc28 is recruited to SGs and modulates SG dynamics

Cdc28 has been colocalized with Pbp1 in foci of stationary-phase cells (Shah et al., 2014) and, although not quantitative, a proteomic survey reported the presence of Cdc28 in SGs (Jain et al., 2016b). To ascertain this possibility, we analyzed Cdc28-GFP and Pub1-mCherry in live cells under stress conditions and found that both proteins displayed extensive colocalization patterns (Fig. 4A). Careful measurement of the relative levels of the two proteins in SGs yielded a steeper slope when Cdc28-GFP was taken as a dependent variable (Fig. 4B), favoring Pub1 as an upstream factor for Cdc28 localization to SGs. Notably, the ratio of Cdc28-GFP to Pub1-mCherry in SGs decreased to ca. 40% when comparing *whi8* with wild-type cells (Fig. 4C and Fig. S3A). Similarly to other components of the SG (Youn et al., 2018), Cdc28 and Pub1 were found to co-immunoprecipitate under non-stress conditions (Fig. 4D). In all, these data underscore the relevance of Whi8 and Pub1 in recruiting Cdc28 to SGs.

A significant number of SG proteins (Jain et al., 2016b) may be phosphorylation targets of Cdc28 (Fig. 4E) and, in addition to Whi8, we found several translation initiation factors that are thought to be involved in translational repression in SGs (Table S1). This observation led us to hypothesize that Cdc28 could play a role in SG assembly and dissolution. To test this possibility, we carefully measured the dissolution kinetics of Pub1-mCherry foci by time-lapse microscopy, and first compared cells carrying wild-type *CDC28* and thermosensitive *cdc28-13* alleles. Glucose was added to induce release from stress, but the temperature was only decreased to 37ºC to maintain a restrictive scenario for the *cdc28-13* allele. As shown in Fig. 4F, wild-type cells readily dissolved SGs under these partial-release conditions, and the levels of Pub1-mCherry in SGs decreased to 50% in only 21 min. By contrast, SG dissolution was much slower in *cdc28-13* cells, taking longer than 60 min to reach a 50% reduction in Pub1-mCherry in SGs (Fig. 4F).

As an independent approach we used a G1-cyclin conditional strain that lacks Cln1,2 and holds Cln3 under the control of a regulatable promoter, which causes cells to arrest in G1 with no Cdk activity under repression conditions. We found a strikingly similar delay in SG dissolution when comparing G1-arrested and cycling cells (Fig. 4G), which confirms the key role of Cdk activity in SG dissolution. Giving further support to this notion, cycling wild-type cells displayed clear differences in SG dissolution kinetics depending on cell cycle position, being slower when Cdk activity is lower, i.e. G1 phase (Fig. S3B). Finally, overexpression of Cln3 produced the opposite effects and reduced by 30% the half-life of SGs after release form stress (Fig. 4F). Albeit surprisingly, the presence of *CLN3-1*, a truncated hyperstable allele that reproduces most phenotypes of *CLN3* overexpression, was much less effective in SG dissolution (Fig. S3C). Cln3-1 lacks a putative 91-aa IDR that could play additional roles in recruiting the Cdc28/Cln3 complex to SGs.

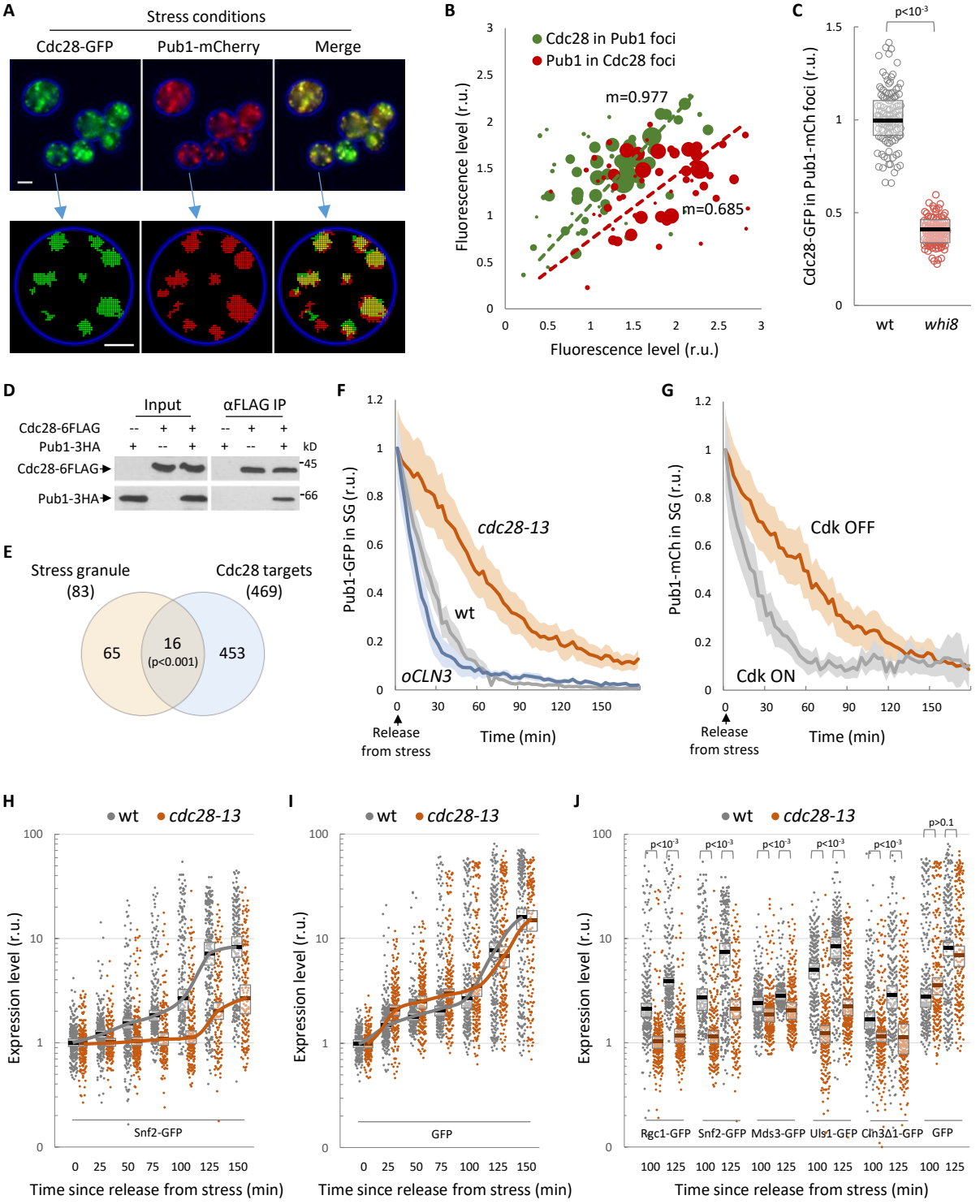

Fig. 4. Cdc28 is recruited to SGs and modulates SG dynamics

(A) Maximum projections of confocal images from cells expressing Cdc8-GFP and Pub1-mCherry after 30 min at 42ºC in the absence of glucose (top). Bar, 2 µm. GFP and mCherry foci detected for quantification in a sample cell with the aid of BudJ are also shown at the bottom (bar, 1 µm). **(B)** Cdc8-GFP levels in Pub1-mCherry foci (n=60), and vice versa, from cells as in A are plotted with point diameter corresponding to foci size. Slope (m) values are also shown. **(C)** Cdc8-GFP levels in Pub1-mCherry foci were measured in wild-type and *whi8* cells stressed for 30 min at 42ºC in the absence of glucose. Individual data (n=125) and median ± Q values are plotted. Shown p-value was obtained using a Mann-Whitney U test. **(D)** Immunoblot of input and αFLAG

immunoprecipitation samples from cells expressing Cdc28-6FLAG and Pub1-3HA. **(E)** Venn diagram showing the overlapping of proteins that (1) were identified as SG components and (2) are putative phosphorylation targets of Cdc28. The indicated p-value was obtained assuming completely independent allocations. **(F)** Wild-type, *cdc28-13* and *oCLN3* (*tetO$_2$-CLN3*) cells expressing Pub1-mCherry were stressed for 30 min at 42ºC in the absence of glucose and, once released at 37ºC in the presence of glucose, Pub1-mCherry levels in foci were measured at different time points. Mean values (n>30) and confidence limits for the mean (α=0.05) are plotted. **(G)** *GAL1p-CLN3 cln1,2* cells expressing Pub1-mCherry were grown in galactose and arrested in G1 by transfer to glucose for 2 h (Cdk OFF). Cells were then stressed for 30 min at 42ºC in the absence of glucose and, once released at 30ºC in the presence of glucose to maintain the G1 arrest, Pub1-mCherry levels in foci were measured at different time points. As control, *CLN3 cln1,2* cells (Cdk ON) were subject to the same experimental conditions. Mean values (n>30) and confidence limits for the mean (α=0.05) are plotted. **(H,I)** Wild-type (gray) and *cdc28-13* (orange) cells expressing the Gal4-hER-VP16 transactivator and plasmid-borne *SNF2-GFP* (H) or GFP (I) from the *GAL1p* promoter were added estradiol and immediately treated for 30 min at 42ºC in the absence of glucose. Once released at 30ºC in the presence of glucose, estradiol was removed to limit further accumulation of the *SNF2-GFP* mRNA. Single-cell fluorescence levels at the indicated time points are plotted. Median values (n>200) and confidence limits for the median (α=0.05) are also shown. **(J)** Wild-type (gray) and *cdc28-13* (orange) cells with plasmids expressing the indicated GFP fusions from the *GAL1p* promoter were analyzed as in panel H. Single-cell fluorescence levels at the indicated time points after release from stress are plotted. Median values (n>200), confidence limits for the median (α=0.05) are p-values using a Mann-Whitney U test are also shown.

Next, we tested whether translation of SG-recruited mRNAs also depended on Cdk activity during release from stress. First, we selected four highly-expressed mRNAs known to accumulate in SGs (Khong et al., 2017) that contain ORFs in the range of 1 to 6 kb and code for proteins readily detectable in the cytoplasm or the nucleus when fused to GFP (Huh et al., 2003): *SNF2*, *RGC1*, *MDS3* and *ULS1*. As a paradigmatic example of a highly-translated transcript (Siwiak and Zielenkiewicz, 2010) we first analyzed the *SNF2* mRNA. Expression of a C-terminal fusion of Snf2 to GFP under the *GAL1* promoter was induced with estradiol immediately after cells were subject to stress. After 30 min cells were placed under normal growth conditions in the absence of estradiol to limit further mRNA accumulation, and fluorescence levels were measured at different times during and after release from stress. In agreement with the fact that overall translation is rapidly inhibited (Crawford and Pavitt, 2019), Snf2-GFP fluorescence did not change significantly (p=0.17) during stress, and gradually increased up to 8-fold when wild-type cells were returned to normal conditions (Fig. 4H). Notably, whereas *SNF2-GFP* mRNA levels in wild-type and *cdc28-13* cells were comparable during recovery from stress (Fig. S3D), Snf2-GFP fluorescence levels were much lower in *cdc28-13* cells and reached only a 2.5-fold increase at the final time point. We used free GFP as control, and observed no significant differences in fluorescence increase when comparing wild-type and *cdc28-13* cells (Fig. 4I and S3D). Finally, we also analyzed other SG-recruited mRNAs such as *RGC1*, *MDS3, ULS1* and *CLN3Δ1,* a hyperstable truncated allele that allows detection of the GFP fusion, and observed a Cdc28-dependent resumption of translation similar to that of *SNF2* (Fig. 4J and S3D). In all, these data demonstrate the important role of the Cdk in relieving translation inhibition of SG-recruited mRNAs, and suggest a cause-effect relationship between SG dissolution and translation resumption.

Mammalian SGs contain Cdk-cyclin factors and are modulated by cell cycle position

SGs from yeast and mammalian cells display a highly significant overlap in composition and share distinct substructural traits (Jain et al., 2016b). Thus, we anticipated that our findings in yeast cells would also apply to mammalian SGs. To test whether G1 cyclin mRNAs are recruited to mammalian SGs we used the MS2-based approach and observed a clear co-localization of a *CCND1-MS2* mRNA with TIA1, the Pub1 mammalian homologue, in SGs of HeLa cells (Fig. S4A). Caprin1, a component of SGs, binds the cyclin D2 mRNA in non-stressed 293T cells (Solomon et al., 2007). Thus, we tested whether Caprin1 would play a role in recruiting the cyclin D1 mRNA to SGs. First, we found that Caprin1 and the *CCND1-MS2* mRNA colocalized in SGs (Fig. 5A). Interestingly, shRNA-driven downregulation of Caprin1 levels was accompanied by a reduction in the number of foci produced by the *CCND1-MS2* mRNA under stress conditions (Fig. 5B). SG formation, as assessed by TIA1 immunofluorescence, was not significantly affected in HeLa cells (Fig. S4B). However, Caprin downregulation has been shown to decrease the number of SGs in AS-treated U2OS cells (Kedersha et al., 2016). This discrepancy may be due to the different cell lines or, alternatively, to the fact that Caprin1 knockdown in our experiments was not as effective as that obtained in U2OS cells (Kedersha et al., 2016). In any event, even considering that SG number is not strongly affected in HeLa cells, the decrease levels of Caprin1 could also affect the ability of SG to recruit other proteins. In all, our data suggest that Caprin1 plays a direct or indirect role in *CCND1* mRNA recruitment to SGs, thus acting as a functional homologue of Whi8 in mammalian cells, where cyclin D1 protein levels are also strongly downregulated during SGs formation (Fig. S4C). Next, we decided to test whether Caprin1 and Cdk4, a G1 Cdk, interact by co-immunoprecipitation as in yeast cells, and found that these proteins are bound in a stress-dependent manner in HeLa cells (Fig. 5C). Moreover, we observed almost overlapping patterns of localization of Caprin1 and Cdk4 in SGs (Fig. 5D).

The rate of SG dissolution has been shown to be strongly diminished by Cdk inhibitors in HeLa and U2OS cells (Wippich et al., 2013b). Hence, the presence of a G1 Cdk and the Caprin1-mediated recruitment of a G1 cyclin mRNA in SGs suggested that cell cycle progression could also play a role in SG dynamics in mammalian cells. As in yeast cells, Cdk activity is low in G1, suddenly increases during the G1/S transition, and becomes maximal during mitosis until anaphase. Using an mCherry-G3BP1 reporter to analyze SG dissolution kinetics in U2OS cells expressing a mVenus-Gem$^{1\text{-}110}$ fusion that is stable from S phase to anaphase, we found that SG half-life was reduced by 2-fold in cells progressing through S-G2-M phases, when Cdk activity is high, compared to G1 cells (Fig. 5E,F). These data confirm our findings in yeast cells and point to the notion that SGs would antagonize Cdk activity by restraining cyclin translation under stress conditions and that, in turn, Cdk would accelerate SGs dissolution during release from stress.

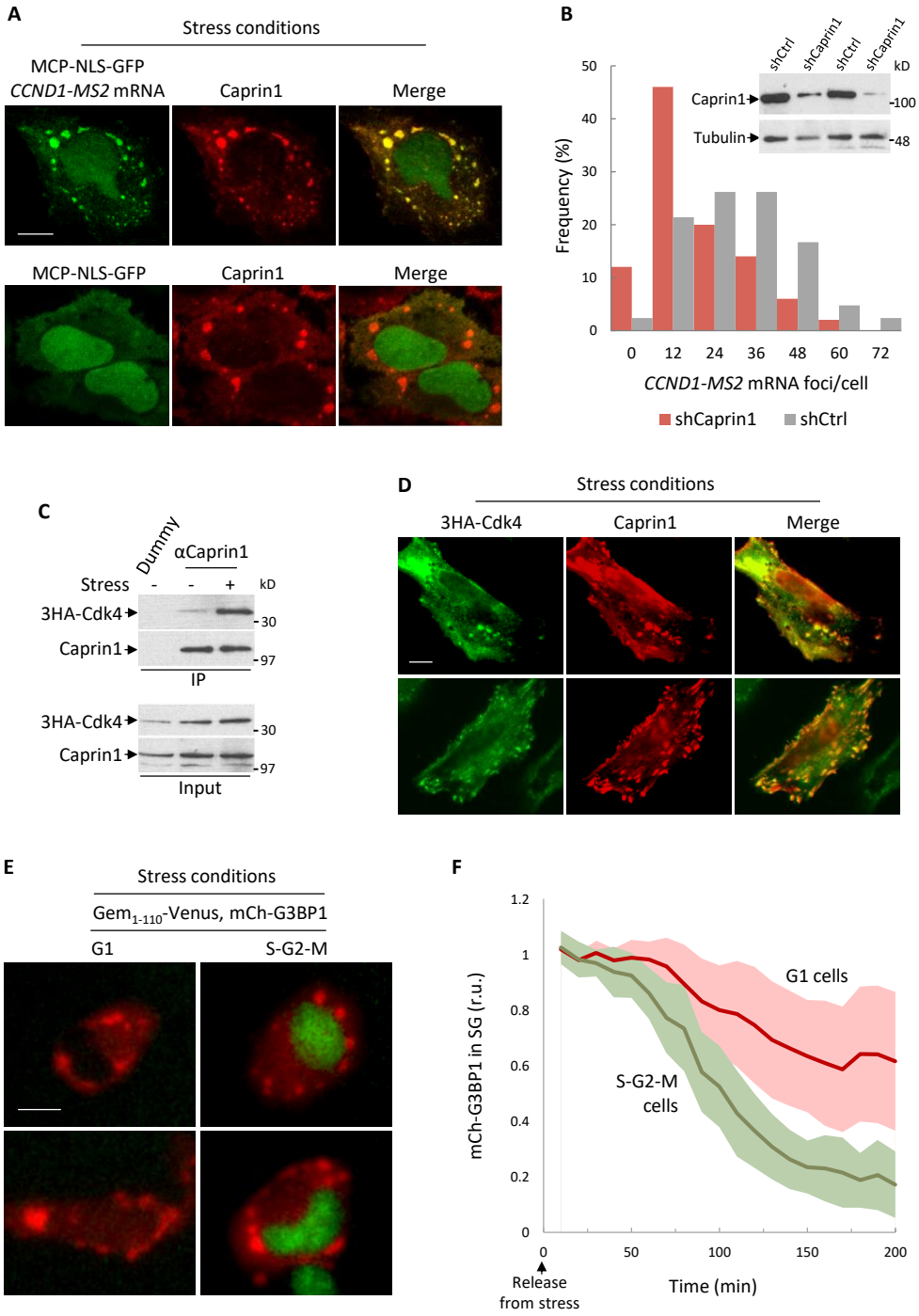

Fig. 5. Mammalian SGs contain Cdk-cyclin factors and are modulated by cell cycle position

(A) HeLa cells expressing NLS-MCP-GFP and *CCND1-MS2* mRNA or none (as control) were subject to 0.5 mM $NaAsO_2$ for 30 min and analyzed by immunofluorescence with a αCaprin1 antibody. Bar, 5 µm. **(B)** HeLa cells as above expressing shCaprin1 or shCtrl were subject to 0.5 mM $NaAsO_2$ for 30 min, and analyzed as in Fig. 4A. Foci frequencies per cell (n=40) are plotted. Inset: Immunoblot analysis of Caprin1 levels. **(C)** Immunoblot of input and αCaprin1 immunoprecipitation samples from HeLa cells expressing 3HA-Cdk4 in the presence (+) or absence (-) of 0.5 mM $NaAsO_2$ for 30 min. **(D)** HeLa cells expressing 3HA-Cdk4 were subject to 0.5 mM $NaAsO_2$ for 30 min and analyzed by immunofluorescence with αHA and αCaprin1 antibodies. Bar, 5 µm. **(E)** Representative images of U2OS cells expressing $Geminin_{1-110}$-mVenus and mCherry-G3BP1 after treatment with 0.5 mM $NaAsO_2$ for 30 min. Bar, 5 µm. **(F)** U2OS cells expressing $Geminin_{1-110}$-mVenus and mCherry-G3BP1 were treated with 0.5 mM $NaAsO_2$ for 30 min as in (E) and, once released in fresh medium, mCherry-G3BP1 levels in foci were measured at different time points. Mean values (n=25) and confidence limits for the mean (α=0.05) are plotted.

Mutual inhibition as a bistable system for SG dynamics

To gain insight into the counteracting effects between SGs and Cdk activity, we modeled a mutual-inhibition system (Fig. 6A and Fig. S5A). Briefly, we assumed that active Cdk (Cdk_{Cyc}) would act with specific catalytic (k_c) and Michaelis-Menten (K_M) constants to promote dissolution of SG factors (SG) as free components (SG_{Comp}). All other processes were defined by simple mass-action laws with explicit rate constants. The model was kept as simple as possible to obtain all the kinetic parameters from experimental data. The K_M for Cdc28 was previously determined *in vitro* (Bouchoux and Uhlmann, 2011), and the maximal substrate concentration in SGs was as described in Fig. S5B. We obtained the basal SG-dissolution rate constant (k_{bd}) by fitting the model to SG dissolution in the *cdc28-13* mutant in the absence of stress (Fig. S5C), where all other variables have no effect. We then used SG formation and dissolution data from wild-type cells to estimate the remaining rate constants (Fig. S5D). With these experimental parameters, the mutual-inhibition model predicted a bistable switch as a function of the stress signal (Fig. 6B). To observe how the bistability of the model arises, in Fig. 6C we plotted the steady-state levels of condensed SG factors (SG) and active Cdk (Cdk_{Cyc}) as independently predicted by each of the two modules of the system, either (1) SG dissolution as a function of Cdk_{Cyc} and the stress level ($Stress$) or (2) Cdk_{Cyc} inactivation as a function of SG. At low stress, SG dissolution and Cdk_{Cyc} inactivation curves intersect only once and the system is monostable, with high active Cdk1 and low condensed SG factors. When stress reaches a certain value, the system creates a saddle-node bifurcation and a new stable steady state, with low active Cdk1 and high levels of condensed SG factors. At higher stress levels, the SG dissolution curve is pushed further and the system becomes monostable again, with low active Cdk1 and high SG condensation (Fig. 6C). The relative K_M, which incorporates SG component concentration, has strong effects on the predicted bistability (Fig. 6D), thus highlighting the importance of substrate accumulation in the SG itself to attain a bistable system.

We then tested whether SG steady states followed a pattern compatible with bistability as a function of stress. As a tunable stress effector we used NaN_3 at different concentrations and measured SG formation after 1h of treatment. We found that steady-state SG levels increased with stressor concentration following bistable kinetics, and displayed a hysteretic behavior as predicted by the model when stressor concentration was reversed (Fig. 6E,F). Finally, we used the G1-cyclin conditional strain to test the effects of Cdk activity in the switch-like behavior of SG formation as a function of NaN_3 concentration. Although a sigmoidal curve was still observed, G1-arrested cells with no Cdk activity advanced SG formation at lower stress levels in a similar fashion to what the model predicts if kinase levels are decreased (Fig. 6G,H). These data support the important role of Cdk in SG dynamics, and suggest that other kinases or factors important for SG formation and dissolution also act in mutual-inhibition modules.

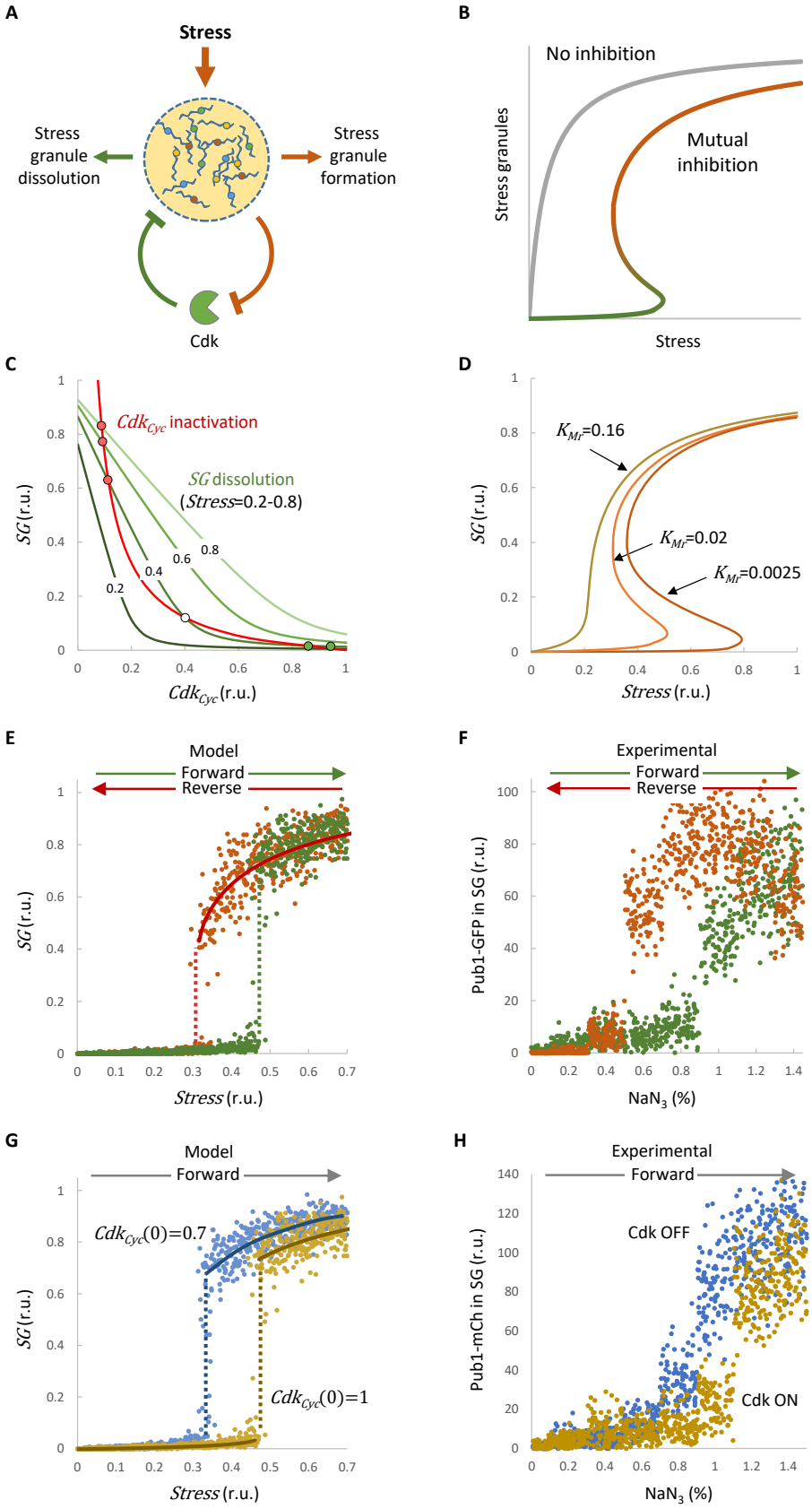

Fig. 6. Mutual inhibition as a bistable system for SG dynamics

(A) SGs maintain cyclin mRNAs translationally inactive and, hence, inactivate the Cdk. In turn, active Cdk promotes SG dissolution and cyclin mRNA release and translation, thus accelerating SG disassembly. **(B)** SG and

Cdk mutual inhibition creates a bistable system that elicits SG formation only above a certain degree of stress and maintains SG integrity until normal conditions are almost fully restored. **(C)** Steady-state balance plots of SG and Cdk_{Cyc} as derived from $Stress$-modulated SG dissolution by active Cdk (green lines) or Cdk inactivation by SGs (red line) reactions. Unstable (white circle) and stable (red and green circles) steady states are indicated. **(D)** SG steady states vs $Stress$ as a function of the K_{Mr}. **(E)** Simulations of SG levels in forward or reverse modes. The plot shows final SG steady states when the initial $Stress$ variable was set to 0 (forward mode, green) or set to 1 (reverse mode, red), simulating non-stressed and stressed cells, respectively. Both deterministic (lines) and stochastic (dots) simulations are shown. **(F)** SG steady-state levels in forward or reverse mode experiments. In forward mode (green), exponentially-growing wild-type cells expressing Pub1-GFP were subject to different NaN_3 concentrations for 60 min. In reverse mode, cells were first subject to 1.4% NaN_3 for 60 min, and then incubated in the presence of different NaN_3 concentrations for an additional 60-min period. Pub1-GFP levels in foci were measured in single cells (n>300) and bootstrapped (n=50) mean values are plotted. **(G)** Simulations of SG levels as a function of the total Cdk levels in forward mode. The plot shows final SG steady states when the initial Cdk_{cyc} variable was set to 1 (yellow) or reduced to 0.7 (blue). Both deterministic (lines) and stochastic (dots) simulations are shown. **(H)** SG steady-state levels in forward mode experiments with cycling and G1-arrested cells with no Cdk activity. *GAL1p-CLN3 cln1,2* expressing Pub1-mCherry were grown in galactose and arrested in G1 by transfer to glucose for 2 hr (Cdk OFF). Then, cells were stressed for 60 min in the presence of different NaN_3 concentrations. As control, *CLN3 cln1,2* cells (Cdk ON) were subject to the same experimental conditions. Pub1-mCherry levels in foci were measured in single cells (n>300) and bootstrapped (n=50) mean values are plotted.

Discussion

Here we identified Whi8 (YGR250C) as a protein that interacts with the Cdc28 Cdk and recruits the *CLN3* cyclin mRNA to SGs for translational repression and, hence, Cdc28 inactivation under stress conditions in G1 cells. Moreover, the yeast Cdk is also recruited to SGs with the important participation of Whi8, and plays a crucial role in SG dissolution and translation resumption of SG-recruited mRNAs when cells are returned to non-stress conditions. We found a similar scenario in mammalian cells, where the *CCND1* cyclin mRNA is translationally repressed by stress and recruited to SGs with the contribution of Caprin1, an RNA-binding protein that interacts with Cdk4, a G1 Cdk, in a stress-dependent manner. While Cdk4 colocalizes with Caprin1 in SGs, SG dissolution is slower in cells where Cdk activity is lower, i.e. G1 cells, when released from stress conditions. Thus, Whi8 and Caprin1 would act as molecular links between Cdk inactivation and Cdk-dependent SG dissolution during adaptation to and recovery from stress, respectively. Finally, our data show that SGs behave as a Cdk-dependent bistable system that only switches when stress levels reach a minimal threshold or normal conditions are almost completely restored.

Recent work analyzed the presence of mRNAs in yeast SGs (Khong et al., 2017), and found that G1 cyclin mRNAs were enriched in the SG fraction, 4-fold for *CLN3* and about 2-fold for *CLN1,2*, but levels of G1 cyclin mRNAs were still significant in the soluble fraction. Moreover, similar data from mammalian cells showed no or only a modest enrichment of *CCND1,2,3* mRNAs in SGs (Khong et al., 2017; Namkoong et al., 2018). Thus, although recruitment to SGs likely plays an important role, other

mechanisms such as eIF2α inhibition by phosphorylation (Crawford and Pavitt, 2019) could act to ensure full inhibition of translation of G1 cyclin mRNAs under stress conditions. On the other hand, recruitment of a fraction of cyclin mRNAs to SGs could increase local Cdk activation when translation resumes after release from stress.

A very significant number of proteins belonging to SGs may be phosphorylated by Cdc28 in yeast cells and, not surprisingly, most of them have functional homologues in mammalian cells (Table S1). The reason Cdc28 would have such a high number of targets in SGs likely resides in their dependence on multivalent protein-protein interactions, which also agrees with the fact that no single protein has been found to be essential for SG formation (Buchan et al., 2013; Yang et al., 2014; Yoon et al., 2010). Intriguingly, a comparative analysis of Cdc28-target phosphosites revealed that their position, rather than being conserved, is very dynamic within disordered regions (Holt et al., 2009b).

We show that SG dynamics obey a bistable system where the Cdk is an important effector, and we have recapitulated this behavior with a simple mutual-inhibition model. Notably, the K_M to substrate ratio was crucial to attaining bistability and, if Cdk substrates were always in a soluble form in the cytoplasm, the model would only predict monostable steady-states at varying stress levels. In other words, the higher substrate concentration attained in SGs is what decreases the K_M/substrate ratio and makes the model bistable. Thus, the effects of mutual-inhibition would be especially relevant during SG dissolution, rather than SG assembly. If this were the case, SG components would not be necessarily phosphorylated when soluble in the cytoplasm under normal conditions and, hence, the Cdc28 phosphoproteome could include many other SG proteins in addition to those listed in Table S1. Alternatively, since many SG components display physical interactions even in the absence of stress (Youn et al., 2018), they could interact with Cdc28 in supramolecular complexes to increase their effective concentration as substrates also under non-stress conditions. Favoring the later possibility, we found that Cdc28 and Whi8 co-immunoprecipitate vey efficiently in the absence of stress.

SG dissolution requires the Cdc48 segregase in yeast (Buchan et al., 2013) and mammalian (Wang et al., 2019) cells, and we previously found that Cdc28 phosphorylates Cdc48 to enhance its segregase activity in releasing Cln3 from the ER during G1 (Parisi et al., 2018b). Therefore, Cdc28 could also act on SG dissolution by modulating the affinity and/or segregase activity of Cdc48 towards components of the SG.

Giving support to our results, a screen in mammalian cells had pinpointed Cdk inhibitors by their marked effects in delaying SG dissolution (Wippich et al., 2013b). These authors identified Dyrk3 as a key factor modulating SG dynamics, and recently showed that this kinase is also important for dissolution of specific membraneless organelles during mitosis (Rai et al., 2018). Also in mammalian

cells, SG dissolution is modulated by FAK-dependent phosphorylation of Grb7 (Tsai et al., 2008a). In yeast, Sky1 is recruited to SGs, where it phosphorylates Npl3 and modulates their dynamics (Shattuck et al.). Therefore, fast and efficient SG assembly and dissolution would result from the concerted action of different protein kinases. Nonetheless, the unique mutual inhibitory roles of Cdk and SGs would provide bistability and hysteresis to prevent SG formation at low levels of stress and sustain their presence until normal conditions are entirely restored. Indeed, as our data suggest, the SG-Cdk mutual inhibitory scenario should also apply to other condensation modulators, thus subjugating SG dynamics to a robust switch as a function of different facets of the cellular physiological status.

Materials and Methods

Cells and growth conditions. Yeast strains and plasmids are listed in Tables S2 and S3, and methods used for chromosomal gene transplacement and PCR-based directed mutagenesis were previously described (Ferrezuelo et al., 2012b). Specific construction details will be made available upon request. Unless noted otherwise, all gene fusions in this study were expressed at endogenous levels in yeast cells. Cells were grown for 7-8 generations in SC medium with 2% glucose at 30ºC unless stated otherwise. *GAL1*p-driven gene expression was induced by addition of 2% galactose to cultures grown in 2% raffinose at OD600=0.5 or, in the presence of glucose, by adding 1 μM β-estradiol to cells expressing the Gal4-hER-VP16 transactivator (Louvion et al., 1993).

When indicated, overexpression of *CLN3* was performed with a *tetO*-based expression system (Garí et al., 1997). SG formation was routinely induced by transferring cells to 42ºC for 30 min in SC medium without glucose, and SG dissolution was assessed by returning stressed cells to 30ºC in SC medium supplemented with glucose. In experiments shown in Fig. 4F, SG dissolution was assessed at 37ºc to maintain restrictive conditions for the thermosensitive *cdc28-13* allele. Finally, SG steady states were analyzed by treating cells with the indicated concentrations of NaN_3 for 60 min at 30ºC in SC plus 1% glucose.

Human HeLa and U2OS cells were grown at 37ºC in Dulbecco's modified Eagle's medium (DMEM) supplemented with glutamine, antibiotics and 10% FBS. Transfection with Caprin1-directed (TRCN0000115972) or control (SHC002) shRNAs and vectors expressing NLS-MCP-GFP, 3HA-Cdk4, $Geminin_{1-110}$-mVenus or mCherry-G3BP1 proteins, or *CCND1-MS2* mRNA, was performed as described (Ruiz-Miro et al., 2011). Cycling cells were analyzed 18 hr after replating, and SG formation was induced by addition of 0.5 mM $NaAsO_2$ for 30 min, unless stated otherwise. SG steady states were analyzed after 60 min in $NaAsO_2$ at the indicated concentrations.

Subcellular fractionation. Briefly, cells (50 OD_{600}) were pelleted and disrupted with glass beads in 200 µl STE10 (10% sucrose, 10 mM Tris-HCl pH7.6, 10 mM EDTA) with protease inhibitors (Vergés et al., 2007b). Cleared extracts were layered on top of a 5-ml, 20–60% linear sucrose gradient, and centrifuged for 18 h at 100,000 g in a SW50.1 rotor (Beckman Instrs., Fullerton, CA). Fractions (0.5 ml) were collected from the top of the gradient, precipitated with 7% trichloroacetic acid and analyzed by immunoblotting as described below.

*Immunoprecipitation***.** Cells (50 OD_{600}) were disrupted with glass beads in 200 µl BFI buffer (0.1% Triton X100, 250 mM NaCl, 50 mM Tris-HCl pH7.5, 5 mM EDTA) with protease inhibitors (Wang et al., 2004). Cleared lysates were incubated with 30 µl αFLAG (clone M2, Sigma) beads which, after three washing steps, were boiled briefly in 2x loading buffer prior to SDS-PAGE.

Immunoblot and immunofluorescence analysis. Immunoblotting was performed essentially as described (Gallego et al., 1997b). Protein gels were transferred to nitrocellulose and probed with primary and secondary antibodies as recommended by the supplier in PBS. Immunofluorescence analysis in yeast (Wang et al., 2004) and HeLa (Ruiz-Miro et al., 2011) cells were performed as described. Used antibodies are listed in Table S4.

mRNA quantification by RT-qPCR. Cells (10 OD600) were disrupted with glass beads in 50 µl of 1:1 phenol/TE, and total RNA was precipitated with ethanol in the presence of 0.3M NaOAc pH 5.2. Determination of mRNA levels by RT-qPCR was done using probes listed in Table S5.

Time-lapse wide-field and confocal microscopy. Yeast cells were analyzed by wide-field epifluorescence microscopy in 35-mm glass-bottom culture dishes (GWST-3522, WillCo) in SC media at 30ºC essentially as described (Ferrezuelo et al., 2012b), using a fully-motorized Leica AF7000 microscope with a HCX PL S-APO 63X/1.3NA oil-immersion objective at room temperature, equipped with a digital CCD camera ORCA-R2. Wide-field images were analyzed with the aid of BudJ, an ImageJ (Wayne Rasband, NIH) plugin to obtain cell dimensions and fluorescence data as described (Ferrezuelo et al., 2012b). Intracellular foci were detected with BudJ as pixels with a fluorescence value above a certain threshold relative to the median cell fluorescence that produced a contiguous area with a minimum size (both set by the user). In a typical set up, pixels were selected if at least 30% brighter than the cell median, with a minimal size of 0.2 µm.

Photobleaching during acquisition was negligible (less than 0.1% per time point) and autofluorescence was always subtracted. Immunofluorescence in mammalian cells was analyzed under a Zeiss 780 confocal microscope with a C-Apochromat 40X/1.2NA water-immersion objective. Time-lapse of U2OS cells was performed as for yeast cells in DMEM supplemented with glutamine and 10% FBS at 37ºC in

5% CO_2. Intracellular foci were analyzed as abovementioned with a plugin derived from BudJ adapted to images from cultured mammalian cells.

Mutual-inhibition mathematical model. A wiring diagram and a set of differential equations were produced with the aid of COPASI (Hoops et al., 2006) to describe the mutual inhibition framework (Fig. S5A). First, we considered SG factors as either free components (SG_{Comp}) or in a condensed state (SG), the stress signal ($Stress$) acting as a positive modulator in their condensation. Regarding SG dissolution, we assumed two independent mechanisms, a basal process that reverses condensation in the absence of stress, and a Cdk-dependent dissolution reaction, in which active Cdk (Cdk_{Cyc}) acts as an enzyme with specific catalytic (k_c) and Michaelis-Menten (K_M) constants. In turn, active Cdk (Cdk_{Cyc}) is inactivated (Cdk) as a function of condensed SG factors (SG) to simulate translation inhibition of G1 cyclin mRNAs by SGs. Finally, we assumed stress-independent reactivation kinetics of the Cdk. With the exception of Cdk-dependent SG dissolution, all processes were defined by mass-action laws with explicit rate constants.

This simplicity allowed us to estimate all kinetic parameters from experimental data using COPASI in deterministic mode. First, the K_M for Cdc28 was previously determined *in vitro* (Bouchoux and Uhlmann, 2011), and the maximal substrate concentration in SGs (SG_{max}) was estimated as described in Fig. S5B, allowing us to obtain a relative $K_{Mr} = K_M / SG_{max}$. We obtained the basal SG-dissolution rate constant (k_{bd}) by fitting the model to SG dissolution in the *cdc28-13* mutant in the absence of stress (Fig. S5C), where all other variables have no effect. We then used SG formation and dissolution data from wild-type cells to estimate the remaining rate constants (Fig. S5D).

Statistical analysis. Sample size is always indicated in the Fig. legend. For single-cell or single-focus data, median and quartile (Q) values are shown. Confidence limits for the median were obtained by bootstrapping-based methods. Pairwise comparisons were performed with a Mann-Whitney U test; and the resulting p-values are shown in the corresponding Fig. panels. Time-lapse data from single cells during SG formation or dissolution are represented as the mean value of the population along time, while the shaded area represents the 95% confidence limits of the mean. Protein and mRNA levels were determined in triplicate samples and mean + SEM values are shown. Venn diagrams were as described (Heberle et al., 2015).

Data and software availability. The model was deposited in the BioModels (Chelliah et al., 2015) database as MODEL2003140002 in SBML format together with a COPASI (Hoops et al., 2006) file to reproduce simulations with the parameter set shown in Fig. S5. BudJ (Ferrezuelo et al., 2012b) can be obtained as an ImageJ (Wayne Rasband, NIH) plugin from ibmb.csic.es/groups/spatial-control-of-cell-cycle-entry.

References

Alberti, S., and Dormann, D. (2019). Liquid–liquid phase separation in disease. Annu. Rev. Genet. 53, 171–196.

Alberti, S., Gladfelter, A., and Mittag, T. (2019). Considerations and challenges in studying liquid-liquid phase separation and biomolecular condensates. Cell 176, 419–434.

Banani, S.F., Lee, H.O., Hyman, A.A., and Rosen, M.K. (2017). Biomolecular condensates: organizers of cellular biochemistry. Nat. Rev. Mol. Cell Biol. 18, 285–298.

Bellí, G., Garí, E., Aldea, M., and Herrero, E. (2001). Osmotic stress causes a G1 cell cycle delay and downregulation of Cln3/Cdc28 activity in Saccharomyces cerevisiae. Mol. Microbiol. 39, 1022–1035.

Bouchoux, C., and Uhlmann, F. (2011). A quantitative model for ordered Cdk substrate dephosphorylation during mitotic exit. Cell 147, 803–814.

Bratek-Skicki, A., Pancsa, R., Meszaros, B., Van Lindt, J., and Tompa, P. (2020). A guide to regulation of the formation of biomolecular condensates. FEBS J. (online ahead of print).

Buchan, J.R., Muhlrad, D., and Parker, R. (2008). P bodies promote stress granule assembly in Saccharomyces cerevisiae. J. Cell Biol. 183, 441–455.

Buchan, J.R., Kolaitis, R.M., Taylor, J.P., and Parker, R. (2013). Eukaryotic stress granules are cleared by autophagy and Cdc48/VCP function. Cell 153, 1461–1474.

Cai, Y., and Futcher, B. (2013). Effects of the yeast RNA-binding protein Whi3 on the half-life and abundance of CLN3 mRNA and other targets. PLoS One 8, e84630.

Chelliah, V., Juty, N., Ajmera, I., Ali, R., Dumousseau, M., Glont, M., Hucka, M., Jalowicki, G., Keating, S., Knight-Schrijver, V., et al. (2015). BioModels: ten-year anniversary. Nucleic Acids Res. 43, D542–D548.

Colomina, N., Ferrezuelo, F., Wang, H., Aldea, M., and Gari, E. (2008). Whi3, a developmental regulator of budding yeast, binds a large set of mRNAs functionally related to the endoplasmic reticulum. J. Biol. Chem. 283, 28670–28679.

Crawford, R.A., and Pavitt, G.D. (2019). Translational regulation in response to stress in Saccharomyces cerevisiae. Yeast 36, 5–21.

Ferrezuelo, F., Colomina, N., Palmisano, A., Garí, E., Gallego, C., Csikász-Nagy, A., and Aldea, M. (2012). The critical size is set at a single-cell level by growth rate to attain homeostasis and adaptation. Nat. Commun. 3, 1012.

Gallego, C., Garí, E., Colomina, N., Herrero, E., and Aldea, M. (1997). The Cln3 cyclin is down-regulated by translational repression and degradation during the G1 arrest caused by nitrogen deprivation in budding yeast. EMBO J. 16, 7196–7206.

Garí, E., Piedrafita, L., Aldea, M., and Herrero, E. (1997). A set of vectors with a tetracycline-regulatable promoter system for modulated gene expression in Saccharomyces cerevisiae. Yeast 13, 837–848.

Garí, E., Volpe, T., Wang, H.Y., Gallego, C., Futcher, B., and Aldea, M. (2001). Whi3 binds the mRNA of the G1 cyclin CLN3 to modulate cell fate in budding yeast. Genes Dev. 15, 2803–2808.

González-Novo, A., Jiménez, J., Clotet, J., Nadal-Ribelles, M., Cavero, S., de Nadal, E., and Posas, F. (2015). Hog1 targets Whi5 and Msa1 transcription factors to downregulate cyclin expression upon stress. Mol. Cell. Biol. 35, 1606–1618.

Heberle, H., Meirelles, G.V., da Silva, F.R., Telles, G.P., and Minghim, R. (2015). InteractiVenn: a web-based tool for the analysis of sets through Venn diagrams. BMC Bioinformatics 16, 169.

Holmes, K.J., Klass, D.M., Guiney, E.L., and Cyert, M.S. (2013). Whi3, an S. cerevisiae RNA-binding protein, is a component of stress granules that regulates levels of its target mRNAs. PLoS One 8, e84060.

Holt, L.J., Tuch, B.B., Villén, J., Johnson, A.D., Gygi, S.P., and Morgan, D.O. (2009). Global analysis of Cdk1 substrate phosphorylation sites provides insights into evolution. Science 325, 1682–1686.

Hoops, S., Sahle, S., Gauges, R., Lee, C., Pahle, J., Simus, N., Singhal, M., Xu, L., Mendes, P., and Kummer, U. (2006). COPASI--a complex pathway simulator. Bioinformatics 22, 3067–3074.

Huh, W.-K., Falvo, J. V., Gerke, L.C., Carroll, A.S., Howson, R.W., Weissman, J.S., and O'Shea, E.K. (2003). Global analysis of protein localization in budding yeast. Nature 425, 686–691.

Jain, S., Wheeler, J.R., Walters, R.W., Agrawal, A., Barsic, A., and Parker, R. (2016). ATPase-modulated stress granules contain a diverse proteome and substructure. Cell 164, 487–498.

Kedersha, N., and Anderson, P. (2007). Mammalian stress granules and processing bodies. Methods Enzymol. 431, 61–81.

Kedersha, N., Panas, M.D., Achorn, C.A., Lyons, S., Tisdale, S., Hickman, T., Thomas, M., Lieberman, J., McInerney, G.M., Ivanov, P., et al. (2016). G3BP-Caprin1-USP10 complexes mediate stress granule condensation and associate with 40S subunits. J. Cell Biol. 212, 845–860.

Khong, A., Matheny, T., Jain, S., Mitchell, S.F., Wheeler, J.R., and Parker, R. (2017). The stress granule transcriptome reveals principles of mRNA accumulation in stress granules. Mol. Cell 68, 808–820.

Kojima, R., Kajiura, S., Sesaki, H., Endo, T., and Tamura, Y. (2016). Identification of multi-copy suppressors for endoplasmic reticulum-mitochondria tethering proteins in Saccharomyces cerevisiae. FEBS Lett. 590, 3061–3070.

Louvion, J.F., Havaux-Copf, B., and Picard, D. (1993). Fusion of GAL4-VP16 to a steroid-binding domain provides a tool for gratuitous induction of galactose-responsive genes in yeast. Gene 131, 129–134.

Moreno, D.F., Parisi, E., Yahya, G., Vaggi, F., Csikász-Nagy, A., and Aldea, M. (2019). Competition in the chaperone-client network subordinates cell-cycle entry to growth and stress. Life Sci. Alliance 2, e201800277.

De Nadal, E.E., Ammerer, G., and Posas, F. (2011). Controlling gene expression in response to stress. Nat. Rev. Genet. 12, 833–845.

Namkoong, S., Ho, A., Woo, Y.M., Kwak, H., and Lee, J.H. (2018). Systematic characterization of stress-induced RNA granulation. Mol. Cell 70, 175–187.

Parisi, E., Yahya, G., Flores, A., and Aldea, M. (2018). Cdc48 / p97 segregase is modulated by Cdk to determine cyclin fate during G1 progression. EMBO J. 37, e98724.

Protter, D.S.W., and Parker, R. (2016). Principles and properties of stress granules. Trends Cell Biol. 26, 668–679.

Rai, A.K., Chen, J.X., Selbach, M., and Pelkmans, L. (2018). Kinase-controlled phase transition of membraneless organelles in mitosis. Nature 559, 211–216.

Rowley, A., Johnston, G.C., Butler, B., Werner-Washburne, M., and Singer, R.A. (1993). Heat shock-mediated cell cycle blockage and G1 cyclin expression in the yeast Saccharomyces cerevisiae. Mol. Cell. Biol. 13, 1034–1041.

Ruiz-Miro, M., Colomina, N., Fernandez, R.M.H., Gari, E., Gallego, C., and Aldea, M. (2011). Translokin (Cep57) interacts with cyclin D1 and prevents its nuclear accumulation in quiescent fibroblasts. Traffic 12, 549–562.

Shah, K.H., Nostramo, R., Zhang, B., Varia, S.N., Klett, B.M., and Herman, P.K. (2014). Protein kinases are associated with multiple cytoplasmic granules in quiescent yeast cells. Genetics 198, 1495–1512.

Shattuck, J.E., Paul, K.R., Cascarina, S.M., and Ross, E.D. (2019). The prion-like protein kinase Sky1 is required for efficient stress granule disassembly. Nat. Commun. 10, 3614.

Shin, Y., and Brangwynne, C.P. (2017). Liquid phase condensation in cell physiology and disease. Science (80-.). 357, eaaf4382.

Siwiak, M., and Zielenkiewicz, P. (2010). A comprehensive, quantitative, and genome-wide model of translation. PLoS Comput. Biol. 6, 4.

Snead, W.T., and Gladfelter, A.S. (2019). The control centers of biomolecular phase separation: how membrane surfaces, PTMs, and active processes regulate condensation. Mol. Cell 76, 295–305.

Solé, C., Nadal-Ribelles, M., de Nadal, E., and Posas, F. (2015). A novel role for lncRNAs in cell cycle control during stress adaptation. Curr. Genet. 61, 299–308.

Solomon, S., Xu, Y., Wang, B., David, M.D., Schubert, P., Kennedy, D., and Schrader, J.W. (2007). Distinct structural features of caprin-1 mediate its interaction with G3BP-1 and its induction of phosphorylation of eukaryotic translation initiation factor 2alpha, entry to cytoplasmic stress granules, and selective interaction with a subset of mRNAs. Mol. Cell. Biol. 27, 2324–2342.

Van Treeck, B., Protter, D.S.W., Matheny, T., Khong, A., Link, C.D., and Parker, R. (2018). RNA self-assembly contributes to stress granule formation and defining the stress granule transcriptome. Proc. Natl. Acad. Sci. U. S. A. 115, 2734–2739.

Tsai, N.-P., Ho, P.-C., and Wei, L.-N. (2008). Regulation of stress granule dynamics by Grb7 and FAK signalling pathway. EMBO J. 27, 715–726.

Vai, M., Popolo, L., and Alberghina, L. (1987). Effect of tunicamycin on cell cycle progression in budding yeast. Exp. Cell Res. 171, 448–459.

Vergés, E., Colomina, N., Garí, E., Gallego, C., and Aldea, M. (2007). Cyclin Cln3 is retained at the ER and released by the J chaperone Ydj1 in late G1 to trigger cell cycle entry. Mol. Cell 26, 649–662.

Wang, B., Maxwell, B.A., Joo, J.H., Gwon, Y., Messing, J., Mishra, A., Shaw, T.I., Ward, A.L., Quan, H., Sakurada, S.M., et al. (2019). ULK1 and ULK2 regulate stress Granule disassembly through phosphorylation and activation of VCP/p97. Mol. Cell 74, 742–757.

Wang, H., Garí, E., Vergés, E., Gallego, C., and Aldea, M. (2004). Recruitment of Cdc28 by Whi3 restricts nuclear accumulation of the G1 cyclin-Cdk complex to late G1. EMBO J. 23, 180–190.

Wippich, F., Bodenmiller, B., Trajkovska, M.G., Wanka, S., Aebersold, R., and Pelkmans, L. (2013). Dual specificity kinase DYRK3 couples stress granule condensation/dissolution to mTORC1 signaling. Cell 152, 791–805.

Yahya, G., Parisi, E., Flores, A., Gallego, C., and Aldea, M. (2014). A Whi7-Anchored Loop Controls the G1 Cdk-Cyclin Complex at Start. Mol. Cell 53, 115–126.

Yang, X., Shen, Y., Garre, E., Hao, X., Krumlinde, D., Cvijović, M., Arens, C., Nyström, T., Liu, B., and Sunnerhagen, P. (2014). Stress granule-defective mutants deregulate stress responsive transcripts. PLoS Genet. 10, e1004763.

Yoon, J.-H., Choi, E.-J., and Parker, R. (2010). Dcp2 phosphorylation by Ste20 modulates stress granule assembly and mRNA decay in Saccharomyces cerevisiae. J. Cell Biol. 189, 813–827.

Youn, J.-Y.Y., Dunham, W.H., Hong, S.J., Knight, J.D.R., Bashkurov, M., Chen, G.I., Bagci, H., Rathod, B., MacLeod, G., Eng, S.W.M., et al. (2018). High-density proximity mapping reveals the subcellular organization of mRNA-associated granules and bodies. Mol. Cell 69, 517–532.

Acknowledgements

We thank E. Rebollo for technical assistance, and B. Futcher, R. Singer and T. Stracker for providing strains, cell lines and plasmids. We also thank C. Rose for editing the manuscript. This work was funded by the Spanish Ministry of Science and Innovation to C.G. (BFU2017-83375-R) and M.A. (BFU2016-80234-R). A.P.P. and D.F.M. received FI fellowships of *Generalitat de Catalunya*.

Author contributions: G. Yahya, Investigation, Methodology; A.P. Pérez, Investigation; M.B. Mendoza, Investigation; E. Parisi, Investigation; D.F. Moreno, Investigation; M. Artés, Investigation; C. Gallego, Conceptualization, Supervision, Funding acquisition, Investigation, Writing—original draft, Writing—review and editing; M. Aldea, Conceptualization, Supervision, Funding acquisition, Investigation, Writing—original draft, Writing—review and editing

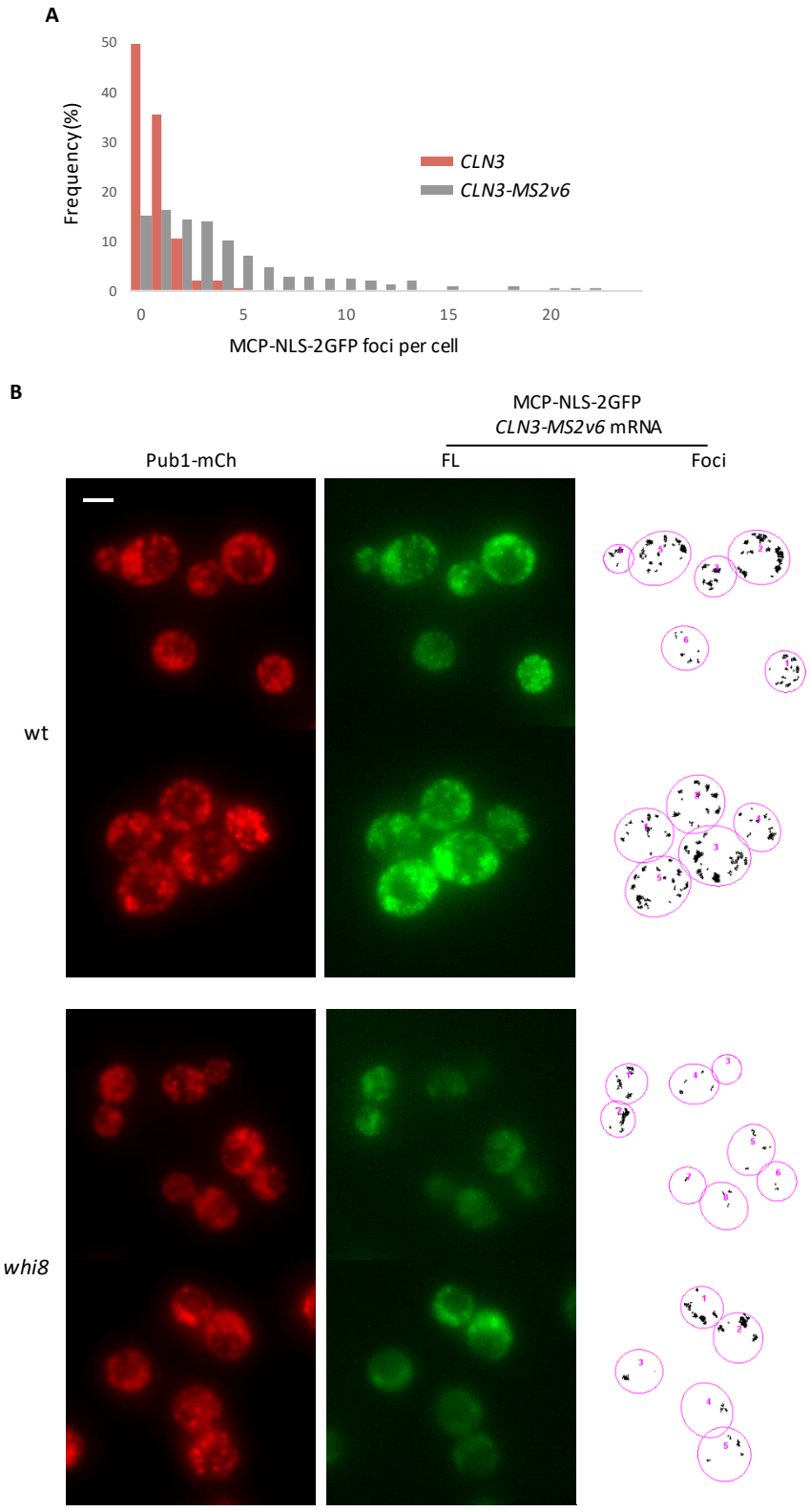

Fig. S1. Whi8 binds and recruits the *CLN3* mRNA to SGs

(A) *MCP-NLS-GFP* foci numbers in *WHI8-mCh* cells (n=200) with plasmids expressing either *CLN3* or *CLN3-MS2v6* after 30 min at 42ºC in the absence of glucose. **(B)** *PUB1-mCh* cells with the indicated genotypes with plasmids expressing *MCP-NLS-GFP* and *CLN3-MS2v6* were stressed for 30 min at 42ºC in the absence of glucose. Foci detected above a fixed local threshold with the aid of BudJ are also shown. Bar, 2 µm.

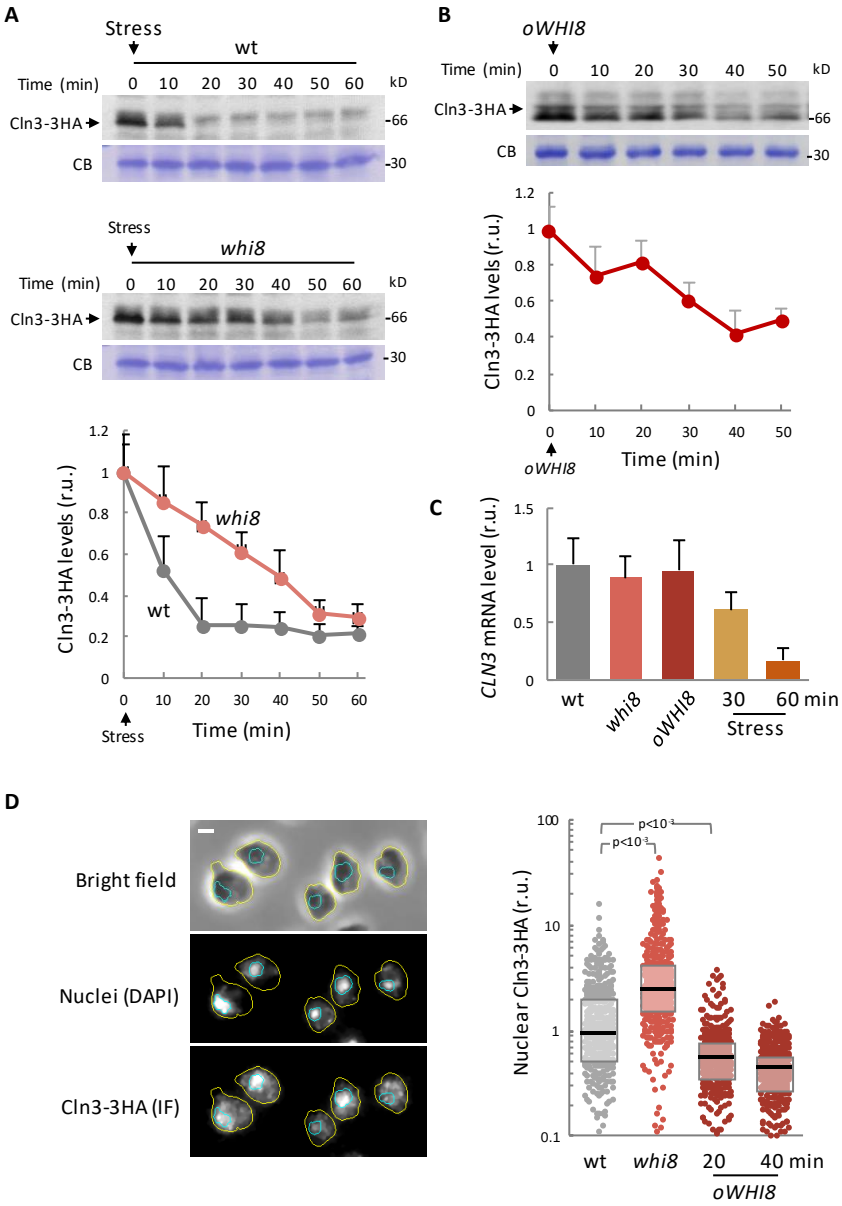

Fig. S2. Whi8 is required to inhibit *CLN3* mRNA translation under stress conditions

(A) Immunoblot analysis of Cln3-3HA after transferring wild-type (top) or *whi8* (bottom) cells to 42ºC in the absence of glucose. Total cell extracts were stained with Coomassie blue and a prominent band is shown as loading control. Cln3-3HA levels were quantified and mean + SEM values (n=3) are plotted. **(B)** Immunoblot analysis of Cln3-3HA after 1 µM β-estradiol addition to induce a plasmid-borne *GAL1p-WHI8* fusion in cells expressing the Gal4-hER-VP16 transactivator. A prominent band in the total cell extract is shown as loading control. Cln3-3HA levels were quantified and mean + SEM values (n=3) are plotted. **(C)** *CLN3* mRNA levels were determined in cells of the indicated genotypes under normal conditions, or 30-60 min after transfer to 42ºC in the absence of glucose. Mean + SEM values (n=3) are plotted. **(D)** Cells with the indicated genotypes were analyzed to determine Cln3-3HA nuclear levels by immunofluorescence (left, Vergés *et al*, 2007). Bar, 2 µm. Individual data (n>400) and median ± Q values are plotted (right). Shown p-values were obtained using a Mann-Whitney U test.

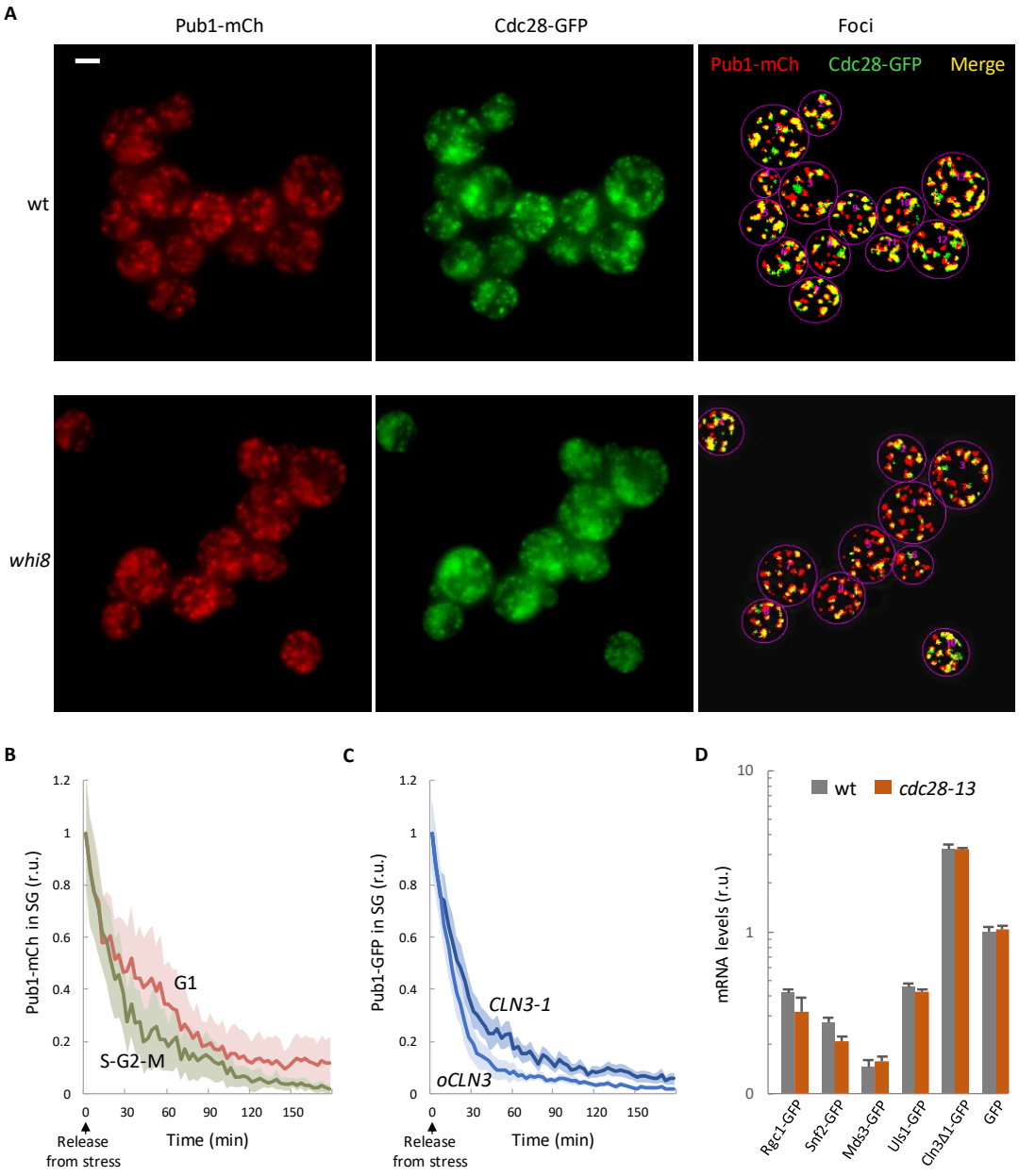

Fig. S3. Cdc28 is recruited to SGs and modulates SG dynamics

(A) Maximum projections of confocal images from wild-type and *whi8* cells expressing Cdc8-GFP and Pub1-mCherry after 30 min at 42ºC in the absence of glucose. Bar, 2 µm. **(B)** Wild-type cells expressing Pub1-mCherry were stressed for 30 min at 42ºC in the absence of glucose and, once released at 30ºC in the presence of glucose, Pub1-mCherry levels in foci were measured at different time points in unbudded (G1) or budded (S-G2-M) cells. Mean values (n>30) and confidence limits for the mean (α=0.05) are plotted. **(C)** *PUB1-mCh* cells with plasmids expressing a hyperstable allele (*CLN3-1*) or overexpressing wild-type Cln3 (*oCLN3*) from the *tetO₂* promoter were stressed for 30 min at 42ºC in the absence of glucose and, once released at 30ºC in the presence of glucose, Pub1-mCherry levels in foci were measured at different time points. Mean values (n>30) and confidence limits for the mean (α=0.05) are plotted. **(D)** Wild-type (gray) and *cdc28-13* (orange) cells with plasmids expressing the indicated GFP fusions as in Fig. 4J were collected 100 min after release form stress and mRNA levels were analyzed by RT-PCR. Relative mean (n=3) and standard error values are plotted.

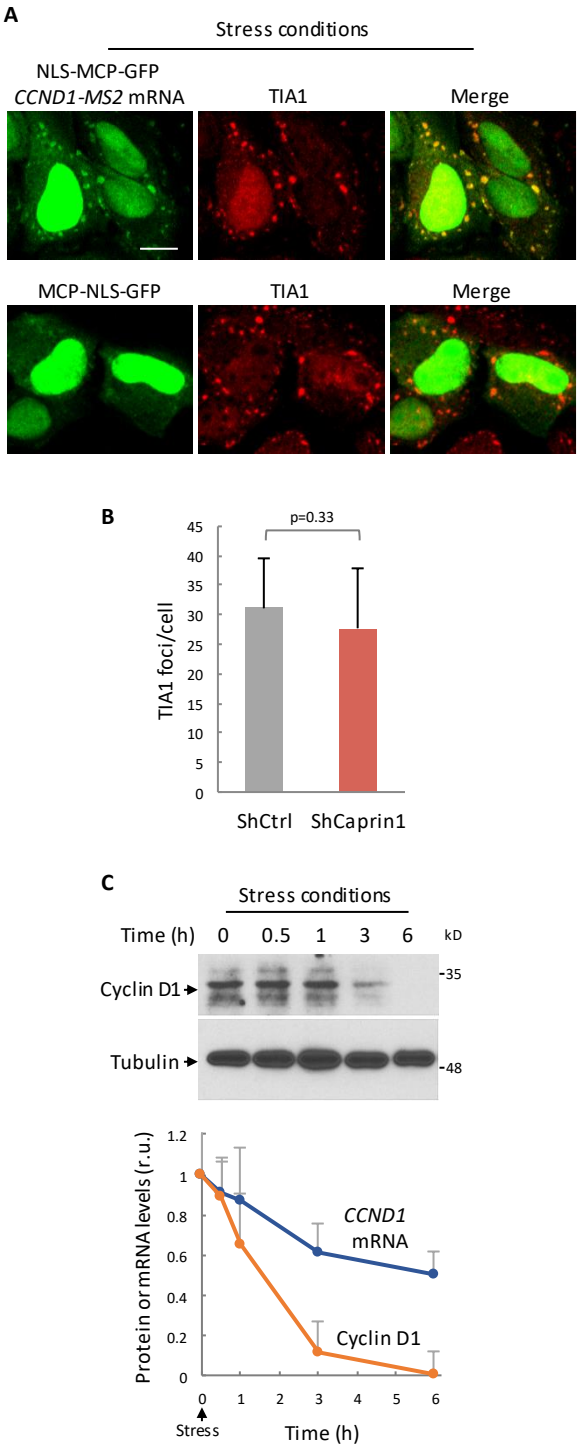

Fig. S4. The *CCND1* mRNA is recruited to SGs and cyclin D1 levels are downregulated by stress
(A) HeLa cells with plasmids expressing NLS-MCP-GFP and either a *CCND1-MS2* mRNA or none (as control) were subject to 0.5 mM $NaAsO_2$ for 30 min, and analyzed by immunofluor-escence with a αTIA1 antibody. Bar, 5 µm. **(B)** HeLa cells with plasmids expressing either shCaprin1 or shCtrl were subject to 0.5 mM $NaAsO_2$ for 30 min, and the number of TIA1 foci per cell was determined by immunofluorescence as in panel A. Mean + CL (n=100, α=0.05) data are plotted. **(C)** Immunoblot analysis of cyclin D1 in HeLa cells at the indicated times after addition of 0.5 mM $NaAsO_2$. Tubulin is shown as loading control. Cyclin D1 protein and *CCND1* mRNA levels were quantified and mean + SEM values (n=3) are plotted.

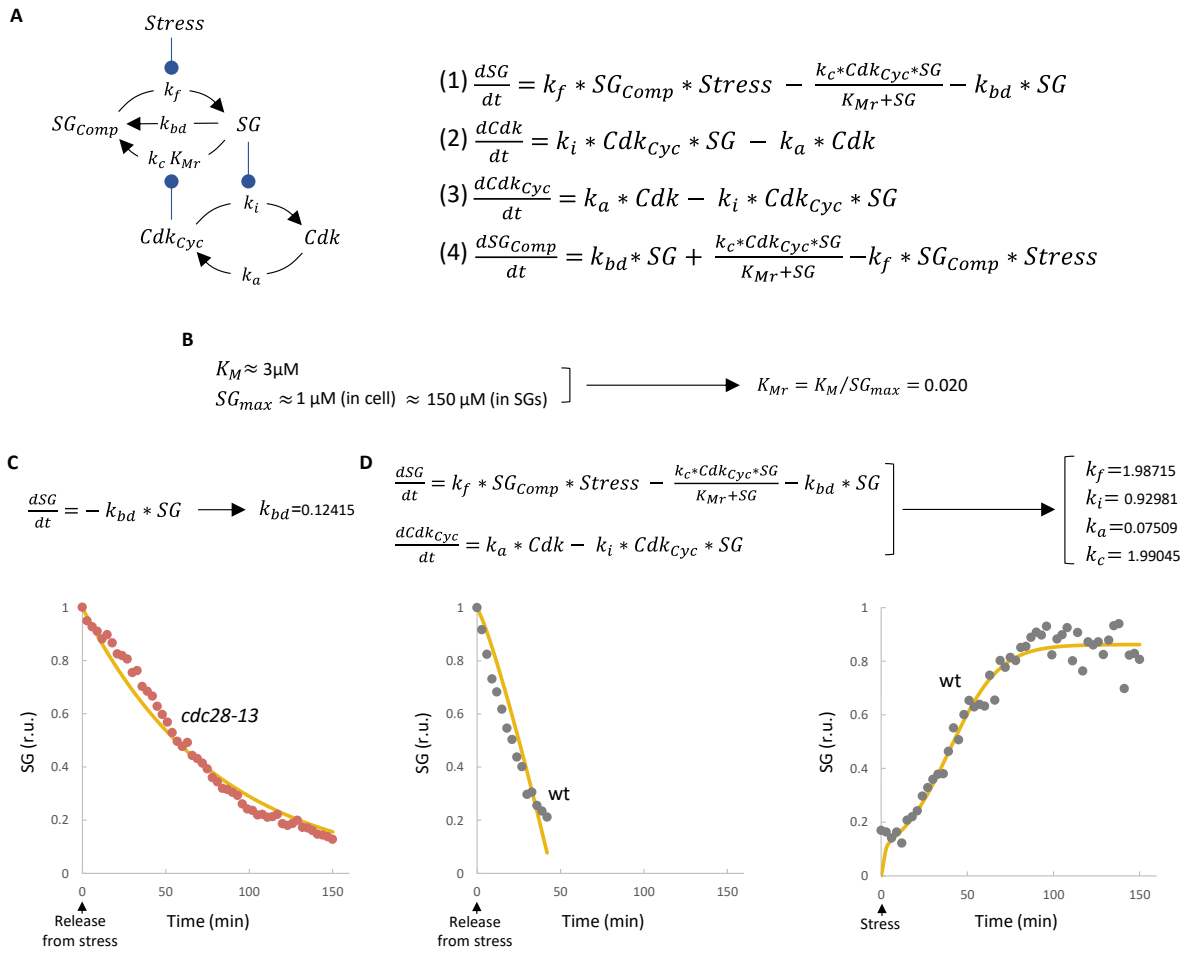

Fig. S5. Equations and parameter fitting in the mutual-inhibition model

(A) Wire diagram of the mutual inhibition model opposing SG formation and Cdk activity. Variables and parameters used in the model are indicated. This model has four state variables: SG_{Comp}, SG free components; SG, SG condensed factors; Cdk_{Cyc}, active Cdk-cyclin complexes; and Cdk, inactive Cdk molecules. With the exception of SG dissolution by Cdk, all reactions are driven by simple mass-action laws with explicit parameters. Stress acts on SG formation by modulating condensation of SG components with k_f, the formation rate constant. SG dissolution, in turn, takes place through (1) a default basal process with rate constant k_{bd}, and (2) a Cdk-mediated enzymatic mechanism with k_c (catalytic constant) and K_{Mr} (relative Michaelis-Menten constant) parameters. Cdk is activated at a constant rate (k_a) and, as cyclin mRNA becomes translationally inhibited, is downregulated by SGs with an inactivation constant k_i. The set of non-linear differential equations used to simulate the model is also shown. **(B)** Cdc28 has a mean $K_M \approx 3$ µM (Bouchoux and Uhlmann, 2016), and putative Cdc28 targets in SGs (Table S1) display an average concentration close to 1 µM (Ho et al., 2018). We carefully analyzed Whi8-GFP and Pub1-GFP levels (as in Fig. 4A) and estimated that these proteins increase their concentration by ca. 150-fold in SGs under stress conditions. Thus, $K_{Mr} = K_M / SG_{max} \approx 0.02$. **(C)** The basal SG-dissolution rate constant (k_{bd}) was obtained by fitting the model to SG dissolution in the *cdc28-13* mutant in the absence of stress, where all other variables have no effect. Equations used and the resulting fitted curve (yellow line) are shown. **(D)** The remaining parameters of the model were obtained by fitting the model to SG formation and dissolution experimental data (gray points) from wild-type cells. Equations used and the resulting fitted curves (yellow lines) are shown.

Table S1. Cdc28 targets in SGs*

Yeast	Human	Gene description
CDC33	EIF4E	Translation initiation factor eIF4E
FUN12	EIF5B	Translation initiation factor eIF5B
HSP26	HSPB1	Small heat shock protein (sHSP) with chaperone activity
KSP1	TBK1	Serine/threonine protein kinase
LEU1	ACO1	Isopropylmalate isomerase
NRP1	--	Putative RNA binding protein that localizes to stress granules
PBP1	ATXN2	Component of glucose deprivation induced stress granules
PPH21	PPP2CB	Catalytic subunit of protein phosphatase 2A, PP2A
RPS0A	RPSA	Subunit of the cytosolic small ribosomal subunit
SRO9	LARP1B	RNA-binding protein involved in cytoplasmic translation
TEF4	EEF1E1	Gamma subunit of translational elongation factor eEF1B
TIF35	EIF3G	eIF3g subunit of the eukaryotic translation initiation factor 3 (eIF3)
TIF4632	EIF4G1	Translation initiation factor eIF4G and scaffold protein
TYS1	YARS1	Tyrosine-tRNA ligase that couples tyrosine to tyrosyl-tRNA
WHI8	CAPRIN1	RNA binding protein that localizes to stress granules (this work)
YEF3	--	Translation elongation factor 3

* Proteins in SGs with phosphosites complying with a Cdk consensus: (S/T)P with at least one basic amino acid from -2 to +3.

Table S2. Yeast strains

Strain name and key genotype	Source
CML128 (*MAT**a** leu2-3,112 ura3-52 trp1-1 his4-1 can^r*)	(Gallego et al., 1997b)
CML203 (*CLN3-3HA::GEN*)	(Gallego et al., 1997b)
CML211 (*cln3::LEU2)*	(Gallego et al., 1997b)
CML391 (*WHI3-3HA::GEN*)	(Garí et al., 2001a)
CYC14 (*WHI3-6FLAG::GEN*)	(Wang et al., 2004)
MAG220 (*GAL4-ER-VP16::URA3*)	(Parisi et al., 2018b)
MAG226 (*whi8::LEU2*)	This study
MAG245 (*CLN3-3HA::GEN whi8::URA3*)	This study
MAG253 (*NAT::GAL1p-CDC28 WHI8-3HA::TRP1*)	This study
MAG279 (*CLN3-3HA::GEN GAL4-ER-VP16::URA3*)	This study
MAG286 (*WHI8-6FLAG::GEN*)	This study
MAG462 (*WHI8-GFP::GEN*)	This study
MAG464 (*cln3::LEU2 whi8::URA3*)	This study
MAG679 (*GAL4-ER-VP16::LEU2*)	This study
MAG717 (*PUB1-mCherry::GEN*)	This study
MAG718 (*WHI8-mCherry::GEN*)	This study
MAG754 (*PUB1-6FLAG::GEN*)	This study
MAG755 (*PUB1-6FLAG::GEN whi8::NAT*)	This study
MAG756 (*PUB1-6FLAG::GEN whi8::NAT whi3::HYG*)	This study
MAG757 (*PUB1-mCherry::GEN whi8::NAT*)	This study
MAG758 (*PUB1-mCherry::GEN whi8::NAT whi3::HYG*)	This study
MAG841 (*WHI8ΔIDR-GFP::GEN*)	This study
MAG842 (*PUB1-3HA::GEN*)	This study
MAG2503 (*PUB1-GFP::GEN*)	This study
MAG2505 (*PUB1-GFP::GEN cdc28-13^{ts}*)	This study
MAG2513 (*CDC28-GFP::GEN PUB1-mCherry::HYG*)	This study
MAG2538 (*CDC28-GFP::GEN PUB1-mCherry::HYG whi8::LEU2*)	This study
MAG2546 (*PUB1-mCh::HYG GAL1p-CLN3::URA3 cln1::HIS3 cln2::TRP1*)	This study
MAG2614 (*GAL4-ER-VP16::LEU2 cdc28-13^{ts}*)	This study

Table S3. Plasmids

Plasmid name and key genotype	Source
pCM192 (*ARS-CEN URA3 CLN3-1-3HA)*	(Gallego et al., 1997b)
pCM194 (*ARS-CEN URA3 CLN3-3HA)*	(Gallego et al., 1997b)
pCM255 (*ARS-CEN URA3 tetO2-CLN3-3HA tTA)*	(Gallego et al., 1997b)
pCYC2077 (*UBIp-3HA-CDK4)*	(Ruiz-Miro et al., 2011)
pET296 (*ARS-CEN LEU2 CYC1p-MCP-NLS-2GFP*)	(Tutucci et al., 2018)
pMAG140 (*ARS-CEN LEU2 CDC28-3FLAG)*	(Yahya et al., 2014)
pMAG141 (*ARS-CEN LEU2 CDC28^{wee}-3FLAG)*	(Yahya et al., 2014)
pMAG231 (*ARS-CEN TRP1 GAL1p-WHI8)*	This study
pMAG610 (*ARS-CEN TRP1 GAL1p-GFP)*	This study
pMAG786 (*CMVp-CCND1-MS2)*	This study
pMAG788 (*CMVp-NLS-MCP-GFP)*	This study
pMAG1307 (*ARS-CEN LEU2 WHI8-6FLAG)*	This study
pMAG2491 (*CMVp-mCherry-G3BP1*)	This study
pMAG2607 (*ARS-CEN URA3 CLN3-MS2v6)*	This study
pMAG2639 (*ARS-CEN TRP1 GAL1p-SNF2-GFP)*	This study
pMAG2640 (*ARS-CEN TRP1 GAL1p-RGC1-GFP)*	This study
pMAG2641 (*ARS-CEN TRP1 GAL1p-MDS3-GFP)*	This study
pMAG2642 (*ARS-CEN TRP1 GAL1p-ULS1-GFP)*	This study
pMAG2643 (*ARS-CEN TRP1 GAL1p-CLN3Δ1-GFP)*	This study

Table S4. Antibodies

Antibody name	Source	Identifier
αCaprin1, polyclonal (rabbit)	Proteintech	15112-1-AP
αCcnD1, clone DCS-6 (mouse)	BD Pharmingen	556470
αDpm1, clone 5C5A7 (mouse)	Invitrogen	A6429
αFLAG, clone M2 (mouse)	Sigma	MAB2200
αGFP, clones 7.1 and 13.1 (mouse)	Roche	11814460001
αHA, clone 12CA5 (mouse)	Roche	11583816001
αHA, clone 3F10 (rat)	Roche	11867423001
αHxk1, polyclonal (rabbit)	US Biological	H2035-03
αTIA1, polyclonal (goat)	Santa Cruz Biotechnology	sc-1751
αTubulin, clone B-5-1-2 (mouse)	Sigma	T5168
αMouse-HRP, polyclonal (sheep)	Amersham	NA931
αRabbit-HRP, polyclonal (donkey)	Amersham	NA934
αMouse-Alexa488, polyclonal (goat)	Invitrogen	A32723
αRat-Alexa488, polyclonal (goat)	Invitrogen	A11006
αRabbit-Alexa555, polyclonal (donkey)	Invitrogen	A31572
αGoat-Alexa555, polyclonal (donkey)	Invitrogen	A21432

Table S5. RT-qPCR probes

Gene	Forward primer, reverse primer, FAM-BHQ probe, or Identifier
ScCLN3	AACCCTAATCTCGTTAAAAG, GACAGTACATGATGAAGTC, ACATCACTCAGCGATCAGCGA
ScHXK1	ACCACTCAATCCAAGTATA, GACCATAAAGTCCTTCAAA, AGAACCACTAAGCACCAAGAGGAG
yeGFP	GATGGTCCAGTCTTGTTA, GCAGCAGTAACAAATTCTA, ACCATTACTTATCCACTCAATCTGCCT
MmGAPDH	Mm99999915_g1
MmCCND1	Mm00432360_m1

DISCUSSION

Cell cycle control in homeostatic and non-homeostatic conditions

Cell cycle regulation is conserved across all living systems. Evolution has sculpted the molecular mechanisms that strive for maintaining cell survival in both homeostatic and non-homeostatic environmental conditions. In normal conditions, one of the most fundamental traits that cells need to preserve is cell size. Otherwise, any imbalance between cell size and biosynthesis would compromise cell survival (Jorgensen and Tyers, 2004; Turner et al., 2012). On the other side, under non-homeostatic conditions, cell survival relies on both cell cycle checkpoints and specific stress responses. In these two situations, the cell cycle control system plays crucial roles restraining cell size to specific ranges and modulating the stress response mainly via the assembly of stress granules. In budding yeast, cell cycle is led by the prevailing activity of the Cdc28 Cdk and its associated cyclins. Consequently, different cyclins modulate the targets of Cdc28 in different cell cycle phases. Despite the importance of all of them, the G1 Cdk is specifically regulated given that it controls cell cycle entry at the Start checkpoint. This involves the function of Cdc28-Cln3 complexes along with other Start components such as Whi5 that participate in cell size regulation (Liu et al., 2015). Here we find that participants confining cell size to certain limits are also key actors in the mechanisms that modulate stress granules assembly and disassembly (Fig. 31).

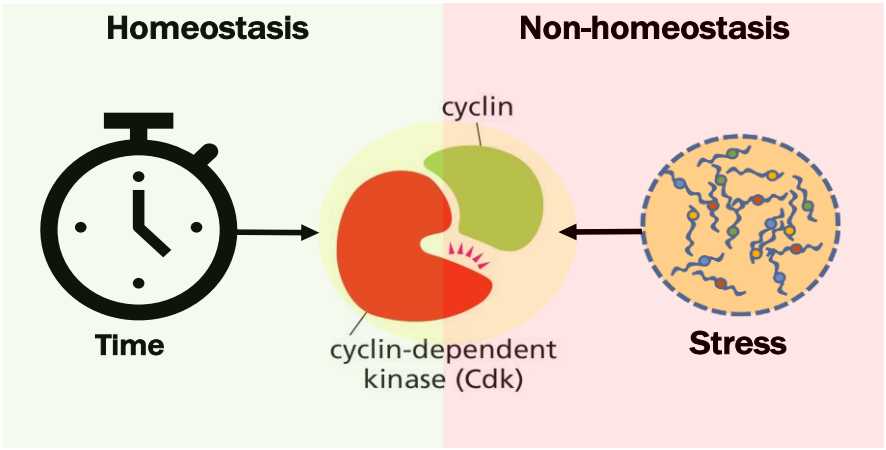

Fig. 31. The cell cycle control machinery executed by Cdk-cyclin complexes are modulated by time and stress.

Cln3 Nuclear levels and stability

Our studies point to cell cycle mechanisms with specific roles in size regulation in which eventually the stability of Cln3 plays a key role. In this context, the influence of Cln3, the most G1 upstream cyclin, has been a matter of debate, probably because a wealth of regulatory mechanisms converge in this cyclin. Cell size reacts to additional copies of the *CLN3* gene in a dose-dependent manner (Cross et al.,

2002; Nash et al., 1988). However, it has been reported that this influence is exerted as long as Whi5 is present in the nucleus during G1 (Talia et al., 2007). Particularly, Cln3 has not a cycling behaviour as other cyclin proteins. Instead, the cellular levels of Cln3 remain nearly constant throughout the cell cycle, mainly due to the constitutive size-scaling transcription and translation of Cln3. This makes difficult to understand the role of Cln3 in the context of cell cycle entry and cell size regulation. With this framework, the post-translational regulation of Cln3 has been explored as a source of molecular regulation. When we tracked the levels of Cln3 at the cellular level, we confirmed that overall protein levels did not change much along the cell cycle. However, supporting the findings by (Wang et al., 2004), we found that Cln3 levels in the nucleus increase during G1 without altering its total cellular amount. Given that the import rate is not limited by importins (Edgington and Futcher, 2001b; Miller and Cross, 2001b), Cln3 accumulation in the nucleus could in principle be modulated by the chaperone machinery (Moreno et al., 2019a; Vergés et al., 2007a). In our model, we used a stabilized and hypoactive version of Cln3 called Cln3-11A. Some of these mutations could have an effect on the ER retention mechanisms that modulate the accumulation of nuclear Cln3 by chaperones. Nonetheless, Cln3-11A is also susceptible to this regulation mainly because cells without Ydj1 (a chaperone with a predominant role in this framework) do not accumulate Cln3-11A in the nucleus (Moreno et al., 2019a). In any event, we have no evidence that chaperone activity and/or availability increases during G1.

As an alternative, the observed accumulation could be due to increased stability of Cln3 in the nucleus during G1. Our work indicates that Mad3 is important for degradation of Cln3 in the nucleus of G1 cells, thus tempering the influence of stochastic-basal Cln3 degradation. As a result, Mad3 would raise the proteolysis rate of Cln3 above the “noise-mediated” degradation. An important piece of the puzzle is Cdc4 and the related F-box proteins that target Cln3 for ubiquitination. The tripartite interaction of Mad3, Cln3 and Cdc4 was reported in a previous study (Martínez-láinez et al., 2018). In this line, our results directly link the G1-phase stability of Cln3 to the presence of Mad3. Consequently, the reported high turnover rates of Cln3 would (in part) rely on the interaction kinetics of Mad3 and Cln3. Possibly with high binding constants remaining invariable in G1. Our Cln3 cycloheximide-chase experiments in G1 do not discard the concurrent effect of additional regulators of Cln3 stability. Cdc4 and Grr1, both F-box proteins of the SCF ubiquitin ligases, redundantly target G1 cyclins (Landry et al., 2012). According to this study, the F-box specificity is commanded by the subcellular localization of each one of them. While Cdc4 is predominantly a nuclear protein, Grr1 is found both in the nuclear and the cytoplasmic compartments. Consequently, in the absence of Cdc4, persistent proteolysis of Cln3 could be partly mediated by Grr1 and thus explain its residual degradation in our conditions. Given that Cdc4 and Grr1 recognize degrons through different recognition motifs (WD40 repeats in Cdc4 and leucine-

rich repeats in Grr1 (Hsiung et al., 2001; Orlicky et al., 2003), one may expect different Cln3 ubiquitination kinetics according to different binding motifs. Whether or not Grr1 makes use of an adapter protein that modulates this process is unknown.

The interweaved activities of Cdc4 and Cdh1 proteins on Cln3 and Mad3 give rise to time control in G1. This assigns an outstanding role in the modulation of G1 length to protein degradation, mainly executed by the SCF and APC complexes. On one hand, Cdc4 targets crucial G1 regulators to degradation (Landry et al., 2012; Liu et al., 2011b; Verma et al., 1997). The importance of these targets for cell survival turns this mechanism into a highly controlled process. Although Mad3 drives the interaction between Cln3 and Cdc4, a previous Cln3 phosphorylation step is necessary for its effective ubiquitination. It is generally assumed that Cdc28 is the responsible kinase that performs these phosphorylation events during G1 progression, similar to the Sic1 Cdk inhibitor, where its multisite phosphorylation by Cdc28 confers cooperative dependence that sets a phosphorylation threshold for Cdc4 binding (Nishizawa et al., 1998; Tang et al., 2012). However, the influence of Cdc28 activity on our framework is yet to be defined. Cln3-11A undergoes Mad3-Cdc4 mediated degradation even being a hypoactive and stable form of Cln3 (with minor effects on other cell parameters, such as cell size). However, the eleven amino acidic substitutions affect putative phosphorylation sites by Cdc28, suggesting that the phospho-regulation of Cln3-11A is likely reduced. Thus, Cln3 phosphorylation would be a necessary but not sufficient requirement for its Cdc4-mediated degradation. Indeed, Cln3 phosphorylation by Cdc28 is assisted by the Ydj1 chaperone, probably with specific roles under heat-shock stress conditions (Yaglom et al., 1996). Future studies may reveal if similar intermediaries either modulate the degradation of Cdc4 targets or are dispensable in cases like Sic1, with a specific phospho-regulation. Eventually we also tried to assess the role of Cdc28 activity in the interaction of Mad3 and Cdc4. Unfortunately, our results displayed a high variability probably due to the intermediate behaviour of the thermosensitive *cdc28-13* strain.

G1 Cdk accumulation in the nucleus during G1

To some extent, the regulation of the Cdc28 kinase is similar to the regulation of Cln3 in terms of nuclear accumulation in G1. The protein levels of Cdc28 remain constant along the cell cycle (Keaton, 2007; Landry et al., 2012), but its activity and specificity are tightly modulated according to different cell cycle phases. In parallel to Cln3, Cdc28 switches its localization from the cytoplasm to the nucleus during G1. This process is assisted by the NLS (nuclear localization signal) of Cln3 and so reinforces the idea that the formation of Cdc28-Cln3 complexes could be limited by the amount of Cln3 (Wang et al., 2004). Our data indicate that the import kinetics of Cdc28 are lower in early G1, and very low in Cln3-

deficient cells. The accumulation of Cln3 in the nucleus steadily increases during G1 and probably during exit from the previous M phase.

Cln3-deficient cells displayed a strong delay in Cdc28 accumulation in early G1. Firstly, this could reflect that the early G1 accumulation of Cdc28 would be assisted by Cln3 and secondly, by the positive feedback mediated by Cdc28-Cln3 complexes that stimulate their own release from the ER and their entry to the nucleus (Yahya et al., 2014). Noteworthy, after this first delay in cln3 cells, the nucleo-cytoplasmic levels of Cdc28 increased with a similar slope in comparison to WT cells. Hence, the lack of Cln3 as a Cdc28 nuclear carrier is possibly compensated by the action of partners like the Cln2 cyclin or other alternative mechanisms (Quilis and Igual, 2012b).

APC^{Cdh1} modulation of Mad3 stability in G1

Unlike SCF^{Cdc4}, the activity of APC^{Cdh1} oscillates during the cell cycle to link the end of the previous mitotic phase with the next Start event. The degradation functions of Cdh1 involve a wide range of targets spanning from late M phase to G1/S transition (Qiao et al., 2010). In parallel, the association of Cdh1 to the APC occurs in the previous late M phase and is maintained in G1, as long there is low Cdc28 activity (Visintin et al., 1997). In this situation, Cdh1 would, constantly degrade Mad3 as a function of time, assuming that the kinetics of Mad3 degradation are independent on cell size. This would be the case for most of the G1 targets of the APC^{Cdh1} complex, including Cdc20. However, Mad3 directly connects the APC^{Cdh1} to the Start machinery. The dynamics of the interaction between Cdh1 and Mad3 depend on the KEN boxes present in Mad3. These KEN boxes are also required for the proper function of the spindle assembly checkpoint (SAC) and for the regulation of the Cdc20 turnover (King et al., 2007; Prinz et al., 1998; Qiao et al., 2016). As a result, the degradation of Mad3 could constitute a case of competition according to the availability of KEN boxes. On one hand the surveillance role of APC^{Cdh1} on Cdc20 is partly mediated through the KEN30 box of Mad3 (King et al., 2007; Robbins and Cross, 2010; Yu, 2007). The accumulation of mitotic targets (included Cdc20) coming from the past phase sustain their degradation in the following cell cycle phase through APC^{Cdh1} and Mad3 in the case of Cdc20. When this happens, part of Mad3 would be focused on Cdc20 proteolysis and consequently it would be free of the APC^{Cdh1}-mediated degradation. In the end, this would stabilize Mad3 in G1 with the corresponding consequences for the concomitant stability of Cln3. In this line, other mitotic targets may keep the APC^{Cdh1} busy and, as before, stabilize Mad3 in G1 (Fig. 32).

The protein levels of Cdh1 are constant along the cell cycle so its activity is predominantly regulated by phosphorylation. After Start, the increasing activity of Cdc28 boosts the association of APC with

Cdc20, but inhibits the assembly of Cdh1 thus allowing Mad3 to recover high levels prior to exit from mitosis.

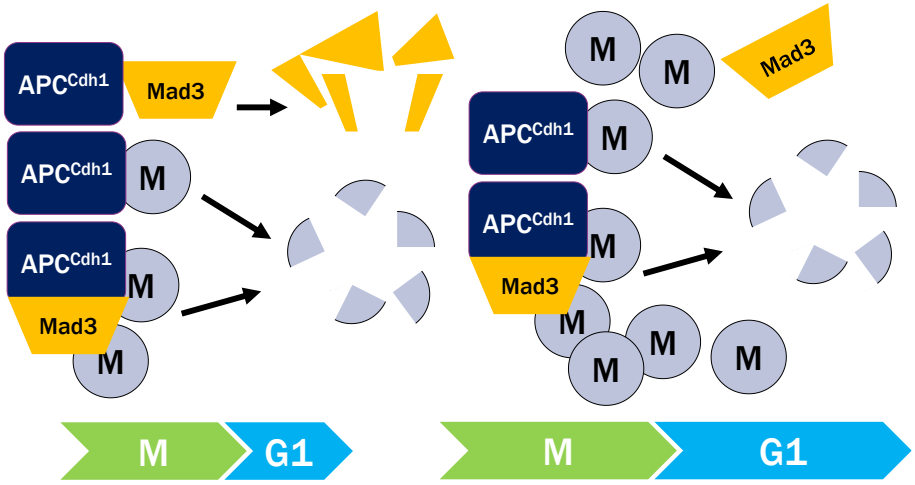

Fig. 32. Hypothetical model for APC^{Cdh1} degradation competition. **(Left)** In normal conditions the APC^{Cdh1} promotes the degradation of mitotic targets (M) along with Mad3 in M-G1. **(Right)** The accumulation of mitotic targets (due to M-phase delays) would directly compete with the degradation kinetics of Mad3 and consequently stabilize Mad3, increasing the degradation rate of Cln3 and lengthening the G1 phase.

Our results point that the regulation of Mad3 at the protein level is mediated by the APC^{Cdh1} complex. The peaks of activity of the APC^{Cdh1} complex are inversely related to the peaks of Mad3 concentration along the cycle. In addition, when we overexpressed Cdh1, the concentration of Mad3 strongly decreased with additional implications on cell size at budding. This highlights the importance of the APC^{Cdh1} activity in G1. Since the ubiquitination activity of APC^{Cdh1} is likely constant over Mad3 and also discarding any special mechanism that may restrict the entry of the APC^{Cdh1} complex to the nucleus, the overall APC^{Cdh1} performance would essentially depend on the inherited amounts of this complex. In this context, the cell cycle would be highly sensitive to the correct regulation of the Cdh1 levels. In fact, overexpression of Cdh1 is lethal and arrests cells mainly in G2 (Martinez et al., 2006). Remarkably, the viability of the cells was considerably compromised when we tried to track the levels of mCherry-Mad3 in a strain with a conditional knockout of Cdh1.

APC^{Cdh1}, Mad3 and Cln3: setting the bases of G1 time control

In G1, the degradation rate of Mad3 mediated by APC^{Cdh1} can be assumed constant. Being Mad3 the FRET limiting factor in the Mad3-Cdc4 interaction according to time-lapse experiments, the expected relaxation of the degradation rate of Cln3 as Mad3 goes away occurs mainly in late G1. This probably comes up because Mad3 is generally inherited in excess in relation to its activity as modulator of Cln3

degradation. Consequently, the degradation rate of Cln3 is mostly constant in G1 despite the fact that Mad3 is degraded as G1 progresses. Following this, all Mad3 inherited proteins are not focused on Cln3 degradation in early G1. Otherwise, Cln3 would not depict such G1 nucleo-cytoplasmic ratios. Indeed, in our cycloheximide-chase experiments following nuclear Cln3 levels, we can find two slopes corresponding to two degradation rates. The first slope governs the degradation rate of Cln3 during much of G1 phase. The second slope is flatter and corresponds to the last 15 minutes of G1, where maybe Mad3 levels have dropped enough for altering the degradation rate of Cln3. A similar but inverse scenario can be found in the nucleo-cytoplasmic plots of Cln3. In this case, the las 15 minutes of G1 show a steeper slope corresponding to an increased accumulation rate, maybe due to the dynamics of Mad3-mediated degradation at this point.

In general, this would add constant proteolytic kinetics to our system and thus the molecular thresholds that drive the transition through Start would fundamentally depend on time if a timer were the only G1 ruler. In the context of G1, when we follow the degradation kinetics of Cln3 at a single-cell level, each cell shows constant rates along most of G1. Nonetheless, at the cellular level, the Cln3 degradation rate varies from one cell to another and is negatively correlated with the cell volume in G1. This would mean that small cells degrade Cln3 rapidly and big cells slow down this process. In other words, Cln3 is generally more stable in cells with a size close the called critical size and thus this points to a deterministic control of the Start transition (Nurse, 1980). Since cells that are about to trigger Start are generally bigger than cells that just have finished cytokinesis, we can think that this negative correlation is just a proxy of the variation of the degradation rate of Cln3 in late G1. However, there is a remarkable budding volume variance that does not correlate with the time spent in G1 (Ferrezuelo et al., 2012; Lord and Wheals, 1981). In addition, cells born already large also show low Cln3 degradation rates without reaching late G1. As a whole, this negative correlation cannot be explained by means of decreased Cln3 degradation rates in late G1. The fact that this correlation disappears when we remove Mad3 from the system adds two levels of control emerging from Mad3 and Cln3. On one hand, each G1 cell depicts a specific and constant Cln3 degradation rate that gives a basal time control to the system. On the other hand, we know that the inherited amounts of Mad3 are independent of the birth volume. This means that we can find small or big cells with high and low concentrations of Mad3 and thus no correlation exists linking Mad3 amounts and cell size at birth. As a result, we can think in a situation in which a small and a big cell display the same concentration of Mad3 but different degradation rates of Cln3. This would discard any dilution mechanism that may soften the activity of Mad3 against Cln3 in big cells. Knowing that Mad3 is still responsible of this negative correlation, there should be something else that stimulates or boosts the activity of Mad3 according to cell size. We can hypothesize about a booster role relying in other members of the SAC

like Bub3, that showed a relevant role in the interface between Mad3 and Cln3 (Martínez-láinez et al., 2018). We can also consider the possibility that Mad3 and Cln3 depict low binding kinetics for avoiding an excess of Cln3 degradation, mostly at early G1. In this situation It is imaginable that this same Bub3 protein could modulate the degradation rate of Cln3. Future experiments will shed light on this aspect.

Finding a timer among the Start network

The idea that a timer can control bud emergence was already raised in the first forays into the study of the cell cycle. Cdc4 mutants arrested cells in G1 and produced multiple buds at a period of about one cell cycle time (Hartwell et al., 1974). Nowadays, the studies of the contribution of time and size to the variability of the critical size grant some clues about the distinction of timers, adders, and sizers (Talia et al., 2007). The relation between the birth size and the volume extension during G1 allows us to identify sizers, timers, or adders as modes of size control. In practical terms, this method is useful for identifying the levels of influence of a sizer in size control. We expect a slope of exactly -1 in the case of a perfect sizer, a slope ≥ 0 in case of a timer and a slope equal to 0 in case of an adder. These plots produce slopes close to -0.3 in wild-type cells, which suggests a combined action of a sizer along with timers or adders. Interestingly, the simulation that fits better with the experimental data corresponds with the mixed contribution of a sizer and a timer. Considering exponential growing, this plot would be the result of adding the positive slope of a timer to the negative slope of the sizer. It appears that this negative slope is sensitive to the grade of influence of timers, adders, or sizers. The predicted behaviour of the sizer-adder combination yields a slope of about -0.5. Considering the expected -1 slope within a full sizer framework, the adder flattens the slope by 50% and the timer does it to a 70% approximately. Nonetheless, in both cases the sizer is dominant but still tempered by either the action of other modes of size control or the intrinsic molecular noise (Talia et al., 2007).

Removing Mad3 from the system is enough for steeping this slope from -0.3 (similar to a mixed sizer-timer influence) to -0.8 and thus, under these circumstances, the sizer would be free to command the setting of a critical cell size. The contribution of such molecular noise in combination to other size regulators no reported yet may impede the expected -1 slope for a full sizer (Honey and Futcher, 2021). In addition, two traits assign time control emerging from Mad3. Firstly, the decreasing levels of Mad3 in G1 are better explained if we think about the combination of constant degradation kinetics along with exponential growing. In case of a sizer, the expected dilution would yield a more linear behaviour in relation to time. Secondly, according to the multivariance logistic analysis, when we delete Mad3, time is no longer a good predictor of bud emergence while volume still is. This suggests that cells use Mad3 as a time sensor for triggering Start.

In our proposal, the timer function involves the participation of the APC^{Cdh1}, Mad3 and Cln3. The setting of the cell size also involves the activity of Cdc28 and the dilution of Whi5. The presence of nuclear Whi5 also acts as a limiting factor of the Start transition. Interestingly, removing Cln3 or Whi5 from this framework is totally epistatic to the concurrent loss of Mad3. In fact, mutant Whi5 cells still show a slope of -0.2, what points to a softer influence of a sizer but still with some level of size control. As a result, the function of the timer needs of the action of the Start components. The deletion of Mad3 produces high and constant levels of Cln3 in G1. In spite of this, we have observed that Whi5 nuclear levels in G1 are slightly lower but remain indistinguishable from their wild-type counterparts at Start. This would explain the small reduction of budding volume in Mad3-deficient cells. Additionally, recently it has been reported that the action of Cdc28-Cln3 complex predominantly phosphorylates the CTD of the RNApol II at the SBF/MBF loci (Kõivomägi et al., 2021). As a result, we can imagine the situation where the activity of Cdc28-Cln3 is modulated by the timer but restricted through the dominant sizer control exerted by Whi5 in G1.

Within this regulatory framework, some layers of control are beyond our knowledge. The analysis of Mad3 lacking the GLEBS domain provided a slope of -0.45 in the birth size – volume extension plots (unpublished data). Knowing that this domain is important for the interaction of Mad3 and Cln3 (Martínez-láinez et al., 2018), we expected a weak effect of the timer in favour of the sizer influence, similar to Mad3-deficient cells. Importantly, Mad3 appear to be more stable when GLEBS is mutated and thus its levels are higher in contrast to wild-type cells. We hypothesize that mutating GLEBS in Mad3 produce opposite phenotypes that in the end may compensate the effect of each other. In other words, less Cln3 degradation may be compensated by high levels of Mad3.

Our experiments with Mad3 lacking the KEN30 box showed and stabilization of Mad3 in G1 as has been reported (King et al., 2007). Surprisingly, these mutants depicted no correlation (slope =0) between birth size and volume extension, as if the sizer had disappeared leaving to timers or adders the control of size in G1 (unpublished data). Actually, we expected a phenotype similar to cells where Mad3 has been totally removed from the system (slope = -0.8). In these cells the nuclear levels of Whi5 were similar to the wild-type control but we found that Whi5 was not diluted in G1. Even without this dilution, our data point to an almost exclusive sizer control of cell size in Mad3-defficient cells. We still have to analyse the dynamics of Whi5 in our Mad3 KEN30 box mutants. As Whi5 is the only reported protein acting as a sizer, it is possible that Mad3 exerts some level of control over the sizer or maybe some compensatory control that works in conjunction with Whi5. In any case, these preliminary results point to a network with different and intricated layers of control that need further attention.

Mad3 executes the G1 time control

Cells receive basal amounts of nuclear Cln3 at birth without any influence of size. This is common for most proteins that diffuse from the mother cell to the daughter promoting a distribution in accordance with their cell size. Intriguingly, Mad3 is segregated in equal amounts from mother to daughter cells after accumulating in the previous G2/M phase. Indeed, our experiments arresting cells in G2/M confirm this Mad3 build-up. The fact that Mad3 is inherited in variable amounts regardless of the birth size points that the G2/M accumulation rate is also independent of size. In this case, we can argue that the time control in G1 executed by Mad3 is a proxy of the previous G2/M state. In this situation, Mad3 is stabilized probably due the lack of Cdh1 activity before anaphase and thus any delay or modulation of this part of the cell cycle can affect the dynamics of the following timer. The addition of three yeast centromeric plasmids (YCPs) to our system caused a delay in the G2/M phase, maybe through the activation of the SAC (Martínez-láinez et al., 2018). Curiously, in this case the amount of Mad3 inherited positively correlated with the birth volume. Assuming that both small and big cells possess three YCPs with the associated G2/M delay, we can reason that, in these conditions, the accumulation rate of Mad3 is related to the cell volume. Maybe through a mechanism involving Cdh1 and a YCP sensing factor. Finally, it would be interesting to test the effects of the activation of the SAC in relation to the following timer in G1.

As stated before, Mad3 amounts are equally segregated during cytokinesis. A similar mode of inheritance is found in the prominent Whi5 sizer, where equal segregation is attained by chromatin-based partitioning. In contrast to *MAD3*, *WHI5* mRNA production is constant and independent of cell size (Schmoller et al., 2015; Swaffer et al., 2021) (Fig. 33).

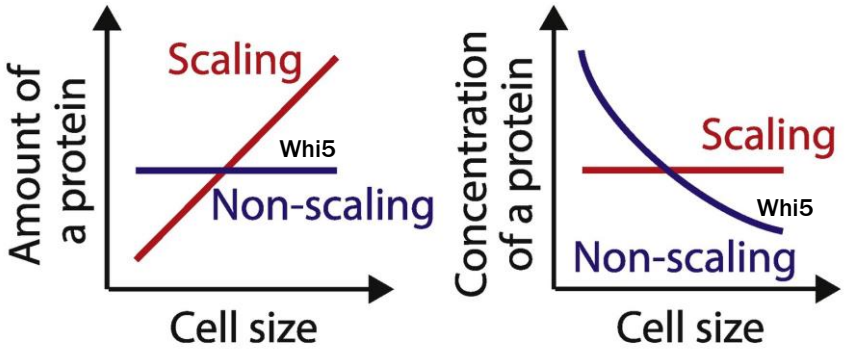

Fig. 33. Protein production and concentration in relation to cell size. **(Left)** Whi5 production (amount of protein) does not scale with cell size while the majority of proteins do. **(Right)** This type of production depict different concentration behaviours according to cell size. Consequently, Whi5 would be diluted as size increases while the concentration of the rest of proteins would remain constant. Modified from (Zatulovskiy and Skotheim, 2020).

The possibility that Mad3 was inherited by chromatin-based partitioning opens the door for linking the timer and also the sizer to ploidy sensing. In the G2/M phase both the Whi5 sizer and the Mad3 timer are accumulated. Nonetheless, this occurs by different mechanisms. The final concentration of a protein depends on the kinetics of mRNA transcription/translation and the degradation kinetics. The mRNA of Whi5 is transcribed mainly in G2/M in a way independent of the cell size. Since Whi5 is essentially not degraded along the cell cycle (Qu et al., 2019), the result is the accumulation of Whi5 during this cell cycle phase. In the case of Mad3, its mRNA production scales with cell size. If Mad3 degradation kinetics were not regulated by cell cycle, its concentration would remain constant. However, the stability of Mad3 depends on the ON/OFF dynamics of Cdh1. During the G2/M phase Cdh1 activity is inhibited and thus Mad3 is stabilized at this point. In the end, both the Mad3 timer and the Whi5 sizer are equally distributed to the lineage. In these circumstances, the timer influence in the next G1 acts as a record of its (random?) accumulation in the previous phase and thus does not correlate with birth size. Regarding the sizer, small cells depict a larger sizer influence than their bigger counterparts promoting a negative correlation with birth size. One point remains to be understood. Knowing that Mad3 stablishes high and low Cln3 degradation rates according to the volume, the timer function still seems to be influenced by the cell size, maybe through the dominant and overlapping effects of the sizer control.

Cdh1 marks the pace of the timer

It is important for understanding the dynamics of a timer the way in which the main Start factors are inherited and the rates or dynamics of their interactions and degradation status. Consequently, all combinatory scenarios would promote high variability in the timer generation at the cellular level, with the consequent addition of variability to the critical size (Talia et al., 2007). Consequently, we could find stochastic timers in different cells according to the inherited levels of Cdh1, Mad3 and Cln3. Cdh1 concentration is constant along the cell cycle and is distributed in proportion to the mother and daughter cell size. The same situation can be found regarding Cln3. Lastly, as stated before, Mad3 is transcribed in consonance with the cell volume, but it is distributed evenly and independently of cell size.

In general, two traits could describe the function of Cdh1. Firstly, we assume constant Cdh1 degradation kinetics over Mad3 and secondly, the activation of Cdh1 after anaphase depict a bistable behaviour (Listovsky and Sale, 2013). This places Cdh1 as the detonator of the timer, like turning an hourglass upside down so that the sand (Mad3) starts to fall (Fig. 34). Hence, the timer variability could come from Mad3 and Cln3. It is plausible to think in a context where the concentration of both proteins at birth does not correlate. The result would be longer or shorter timers according to the

Cln3/Mad3 ratios. Nevertheless, if we discard any restriction or modulator acting in G2/M, it is also possible that Mad3 trigger the degradation of Cln3 already in G2/M.

Within this framework, the concentration of both proteins at birth would negatively correlate in a way that high levels of Mad3 would cause less Cln3 concentrations at birth. Given the bistable dynamics of Cdh1, the real timer would span from G2/M to the next G1/S phase, corresponding to the Cdh1 periods of activity.

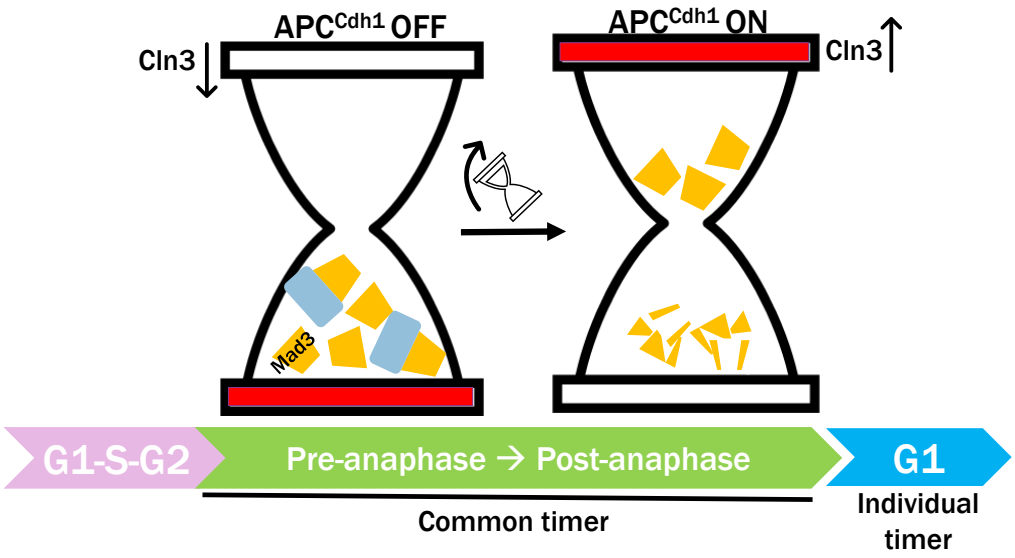

Fig. 34. An hourglass model for the detonation of the molecular timer. Cln3 degradation may start when the APC^{Cdh1} complex is still not active (pre-anaphase) and Mad3 starts accumulating. The hourglass is resting. Once anaphase is triggered, the APC^{Cdh1} complex is activated (the hourglass is turned upside down) and starts the constant degradation of Mad3. Consequently, as Mad3 disappears, Cln3 stability increases and modulates Start at the next G1 phase. Mad3 degradation before cytokinesis would stablish a mother-daughter common timer while its degradation after cytokinesis would depict the effective regulation of the single-cell timer.

This would split the timer function in two periods, the common timer (G2/M) and the individual timer (from mitotic exit to G1/S), maybe with different layers of regulation but both interdependent. Noteworthy, a gap exists between the activation of Cdh1 (post-anaphase) and the moment from which Cln3 degradation begins (pre-anaphase). Consequently, Cln3 degradation starts before the activation of the time pacer. Any delay in the pre-anaphase period would promote the accumulation of Mad3 with a concurrent reduction of the stability of Cln3. Following the hourglass metaphor, the accumulation of Mad3 would correspond to an hourglass more loaded with sand and with an increased time spanning.

A timer, what for?

In rich environments, cells grow exponentially and attain a limited range of sizes before triggering Start. This behaviour has long been studied from the deterministic and stochastic point of view. In this line, the existence of a critical size goes in conjunction with a remarkable variability of sizes for triggering Start. One of the main modulators of this variability is the control of size, without discarding the effects of the molecular noise (Talia et al., 2007). At the molecular level, Whi5 is the only reported sizer. Also, the cell growth rate might be treated as a sizer control (Ferrezuelo et al., 2012; Schmoller et al., 2015). Our results point to a timer adding an extra control of cell size in G1 and thus it is possible that what in reality was time control variability has been interpreted as molecular noise. Nonetheless, most studies report a dominant size control over time control (Schmoller et al., 2015; Schneider et al., 2004; Talia et al., 2007; Turner et al., 2012). In fact, other studies discard a significant effect of time for Start execution. One model found no correlation between volume at Start and the time to reach Start (Ferrezuelo et al., 2012). Other studies stablished a model where cell size variability exerted by an imperfect sizer was enough for explaining the characteristics of Start transition (Chandler-Brown et al., 2017). However, our analysis shows that at a fixed cell volume, the time spent in G1 is also a valid parameter for predicting budding. Importantly, this time predictor trait was lost when Mad3 was out of the system.

In any case, size control is still dominantly executed by a sizer. This does not discard the influence of other overlapping modes that contribute to size control. In a deterministic model, size control should always lessen the variability of size at Start. Nevertheless, a more stochastic size control explains this variability as the result of volume-induced probabilities for Start execution (Chandler-Brown et al., 2017). At the population level, the range of cell sizes points to a variability that may be beneficial for organisms that are expected to be ready for a wide range of hostilities. Consequently, it is possible to think that not all layers of size control work for setting or limiting the size at which a cell triggers Start. This should be in harmony with a size control that ensures the efficient coordination of size with product biosynthesis. The addition of different strata of size control also add noise to this process. While the sizer may work in limiting size, its combination with a timer may add variability at the population by relaxing the size requirements for triggering the cell cycle. Under a full sizer control, the inherent variability in yeast populations would decrease by restricting too small or too large cells. In this case, cells that are able to acquire an optimal size are usually the ones that grow faster. Conversely, evolution has selected an equilibrium of small – normal – big cells that is maintained due to its beneficial characteristics. The variability of cell sizes emerges from the diversity of growth rates at the cellular level. In this situation, a timer could assist cells growing slower by allowing them to trigger Start even if they have not reached an optimal size (Fig. 35). This would help to maintain a

population of small cells that would be otherwise counter-selected if they only depended on sizers. In a more general context, a timer could work as an emergency mode for triggering the cell cycle when it is not possible to grow for reaching certain cell sizes, as in hostile environments. Under these conditions, cells would give priority to entering the cell cycle in spite of not having a proper size.

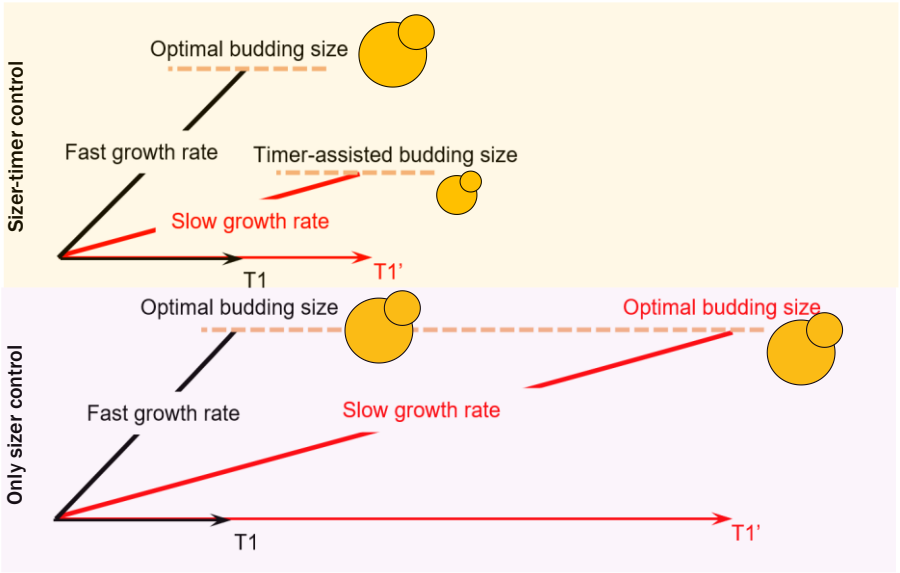

Fig. 35. Cell-size population consequences of different modes of size control. (Above) The combination of sizers and timers modes of control allow small cells to trigger Start even under sub-optimal size conditions. This would maintain a basal number of small cells. (Below) Only-sizer conditions would be detrimental for slow growing cells since they would need too much time for attaining the optimal budding size. T=time.

All studies regarding mammalian cells have been hindered by the technical limitations of measuring cell volumes and tracking these parameters at the single-cell level. Firstly, data from *in vitro* cultured cell lines quantified the cell volume by fluorescent exclusion measurement. The results from the birth volume vs volume extension plots mimicked the slopes found in budding yeast (Cadart et al., 2018b). Importantly, size was modulated through growth rate and time for generating the adder mode of size control. This is similar to studies in *E. coli* and budding yeast (Campos et al., 2014; Chandler-Brown et al., 2017; Soifer et al., 2016). In budding yeast, the adder would emerge from the analysis of the whole cell cycle and not only from G1 (Chandler-Brown et al., 2017).

As being stated, mammalian cells also show some level of time control, at least *in vitro*. The study of cell size *in vivo* can be a daunting task. In this line, the first approach was done in mouse epidermal stem cells. The histological characteristics of this tissue along with a cell cycle reporter depicted a sizer control in this organ (Xie and Skotheim, 2020). *In vivo* systems contain additional layers of complexity since growth and division is not always a coordinated process or directly depend on the micro-environment. Some tissues are phenotypically large but, in some cases, this is due to a general increase in cell size while in others it is produced by additional cell numbers. We cannot discard the

concurrent influence of other and yet to be identified modes of size control (Zatulovskiy and Skotheim, 2020). The exceptional adaptability of life to different scenarios directly affects the decision of cell cycle entry and the consequent size that ensures an optimal scaling with the biosynthetic program.

Whi8 dynamic interactions within SGs

The emergence of stress granules (SGs) as phase-separated condensates that mediate translational restriction and signalling modulation is one of the main responses against stress conditions. Their formation is mainly cytoplasmic, with presumably small nuclear contribution to their assembly (Zhang et al., 2018). As a conserved mechanism, most living systems have been reported to trigger their formation, with crucial functions in cell homeostasis and disease. The promiscuous composition of stress granules bestows them high interaction dynamics that adapt their formation to almost any stress circumstance. Stalling translation virtually restrains any biological process inside cells, with special influence on proteins that are regulated through gene expression.

Our work links the stress response to the machinery of the cell cycle through the action of well-known Start participants. In this context, Whi8 couples both processes with characteristics that make it suitable as a dual molecular player. First, Whi8 contains intrinsic disordered regions (IDRs) that are commonly found participating in liquid-liquid phase separation (LLPS) (Kuechler et al., 2020). Second, Whi8 is capable of capturing RNAs through its RRM (RNA recognition motifs). Third, it is able to interact with Cdc28 and phenotypically modulate the budding volume. Our work confirms the interaction between Cdc28 and Whi8 but also places Whi8 close to the nuclear SG core given the presence of Pub1 in Whi8 immunoprecipitations (IPs). We cannot discard an indirect Whi8-Pub1 interaction. Indeed, it appears that RNA does not mediate this interplay, at least in steady state. On the contrary, it could be that RNA assists but not stabilizes the interaction between Whi8 and Pub1 during SGs formation (Campos-Melo et al., 2021). In general, protein-protein interactions depict slow turnover interactions and consequently are associated to stable internal structures of stress granules. In fact, some results point that phase separation emerges from the cores of stress granules (Wheeler et al., 2016). Given the intrinsic properties of Pub1 for generating stress granule condensates (Kroschwald et al., 2018), Cdc28 may be one of the first proteins recruited to SGs that do not contain neither IDRs nor RRMs. Also, these entities need to be dissolved before cell cycle re-entry.

Whi8 multivalency is probably attained through the combination of IDRs and RRMs. This feature is crucial for priming the formation of phase separation (Protter and Parker, 2016a). Importantly, Whi8 can bind and recruit the mRNA of *CLN3* to stress granules (Fig. 36). Actually, other partners related to Whi8, like Whi3, depict similar roles. As Whi8, Whi3 interacts with Cdc28 and binds the *CLN3* mRNA. Whi3 is also driven to stress granules under stress (Holmes et al., 2013). However, its loss does not

affect the translation of target mRNAs but can influence mRNA abundancy (Holmes et al., 2013). Interestingly, in normal conditions, our data suggest that the overexpression of Whi8 has not any effect on neither the translation of the *CLN3* mRNA nor the total mRNA amounts.

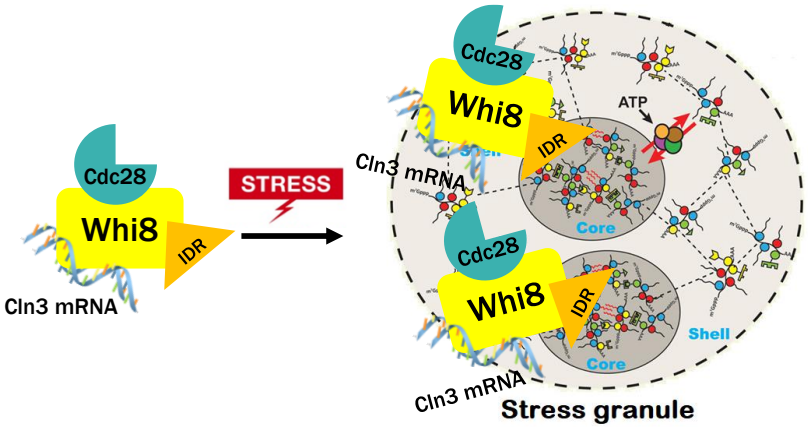

Fig. 36. Whi8 is localized in stress granules and interacts with the mRNA of Cln3 and the Cdc28 protein. Under stress conditions it drives the localization of Cdc28 and the mRNA of Cln3 to stress granules, probably close to the core section.

As in other proteins related to LLPS, the IDRs present in Whi8 are important for its localization in stress granules. IDRs may intercede in the Pub1-Whi8 interaction albeit their multivalency could be more focused on interactions with faster turnovers. Intriguingly, the IDR region is also important for placing Whi8 in the endoplasmic reticulum (ER) fraction. The first reported function of Whi8 is related to the ER as an enhancer of ER – mitochondria tethering protein (Kojima et al., 2016). The duality of Whi8 as a *bona fide* stress granule protein and as a component of the ER raises the possibility that Whi8 participates in the regulation of SGs at ER contact sites (Lee et al., 2020). Other similar proteins like Whi3 may also have a role in this mechanism of SG regulation.

Recruiting the mRNA of Cln3 to stress granules

The relation of Whi8 and Whi3 is closely related to the *CLN3* mRNAs. Firstly, Whi8 and Whi3 interaction depends on the presence of RNA. Second, both proteins bind the mRNA of *CLN3* and promote its immunoprecipitation (IP) with Pub1. Similar to Whi3, the deletion of Whi8 increases the basal amounts of some mRNAs bound to Pub1, as in the case of the mRNA of *HXK1*. In the IP of Pub1 the enrichment of *CLN3* mRNA is dramatically affected when Whi8 is absent, with a less important role of Whi3 in these circumstances. This is confirmed when quantifying the colocalization with the *CLN3* mRNA foci. The deletion of *WHI8* almost totally abrogated the formation of *CLN3* mRNA foci. Also, the concomitant deletion of *WHI3* had almost no effect on the foci number in the same way that there is no data confirming the interaction of Whi3 with Pub1. This points to a specific role of Whi8 directing

the mRNA of *CLN3* to SGs foci. This is interesting given the similarity of Whi8 and Whi3. Across evolution Whi8 acquired a specialized role recruiting the mRNA of *CLN3* to stress granules. By contrast, Whi3 has roles more related to mother-daughter asymmetric inheritance. The promiscuous nature of transcriptome and interaction network of SGs makes difficult to assign specificity in this framework. Consequently, the transport of *CLN3* mRNA to stress granules may be relevant for SG homeostasis and cell survival. Little is known about the dynamics that make Whi8 suitable for this specific transport. We can imagine that Whi8 is able to stabilize the mRNA of *CLN3* (half life = 1.4 minutes) with high affinity constants and promoting stable RNA conformations.

Considering that only about 10% of total mRNA is present in SGs, G1 cyclins and Clb2 are the only mRNAs of cyclins that are enriched in SGs. Among them, the mRNA of *CLN3* is the most enriched RNA in SGs among all cyclins (4-fold) (Khong et al., 2017). This can be partly explained through the directed action of Whi8. Given the bistable and rapid formation kinetics of stress granules along with the low stability of the mRNA of Cln3, the association constant of Whi8 to stress granules should be high. This can occur through multivalent interactions (mediated by IDRs?) that drive the association of Whi8 and Pub1, or maybe by a direct interaction of Pub1 and Whi8at the SG core. The fact that core particles have been reported as the first SGs structures to form, suggests that the second option is very likely. Still, we know that after stress the mRNA of *CLN3* is partially degraded (40% reduction the first 30 minutes). The remaining mRNA probably corresponds to the sum of the SG-associated and the cytoplasmic mRNA of *CLN3*. After 60 minutes of constant stress, we quantified just 10% remaining from the initial level of mRNA. This last half of mRNA probably corresponds to the real percentage of mRNA recruited to stress granules. Nonetheless, when stress is sustained or surpasses some intensity levels the structure of stress granules is weakened and thus SGs may undergo non-regulated dissolution.

Noteworthy, under stress conditions the protein levels of Cln3 sharply decrease during the first 20 minutes and then stabilize at very low levels. This means that the protein degradation machinery still works at least during the first minutes after stress. This could be possibly helpful for degrading truncated or misfolded proteins that can be harmful for the cell. Besides, the inhibition of the ubiquitin-proteasome system could stimulate the formation of stress granules that can unbalance the SG homeostatic amounts (Mazroui et al., 2007). Interestingly, when Whi8 is deleted the protein levels of Cln3 decrease slower. Since protein translation is gradually stalled and the mRNA levels of *CLN3* are not altered by removing Whi8, we can think in two combinatorial options. First, it is possible that Whi8 mimics the mRNA interactions already depicted by Whi3 (Garí et al., 2001b). As a result, under stress we can imagine that most of *CLN3* mRNAs will be cytoplasmic in absence of Whi8. In this context, even under stress conditions is possible that cells depict basal levels of mRNA translation that stabilize Cln3

protein production. One clue about this possibly is the fact that eIF2α phosphorylation is gradual and thus translation is not totally inhibited 20 minutes after stress (Wheeler et al., 2016). Last, Whi8 could participate as regulator of the degradation machinery of Cln3 and thus without Whi8 the degradation machinery would become compromised. In summary, keeping high protein levels of Cln3 may compromise the stability of stress granules due to a probable increase of the stochastic activation of Cdc28. Alternatively, the lack of Whi8 probably alters the translation of mRNAs localized to SGs (Mateju et al., 2020), as in the case of *CLN3*. Future studies will provide the real implications of impaired mRNA recruitment to stress granules.

It is also possible that other proteins recruit the mRNA of *CLN3* to SGs. In any case the role of such proteins seems not to compensate the lack of Whi8. Given the great interplay between P bodies and stress granules, we can think of a mechanism that recruits important mRNAs to P bodies when their recruitment to SGs is compromised. The dynamic interchange of material between these two entities supports this possibility (Luo et al., 2018; Stoecklin and Kedersha, 2013). In this line, this does not discard that other mRNAs can travel with Whi8. Whi8 RRM binding motifs depict high binding versatility (Maris et al., 2005) capable of recruiting the mRNAs of *WHI3*, *WHI8* and even the mRNA of *CDC28* in smaller amounts (our unpublished data).

Cdc28 functional roles in stress granules

The presence of Cdc28 in stress granules has been reported through proteomic analysis and indirect methods (Jain et al., 2016a; Wippich et al., 2013a). Pub1 was immunoprecipitated along with Cdc28 in our lysates. In addition, we confirmed the presence of Cdc28 in stress granules by fluorescence co-localization with Pub1.The fact that Cdc28 is enriched in SGs does not mean that all Cdc28 moves to this location. Under the microscope it is possible to observe a considerable signal from cytoplasmatic Cdc28. Cdc28 has not any IDR or RRM segment. This reinforces the idea that Cdc28 is driven to stress granules by an assistant protein in the same way that (probably) discards Cdc28 as a nucleation factor in SGs formation. In this context, we found that deletion of *WHI8* decreased the localization of Cdc28 in Pub1 foci. In these cells Cdc28 was still found to co-localize with Pub1 albeit to a less extend. Our results point to Whi8 as the main partner that directs Cdc28 to SGs, but Whi3 may also depict some effect that remains to be assessed. As a whole, Whi8 displays an outstanding role as a cell cycle control recruiter to SGs, where both Cdc28 protein and the mRNA of *CLN3* connect to SGs through this protein. As a whole, this highlights the multivalency nature of SGs-related proteins as general modulators of cell homeostasis.

The stress response is able to arrest the advance of the cell cycle regardless the activation of additional checkpoints. This allows the cell cycle to be stopped at any point. Given that the stress granule

formation is triggered by stalling translation, arresting the cell cycle may be a consequence of the activation of the stress response. In the same way, all processes involved in cell growth and cell size regulation (tightly related to the cell cycle control) remain arrested. So far, proteomic analyses of SGs only found Cdc28 as a representative member of the canonical cell cycle control system (Jain et al., 2016a). Other participants such as Cdc33 or Cdc48 are respectively related to protein translation and SGs clearance. At the mRNA level, all *CLN* cyclins along with *CLB2* are also displaced to SGs. This discrepancy between either protein or mRNA recruitment depending on the cell cycle regulator suggests different roles in the context of the stress response. One can imagine that mRNAs present in stress granules may represent ready-to-translate mRNAs in contrast to their cytoplasmatic counterparts (Mateju et al., 2020). Alternatively, given that in some cases both mRNA and protein entities depict low stability, the recruitment of mRNA could be favoured probably because it works in close contact with SGs-related proteins. Knowing that Cln3 protein is quickly degraded after stress supports the possibility that cyclin degradation may be a side effect of the stress response that allows effective cell cycle arrest. In this case, directly recruiting Cln3 protein instead of mRNA would delay the translation of Cln3 during stress. In case of Cdc28 (and translation factors), the direct recruitment at the protein level may involve either direct roles on SGs dynamics (Shattuck et al., 2019; Wippich et al., 2013a) or induce localized translation upon stress relief (Mateju et al., 2020).

We assessed these last possibilities in the case of Cdc28 since many Cdc28 targets were present in stress granules. Our time-lapse experiments showed a significant delay in SGs dissolution when Cdc28 was destabilized in a thermosensitive budding yeast strain. Conversely, the overexpression of *CLN3* made SGs dissolve faster. This last situation points to an imbalance in the ratio of cytoplasmic-stress granule localization of this G1 cyclin, probably at the protein and the mRNA level. In this line, problems with the homeostasis of SGs formation and dissolution are closely related to many diseases (Asadi et al., 2021; Dubinski and Vande Velde, 2021; Song and Grabocka, 2020). Also, cells do not restart growth and cell cycle until the stress granules are disassembled. Further studies are needed for assessing the consequences of too slow and too fast disassembly kinetics of stress granules in budding yeast. In support to our first results, we performed an experiment in which we modulated the activation of Cdc28 according to the expression of *CLN3* in a *cln1,2* mutant strain (Cdc28 OFF). The inhibition of *CLN3* expression in this strain causes a strong G1 arrest in a state of low Cdk activity. Within this framework, the dissolution of SGs was delayed in comparison to a cln1,2 strain with high expression of *CLN3* (Cdc28 ON). Hence, here we are considering the disassembly kinetics of SGs according to the activation states of the Cdk. Interestingly, the initial number of stress granules was comparable in both cases and thus points that the influence of Cdc28 activity was marginal in the context of SG formation (similarly to the *cdc28-13* strain). The same would occur with the G1 cyclin mRNAs and with the carrier

functions of Whi8. Additionally, it would be interesting to know if the activity of Cdc28 is related to its localization in SGs. Even so, since we apply stress saturating conditions, we still cannot discard differences in the assembly kinetics of stress granules. Noteworthy, our wild-type cells trigger the entry to the cell cycle in comparison to the G1-arrested strain. Consequently, maybe some effectors that are not directly related to Cdk activity may still regulate SGs dismantling, such as the activity of the non-canonical Cdk Pho85 (Carroll et al., 2001). In any case, we can confirm that the activity of Cdc28 has a major impact on the dynamics of stress dissolution.

Regarding our time-lapse experiments tracking the disassembly of stress granules, the dissolution kinetics of both control strains were similar (WT and *CLN3 cln1,2*). However, they depicted slight differences 120 minutes after the release from stress. It appears that in the case of the *cln1,2* mutant, the basal levels of stress granules were higher than the wild-type strain. Interestingly, there were no significant differences between the dissolution kinetics of *cdc18-13* and Cdc28 OFF strains. These differences probably arise from the combination of the recovery conditions that promote the total dissolution of SGs (37°C in the case of WT) with genetical differences. Therefore, the lack of Cln1 and Cln2 may have an effect that increase the basal number of stress granules.

Quick environmental changes test the stress response and its dynamics. Given the relevance of Cdc28 in the kinetics of SGs, the stress response is different according to the moment of cycle in which cells are exposed to stress. The disassembly of SGs is delayed if the stress appeared in G1, a state of low Cdk activity. Conversely, stress granules are dissolved faster in the rest of phase (S-G2-M), where Cdk activity is higher. This could adapt the stress response to the cell cycle. Thinking on the biochemical reactions present in different cell cycle phases, it is possible to imagine that the formation of SGs during DNA replication or segregation is more delicate than SGs formation during G1. High activity of the Cdk may guarantee a rapid recovery from stress for ensuring the completion of the cell cycle. Besides, the next G1 phase contains specific cell cycle responses that may delay the entry to the cell cycle in cooperation to the stress response.

Stress granule regulation of translation

One key point about the implications of stress granules is their influence on post-stress translation dynamics. So far, we knew that localized translation is a common in event among the functional roles of SGs (Mateju et al., 2020). Besides, Cdc28 phosphorylates some members of the translation machinery. For that reason, one important question would be if stress granules directly participate in the inhibition of translation until stress relief. Our results point that SGs act as translational repressors of specific mRNAs through the activation state of Cdc28 (Fig. 37). The formation of stress granules through the initial cores recruits many RNA-binding proteins and mRNAs that will generate liquid-

liquid phase separation. During this process, the mRNA of virtually all genes can be recruited to SGs. Nonetheless, some of them are specially enriched and detected by the analysis of the transcriptome (Khong et al., 2017).

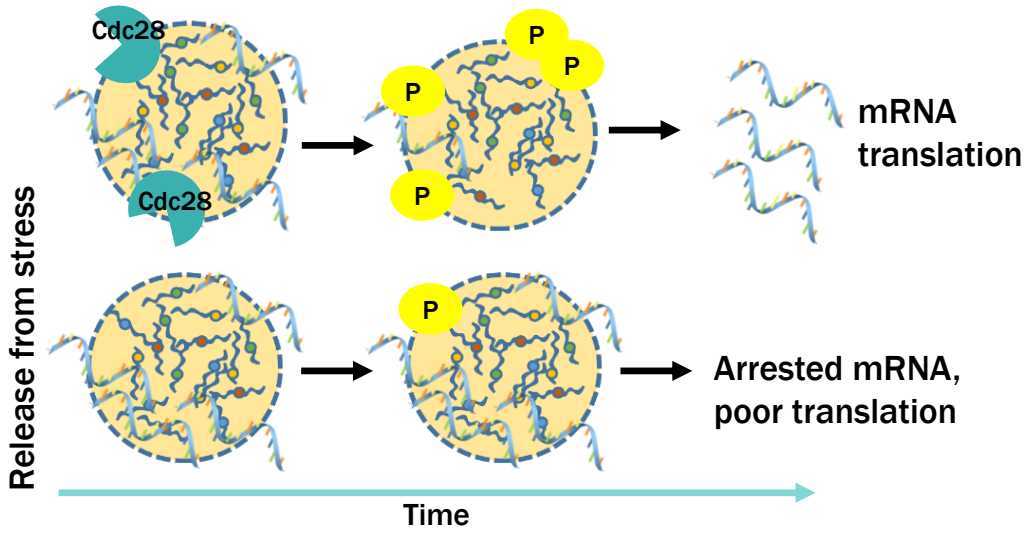

Fig. 37. The Cdk modulate the translation of mRNAs associated to stress granules (SGs). **(Above)** Upon stress relief, SGs disassemble (in part) by the action of Cdk-mediated phosphorylations. These phosphorylations also stimulate the expression of mRNAs that were arrested in SGs. **(Below)** When Cdc28 activity is compromised, stress granule dissolution is delayed in the same way that SG-associated mRNAs are poorly translated.

When we analysed the post-stress translation of mRNAs that are poorly recruited to stress granules, the result was that their translation was efficient regardless of the presence of Cdc28. Conversely, mRNAs enriched in stress granules depicted low post-stress translation when Cdc28 was destabilized. As a result, Cdc28 modulates the kinetics of SGs disassembly and the consequent translation dynamics of SG-related mRNAs. For instance, the expression of *SNF2* was almost negligible during the first 100 minutes after stress relief in the *cdc28-13* strain. At this point the dissolution of stress granules has probably reached to 75% in the *cdc28-13* strain. Curiously, *SNF2* translation did not started even with most stress granules already disassembled in the *cdc28-13* strain. This last result points to a second mechanism of translation resumption that does not depend on Cdc28 but may work in cooperation with it. In parallel, the function of Cdc28 not only modulates intra-SGs translational dynamics but also stimulates the translation of released mRNAs. In the wild-type strain, SGs mRNAs start to translate from the very beginning of stress release. Actually, our expression level plots depict different behaviours according to different post-stress moments. From minute 100, the expression level increases sharply in comparison to earlier post-stress translation. We hypothesized that at this point exists a cooperative mechanism of expression that assists the translation of cytoplasmic mRNAs that have been freed from stress granules independently of Cdc28. In conclusion, this would assign to

stress granules an inhibitory role to the expression of the mRNAs in a way that their formation would work in cooperation with the phosphorylated form of eIF2α. All this knowing that the phosphorylation of eIF2α usually precedes the formation of stress granules.

Bistable dynamics of stress granules

Membranes in life have multiple advantages both at the structural and the signalling level. However, their nature also may be limiting under certain circumstances. When cells detect any hostile condition, they are ready for triggering a quick and reliable response: the formation of stress granules. If stress granules would require the assembly of an external membrane, it would become a time and energy consuming process. In this line, the bistable dynamics showed by stress granules would be more complex in the context of membrane-surrounded entities. The generation of multivalent interactions mediated by the nature of RBPs and RNAs creates a thermodynamically stable state from which liquid-liquid phase separation emerges. In consequence, even going against entropy, the enthalpic contributions of SGs multivalent interactions would contribute to a suitable energy state (Shin and Brangwynne, 2017).

The assembly of stress granules recruits a rich diversity of molecules and interactions. Importantly, the formation of SGs inhibits the function of Cdc28 by sequestering the mRNAs of some cyclins and also by restricting the activity of Cdc28 close to SGs. In the same way, the kinase activity of Cdc28 destabilizes the interactions that balance the thermodynamics of LLPS. In consequence, SGs recruit their own kinase inhibitors. As a whole, this mutual inhibition framework promotes the generation of bistability to the dynamics of stress granules. When we modelled mutual inhibition with experimental parameters, we can divide this simulation into two sub-processes. One corresponds to the assembly/disassembly kinetics of stress granules in a way that is stimulated by stress and inhibited by the activity of the Cdk. The other corresponds to the activation/inhibition of Cdc28 according to the formation of SGs. The combination of both processes (mutual inhibition) depicts two steady states in which the dynamics of SG assembly/disassembly are balanced with the dynamics of Cdc28 activation and inhibition. The model predicts a stress level threshold from which the formation of SGs is dramatically increased.

Our experimental data testing different levels of stress by using sodium azide (NaN_3) coincides with our simulations. In this line, the system possessed a hysteretic behaviour confirmed through our experimental data. Consequently, in the context of bistable SGs it is not the same moving from low stress (few SGs – high Cdk) to high stress (many SGs – low Cdk) than moving from high stress to low stress. When cells return from high stress, they need lower levels of stress for achieving the dissolution of SGs in comparison to the level of stress needed for triggering the formation of SGs. At the molecular

level, this could occur due to the different dependency on Cdc28 in relation to formation and dissolution of stress granules. Our model assigns a major role to the Cdc28 Michaelis-Menten (K_m) constant for generating bistability to stress granules. This is directly related to the substrate concentration ([substrate]) inside SGs. Low substrate concentrations (cytoplasmatic concentrations) bypass the generation of bistability in favour to gradual formation of SGs. Conversely, when [substrate] increases due to the accumulation of many Cdc28 targets in stress granules, the model predicts good bistability. In consequence, stress granule formation may induce the formation of low substrate concentrated structures (or at least similar to cytoplasmatic substrate concentration) at low levels of stress. In this situation, Cdc28 activity would not be localized in stress granules. By contrast, if stress reaches certain levels, the localized [substrate] in SGs would increase in the same way that many mRNAs are recruited to them, setting the conditions that favour Cdc28-mediated bistability. We can imagine that Cdc28 modulates the hysteretic behaviour of SGs according to the substrate concentration direction. Within this framework, the effective Cdc28-substrate concentration in SGs increases with the intensity of the stress going from low to high [substrate]. By contrast, cells transferred from stress to normal conditions need to reach less stress intensity for depicting bistability in the high to low [substrate] direction. In this context, the activation status of Cdc28 is different when going from stress conditions to stress release in comparison to the inverted path. Consequently, the Cdk activity may modulate hysteresis according to the direction of the effective SGs substrate concentration (Fig. 38).

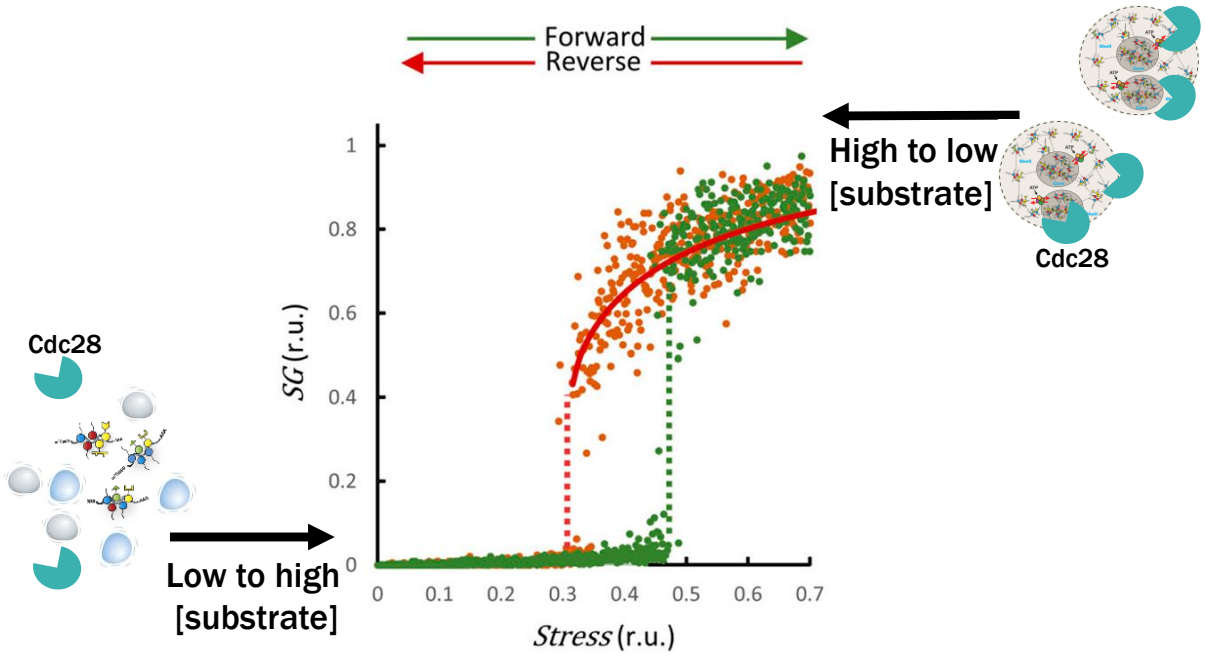

Fig. 38. The hysteretic behaviour of SGs could be modulated by Cdk. According to stress intensity, the local concentration of substrates increases in stress granules until bistability emerges at a certain level of stress.

Certain level of stress is needed for reaching the optimal substrate concentration for generating Cdc28-mediated bistability. On the other way, If we start from high stress conditions, stress granules are potentially stabilized through several multivalent interactions. At this point, different initial substrate concentration and Cdc28 activation status promote a displacement of the bistable jump.

The cell cycle – stress response interplay is conserved in mammal cells

The stress response encompasses a large number of strategies that vary according to the type of stress, the intensity, and the cellular context. Nonetheless, the traits underlying the most fundamental properties of the stress response are conversed across life. Consequently, mammalian cell lines also depict the formation of mRNA-RBP condensates also called stress granules. Previous works already reported Caprin1 as a *bona fide* stress granule component (Kedersha et al., 2016). It also contains both IDR and RRM regions that can bind the mRNA of cyclin D2 (Solomon et al., 2007; Yang et al., 2019) . Although not sharing sequence similarities, we tested the possibility that Caprin1 could acts as a functional homolog of Whi8. First, under stress conditions, we have showed that Caprin1 was able to recruit the mRNA of cyclin D1 to Caprin1 fluorescent foci. To support this observation, when Caprin1 was silenced, the number of cyclin D1 mRNA foci was reduced. In line with Whi8, Caprin1 was able to interact with Cdk4 under stress conditions. Importantly, when we checked TIA-1 (Pub1 homolog) localization as a proxy of SG formation, the silencing of Caprin1 did not affect the basal formation of SGs. Hence, Caprin1 appears to mimic the functional role Whi8. One important difference with budding yeast is the fact that transcriptomic analysis of G1 cyclins shows no enrichment in SGs (Khong et al., 2017). Still, the recruitment of G1 cyclins to SGs would aid to reduce cyclin protein levels during stress. In summary, Caprin1 carries the mRNA of G1 cyclins to stress granules albeit they are not specifically enriched into these condensates. Actually, the only cell-cycle related cyclins are cyclin E1 and all B cyclins along with other atypical cyclins (Khong et al., 2017). In any way, both cyclin D1,2 and Cdk4 belong to G1 regulation in mammalian cells. Given the complexity of Cdk-cyclin combinations in mammalian models, it is tempting to think in a model of different Cdk partners driving the SG localization of different Cdks according to the corresponding cell cycle phase. Intriguingly, the phosphorylation status of Caprin1 modulates the translation/deadenylation fate of stress granule mRNAs (Kim et al., 2019). In this context, the activity of different Cdks may regulate the dynamics of mRNA through specific phosphorylation of RBPs like Caprin1.

When assessing the possible roles of Cdks in stress granules we thought that it would be difficult to obtain significant results by just removing one Cdk from the system. The general detrimental effects of gene silencing or genetic manipulation prompted us to analyze the influence of Cdk activity by a different approach. The Cdk activity levels intercalate G1 low-activity states with S-G2-M high activity states. In parallel to budding yeast, we followed SG dissolution at both G1 and S-G2-M phases in the

U20S cell line. Interestingly, we found remarkable SG disassembly kinetics comparing this two Cdk activation states. G1 cells depicted delayed dissolution dynamics in comparison to cells that were caught at a different cell cycle phase. Consequently, Cdk activity also appears to modulate the stability of SGs in mammal cells. When we compared budding yeast and U2OS cells, they presented different dissolution kinetics according to cell cycle phase. In the case of budding yeast, the differences between G1 and S-G2-M dissolution kinetics were smaller in comparison to their mammal cells counterparts. This points to a more relevant link between cell cycle and SG kinetics in mammalian cells. In fact, previous studies showed that the inhibition of Cdks impairs the disassembly of stress granules (Wippich et al., 2013a). We cannot discard that these differences may emerge due to differences in the nature of the stress. Further studies are needed for assessing if impaired Cdk activation may lead to hyperstable stress condensates. In the end this would stablish stress granules as potential targets for treating many life-threating diseases (Mahboubi and Stochaj, 2017; Wang et al., 2020).

Timer and stress granule possible synergies

Mechanisms that control size and stress are ubiquitous and well preserved among living systems. At any or other point the molecular apparatus is well embedded for attaining good coordination in different contexts. In this work we describe a molecular mechanism that stablishes different degradation dynamics of Cln3 according to a specific moment of the cell cycle. This in the end modulates the activity of Cdc28. This kinase is also modulated when stress promotes the formation or dissolution of stress granules (SGs). As stated before, cells are ready for responding against many hostile and unexpected situations. Our results in fact show that the dissolution of stress granules is influenced by the moment of the cycle in which the stress response has been launched.

Phase separation, namely, liquid-liquid phase separation (LLPS) has been reported to influence cell cycle mostly in mitosis (Liu et al., 2020). The material properties of chromatin along with the mitotic spindle promote the formation of transient LLPS structures that are thought to regulate mitosis. Interestingly, the phosphorylation of the RNA pol II C-terminal domain (CTD) is important for triggering Start (Kõivomägi et al., 2021). At the same time, other reports point that the hyperphosphorylation of the RNA pol II CTD is promoted by liquid-liquid phase separation (Lu et al., 2018).

One important feature of the stress response is that its assembly is mostly cell cycle or checkpoint independent. This does not contradict the fact that crucial components of the cell cycle machinery participate in the dynamics of stress granules, as it has been shown here. In this regard, the kinetics of stress granules could be modulated through crucial elements of the cell cycle control system such as Cdc28 or Cln3. While stress granules are cytosolic structures, Cdc28 navigates from the cytoplasm to the nucleus at different cell cycle stages. Cln3 also depicts a cytosolic to nuclear migration while

Mad3 and Cdh1 are mainly nuclear proteins. We propose that small slow-growing cells are the ones in which the timer would have a prominent role. In this context, slow-growing cells would spend more time in G1 increasing the probabilities that stress conditions occur mostly in this phase. Given this, the assembly of stress granules would set a new scenario in the molecular timer. Upon stress, the recruitment of the mRNA of Cln3 to SGs occurs in parallel with its degradation at the protein level. This is supported by the fact that Mad3 has not been found at neither proteomic nor transcriptomic databases related to stress granules. Thus, we presume that nuclear Cln3 degradation is still mediated by Mad3-Cdc4 under stress conditions. At this point cells not only remain arrested in G1, but also halt growth. Mad3 expression is not stimulated under stress according to the SPELL database, suggesting that Mad3 levels remain constant during stress. Interestingly, the Cdh1 mRNA is enriched in SGs. We imagine a situation in which accumulating the mRNA of Cdh1 in granules would be useful for modulating G1 phase. Regarding the timer functions, it would be interesting to see that, under stress, small G1 cells accumulate more mRNA of Cdh1 than bigger G1 cells. This should be in concordance with our observation that small G1 cells degrade Cln3 at higher rates in comparison to bigger cells. The influence of stress on this or other related mechanisms regarding cell size are yet to be discovered. However, the stress response is also active at S-G2-M phases. In this line, the accumulation of Cdh1 in stress granules may also favor the bistable behaviour of the activation of Cdh1 and thus promote a quick and neat exit from mitosis when stress is relieved.

CONCLUSIONS

G1-Cdk modulation by time

1. Cln3 accumulates in the nucleus during G1 and modulates the nuclear import rate of Cdc28
2. The stability of Cln3 in G1 greatly depends on the presence of Mad3
3. Mad3 protein is degraded during G1 according to the activity of the APC^{Cdh1} complex
4. Mad3 amounts are equally segregated in mother and daughter cells
5. Mad3 allows the scaling of Cln3 degradation rate with cell size
6. Wild-type cell size regulation corresponds to a mixed contribution of sizers and timers
7. Mad3 is a key component of the timer device.

G1-Cdk modulation by stress

1. Whi8 localizes to stress granules (SGs) and modulates the budding volume
2. Whi8 requires an intrinsically disordered region (IDR) for SG localization
3. Whi8 tethers the *CLN3* mRNA to SGs
4. Whi8 interacts with Cdc28 and promotes its recruitment to SGs
5. Cdc28 activity modulates the disassembly kinetics of SGs
6. Cdc28 modulates the translation of mRNAs recruited to SGs
7. Cdc28 and SGs mutual inhibition display bistable and hysteretic dynamics
8. Low-high Cdk during the cell cycle modulates disassembly kinetics of mammalian SGs
9. Caprin1 acts as a functional homolog of Whi8 in mammalian cell lines

BIBLIOGRAPHY

Adjibade, P., St-Sauveur, V.G., Huberdeau, M.Q., Fournier, M.J., Savard, A., Coudert, L., Khandjian, E.W., and Mazroui, R. (2015). Sorafenib, a multikinase inhibitor, induces formation of stress granules in hepatocarcinoma cells. Oncotarget *6*, 43927–43943.

Aizer, A., Kalo, A., Kafri, P., Shraga, A., Ben-Yishay, R., Jacob, A., Kinor, N., and Shav-Tal, Y. (2014). Quantifying mRNA targeting to P-bodies in living human cells reveals their dual role in mRNA decay and storage. J. Cell Sci. *127*, 4443–4456.

Alberti, S., and Dormann, D. (2019). Liquid–liquid phase separation in disease. Annu. Rev. Genet. *53*, 171–196.

Alberti, S., Gladfelter, A., and Mittag, T. (2019). Considerations and challenges in studying liquid-liquid phase separation and biomolecular condensates. Cell *176*, 419–434.

Aldea, M., Jenkins, K., and Csikász-Nagy, A. (2017). Growth rate as a direct regulator of the start network to set cell size. Front. Cell Dev. Biol. *5*, 57.

Anders, M., Chelysheva, I., Goebel, I., Trenkner, T., Zhou, J., Mao, Y., Verzini, S., Qian, S.B., and Ignatova, Z. (2018). Dynamic m6a methylation facilitates mRNA triaging to stress granules. Life Sci. Alliance *1*.

Anderson, P., and Kedersha, N. (2009). RNA granules: Post-transcriptional and epigenetic modulators of gene expression. Nat. Rev. Mol. Cell Biol. *10*, 430–436.

Anderson, P., Kedersha, N., and Ivanov, P. (2015). Stress granules, P-bodies and cancer. Biochim. Biophys. Acta - Gene Regul. Mech. *1849*, 861–870.

Ang, X.L., and Harper, J.W. (2005). SCF-mediated protein degradation and cell cycle control. Oncogene *24*, 2860–2870.

Armstrong, C., and Spencer, S.L. (2021). Replication-dependent histone biosynthesis is coupled to cell-cycle commitment. Proc. Natl. Acad. Sci. U. S. A. *118*.

Artom, C. (1926). Tetraploidismo e Gigantismo. Esame comparativo degli stadi postembrionali dell'Artemia salina diploide e tetraploide. Int. Rev. Der Gesamten Hydrobiol. Und Hydrogr. *16*, 51–80.

Asadi, M.R., Sadat Moslehian, M., Sabaie, H., Jalaiei, A., Ghafouri-Fard, S., Taheri, M., and Rezazadeh, M. (2021). Stress Granules and Neurodegenerative Disorders: A Scoping Review. Front. Aging Neurosci. *13*, 310.

Baena, E., Gandarillas, A., Vallespinós, M., Zanet, J., Bachs, O., Redondo, C., Fabregat, I., Martinez-A., C., and De Alborán, I.M. (2005). c-Myc regulates cell size and ploidy but is not essential for postnatal proliferation in liver. Proc. Natl. Acad. Sci. U. S. A. *102*, 7286–7291.

Banani, S.F., Lee, H.O., Hyman, A.A., and Rosen, M.K. (2017). Biomolecular condensates: organizers of cellular biochemistry. Nat. Rev. Mol. Cell Biol. *18*, 285–298.

Barbarese, E., Ifrim, M.F., Hsieh, L., Guo, C., Tatavarty, V., Maggipinto, M.J., Korza, G., Tutolo, J.W., Giampetruzzi, A., Le, H., et al. (2013). Conditional Knockout of Tumor Overexpressed Gene in Mouse Neurons Affects RNA Granule Assembly, Granule Translation, LTP and Short Term Habituation. PLoS One *8*, e69989.

Barber, F., Amir, A., Murray, A.W., and Murray, A.W. (2020). Cell-size regulation in budding yeast does not depend on linear accumulation of Whi5. Proc. Natl. Acad. Sci. U. S. A. *117*, 14243–14250.

Bell, S.D., and Botchan, M.R. (2013). The minichromosome maintenance replicative helicase. Cold Spring Harb. Perspect. Biol. *5*, 12807–12808.

Bellí, G., Garí, E., Aldea, M., and Herrero, E. (2001). Osmotic stress causes a G1 cell cycle delay and downregulation of Cln3/Cdc28 activity in Saccharomyces cerevisiae. Mol. Microbiol. *39*, 1022–1035.

Bentmann, E., Haass, C., and Dormann, D. (2013). Stress granules in neurodegeneration - Lessons learnt from TAR DNA binding protein of 43 kDa and fused in sarcoma. FEBS J. *280*, 4348–4370.

Bertoli, C., Skotheim, J.M., and De Bruin, R.A.M. (2013). Control of cell cycle transcription during G1 and S phases. Nat. Rev. Mol. Cell Biol. *14*, 518–528.

Boettcher, B., and Barral, Y. (2013). The cell biology of open and closed mitosis. Nucl. (United States) *4*, 160–165.

Boeynaems, S., Alberti, S., Fawzi, N.L., Mittag, T., Polymenidou, M., Rousseau, F., Schymkowitz, J., Shorter, J., Wolozin, B., Van Den Bosch, L., et al. (2018). Protein Phase Separation: A New Phase in Cell Biology. Trends Cell Biol. *28*, 420–435.

Bouchoux, C., and Uhlmann, F. (2011). A quantitative model for ordered Cdk substrate dephosphorylation during mitotic exit. Cell *147*, 803–814.

Brangwynne, C.P., Eckmann, C.R., Courson, D.S., Rybarska, A., Hoege, C., Gharakhani, J., Jülicher, F., and Hyman, A.A. (2009). Germline P granules are liquid droplets that localize by controlled dissolution/condensation. Science (80-.). *324*, 1729–1732.

Bratek-Skicki, A., Pancsa, R., Meszaros, B., Van Lindt, J., and Tompa, P. (2020). A guide to regulation of the formation of biomolecular condensates. FEBS J. (online ahead of print).

Bruce Alberts (University of California, San Francisco, U., Alexander Johnson (University of California, San Francisco, U., Julian Lewis (Cancer Research UK), David Morgan, (University of California, San Francisco, U., Martin Raff (University College London, U., Keith Roberts (Emeritus, University of East Anglia, U., and Peter Walter (University of California, San Francisco, U. (2018). Molecular Biology of the Cell: Sixth International Student Edition. Garl. Sci. 1106.

Buchan, J.R., and Parker, R. (2009). Eukaryotic Stress Granules: The Ins and Outs of Translation. Mol. Cell *36*, 932–941.

Buchan, J.R., Muhlrad, D., and Parker, R. (2008). P bodies promote stress granule assembly in Saccharomyces cerevisiae. J. Cell Biol. *183*, 441–455.

Buchan, J.R., Kolaitis, R.M., Taylor, J.P., and Parker, R. (2013). XEukaryotic stress granules are cleared by autophagy and Cdc48/VCP function. Cell *153*, 1461.

Cadart, C., Monnier, S., Grilli, J., Sáez, P.J., Srivastava, N., Attia, R., Terriac, E., Baum, B., Cosentino-Lagomarsino, M., and Piel, M. (2018a). Size control in mammalian cells involves modulation of both growth rate and cell cycle duration. Nat. Commun. *9*, 3275.

Cadart, C., Monnier, S., Grilli, J., Sáez, P.J., Srivastava, N., Attia, R., Terriac, E., Baum, B., Cosentino-Lagomarsino, M., and Piel, M. (2018b). Size control in mammalian cells involves modulation of both growth rate and cell cycle duration. Nat. Commun. *9*, 1–15.

Cai, Y., and Futcher, B. (2013). Effects of the yeast RNA-binding protein Whi3 on the half-life and abundance of CLN3 mRNA and other targets. PLoS One *8*, e84630.

Campos-Melo, D., Hawley, Z.C.E., Droppelmann, C.A., and Strong, M.J. (2021). The Integral Role of RNA in Stress Granule Formation and Function. Front. Cell Dev. Biol. *9*, 808.

Campos, M., Surovtsev, I. V., Kato, S., Paintdakhi, A., Beltran, B., Ebmeier, S.E., and Jacobs-Wagner, C. (2014). A constant size extension drives bacterial cell size homeostasis. Cell *159*, 1433–1446.

Carroll, A.S., Bishop, A.C., DeRisi, J.L., Shokat, K.M., and O'Shea, E.K. (2001). Chemical inhibition of the Pho85 cyclin-dependent kinase reveals a role in the environmental stress response. Proc. Natl. Acad. Sci. U. S. A. *98*, 12578–12583.

Chandler-Brown, D., Schmoller, K.M., Winetraub, Y., and Skotheim, J.M. (2017). The Adder Phenomenon Emerges from Independent Control of Pre- and Post-Start Phases of the Budding Yeast Cell Cycle. Curr. Biol. *27*, 2774-2783.e3.

Chang, L., Zhang, Z., Yang, J., McLaughlin, S.H., and Barford, D. (2014). Molecular architecture and mechanism of the anaphase-promoting complex. Nature *513*, 388–393.

Chelliah, V., Juty, N., Ajmera, I., Ali, R., Dumousseau, M., Glont, M., Hucka, M., Jalowicki, G., Keating, S., Knight-Schrijver, V., et al. (2015). BioModels: ten-year anniversary. Nucleic Acids Res. *43*, D542–D548.

Chen, Y., and Futcher, B. (2021). Scaling gene expression for cell size control and senescence in Saccharomyces cerevisiae. Curr. Genet. *67*, 41–47.

Chen, Y., Zhao, G., Zahumensky, J., Honey, S., and Futcher, B. (2020). Differential Scaling of Gene Expression with Cell Size May Explain Size Control in Budding Yeast. Mol. Cell *78*, 359-370.e6.

Cherkasov, V., Hofmann, S., Druffel-Augustin, S., Mogk, A., Tyedmers, J., Stoecklin, G., and Bukau, B. (2013). Coordination of translational control and protein homeostasis during severe heat stress. Curr. Biol. *23*, 2452–2462.

Chernov, K.G., Barbet, A., Hamon, L., Ovchinnikov, L.P., Curmi, P.A., and Pastré, D. (2009). Role of microtubules in stress granule assembly: Microtubule dynamical instability favors the formation of micrometric stress granules in cells. J. Biol. Chem. *284*, 36569–36580.

Colomina, N., Ferrezuelo, F., Wang, H., Aldea, M., and Gari, E. (2008). Whi3, a developmental regulator of budding yeast, binds a large set of mRNAs functionally related to the endoplasmic reticulum. J. Biol. Chem. *283*, 28670–28679.

Costanzo, M., Nishikawa, J.L., Tang, X., Millman, J.S., Schub, O., Breitkreuz, K., Dewar, D., Rupes, I., Andrews, B., and Tyers, M. (2004). CDK activity antagonizes Whi5, an inhibitor of G1/S transcription in yeast. Cell *117*, 899–913.

Crawford, R.A., and Pavitt, G.D. (2019). Translational regulation in response to stress in Saccharomyces cerevisiae. Yeast *36*, 5–21.

Cross, F.R., Archambault, V., Miller, M., and Klovstad, M. (2002). Testing a mathematical model of the yeast cell cycle. Mol. Biol. Cell *13*, 52–70.

Cross, F.R., Buchler, N.E., and Skotheim, J.M. (2011). Evolution of networks and sequences in eukaryotic cell cycle control. Philos. Trans. R. Soc. B Biol. Sci. *366*, 3532–3544.

D'Ario, M., and Sablowski, R. (2019). Cell Size Control in Plants. Annu. Rev. Genet. *53*, 45–65.

D'Ario, M., Tavares, R., Schiessl, K., Desvoyes, B., Gutierrez, C., Howard, M., and Sablowski, R. (2021). Cell size controlled in plants using DNA content as an internal scale. Science *372*, 1176–1181.

Daga, R.R., and Jimenez, J. (1999). Translational control of the Cdc25 cell cycle phosphatase: A molecular mechanism coupling mitosis to cell growth. J. Cell Sci. *112*, 3137–3146.

Dann, S.G., and Thomas, G. (2006). The amino acid sensitive TOR pathway from yeast to mammals. FEBS Lett. *580*, 2821–2829.

Diehl, J., Zindy, F., and Sherr, C. (1997). Inhibition of cyclin D1 phosphorylation on threonine-286

prevents its rapid degradation via the ubiquitin-proteasome pathway. Genes Dev. *11*, 957–972.

Dougherty, J.D., Tsai, W.C., and Lloyd, R.E. (2015). Multiple poliovirus proteins repress cytoplasmic RNA granules. Viruses *7*, 6127–6140.

Dubinski, A., and Vande Velde, C. (2021). Altered stress granule disassembly: links to neurodegenerative disease? Trends Neurosci. *44*, 765–766.

Edgington, N.P., and Futcher, B. (2001a). Relationship between the function and the location of G1 cyclins in S. cerevisiae. J. Cell Sci. *114*, 4599–4611.

Edgington, N.P., and Futcher, B. (2001b). Relationship between the function and the location of G1 cyclins in S. cerevisiae. J. Cell Sci. *114*, 4599–4611.

Elbaum-Garfinkle, S., Kim, Y., Szczepaniak, K., Chen, C.C.H., Eckmann, C.R., Myong, S., and Brangwynne, C.P. (2015). The disordered P granule protein LAF-1 drives phase separation into droplets with tunable viscosity and dynamics. Proc. Natl. Acad. Sci. U. S. A. *112*, 7189–7194.

Epstein, C.B., and Cross, F.R. (1994). Genes that can bypass the CLN requirement for Saccharomyces cerevisiae cell cycle START. Mol. Cell. Biol. *14*, 2041–2047.

Facchetti, G., Chang, F., and Howard, M. (2017a). Controlling cell size through sizer mechanisms. Curr. Opin. Syst. Biol. *5*, 86–92.

Facchetti, G., Chang, F., and Howard, M. (2017b). Controlling cell size through sizers mechanisms. Curr. Opin. Syst. Biol. *5*, 86–92.

Facchetti, G., Knapp, B., Chang, F., and Howard, M. (2019). Reassessment of the Basis of Cell Size Control Based on Analysis of Cell-to-Cell Variability. Biophys. J. *117*, 1728–1738.

Fantes, P.A. (1977). Control of cell size and cycle time in Schizosaccharomyces pombe. J. Cell Sci. *24*, 51–67.

Fay, M.M., Anderson, P.J., and Ivanov, P. (2017). ALS/FTD-Associated C9ORF72 Repeat RNA Promotes Phase Transitions In Vitro and in Cells. Cell Rep. *21*, 3573–3584.

Ferrezuelo, F., Aldea, M., and Futcher, B. (2009). Bck2 is a phase-independent activator of cell cycle-regulated genes in yeast. Cell Cycle *8*, 239–252.

Ferrezuelo, F., Colomina, N., Palmisano, A., Garí, E., Gallego, C., Csikász-Nagy, A., and Aldea, M. (2012a). The critical size is set at a single-cell level by growth rate to attain homeostasis and adaptation. Nat. Commun. *3*, 1–11.

Ferrezuelo, F., Colomina, N., Palmisano, A., Garí, E., Gallego, C., Csikász-Nagy, A., and Aldea, M. (2012b). The critical size is set at a single-cell level by growth rate to attain homeostasis and adaptation. Nat. Commun. *3*, 1012.

Fingar, D.C., Salama, S., Tsou, C., Harlow, E., and Blenis, J. (2002). Mammalian cell size is controlled by mTOR and its downstream targets S6K1 and 4EBP1/eIF4E. Genes Dev. *16*, 1472–1487.

Foley, E.A., and Kapoor, T.M. (2013). Microtubule attachment and spindle assembly checkpoint signalling at the kinetochore. Nat. Rev. Mol. Cell Biol. *14*, 25–37.

Fournier, M.-J., Coudert, L., Mellaoui, S., Adjibade, P., Gareau, C., Côté, M.-F., Sonenberg, N., Gaudreault, R.C., and Mazroui, R. (2013). Inactivation of the mTORC1-Eukaryotic Translation Initiation Factor 4E Pathway Alters Stress Granule Formation. Mol. Cell. Biol. *33*, 2285–2301.

Freire, P., Vinod, P., and Novak, B. (2012). Interplay of transcriptional and proteolytic regulation in driving robust cell cycle progression. Mol. Biosyst. *8*, 863–870.

Fu, Y., and Zhuang, X. (2020). m6A-binding YTHDF proteins promote stress granule formation. Nat. Chem. Biol. *16*, 955–963.

Futcher, B. (1996). Cyclins and the wiring of the yeast cell cycle. Yeast *12*, 1635–1646.

Futcher, B., and Carbon, J. (1986). Toxic effects of excess cloned centromeres. Mol. Cell. Biol. *6*, 2213–2222.

Gal, J., Chen, J., Na, D.-Y., Tichacek, L., Barnett, K.R., and Zhu, H. (2019). The Acetylation of Lysine-376 of G3BP1 Regulates RNA Binding and Stress Granule Dynamics. Mol. Cell. Biol. *39*.

Gallego, C., Garí, E., Colomina, N., Herrero, E., and Aldea, M. (1997a). The Cln3 cyclin is down-regulated by translational repression and degradation during the G1 arrest caused by nitrogen deprivation in budding yeast. EMBO J. *16*, 7196–7206.

Gallego, C., Garí, E., Colomina, N., Herrero, E., and Aldea, M. (1997b). The Cln3 cyclin is down-regulated by translational repression and degradation during the G1 arrest caused by nitrogen deprivation in budding yeast. EMBO J. *16*, 7196–7206.

Ganassi, M., Mateju, D., Bigi, I., Mediani, L., Poser, I., Lee, H.O., Seguin, S.J., Morelli, F.F., Vinet, J., Leo, G., et al. (2016). A Surveillance Function of the HSPB8-BAG3-HSP70 Chaperone Complex Ensures Stress Granule Integrity and Dynamism. Mol. Cell *63*, 796–810.

Garí, E., Piedrafita, L., Aldea, M., and Herrero, E. (1997). A set of vectors with a tetracycline-regulatable promoter system for modulated gene expression in Saccharomyces cerevisiae. Yeast *13*, 837–848.

Garí, E., Volpe, T., Wang, H.Y., Gallego, C., Futcher, B., and Aldea, M. (2001a). Whi3 binds the mRNA of the G1 cyclin CLN3 to modulate cell fate in budding yeast. Genes Dev. *15*, 2803–2808.

Garí, E., Volpe, T., Wang, H., Gallego, C., Futcher, B., and Aldea, M. (2001b). Whi3 binds the mRNA of the G1 cyclin CLN3 to modulate cell fate in budding yeast. Genes Dev. *15*, 2803–2808.

Garmendia-torres, C., Tassy, O., Matifas, A., Molina, N., and Charvin, G. (2017). Multiple inputs ensure yeast cell size homeostasis during cell cycle progression. ELife (Preprint Server) *7*, e34025.

Gartner, A., Jovanović, A., Jeoung, D.-I., Bourlat, S., Cross, F.R., and Ammerer, G. (1998). Pheromone-Dependent G 1 Cell Cycle Arrest Requires Far1 Phosphorylation, but May Not Involve Inhibition of Cdc28-Cln2 Kinase, In Vivo . Mol. Cell. Biol. *18*, 3681–3691.

Gibson, D.G., Benders, G.A., Axelrod, K.C., Zaveri, J., Algire, M.A., Moodie, M., Montague, M.G., Venter, J.C., Smith, H.O., and Hutchison, C.A. (2008). One-step assembly in yeast of 25 overlapping DNA fragments to form a complete synthetic Mycoplasma genitalium genome. Proc. Natl. Acad. Sci. U. S. A. *105*, 20404–20409.

Gilks, N., Kedersha, N., Ayodele, M., Shen, L., Stoecklin, G., Dember, L.M., and Anderson, P. (2004). Stress granule assembly is mediated by prion-like aggregation of TIA-1. Mol. Biol. Cell *15*, 5383–5398.

Ginzberg, M.B., Kafri, R., and Kirschner, M. (2015). On being the right (cell) size. Science (80-.). *348*.

Gomar-Alba, M., Méndez, E., Quilis, I., Bañó, M.C., and Igual, J.C. (2017). Whi7 is an unstable cell-cycle repressor of the Start transcriptional program /631/80/641 /631/337/641 article. Nat. Commun. *8*, 1–13.

González-Novo, A., Jiménez, J., Clotet, J., Nadal-Ribelles, M., Cavero, S., de Nadal, E., and Posas, F. (2015). Hog1 targets Whi5 and Msa1 transcription factors to downregulate cyclin expression upon stress. Mol. Cell. Biol. *35*, 1606–1618.

Goulet, I., Boisvenue, S., Mokas, S., Mazroui, R., and Côté, J. (2008). TDRD3, a novel Tudor domain-containing protein, localizes to cytoplasmic stress granules. Hum. Mol. Genet. *17*, 3055–3074.

Gregory, T.R. (2001). Coincidence, coevolution, or causation? DNA content, cellsize, and the C-value enigma. Biol. Rev. *76*, 65–101.

Guillén-Boixet, J., Kopach, A., Holehouse, A.S., Wittmann, S., Jahnel, M., Schlüßler, R., Kim, K., Trussina, I.R.E.A., Wang, J., Mateju, D., et al. (2020). RNA-Induced Conformational Switching and Clustering of G3BP Drive Stress Granule Assembly by Condensation. Cell *181*, 346-361.e17.

Günesdogan, U., Jäckle, H., and Herzig, A. (2014). Histone supply regulates S phase timing and cell cycle progression. Elife *3*, e02443.

Guo, H.J., and Tadi, P. (2020). Biochemistry, Ubiquitination. StatPearls.

Hardwick, K.G., Johnston, R.C., Smith, D.L., and Murray, A.W. (2000). MAD3 encodes a novel component of the spindle checkpoint which interacts with Bub3p , Cdc20p , and Mad2p. J. Cell Biol. *148*, 871–882.

Hartwell, L.H., and Unger, M.W. (1977). Unequal division in Saccharomyces cerevisiae and its implications for the control of cell division. J. Cell Biol. *75*, 422–435.

Hartwell, L.H., Culotti, J., Pringle, J.R., and Reid, B.J. (1974). Genetic control of the cell division cycle in yeast. Science (80-.). *183*, 46–51.

Hasan, M.M., Brocca, S., Sacco, E., Spinelli, M., Papaleo, E., Lambrughi, M., Alberghina, L., and Vanoni, M. (2014). A comparative study of Whi5 and retinoblastoma proteins: From sequence and structure analysis to intracellular networks. Front. Physiol. *4 JAN*, 315.

Heberle, H., Meirelles, G.V., da Silva, F.R., Telles, G.P., and Minghim, R. (2015). InteractiVenn: a web-based tool for the analysis of sets through Venn diagrams. BMC Bioinformatics *16*, 169.

Heldt, F.S., Lunstone, R., Tyson, J.J., and Novak, B. (2018). Dilution and titration of cell-cycle regulators may control cell size in budding yeast. PLoS Comput. Biol. *14*, e1006548.

Hill, N.S., Kadoya, R., Chattoraj, D.K., and Levin, P.A. (2012). Cell size and the initiation of DNA replication in bacteria. PLoS Genet. *8*.

Hilliker, A., Gao, Z., Jankowsky, E., and Parker, R. (2011). The DEAD-Box Protein Ded1 Modulates Translation by the Formation and Resolution of an eIF4F-mRNA Complex. Mol. Cell *43*, 962–972.

Ho, B., Baryshnikova, A., and Brown, G.W. (2018). Unification of Protein Abundance Datasets Yields a Quantitative Saccharomyces cerevisiae Proteome. Cell Syst. *6*, 192-205.e3.

Hofmann, S., Kedersha, N., Anderson, P., and Ivanov, P. (2021). Molecular mechanisms of stress granule assembly and disassembly. Biochim. Biophys. Acta - Mol. Cell Res. *1868*, 118876.

Holmes, K.J., Klass, D.M., Guiney, E.L., and Cyert, M.S. (2013). Whi3, an S. cerevisiae RNA-binding protein, is a component of stress granules that regulates levels of its target mRNAS. PLoS One *8*.

Holt, L.J., Tuch, B.B., Villen, J., Johnson, A.D., Gygi, S.P., and Morgan, D.O. (2009a). Global analysis of cdk1 substrate phosphorylation sites provides insiqhts into evolution. Science (80-.). *325*, 1682–1686.

Holt, L.J., Tuch, B.B., Villen, J., Johnson, A.D., Gygi, S.P., and Morgan, D.O. (2009b). Global analysis of cdk1 substrate phosphorylation sites provides insiqhts into evolution. Science (80-.). *325*, 1682–1686.

Honey, S., and Futcher, B. (2021). Whi5 and Stb1 define redundant pathways through which the G1

cyclin Cln3 promotes cell division. BioRxiv 2021.11.04.467365.

Hoops, S., Sahle, S., Gauges, R., Lee, C., Pahle, J., Simus, N., Singhal, M., Xu, L., Mendes, P., and Kummer, U. (2006). COPASI--a complex pathway simulator. Bioinformatics *22*, 3067–3074.

Horst Feldmann (2012). Yeast Cell Architecture and Functions. Yeast Mol. Cell Biol. Second Ed. 5–24.

Hsiung, Y.G., Chang, H.-C., Pellequer, J.-L., La Valle, R., Lanker, S., and Wittenberg, C. (2001). F-Box Protein Grr1 Interacts with Phosphorylated Targets via the Cationic Surface of Its Leucine-Rich Repeat. Mol. Cell. Biol. *21*, 2506–2520.

Huh, W.-K., Falvo, J. V., Gerke, L.C., Carroll, A.S., Howson, R.W., Weissman, J.S., and O'Shea, E.K. (2003). Global analysis of protein localization in budding yeast. Nature *425*, 686–691.

Inoki, K., Zhu, T., and Guan, K.L. (2003). TSC2 Mediates Cellular Energy Response to Control Cell Growth and Survival. Cell *115*, 577–590.

Ivanova, T., Maier, M., Missarova, A., Ziegler-Birling, C., Dam, M., Gomar-Alba, M., Carey, L.B., and Mendoza, M. (2020). Budding yeast complete DNA synthesis after chromosome segregation begins. Nat. Commun. *11*, 1–13.

Iyer, V.R., Horak, C.E., Scafe, C.S., Botstein, D., Snyder, M., and Brown, P.O. (2001). Genomic binding sites of the yeast cell-cycle transcription factors SBF and MBF. Nature *409*, 533–538.

Jain, A., and Vale, R.D. (2017). RNA phase transitions in repeat expansion disorders. Nature *546*, 243–247.

Jain, S., Wheeler, J.R., Walters, R.W., Agrawal, A., Barsic, A., and Parker, R. (2016a). ATPase-Modulated Stress Granules Contain a Diverse Proteome and Substructure. Cell *164*, 487–498.

Jain, S., Wheeler, J.R., Walters, R.W., Agrawal, A., Barsic, A., and Parker, R. (2016b). ATPase-Modulated Stress Granules Contain a Diverse Proteome and Substructure. Cell *164*, 487–498.

Jentsch, S., and Rumpf, S. (2007). Cdc48 (p97): a "molecular gearbox" in the ubiquitin pathway? Trends Biochem. Sci. *32*, 6–11.

Johnson, A., and Skotheim, J.M. (2013). Start and the restriction point. Curr. Opin. Cell Biol. *25*, 717–723.

Johnston, G.C., Pringle, J.R., and Hartwell, L.H. (1977). Coordination of growth with cell division in the yeast Saccharomyces cerevisiae. Exp. Cell Res. *105*, 79–98.

Jonas, S., and Izaurralde, E. (2013). The role of disordered protein regions in the assembly of decapping complexes and RNP granules. Genes Dev. *27*, 2628–2641.

Jorgensen, P., and Tyers, M. (2004). How cells coordinate growth and division. Curr. Biol. *14*, R1014–R1027.

Jorgensen, P., Rupes, I., Sharom, J.R., Schneper, L., Broach, J.R., and Tyers, M. (2004). A dynamic transcriptional network communicates growth potential to ribosome synthesis and critical cell size. Genes Dev. *18*, 2491–2505.

Jorgensen, P., Edgington, N.P., Schneider, B.L., Rupes, I., Tyers, M., and Futcher, B. (2007). The size of the nucleus increases as yeast cells grow. Mol. Biol. Cell *18*, 3523–3532.

Kato, M., Han, T.W., Xie, S., Shi, K., Du, X., Wu, L.C., Mirzaei, H., Goldsmith, E.J., Longgood, J., Pei, J., et al. (2012). Cell-free formation of RNA granules: Low complexity sequence domains form dynamic fibers within hydrogels. Cell *149*, 753–767.

Keaton, M.A. (2007). The Cell Cycle: Principles of Control" by David O. Morgan. Cell Div. *2*, 27.

Kedersha, N., and Anderson, P. (2007). Mammalian stress granules and processing bodies. Methods Enzymol. *431*, 61–81.

Kedersha, N., Cho, M.R., Li, W., Yacono, P.W., Chen, S., Gilks, N., Golan, D.E., and Anderson, P. (2000). Dynamic shuttling of TIA-1 accompanies the recruitment of mRNA to mammalian stress granules. J. Cell Biol. *151*, 1257–1268.

Kedersha, N., Stoecklin, G., Ayodele, M., Yacono, P., Lykke-Andersen, J., Fitzler, M.J., Scheuner, D., Kaufman, R.J., Golan, D.E., and Anderson, P. (2005). Stress granules and processing bodies are dynamically linked sites of mRNP remodeling. J. Cell Biol. *169*, 871–884.

Kedersha, N., Panas, M.D., Achorn, C.A., Lyons, S., Tisdale, S., Hickman, T., Thomas, M., Lieberman, J., McInerney, G.M., Ivanov, P., et al. (2016). G3BP-Caprin1-USP10 complexes mediate stress granule condensation and associate with 40S subunits. J. Cell Biol. *212*, 845–860.

Kedersha, N.L., Gupta, M., Li, W., Miller, I., and Anderson, P. (1999). RNA-binding proteins TIA-1 and TIAR link the phosphorylation of eIF-2α to the assembly of mammalian stress granules. J. Cell Biol. *147*, 1431–1441.

Keiten-Schmitz, J., Wagner, K., Piller, T., Kaulich, M., Alberti, S., and Müller, S. (2020). The Nuclear SUMO-Targeted Ubiquitin Quality Control Network Regulates the Dynamics of Cytoplasmic Stress Granules. Mol. Cell *79*, 54-67.e7.

Khong, A., Matheny, T., Jain, S., Mitchell, S.F., Wheeler, J.R., and Parker, R. (2017). The Stress Granule Transcriptome Reveals Principles of mRNA Accumulation in Stress Granules. Mol. Cell *68*, 808-820.e5.

Kim, T.H., Tsang, B., Vernon, R.M., Sonenberg, N., Kay, L.E., and Forman-Kay, J.D. (2019). Phospho-dependent phase separation of FMRP and CAPRIN1 recapitulates regulation of translation and deadenylation. Science (80-.). *365*, 825–829.

King, E.M.J., van der Sar, S.J.A., and Hardwick, K.G. (2007). Mad3 KEN boxes mediate both Cdc20 and Mad3 turnover, and are critical for the spindle checkpoint. PLoS One *2*, e342.

Kõivomägi, M., Swaffer, M.P., Turner, J.J., Marinov, G., and Skotheim, J.M. (2021). G1 cyclin-Cdk promotes cell cycle entry through localized phosphorylation of RNA polymerase II. Science (80-.). *374*, 347–351.

Kojima, R., Kajiura, S., Sesaki, H., Endo, T., and Tamura, Y. (2016). Identification of multi-copy suppressors for endoplasmic reticulum-mitochondria tethering proteins in Saccharomyces cerevisiae. FEBS Lett. *590*, 3061–3070.

Kondorosi, E., Roudier, F., and Gendreau, E. (2000). Plant cell-size control: Growing by ploidy? Curr. Opin. Plant Biol. *3*, 488–492.

Krenn, V., and Musacchio, A. (2015). The Aurora B kinase in chromosome bi-orientation and spindle checkpoint signaling. Front. Oncol. *5*.

Kroschwald, S., Munder, M.C., Maharana, S., Franzmann, T.M., Richter, D., Ruer, M., Hyman, A.A., and Alberti, S. (2018). Different Material States of Pub1 Condensates Define Distinct Modes of Stress Adaptation and Recovery. Cell Rep. *23*, 3327–3339.

Kuechler, E.R., Budzyńska, P.M., Bernardini, J.P., Gsponer, J., and Mayor, T. (2020). Distinct Features of Stress Granule Proteins Predict Localization in Membraneless Organelles. J. Mol. Biol. *432*, 2349–2368.

Landry, B.D., Doyle, J.P., Toczyski, D.P., and Benanti, J.A. (2012). F-box protein specificity for G1 cyclins is dictated by subcellular localization. PLoS Genet. *8*, e1002851.

Langdon, E.M., Qiu, Y., Niaki, A.G., McLaughlin, G.A., Weidmann, C.A., Gerbich, T.M., Smith, J.A., Crutchley, J.M., Termini, C.M., Weeks, K.M., et al. (2018). mRNA structure determines specificity of a polyQ-driven phase separation. Science (80-.). *360*, 922–927.

Lee, J.E., Cathey, P.I., Wu, H., Parker, R., and Voeltz, G.K. (2020). Endoplasmic reticulum contact sites regulate the dynamics of membraneless organelles. Science (80-.). *367*.

Li, P., Liu, X., Hao, Z., Jia, Y., Zhao, X., Xie, D., Dong, J., and Zeng, F. (2020). Dual Repressive Function by Cip1, a Budding Yeast Analog of p21, in Cell-Cycle START Regulation. Front. Microbiol. *11*, 1623.

Li, Y.R., King, O.D., Shorter, J., and Gitler, A.D. (2013). Stress granules as crucibles of ALS pathogenesis. J. Cell Biol. *201*, 361–372.

Lin, Y., Protter, D.S.W., Rosen, M.K., and Parker, R. (2015). Formation and Maturation of Phase-Separated Liquid Droplets by RNA-Binding Proteins. Mol. Cell *60*, 208–219.

Listovsky, T., and Sale, J.E. (2013). Sequestration of cdh1 by mad2l2 prevents premature apc/c activation prior to anaphase onset. J. Cell Biol. *203*, 87–100.

Liti, G. (2015). The fascinating and secret wild life of the budding yeast S. cerevisiae. Elife *4*.

Litsios, A., Huberts, D.H.E.W., Terpstra, H.M., Guerra, P., Schmidt, A., Buczak, K., Papagiannakis, A., Rovetta, M., Hekelaar, J., Hubmann, G., et al. (2019). Differential scaling between G1 protein production and cell size dynamics promotes commitment to the cell division cycle in budding yeast. Nat. Cell Biol. *21*, 1382–1392.

Liu, C., Van Dyk, D., Choe, V., Yan, J., Majumder, S., Costanzo, M., Bao, X., Boone, C., Huo, K., Winey, M., et al. (2011a). Ubiquitin ligase Ufd2 is required for efficient degradation of Mps1 kinase. J. Biol. Chem. *286*, 43660–43667.

Liu, Q., Larsen, B., Ricicova, M., Orlicky, S., Tekotte, H., Tang, X., Craig, K., Quiring, A., Le Bihan, T., Hansen, C., et al. (2011b). SCF Cdc4 Enables Mating Type Switching in Yeast by Cyclin-Dependent Kinase-Mediated Elimination of the Ash1 Transcriptional Repressor . Mol. Cell. Biol. *31*, 584–598.

Liu, X., Wang, X., Yang, X., Liu, S., Jiang, L., Qu, Y., Hu, L., Ouyang, Q., and Tang, C. (2015). Reliable cell cycle commitment in budding yeast is ensured by signal integration. Elife *2015*.

Liu, X., Liu, X., Wang, H., Dou, Z., Ruan, K., Hill, D.L., Li, L., Shi, Y., and Yao, X. (2020). Phase separation drives decision making in cell division. J. Biol. Chem. *295*, 13419–13431.

Lord, P.G., and Wheals, A.E. (1981). Variability in individual cell cycles of Saccharomyces cerevisiae. J. Cell Sci. *Vol. 50*, 361–376.

Louvion, J.F., Havaux-Copf, B., and Picard, D. (1993). Fusion of GAL4-VP16 to a steroid-binding domain provides a tool for gratuitous induction of galactose-responsive genes in yeast. Gene *131*, 129–134.

Lu, H., Yu, D., Hansen, A.S., Ganguly, S., Liu, R., Heckert, A., Darzacq, X., and Zhou, Q. (2018). Phase-separation mechanism for C-terminal hyperphosphorylation of RNA polymerase II. Nature *558*, 318–323.

Lucena, R., Alcaide-Gavilán, M., Schubert, K., He, M., Domnauer, M.G., Marquer, C., Klose, C., Surma, M.A., and Kellogg, D.R. (2018). Cell Size and Growth Rate Are Modulated by TORC2-Dependent Signals. Curr. Biol. *28*, 196-210.e4.

Luo, X., Tang, Z., Xia, G., Wassmann, K., Matsumoto, T., Rizo, J., and Yu, H. (2004). The Mad2 spindle checkpoint protein has two distinct natively folded states. Nat. Struct. Mol. Biol. *11*, 338–345.

Luo, Y., Na, Z., and Slavoff, S.A. (2018). P-Bodies: Composition, Properties, and Functions. Biochemistry *57*, 2424–2431.

Maekawa, H., Usui, T., Knop, M., and Schiebel, E. (2003). Yeast Cdk1 translocates to the plus end of cytoplasmic microtubules to regulate bud cortex interactions. EMBO J. *22*, 438–449.

Mahboubi, H., and Stochaj, U. (2017). Cytoplasmic stress granules: Dynamic modulators of cell signaling and disease. Biochim. Biophys. Acta - Mol. Basis Dis. *1863*, 884–895.

Mapa, C.E., Arsenault, H.E., Conti, M.M., Poti, K.E., and Benanti, J.A. (2018). A balance of deubiquitinating enzymes controls cell cycle entry. Mol. Biol. Cell *29*, 2821–2834.

Maris, C., Dominguez, C., and Allain, F.H.T. (2005). The RNA recognition motif, a plastic RNA-binding platform to regulate post-transcriptional gene expression. FEBS J. *272*, 2118–2131.

Marmor-Kollet, H., Siany, A., Kedersha, N., Knafo, N., Rivkin, N., Danino, Y.M., Moens, T.G., Olender, T., Sheban, D., Cohen, N., et al. (2020). Spatiotemporal Proteomic Analysis of Stress Granule Disassembly Using APEX Reveals Regulation by SUMOylation and Links to ALS Pathogenesis. Mol. Cell *80*, 876-891.e6.

Marshall, W.F., Young, K.D., Swaffer, M., Wood, E., Nurse, P., Kimura, A., Frankel, J., Wallingford, J., Walbot, V., Qu, X., et al. (2012). What determines cell size? BMC Biol. *10*, 101.

Martínez-láinez, J.M., Moreno, D.F., Parisi, E., Clotet, J., and Aldea, M. (2018). Centromeric signaling proteins boost G1 cyclin degradation and modulate cell size in budding yeast. PLOS Biol. *16*, 1–23.

Martinez, J.S., Jeong, D.-E., Choi, E., Billings, B.M., and Hall, M.C. (2006). Acm1 Is a Negative Regulator of the Cdh1-Dependent Anaphase-Promoting Complex/Cyclosome in Budding Yeast. Mol. Cell. Biol. *26*, 9162–9176.

Masur, L. (2009). Saccharomyces cerevisiae cells in DIC microscopy. 1.

Mateju, D., Franzmann, T.M., Patel, A., Kopach, A., Boczek, E.E., Maharana, S., Lee, H.O., Carra, S., Hyman, A.A., and Alberti, S. (2017). An aberrant phase transition of stress granules triggered by misfolded protein and prevented by chaperone function. EMBO J. *36*, 1669–1687.

Mateju, D., Eichenberger, B., Voigt, F., Eglinger, J., Roth, G., and Chao, J.A. (2020). Single-Molecule Imaging Reveals Translation of mRNAs Localized to Stress Granules. Cell *183*, 1801-1812.e13.

Matsumura, K., Yagi, T., and Yasuda, K. (2003). Role of timer and sizer in regulation of Chlamydomonas cell cycle. Biochem. Biophys. Res. Commun. *306*, 1042–1049.

Mazroui, R., Di Marco, S., Kaufman, R.J., and Gallouzi, I.E. (2007). Inhibition of the ubiquitin-proteasome system induces stress granule formation. Mol. Biol. Cell *18*, 2603–2618.

McShane, E., Sin, C., Zauber, H., Wells, J.N., Donnelly, N., Wang, X., Hou, J., Chen, W., Storchova, Z., Marsh, J.A., et al. (2016). Kinetic analysis of protein stability reveals age-dependent degradation. Cell *167*, 803–815.

Menoyo, S., Ricco, N., Bru, S., Hernández-Ortega, S., Escoté, X., Aldea, M., and Clotet, J. (2013). Phosphate-Activated Cyclin-Dependent Kinase Stabilizes G 1 Cyclin To Trigger Cell Cycle Entry . Mol. Cell. Biol. *33*, 1273–1284.

Miller, M.E., and Cross, F.R. (2001a). Mechanisms controlling subcellular localization of the G1 cyclins Cln2p and Cln3p in budding yeast. Mol. Cell. Biol. *21*, 6292–6311.

Miller, M.E., and Cross, F.R. (2001b). Cyclin specificity: How many wheels do you need on a unicycle? J. Cell Sci. *114*, 1811–1820.

Mitchison, J.M. (1988). Synchronous cultures and age fractionation. In Yeast, a Practical Approach, I. Campbell, and J. Duffus, eds. (Oxford, UK: IRL Press), pp. 51–64.

Moeller, B.J., Cao, Y., Li, C.Y., and Dewhirst, M.W. (2004). Radiation activates HIF-1 to regulate vascular radiosensitivity in tumors: Role of reoxygenation, free radicals, and stress granules. Cancer Cell *5*, 429–441.

Molliex, A., Temirov, J., Lee, J., Coughlin, M., Kanagaraj, A.P., Kim, H.J., Mittag, T., and Taylor, J.P. (2015). Phase Separation by Low Complexity Domains Promotes Stress Granule Assembly and Drives Pathological Fibrillization. Cell *163*, 123–133.

Montagne, J., Stewart, M.J., Stocker, H., Hafen, E., Kozma, S.C., and Thomas, G. (1999). Drosophila S6 kinase: A regulator of cell size. Science (80-.). *285*, 2126–2129.

Morcinek-Orlowska, J., Galinska, J., and Glinkowska, M. (2019). When size matters-coordination of growth and cell cycle in bacteria. Acta Biochim. Pol. *66*, 139–146.

Moreno-Torres, M., Jaquenoud, M., and De Virgilio, C. (2015). TORC1 controls G 1 -S cell cycle transition in yeast via Mpk1 and the greatwall kinase pathway. Nat. Commun. *6*, 1–10.

Moreno, D.F., Parisi, E., Yahya, G., Vaggi, F., Csikász-Nagy, A., and Aldea, M. (2019a). Competition in the chaperone-client network subordinates cell-cycle entry to growth and stress. Life Sci. Alliance *2*.

Moreno, D.F., Jenkins, K., Morlot, S., Charvin, G., Csikász-Nagy, A., and Aldea, M. (2019b). Proteostasis collapse, a hallmark of aging, hinders the chaperone-Start network and arrests cells in G1. Elife *8*, e48240.

Morgan, D.O. (2007). The Cell Cycle: Principles of Control (New Science Press Ltd).

Morita, T., Satoh, R., Umeda, N., Kita, A., and Sugiura, R. (2012). The stress granule protein Vgl1 and poly(A)-binding protein Pab1 are required for doxorubicin resistance in the fission yeast Schizosaccharomyces pombe. Biochem. Biophys. Res. Commun. *417*, 399–403.

Moseley, J.B. (2017). Wee1 and Cdc25: Tools, pathways, mechanisms, questions. Cell Cycle *16*, 599–600.

De Nadal, E.E., Ammerer, G., and Posas, F. (2011). Controlling gene expression in response to stress. Nat. Rev. Genet. *12*, 833–845.

Nadezhdina, E.S., Lomakin, A.J., Shpilman, A.A., Chudinova, E.M., and Ivanov, P.A. (2010). Microtubules govern stress granule mobility and dynamics. Biochim. Biophys. Acta - Mol. Cell Res. *1803*, 361–371.

Nakada, D., Shimomura, T., Matsumoto, K., and Sugimoto, K. (2003). The ATM-related Tel1 protein of Saccharomyces cerevisiae controls a checkpoint response following phleomycin treatment. Nucleic Acids Res. *31*, 1715–1724.

Namkoong, S., Ho, A., Woo, Y.M., Kwak, H., and Lee, J.H. (2018). Systematic characterization of stress-induced RNA granulation. Mol. Cell *70*, 175–187.

Nash, P., Tang, X., Orlicky, S., Chen, Q., Gertler, F.B., Mendenhall, M.D., Sicheri, F., Pawson, T., and Tyers, M. (2001). Multisite phosphorylation of a CDK inhibitor sets a threshold for the onset of DNA replication. Nature *414*, 514–521.

Nash, R., Tokiwa, G., Anand, S., Erickson, K., and Futcher, A.B. (1988). The WHI1+ gene of

Saccharomyces cerevisiae tethers cell division to cell size and is a cyclin homolog. EMBO J. *7*, 4335–4346.

von Neumann, J. (1951). The general and logical theory of automata. In Systems Research for Behavioral Science: A Sourcebook, pp. 97–107.

Newcomb, L.L., Hall, D.D., and Heideman, W. (2002). AZF1 is a glucose-dependent positive regulator of CLN3 transcription in Saccharomyces cerevisiae. Mol. Cell. Biol. *22*, 1607–1614.

Nickels, J.T., and Broach, J.R. (1996). A ceramide-activated protein phosphatase mediates ceramide-induced G1 arrest of Saccharomyces cerevisiae. Genes Dev. *10*, 382–394.

Niewidok, B., Igaev, M., da Graca, A.P., Strassner, A., Lenzen, C., Richter, C.P., Piehler, J., Kurre, R., and Brandt, R. (2018). Single-molecule imaging reveals dynamic biphasic partition of RNA-binding proteins in stress granules. J. Cell Biol. *217*, 1303–1318.

Nishizawa, M., Kawasumi, M., Fujino, M., and Toh-e, A. (1998). Phosphorylation of Sic1, a cyclin-dependent kinase (Cdk) inhibitor, by Cdk including Pho85 kinase is required for its prompt degradation. Mol. Biol. Cell *9*, 2393–2405.

Nott, T.J., Petsalaki, E., Farber, P., Jervis, D., Fussner, E., Plochowietz, A., Craggs, T.D., Bazett-Jones, D.P., Pawson, T., Forman-Kay, J.D., et al. (2015). Phase Transition of a Disordered Nuage Protein Generates Environmentally Responsive Membraneless Organelles. Mol. Cell *57*, 936–947.

Nurse, P. (1980). Cell cycle control - Both deterministic and probabilistic? Nature *286*, 9–10.

Ohn, T., Kedersha, N., Hickman, T., Tisdale, S., and Anderson, P. (2008). A functional RNAi screen links O-GlcNAc modification of ribosomal proteins to stress granule and processing body assembly. Nat. Cell Biol. *10*, 1224–1231.

Örd, M., Puss, K.K., Kivi, R., Möll, K., Ojala, T., Borovko, I., Faustova, I., Venta, R., Valk, E., Kõivomägi, M., et al. (2020). Proline-Rich Motifs Control G2-CDK Target Phosphorylation and Priming an Anchoring Protein for Polo Kinase Localization. Cell Rep. *31*.

Orlicky, S., Tang, X., Willems, A., Tyers, M., and Sicheri, F. (2003). Structural basis for phosphodependent substrate selection and orientation by the SCFCdc4 ubiquitin ligase. Cell *112*, 243–256.

Pan, T., Qin, Q., Nong, C., Gao, S., Wang, L., Cai, B., Zhang, M., Wu, C., Chen, H., Li, T., et al. (2021). A novel WEE1 pathway for replication stress responses. Nat. Plants *7*, 209–218.

Panas, M.D., Schulte, T., Thaa, B., Sandalova, T., Kedersha, N., Achour, A., and McInerney, G.M. (2015). Viral and Cellular Proteins Containing FGDF Motifs Bind G3BP to Block Stress Granule Formation. PLoS Pathog. *11*.

Parisi, E., Yahya, G., Flores, A., and Aldea, M. (2018a). Cdc48/p97 segregase is modulated by cyclin-dependent kinase to determine cyclin fate during G1 progression. EMBO J. *37*, e98724.

Parisi, E., Yahya, G., Flores, A., and Aldea, M. (2018b). Cdc48 / p97 segregase is modulated by Cdk to determine cyclin fate during G1 progression. EMBO J. *37*, e98724.

Parviz, F., and Heideman, W. (1998). Growth-independent regulation of CLN3 mRNA levels by nutrients in Saccharomyces cerevisiae. J. Bacteriol. *180*, 225–230.

Patel, A., Lee, H.O., Jawerth, L., Maharana, S., Jahnel, M., Hein, M.Y., Stoynov, S., Mahamid, J., Saha, S., Franzmann, T.M., et al. (2015). A Liquid-to-Solid Phase Transition of the ALS Protein FUS Accelerated by Disease Mutation. Cell *162*, 1066–1077.

Patterson, J.O., Basu, S., Rees, P., and Nurse, P. (2021). Cdk control pathways integrate cell size and ploidy information to control cell division. Elife *10*.

Poblete-Durán, N., Prades-Pérez, Y., Vera-Otarola, J., Soto-Rifo, R., and Valiente-Echeverría, F. (2016). Who regulates whom? An overview of RNA granules and viral infections. Viruses *8*, 1–28.

Polymenis, M., and Schmidt, E. V. (1997a). Coupling of cell division to cell growth by translational control of the G1 cyclin CLN3 in yeast. Genes Dev. *11*, 2522–2531.

Polymenis, M., and Schmidt, E. V (1997b). Coupling of cell division to cell growth by translational control of the G1 cyclin CLN3 in yeast. Genes Dev. *11*, 2522–2531.

Del Pozo, J.C., and Ramirez-Parra, E. (2015). Whole genome duplications in plants: An overview from Arabidopsis. J. Exp. Bot. *66*, 6991–7003.

Prinz, S., Hwang, E.S., Visintin, R., and Amon, A. (1998). The regulation of Cdc20 proteolysis reveals a role for the APC components Cdc23 and Cdc27 during S phase and early mitosis. Curr. Biol. *8*, 750–760.

Protter, D.S.W., and Parker, R. (2016a). Principles and Properties of Stress Granules. Trends Cell Biol. *26*, 668–679.

Protter, D.S.W., and Parker, R. (2016b). Principles and Properties of Stress Granules. Trends Cell Biol. *26*, 668–679.

Qiao, R., Weissmann, F., Yamaguchi, M., Brown, N.G., VanderLinden, R., Imre, R., Jarvis, M.A., Brunner, M.R., Davidson, I.F., Litos, G., et al. (2016). Mechanism of APC/CCDC20 activation by mitotic phosphorylation. Proc. Natl. Acad. Sci. U. S. A. *113*, E2570–E2578.

Qiao, X., Zhang, L., Gamper, A.M., Fujita, T., and Wan, Y. (2010). APC/C-Cdh1: From cell cycle to cellular differentiation and genomic integrity. Cell Cycle *9*, 3904–3912.

Qu, Y., Jiang, J., Liu, X., Wei, P., Yang, X., and Tang, C. (2019). Cell Cycle Inhibitor Whi5 Records Environmental Information to Coordinate Growth and Division in Yeast. Cell Rep. *29*, 987-994.e5.

Quilis, I., and Igual, J.C. (2012a). Molecular basis of the functional distinction between Cln1 and Cln2 cyclins. Cell Cycle *11*, 3117–3131.

Quilis, I., and Igual, J.C. (2012b). Molecular basis of the functional distinction between Cln1 and Cln2 cyclins. Cell Cycle *11*, 3117–3131.

Rai, A.K., Chen, J.-X., Selbach, M., and Pelkmans, L. (2018). Kinase-controlled phase transition of membraneless organelles in mitosis. Nature *559*, 211–216.

Ramaswami, M., Taylor, J.P., and Parker, R. (2013). XAltered ribostasis: RNA-protein granules in degenerative disorders. Cell *154*.

Repici, M., Hassanjani, M., Maddison, D.C., Garção, P., Cimini, S., Patel, B., Szegö, É.M., Straatman, K.R., Lilley, K.S., Borsello, T., et al. (2019). The Parkinson's Disease-Linked Protein DJ-1 Associates with Cytoplasmic mRNP Granules During Stress and Neurodegeneration. Mol. Neurobiol. *56*, 61–77.

Ries, R.J., Zaccara, S., Klein, P., Olarerin-George, A., Namkoong, S., Pickering, B.F., Patil, D.P., Kwak, H., Lee, J.H., and Jaffrey, S.R. (2019). m6A enhances the phase separation potential of mRNA. Nature *571*, 424–428.

Robbins, J.A., and Cross, F.R. (2010). Regulated degradation of the APC coactivator Cdc20. Cell Div. *5*, 23.

Robinson, D.O., Coate, J.E., Singh, A., Hong, L., Bush, M., Doyle, J.J., and Roeder, A.H.K. (2018). Ploidy

and size at multiple scales in the arabidopsis sepal[open]. Plant Cell *30*, 2308–2329.

Rowley, A., Johnston, G.C., Butler, B., Werner-Washburne, M., and Singer, R.A. (1993). Heat shock-mediated cell cycle blockage and G1 cyclin expression in the yeast Saccharomyces cerevisiae. Mol. Cell. Biol. *13*, 1034–1041.

Ruiz-Miro, M., Colomina, N., Fernandez, R.M.H., Gari, E., Gallego, C., and Aldea, M. (2011). Translokin (Cep57) interacts with cyclin D1 and prevents its nuclear accumulation in quiescent fibroblasts. Traffic *12*, 549–562.

Sanders, D.W., Kedersha, N., Lee, D.S.W., Strom, A.R., Drake, V., Riback, J.A., Bracha, D., Eeftens, J.M., Iwanicki, A., Wang, A., et al. (2020). Competing Protein-RNA Interaction Networks Control Multiphase Intracellular Organization. Cell *181*, 306-324.e28.

Santocanale, C., and Diffley, J.F.X. (1998). A Mec1-and Rad53-dependent checkpoint controls late-firing origins of DNA replication. Nature *395*, 615–618.

Schaechter, M., MaalOe, O., and Kjeldgaard, N.O. (1958). Dependency on Medium and Temperature of Cell Size and Chemical Composition during Balanced Growth of Salmonella typhimurium. J. Gen. Microbiol. *19*, 592–606.

Schmoller, K.M., and Skotheim, J.M. (2015). The biosynthetic basis of cell size control. Trends Cell Biol. *25*, 793–802.

Schmoller, K.M., Turner, J.J., Kõivomägi, M., and Skotheim, J.M. (2015a). Dilution of the cell cycle inhibitor Whi5 controls budding-yeast cell size. Nature *526*, 268–272.

Schmoller, K.M., Turner, J.J., Kõivomägi, M., and Skotheim, J.M. (2015b). Dilution of the cell cycle inhibitor Whi5 controls budding yeast cell size. Nature *526*, 268–272.

Schneider, B., Patton, E., Lanker, S., Mendenhall, M., Wittenberg, C., Futcher, B., and Tyers, M. (1998). Yeast G1 cyclins are unstable in G1 phase. Nature *395*, 86–89.

Schneider, B.L., Zhang, J., Markwardt, J., Tokiwa, G., Volpe, T., Honey, S., and Futcher, B. (2004). Growth Rate and Cell Size Modulate the Synthesis of, and Requirement for, G 1 -Phase Cyclins at Start . Mol. Cell. Biol. *24*, 10802–10813.

Shah, K.H., Nostramo, R., Zhang, B., Varia, S.N., Klett, B.M., and Herman, P.K. (2014). Protein kinases are associated with multiple, distinct cytoplasmic granules in quiescent yeast cells. Genetics *198*, 1495–1512.

Shashni, B., Ariyasu, S., Takeda, R., Suzuki, T., Shiina, S., Akimoto, K., Maeda, T., Aikawa, N., Abe, R., Osaki, T., et al. (2018). Size-based differentiation of cancer and normal cells by a particle size analyzer assisted by a cell-recognition PC software. Biol. Pharm. Bull. *41*, 487–503.

Shattuck, J.E., Paul, K.R., Cascarina, S.M., and Ross, E.D. The prion-like protein kinase Sky1 is required for efficient stress granule disassembly.

Shattuck, J.E., Paul, K.R., Cascarina, S.M., and Ross, E.D. (2019). The prion-like protein kinase Sky1 is required for efficient stress granule disassembly. Nat. Commun. *10*, 1–11.

Shima, H. (1998). Disruption of the p70s6k/p85s6k gene reveals a small mouse phenotype and a new functional S6 kinase. EMBO J. *17*, 6649–6659.

Shin, Y., and Brangwynne, C.P. (2017). Liquid phase condensation in cell physiology and disease. Science (80-.). *357*.

Shukla, S., and Parker, R. (2016). Hypo- and Hyper-Assembly Diseases of RNA–Protein Complexes.

Trends Mol. Med. *22*, 615–628.

Sivakumar, S., and Gorbsky, G.J. (2015). Spatiotemporal regulation of the anaphase-promoting complex in mitosis. Nat. Rev. Mol. Cell Biol. *16*, 82–94.

Siwach, P., and Kaganovich, D. (2017). Getting stress out of stressed-out stress granules. EMBO J. *36*, 1647–1649.

Siwiak, M., and Zielenkiewicz, P. (2010). A comprehensive, quantitative, and genome-wide model of translation. PLoS Comput. Biol. *6*, 4.

Skinner, J.J., Wood, S., Shorter, J., Englander, S.W., and Black, B.E. (2008). The Mad2 partial unfolding model: Regulating mitosis through Mad2 conformational switching. J. Cell Biol. *183*, 761–768.

Skotheim, J.M., Di Talia, S., Siggia, E.D., and Cross, F.R. (2008). Positive feedback of G1 cyclins ensures coherent cell cycle entry. Nature *454*, 291–296.

Smets, B., Ghillebert, R., De Snijder, P., Binda, M., Swinnen, E., De Virgilio, C., and Winderickx, J. (2010). Life in the midst of scarcity: Adaptations to nutrient availability in Saccharomyces cerevisiae. Curr. Genet. *56*, 1–32.

Ńnchez, L., Granadino, B., and Torres, M. (1994). Sex determination in Drosophila melanogaster: X-linked genes involved in the initial step of Sex-lethal activation. Dev. Genet. *15*, 251–264.

Snead, W.T., and Gladfelter, A.S. (2019). The control centers of biomolecular phase separation: how membrane surfaces, PTMs, and active processes regulate condensation. Mol. Cell *76*, 295–305.

Soifer, I., Robert, L., and Amir, A. (2016). Single-cell analysis of growth in budding yeast and bacteria reveals a common size regulation strategy. Curr. Biol. *26*, 356–361.

Solé, C., Nadal-Ribelles, M., de Nadal, E., and Posas, F. (2015). A novel role for lncRNAs in cell cycle control during stress adaptation. Curr. Genet. *61*, 299–308.

Solomon, S., Xu, Y., Wang, B., David, M.D., Schubert, P., Kennedy, D., and Schrader, J.W. (2007). Distinct Structural Features ofCaprin-1 Mediate Its Interaction with G3BP-1 and Its Induction of Phosphorylation of Eukaryotic Translation InitiationFactor 2α, Entry to Cytoplasmic Stress Granules, and Selective Interaction with a Subset of mRNAs. Mol. Cell. Biol. *27*, 2324–2342.

Somasekharan, S.P., El-Naggar, A., Leprivier, G., Cheng, H., Hajee, S., Grunewald, T.G.P., Zhang, F., Ng, T., Delattre, O., Evdokimova, V., et al. (2015). YB-1 regulates stress granule formation and tumor progression by translationally activating G3BP1. J. Cell Biol. *208*, 913–929.

Sommer, R.A., DeWitt, J.T., Tan, R., and Kellogg, D.R. (2021). Growth-dependent signals drive an increase in early G1 cyclin concentration to link cell cycle entry with cell growth. Elife *10*, e64364.

Song, M.-S., and Grabocka, E. (2020). Stress Granules in Cancer. Rev. Physiol. Biochem. Pharmacol.

Souquere, S., Mollet, S., Kress, M., Dautry, F., Pierron, G., and Weil, D. (2009). Unravelling the ultrastructure of stress granules and associated P-bodies in human cells. J. Cell Sci. *122*, 3619–3626.

Spellman, P.T., Sherlock, G., Zhang, M.Q., Iyer, V.R., Anders, K., Eisen, M.B., Brown, P.O., Botstein, D., and Futcher, B. (1998). Comprehensive identification of cell cycle-regulated genes of the yeast Saccharomyces cerevisiae by microarray hybridization. Mol. Biol. Cell *9*, 3273–3297.

Spiesser, T.W., Kühn, C., Krantz, M., and Klipp, E. (2015). Bud-localization of CLB2 mRNA can constitute a growth rate dependent daughter sizer. PLOS Comput. Biol. *11*, e1004223.

Stoecklin, G., and Kedersha, N. (2013). Relationship of GW/P-bodies with stress granules. Adv. Exp. Med. Biol. *768*, 197–211.

Storti, R. V., Scott, M.P., Rich, A., and Pardue, M. Lou (1980). Translational control of protein synthesis in response to heat shock in D. melanogaster cells. Cell *22*, 825–834.

Swaffer, M.P., Kim, J., Chandler-Brown, D., Langhinrichs, M., Marinov, G.K., Greenleaf, W.J., Kundaje, A., Schmoller, K.M., and Skotheim, J.M. (2021). Transcriptional and chromatin-based partitioning mechanisms uncouple protein scaling from cell size. Mol. Cell *81*, 4861-4875.e7.

Szaflarski, W., Fay, M.M., Kedersha, N., Zabel, M., Anderson, P., and Ivanov, P. (2016). Vinca alkaloid drugs promote stress-induced translational repression and stress granule formation. Oncotarget *7*, 30307–30322.

Talarek, N., Gueydon, E., and Schwob, E. (2017). Homeostatic control of START through negative feedback between Cln3-Cdk1 and Rim15/Greatwall kinase in budding yeast. Elife *6*, e26233.

Talia, S. Di, Skotheim, J.M., Bean, J.M., Siggia, E.D., and Cross, F.R. (2007). The effects of molecular noise and size control on variability in the budding yeast cell cycle. Nature *448*, 947–951.

Di Talia, S., Wang, H., Skotheim, J.M., Rosebrock, A.P., Futcher, B., and Cross, F.R. (2009). Daughter-specific transcription factors regulate cell size control in budding yeast. PLoS Biol. *7*, e1000221.

Tang, X., Orlicky, S., Mittag, T., Csizmok, V., Pawson, T., Forman-Kay, J.D., Sicheri, F., and Tyers, M. (2012). Composite low affinity interactions dictate recognition of the cyclin-dependent kinase inhibitor Sic1 by the SCF Cdc4 ubiquitin ligase. Proc. Natl. Acad. Sci. U. S. A. *109*, 3287–3292.

Tian, S., Curnutte, H.A., and Trcek, T. (2020). RNA granules: A view from the RNA perspective. Molecules *25*, 3130.

Tourrière, H., Chebli, K., Zekri, L., Courselaud, B., Blanchard, J.M., Bertrand, E., and Tazi, J. (2003). The RasGAP-associated endoribonuclease G3BP assembles stress granules. J. Cell Biol. *160*, 823–831.

Van Treeck, B., and Parker, R. (2018). Emerging Roles for Intermolecular RNA-RNA Interactions in RNP Assemblies. Cell *174*, 791–802.

Van Treeck, B., Protter, D.S.W., Matheny, T., Khong, A., Link, C.D., and Parker, R. (2018). RNA self-assembly contributes to stress granule formation and defining the stress granule transcriptome. Proc. Natl. Acad. Sci. U. S. A. *115*, 2734–2739.

Tsai, N.-P., Ho, P.-C., and Wei, L.-N. (2008a). Regulation of stress granule dynamics by Grb7 and FAK signalling pathway. EMBO J. *27*, 715–726.

Tsai, N.P., Ho, P.C., and Wei, L.N. (2008b). Regulation of stress granule dynamics by Grb7 and FAK signalling pathway. EMBO J. *27*, 715–726.

Tsukaya, H. (2008). Controlling size in multicellular organs: Focus on the leaf. PLoS Biol. *6*, 1373–1376.

Tsunematsu, T., Arakaki, R., Yamada, A., Ishimaru, N., and Kudo, Y. (2015). The non-canonical role of Aurora-A in DNA replication. Front. Oncol. *5*, 187.

Turner, J.J., Ewald, J.C., and Skotheim, J.M. (2012). Cell size control in yeast. Curr. Biol. *22*, R350-9.

Tutucci, E., Vera, M., Biswas, J., Garcia, J., Parker, R., and Singer, R.H. (2018). An improved MS2 system for accurate reporting of the mRNA life cycle. Nat. Methods *15*.

Tyers, M., Tokiwa, G., and Futcher, B. (1993). Comparison of the saccharomyces cerevisiae G1 cyclins: Cln3 may be an upstream activator of cln1, cln2 and other cyclins. EMBO J. *12*, 1955–1968.

Vai, M., Popolo, L., and Alberghina, L. (1987). Effect of tunicamycin on cell cycle progression in budding yeast. Exp. Cell Res. *171*, 448–459.

Valiente-Echeverría, F., Melnychuk, L., and Mouland, A.J. (2012). Viral modulation of stress granules. Virus Res. *169*, 430–437.

Valiente-Echeverría, F., Melnychuk, L., Vyboh, K., Ajamian, L., Gallouzi, I.E., Bernard, N., and Mouland, A.J. (2014). EEF2 and Ras-GAP SH3 domain-binding protein (G3BP1) modulate stress granule assembly during HIV-1 infection. Nat. Commun. *5*.

Vanderweyde, T., Yu, H., Varnum, M., Liu-Yesucevitz, L., Citro, A., Ikezu, T., Duff, K., and Wolozin, B. (2012). Contrasting pathology of the stress granule proteins TIA-1 and G3BP in Tauopathies. J. Neurosci. *32*, 8270–8283.

Vanderweyde, T., Apicco, D.J., Youmans-Kidder, K., Ash, P.E.A., Cook, C., Lummertz da Rocha, E., Jansen-West, K., Frame, A.A., Citro, A., Leszyk, J.D., et al. (2016). Interaction of tau with the RNA-Binding Protein TIA1 Regulates tau Pathophysiology and Toxicity. Cell Rep. *15*, 1455–1466.

Varshavsky, A. (2011). The N-end rule pathway and regulation by proteolysis. Protein Sci. *20*, 1298.

Vergés, E., Colomina, N., Garí, E., Gallego, C., and Aldea, M. (2007a). Cyclin Cln3 Is Retained at the ER and Released by the J Chaperone Ydj1 in Late G1 to Trigger Cell Cycle Entry. Mol. Cell *26*, 649–662.

Vergés, E., Colomina, N., Garí, E., Gallego, C., and Aldea, M. (2007b). Cyclin Cln3 Is Retained at the ER and Released by the J Chaperone Ydj1 in Late G1 to Trigger Cell Cycle Entry. Mol. Cell *26*, 649–662.

Verma, R., Feldman, R.M.R., and Deshaies, R.J. (1997). SIC1 is ubiquitinated in vitro by a pathway that requires CDC4, CDC34, and cyclin/CDK activities. Mol. Biol. Cell *8*, 1427–1437.

Vilas-Boas, F. de A.S., da Silva, A.M., de Sousa, L.P., Lima, K.M., Vago, J.P., Bittencourt, L.F.F., Dantas, A.E., Gomes, D.A., Vilela, M.C., Teixeira, M.M., et al. (2016). Impairment of stress granule assembly via inhibition of the eIF2alpha phosphorylation sensitizes glioma cells to chemotherapeutic agents. J. Neurooncol. *127*, 253–260.

Visintin, R., Prinz, S., and Amon, A. (1997). CDC20 and CDH1: A family of substrate-specific activators of APC- dependent proteolysis. Science (80-.). *278*, 460–463.

Wallden, M., Fange, D., Lundius, E.G., Baltekin, Ö., and Elf, J. (2016). The synchronization of replication and division cycles in individual E. coli cells. Cell *166*, 729–739.

Walters, R.W., Muhlrad, D., Garcia, J., and Parker, R. (2015). Differential effects of Ydj1 and Sis1 on Hsp70-mediated clearance of stress granules in Saccharomyces cerevisiae. Rna *21*, 1660–1671.

Wang, B., Maxwell, B.A., Joo, J.H., Gwon, Y., Messing, J., Mishra, A., Shaw, T.I., Ward, A.L., Quan, H., Sakurada, S.M., et al. (2019). ULK1 and ULK2 regulate stress Granule disassembly through phosphorylation and activation of VCP/p97. Mol. Cell *74*, 742–757.

Wang, F., Li, J., Fan, S., Jin, Z., and Huang, C. (2020). Targeting stress granules: A novel therapeutic strategy for human diseases. Pharmacol. Res. *161*, 105143.

Wang, H., Garí, E., Vergés, E., Gallego, C., and Aldea, M. (2004). Recruitment of Cdc28 by Whi3 restricts nuclear accumulation of the G1 cyclin-Cdk complex to late G1. EMBO J. *23*, 180–190.

Wang, H., Carey, L.B., Cai, Y., Wijnen, H., and Futcher, B. (2009). Recruitment of Cln3 cyclin to promoters controls cell cycle entry via histone deacetylase and other targets. PLoS Biol. *7*, e1000189.

Weinert, T.A., Kiser, G.L., and Hartwell, L.H. (1994). Mitotic checkpoint genes in budding yeast and the dependence of mitosis on DNA replication and repair. Genes Dev. *8*, 652–665.

Wheeler, J.R., Matheny, T., Jain, S., Abrisch, R., and Parker, R. (2016). Distinct stages in stress granule assembly and disassembly. Elife *5*.

Wijnen, H., Landman, A., and Futcher, B. (2002). The G 1 Cyclin Cln3 Promotes Cell Cycle Entry via the Transcription Factor Swi6 . Mol. Cell. Biol. *22*, 4402–4418.

Wippich, F., Bodenmiller, B., Trajkovska, M.G., Wanka, S., Aebersold, R., and Pelkmans, L. (2013a). Dual specificity kinase DYRK3 couples stress granule condensation/ dissolution to mTORC1 signaling. Cell *152*, 791–805.

Wippich, F., Bodenmiller, B., Trajkovska, M.G., Wanka, S., Aebersold, R., and Pelkmans, L. (2013b). Dual specificity kinase DYRK3 couples stress granule condensation/ dissolution to mTORC1 signaling. Cell *152*, 791–805.

Wood, E., and Nurse, P. (2015). Sizing up to divide: mitotic cell-size control in fission yeast. Annu Rev Cell Dev Biol *31*, 11–29.

Xie, S., and Skotheim, J.M. (2020). A G1 Sizer Coordinates Growth and Division in the Mouse Epidermis. Curr. Biol. *30*, 916-924.e2.

Xie, Z., Jay, K.A., Smith, D.L., Zhang, Y., Liu, Z., Zheng, J., Tian, R., Li, H., and Blackburn, E.H. (2015). Early telomerase inactivation accelerates aging independently of telomere length. Cell *160*, 928–939.

Yaglom, J., Linskens, M.H.K., Sadis, S., Rubin, D.M., Futcher, B., and Finley, D. (1995). p34 Cdc28 - mediated control of Cln3 cyclin degradation. Mol. Cell. Biol. *15*, 731–741.

Yaglom, J.A., Goldberg, A.L., Finley, D., and Sherman, M.Y. (1996). The molecular chaperone Ydj1 is required for the p34CDC28-dependent phosphorylation of the cyclin Cln3 that signals its degradation. Mol. Cell. Biol. *16*, 3679–3684.

Yahya, G., Parisi, E., Flores, A., Gallego, C., and Aldea, M. (2014). A Whi7-Anchored Loop Controls the G1 Cdk-Cyclin Complex at Start. Mol. Cell *53*, 115–126.

Yang, P., Mathieu, C., Kolaitis, R.M., Zhang, P., Messing, J., Yurtsever, U., Yang, Z., Wu, J., Li, Y., Pan, Q., et al. (2020). G3BP1 Is a Tunable Switch that Triggers Phase Separation to Assemble Stress Granules. Cell *181*, 325-345.e28.

Yang, X., Shen, Y., Garre, E., Hao, X., Krumlinde, D., Cvijović, M., Arens, C., Nyström, T., Liu, B., and Sunnerhagen, P. (2014). Stress granule-defective mutants deregulate stress responsive transcripts. PLoS Genet. *10*, e1004763.

Yang, Z.S., Qing, H., Gui, H., Luo, J., Dai, L.J., and Wang, B. (2019). Role of caprin-1 in carcinogenesis (Review). Oncol. Lett. *18*, 15–21.

Yoneyama, M., Jogi, M., and Onomoto, K. (2015). Regulation of antiviral innate immune signaling by stress-induced RNA granules. J. Biochem. *159*, 279–286.

Yoon, J.-H., Choi, E.-J., and Parker, R. (2010). Dcp2 phosphorylation by Ste20 modulates stress granule assembly and mRNA decay in Saccharomyces cerevisiae. J. Cell Biol. *189*, 813–827.

Youn, J.-Y.Y., Dunham, W.H., Hong, S.J., Knight, J.D.R., Bashkurov, M., Chen, G.I., Bagci, H., Rathod, B., MacLeod, G., Eng, S.W.M., et al. (2018). High-density proximity mapping reveals the subcellular organization of mRNA-associated granules and bodies. Mol. Cell *69*, 517–532.

Yu, H. (2007). Cdc20: A WD40 Activator for a Cell Cycle Degradation Machine. Mol. Cell *27*, 3–16.

Zapata, J., Dephoure, N., Macdonough, T., Yu, Y., Parnell, E.J., Mooring, M., Gygi, S.P., Stillman, D.J., and Kellogg, D.R. (2014). PP2ARts1 is a master regulator of pathways that control cell size. J. Cell Biol. *204*, 359–376.

Zatulovskiy, E., and Skotheim, J.M. (2020). On the Molecular Mechanisms Regulating Animal Cell Size

Homeostasis. Trends Genet. *36*, 360–372.

Zhang, H., Elbaum-Garfinkle, S., Langdon, E.M., Taylor, N., Occhipinti, P., Bridges, A.A., Brangwynne, C.P., and Gladfelter, A.S. (2015). RNA Controls PolyQ Protein Phase Transitions. Mol. Cell *60*, 220–230.

Zhang, K., Daigle, J.G., Cunningham, K.M., Coyne, A.N., Ruan, K., Grima, J.C., Bowen, K.E., Wadhwa, H., Yang, P., Rigo, F., et al. (2018). Stress Granule Assembly Disrupts Nucleocytoplasmic Transport. Cell *173*, 958-971.e17.